STOCHASTIC ANALYSIS OF THE EFFECT OF SPATIAL VARIATIONS OF HYDRAULIC CONDUCTIVITY ON GROUNDWATER FLOW

by

Adel Ahmed Mohammed Bakr

Submitted in Partial Fulfillment
of the Requirements for the Degree of
Doctor of Philosophy

NEW MEXICO INSTITUTE OF MINING AND TECHNOLOGY

Socorro, New Mexico

July, 1976

ACKNOWLEDGMENTS

I would like to express my appreciation and sincere gratitude to my thesis advisor, Professor Lynn W. Gelhar, for his unfailing support, helpful suggestions, and prodding encouragement which contributed to the success of this study. The author is particularly indebted to Professor Gelhar for suggesting a spectral analysis approach to characterizing the spatial correlation structure of hydrogeologic variables.

I would also like to express my gratitude to the remaining members of my committee for their interest throughout this work. In particular the author benefited from discussions on the estimation of spectra with Dr. Allan L. Gutjahr of the mathematics department.

The help of Mr. Adrian P. Visocky of the Illinois State Water Survey in securing the core analysis data used herein is greatly appreciated.

The author would like to express his gratitude to his colleague Richard L. Naff for critically editing the rough draft which led to its improvement. The author is indebted to Lisa Cole for drafting the figures and to Patricia Valentine and Barbara Zamora for typing the manuscript.

The writer expresses his thanks to the Middle Eastern Regional Radioisotope Centre for the Arab Countries, Egypt, for granting him a study leave.

Special gratitude is due my wife, Salwa, and children, Noha and Yasser whose affection, encouragement, and understanding made this accomplishment possible.

ABSTRACT

The objective of this study is to use spectral analysis techniques to examine the predicted hydraulic head in one- and three-dimensional flow systems in which both the hyraulic conductivity and the head are taken to be spatially random variables characterized by appropriate covariance functions. The main features of this work are the statistical representation of medium properties (e.g. hydraulic conductivity) in terms of spatial correlation structure, a feature which is inherent to the description of a porous medium flow as a continuum, and the stochastic analysis of the problem of groundwater flow in three dimensions.

The theoretical analyses of the problem of groundwater flow in one and three dimensions is based on the stochastic representation of random function in terms of Fourier-Stieltjes integrals. Solutions of equations governing groundwater flow result in spectral expressions relating fluctuations in conductivity (or input) to those of hydraulic head (or output). These input-output spectral relationships are then used to establish forms of the covariance functions describing spatial variations of both input and output.

Estimated covariance functions for permeability and porosity of field data are used to test the validity of the assumed autocovariance functions characterizing conductivity fluctuations; the agreement between the assumed and estimated covariances was found to be reasonable. This portion of the study leads to the estimation of a length scale indicating the distance over which neighboring values of conductivity are correlated.

Applicability of the results obtained are demonstrated through two hypothetical one-dimensional network design problems. In the first, the optimum well spacing required for achieving a specified degree of accuracy in estimation of the hydraulic conductivity from permeameter experiments is determined, and in the second problem, the errors in specific discharge measurements between two points across an aquitard are estimated.

An important result of the three-dimensional analysis is an order of magnitude reduction in the variance of predicted hydraulic head relative to that in one dimension. It is of interest to note that although the conductivity field was assumed to be statistically isotropic, the correlation function of hydraulic head in three dimensions turned out to be statistically anisotropic.

TABLE OF CONTENTS

LIST OF FIGURES

LIST OF TABLES

LIST OF SYMBOLS

The following list covers the symbols which are widely used herein. The dimensions of dimensional quantities are given in brackets.

Symbol	Definition
a	correlation parameter in one-dimensional analysis (1/L)
dV	elemental volume (L^3)
$dZ_f(k)$	complex Fourier amplitude of fluctuations in ln K
$dZ_\phi(k)$	complex Fourier amplitude of hydraulic head fluctuations (L)
$dZ_K(k)$	complex Fourier amplitude of hydraulic conductivity fluctuations (L/T)
$dZ_W(k)$	complex Fourier amplitude of hydraulic resistivity fluctuations (T/L)
e	relative error in specific discharge estimates
$\bar{e}$	average relative error in specific discharge estimates
$\overline{e'^2}$	relative variance of specific discharge estimates
$E[X(t)]$	the expected value or ensemble average of X(t)
f'	fluctuation in the logarithm of the ratio $\frac{K}{K_\ell}$ where K and K_ℓ are defined below
$\bar{f}$	mean of log K
$\overline{f'^2}$	variance of log K
F	frequency; number of oscillations per unit distance (1/L)
i	$\sqrt{-1}$
J	hydraulic gradient

Symbol	Definition
k	wave number (1/L)
K	hydraulic conductivity of the medium (L/T)
K'	fluctuation in hydraulic conductivity about the mean (L/T)
K_ℓ	$\log K_\ell$ is the mean of log K
$\bar{K}$	mean hydraulic conductivity (L/T)
$\overline{K'^2}$	variance of hydraulic conductivity (L^2/T^2)
ℓ	correlation length (L)
M	number of lags used to compute the autocovariance function
N	length of record (L)
$p(X)$	probability density of some event X
$p(X_1, X_2)$	joint probability density of events X_1 and X_2
q	specific discharge vector (L/T)
$\bar{q}$	mean specific discharge (L/T)
$\hat{q}$	an estimate of the specific discharge (L/T)
$R_{ff}(\xi)$	$= E[f(x+\xi)f(x)]$, autocovariance of fluctuation in log K
$R_{KK}(\xi)$	autocovariance of fluctuations in hydraulic conductivity (L^2/T^2)
$R_{WW}(\xi)$	autocovariance of fluctuations in hydraulic resistivity (T^2/L^2)
$R_{\phi\phi}(\xi)$	autocovariance of hydraulic head fluctuations (L^2)
$R_{\phi\phi}(\xi, \chi)$	autocovariance of hydraulic head fluctuations in three dimensions (L^2)
$\hat{R}(\xi)$	an estimate of the autocovariance function

Symbol	Definition
$R_{xx}(o)$	variance of fluctuations in X
W	hydraulic resistivity (T/L)
W'	fluctuations in hydraulic resistivity (T/L)
$\bar{W}$	mean of hydraulic resistivity (T/L)
$\hat{W}$	an estimate of hydraulic resistivity (T/L)
$\overline{W'^2}$	variance of fluctuations in hydraulic resistivity (T^2/L^2)
$\overline{W'_3\phi'_2} = R_{W\phi}(\xi)$	$= E[W(x+\xi)\phi(x)]$, cross covariance of hydraulic resistivity and hydraulic head (T)
x	horizontal spatial coordinate (L)
γ	correlation parameter in three-dimensional analysis (1/L)
Δ	spacing between samples (L)
λ	integral scale (L)
ν	number of degrees of freedom used to compute confidence intervals
ξ	separation or lag (L)
$\rho_{ff}(\xi)$	autocorrelation function of fluctuations in log K
$\rho_{KK}(\xi)$	autocorrelation function of fluctuations in hydraulic conductivity
$\rho_{nn}(\xi)$	autocorrelation function of porosity fluctuations
$\rho_{WW}(\xi)$	autocorrelation function of fluctuations in hydraulic resistivity
$\rho_{\phi\phi}(\xi)$	autocorrelation function of fluctuations in hydraulic head
σ	standard deviation of log K

Symbol	Definition
ϕ	hydraulic head elevation (L)
ϕ'	fluctuation in hydraulic head (L)
$\bar{\phi}$	mean of hydraulic head (L)
$\hat{\phi}$	an estimate of hydraulic head (L)
$\overline{\phi'^2}$	variance of fluctuations in hydraulic head (L^2)
$\overline{\phi_1' W_3'}=R_{\phi W}(\xi)$	cross covariance of hydraulic head and hydraulic resistivity (T)
$\Phi_{ff}(k)$	spectral density function or spectrum of fluctuations in log K
$\Phi_{KK}(k)$	spectral density function of fluctuations in hydraulic conductivity (L)
$\Phi_{nn}(k)$	spectral density function of fluctuations in porosity (L)
$\Phi_{WW}(k)$	spectral density function of fluctuations in hydraulic resistivity (L)
$\Phi_{W\phi}(k)$	cross spectrum of resistivity and head fluctuations (L)
$\Phi_{\phi\phi}(k)$	spectral density function of hydraulic head fluctuations (L)
$\hat{\Phi}(k)$	an estimate of the spectral density function

CHAPTER 1

INTRODUCTION

1.1 Background

Numerical studies of groundwater movement, based on mathematical solutions to deterministic models of flow through porous media often assume that individual aquifers or geologic units are homogenous and isotropic and that large scale heterogeneity exists only between adjoining geologic units. However, observation indicates that natural depositional processes do not produce perfectly homogenous geologic units. It is this homogeneity which we wish to examine in the following paragraphs.

Few investigations have attempted to account for the high degree of variability in hydrologic properties of aquifer materials (e.g. Warren and Price, 1961; McMillan, 1966; and Freeze, 1975). In these studies, values of the hydrologic parameters of the individual layers or blocks constituting the flow system were assigned to various regions of the modelled aquifer according to some frequency distribution. Random numbers were used to generate values of the hydrologic parameters in each unit in which the values were assumed to be statistically independent and therefore totally uncorrelated in space. However, the mode of deposition of most clastic geologic formations suggests the existence of correlation patterns for properties within a given deposit. Furthermore, the simulations by Freeze (1975, Fig. 5) demonstrate that the number of layers included in the model has a definite effect on the magnitude of the standard deviation of predicted hydraulic head; the errors in head decreased as the number of layers increased. This observation implies the need for a better way of defining the spatial variability

in a flow system other than by deterministic blocks or units as usually done in the literature.

As previously noted, a major limitation of the investigations cited above is that the spatial statistical structure of medium properties (e.g. porosity and permeability) is completely ignored. Though it is recognized that properties such as permeability are spatially variable, the effects of the variability in the transmitting medium on subsurface flow are largely unexplored. Though the last decade witnessed major advances in the subsurface flow modelling, it is recognized that predictive capabilities of these models are seriously limited because of uncertainty in the model parameters. This uncertainty is fundamentally related to the spatial variability of the medium and its effect on the flow. Therefore, statistical techniques are needed which incorporate spatial variability of the hydrologic properties in order that the effects of their variations on the flow be ascertained.

A statistically complete description of the hydraulic conductivity continuum requires joint probability density functions of conductivity at various locations. However, these are seldom available in real life situations. Instead, certain moments of the distributions, such as covariances, can be used to characterize the spatial statistical structure of permeability variations (see e.g. Gelhar, 1976). Techniques of spectral analysis have been applied by Bennion and Hope (1974) to analyze one-dimensional permeability and porosity data from oil reservoirs. Spectral analysis of two-dimensional processes has been utilized in the analysis of several types of data; these include data on topographic variations in forest land surveys (Matern, 1947), agricultural yields (Whittle, 1954), mineral deposits (Agterberg, 1974, Ch. 10 & 11), and

precipitation (Rodriguez-Iturbe and Mejia, 1974). In this work we use spectral analysis techniques to describe the relationship between the spatial variability of medium flow properties and variability in the resulting hydraulic head for steady, saturated groundwater flow problems.

1.2 Objectives and Scope of This Study

The general goal of this study is to develop methods by which the effects of the spatial variability of hydrologic properties can be evaluated and predicted for natural subsurface materials. The main features of this work are the statistical description of medium properties such as hydraulic conductivity and porosity in relation to the geologic features of natural deposits, and the stochastic analysis of the problem of groundwater flow in three dimensions. The immediate goal of this work is to use spectral analysis techniques to examine the predicted hydraulic head in one- and three-dimensional groundwater systems in which the conductivity and head are taken to be spatially random variables. The following specific objectives are established:

(1) to develop solutions to the problem of steady, saturated, groundwater flow in one dimension in which a stochastic representation is used to describe fluctuations in hydraulic conductivity and hydraulic head,

(2) to demonstrate the applicability of the results obtained from the previous step in examples of simple network design problems,

(3) to extend the approach of step (1) to the solution of the problem of steady, saturated, groundwater flow in three dimensions in an isotropic medium,

(4) to examine how estimated covariance functions from permeability and porosity field data fit the theoretical covariance functions assumed in the course of the spectral analysis of steps (1) and (3),

(5) to compare among results of the analysis of the problem of one-dimensional groundwater flow and those obtained from the three-dimensional solution. The purpose in performing these comparisons is to examine the range of validity of the one-dimensional results.

The theoretical analysis of the problem of groundwater flow in one and three dimensions is based on the stochastic representation of random functions in terms of Fourier-Stieltjes integrals. Solutions of equations governing groundwater flow result in spectral expressions relating fluctuations in conductivity (or input) to those of hydraulic head (output). These input-output spectral relationships are then used to establish forms of the covariance functions describing spatial variations of both input and output.

Estimated covariance functions for permeability and porosity field data are used to examine the validity of the assumed theoretical autocovariance functions characterizing conductivity fluctuations. The outcome of this portion of the study leads to a length scale indicating the distance over which neighboring values of conductivity are positively correlated. The significance and implications of this concept are explored.

Applicability of the results obtained are demonstrated through two hypothetical one-dimensional network design problems. The first addresses the optimum well spacing required for achieving a specified

degree of accuracy in estimation of the hydraulic conductivity from permeameter experiments and the second the estimation of the errors in specific discharge measurement between two points across an aquitard.

CHAPTER 2

STOCHASTIC REPRESENTATION OF HYDRAULIC CONDUCTIVITY VARIATIONS IN NATURAL DEPOSITS

2.1 Introduction

In order to understand the motivation behind a stochastic representation for hydraulic conductivity fluctuations in natural deposits, it is necessary to examine the range of variation of such a property in different geologic formations. This constitutes the first objective of this chapter. The second objective of this chapter is to review previous work on analysis of fluid flow in subsurface materials with a view toward the methods through which variations of flow system conductivity are incorporated. Finally, we discuss both the reasons for a stochastic representation of conductivity fluctuations in a given formation and the basis for such a representation.

2.2 Hydraulic Conductivity of Subsurface Materials

The hydraulic conductivity expresses the capacity of a porous material to transmit fluids. It is a property of both the fluid and the porous material. The hydraulic conductivity of a porous medium is defined (U. S. Geological Survey, 1972, p. 4) as the volume of water at the existing kinematic viscosity that will move in unit time under a unit hydraulic gradient through a unit area measured at right angles to the direction of flow.

The hydraulic conductivity of clastic rocks is one of their most variable properties, far exceeding that of porosity (see for example fig. 2-1). Variation in hydraulic conductivity is enormous and can

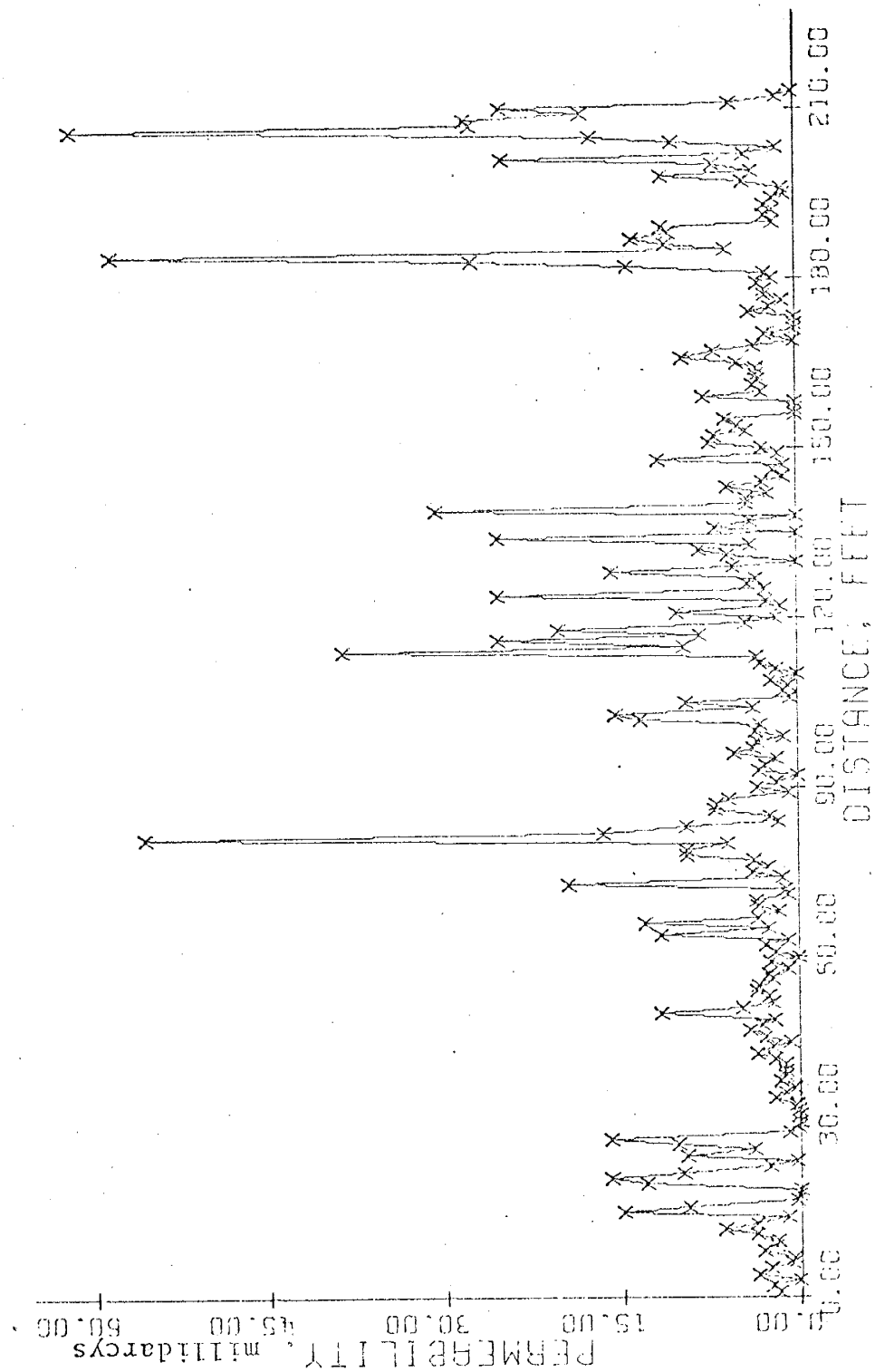

Fig. 2-1: Original permeability series versus spacing between samples for IL042H.

range from thousands of meters per day in well-washed, unconsolidated terrace and river sands to 4×10^{-4} m/day in unweathered silts and clays (Todd, 1959, p. 53). Moreover, small- and large-scale spatial variations in hydraulic conductivity can also be large. This high degree of variability has made conductivity a difficult parameter to predict.

Pettijohn et al. (1972) present a detailed discussion of the geologic factors controlling variations in hydraulic conductivity and list several related references. On the microscale of a few grains, medium properties affecting the hydraulic conductivity are grain size, sorting, orientation and packing of grains, and cementation and bedding on the scale of core samples, all interrelated in a manner which defies analysis. It has been found experimentally (Krumbein and Monk, 1942), that the finer the grain size and the poorer the sorting of loose sand, the smaller its hydraulic conductivity. The influence of the uniformity in grain size or sorting on the conductivity is significant in clastic materials; the poorer the sorting the lower the conductivity. The tighter the packing of sand the lower its effective porosity and hence the lower its conductivity, all other factors remaining equal. However, in nature, tighter packing tends to prevail since it is the most stable, hence the importance of variation in packing is minimized. Mast and Potter (1963, p. 588) indicated that orientation and packing of grains of a sandstone appear to have a weak control on permeability in the plane of bedding and a much stronger control in vertical sections parallel to sand transport direction.

The most important primary depositional control on permeability distribution in a sandstone body on the scale of core samples or larger

is its bedding facies (Pettijohn et al. 1972, p. 526) because slight pauses in sand deposition are commonly marked by an accumulation of thin mud laminations of low permeability. It is recognized that siltstone and shale beds act as barriers to flow within a sandstone body and consequently inhibiting vertical flow. Polesek and Hutchinson (1967, p. 397) emphasized that it is the arrangement of such barriers within a sand body, and not the permeability variations within the sand, that are of critical significance in reservoir analysis. Note that both grain fabric and laminations cause vertical permeabilities to be smaller than horizontal ones while grain orientation imparts a weak anisotropy to permeability in the plane of the bedding.

2.3 Statistical Distribution of Hydraulic Conductivity

It is generally recognized that the probability density function for hydraulic conductivity measurements from the same geologic unit tends to be lognormally distributed (Davis, 1969, p. 76). Direct evidence to support this statement is provided by several studies. Freeze (1975) presents a good summary of relevant works. On the basis of core analysis data from a sand oil reservoir, Law (1944) proposed a lognormal distribution for hydraulic conductivity values. Bulnes (1946) working with cores from carbonate rocks and later Warren et al. (1961) using cores from sand and dolomite oil reservoirs observed a lognormal distribution for the conductivity of these data. Based on over 250 auger hole measurements in 12 fields in Australia and on close to 1500 samples from seven soil types in California, Willardson and Hurst (1965) found that a lognormal distribution best described the hydraulic conductivity of soils. Brust et al. (1968) and more recently

Nielsen et al. (1973) reached the same conclusion with regard to soils. McMillan (1966) found the transmissivity for the water bearing units of the Los Angeles basin to be lognormally distributed. Bennion and Griffiths (1966) have compiled data from several thousand samples of conglomerate, sandstone, and limestone units, and have found permeabilities to be lognormally distributed, although occasionally somewhat skewed. Finally, part of the log of conductivity data to be analyzed herein was plotted on normal probability paper as shown in figure 2-2. That these data points fall on a straight line confirms that conductivity values tend to be lognormally distributed.

In addition to the direct evidence reflected from the studies cited above, there exists in the literature a large body of indirect evidence providing support for a lognormal frequency distribution for hydraulic conductivity. Extensive studies of the specific capacities (which are an indirect function of aquifer permeabilities) of several thousand water wells in various geologic units, have shown that their values are lognormally distributed (Csallany and Walton, 1963; Seaber and Hollyday, 1968). It is also widely recognized that grain size distributions are lognormal (Krumbein, 1936; and Griffiths, 1967), with the exception of Bagnold (1968), and that hydraulic conductivity can be expressed in terms of some representative grain size diameter. Furthermore, in most empirical formulae, hydraulic conductivity is expressed as an exponential function of porosity. Since porosity values from a single formation have been reported (Law, 1944; Bennion and Griffiths, 1966) as being normally distributed, the exponential relationship between conductivity and porosity implies that the hydraulic conductivity is lognormally distributed.

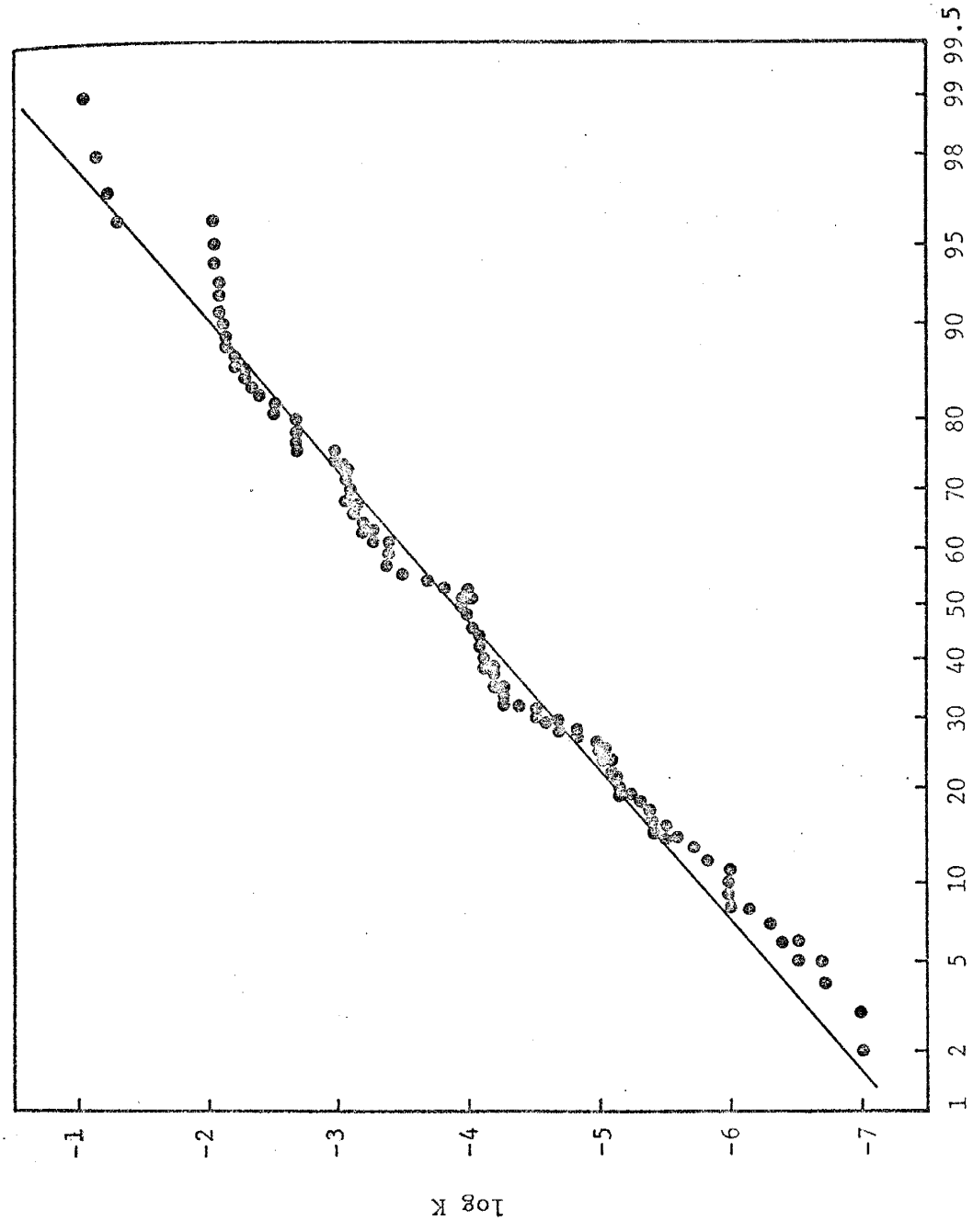

Fig. 2-2: A check for the normality of log conductivity data from Gambolati et al. (1974).

2.4 Review of Previous Work

We start this review by discussing the estimation of permeability of unconsolidated sediments from grain size analysis. Flow models incorporating some statistical variability in the parameters of porous materials and also deterministic models addressing the same problem are briefly examined. Finally, we mention the few studies describing spatial variability of geologic parameters and also briefly comment on the small number of investigations dealing with the stochastic analysis of groundwater systems.

Estimation of the permeability of unconsolidated sediments from grain size analysis has been attempted by several authors with varying degrees of success (Krumbein and Monk, 1942; Cohen, 1963; Masch and Denny, 1966; and Rose and Smith, 1957). Statistical analysis of data from cores (Law, 1944; Bulnes, 1946; and Warren et al. 1961) and from field soil tests (Brust et al. 1968; Nielson et al. 1973; Rogowski, 1972; and Willardson and Hurst, 1965) have been performed. In all of these studies, it was assumed that the permeability measurements are statistically independent in space. Greenkorn and others (1964) used a permeability tensor to explain and correlate directional air permeabilities from core data with lithology. They found that the anisotropy component correlates with bedding while the heterogeneity part correlates with grain size.

Cardwell and Parsons (1945), working with blocks of different permeabilities arranged in a number of patterns, arrived at expressions for the average permeability of heterogeneous oil sands while Bouwer (1969), among others, discussed the problem of sampling and design of

experiments for measuring the hydraulic conductivity of soils and other natural materials. Mason and others (1957) using approximately 10,000 core samples, discussed the interrelationships between hydraulic conductivity, percent drainable pores, and bulk density in a number of soil groups and also the magnitude of the sampling error involved over a wide range of soil conditions.

Statistical interpretation of permeability data from cores enabled Warren et al. (1961) to correlate them with field data. Willardson and Hurst (1965) suggested the use of confidence intervals to estimate the number of field hydraulic conductivity measurements required to represent a given formation. Sagar and Kisiel (1972) estimated the errors in hydraulic head measurements near a pumping well due to uncertainties in aquifer parameters and noted that these errors grow with time, thus limiting the validity of long range predictions.

A number of flow models incorporating some statistical variability in hydrologic parameters of the porous materials will now be discussed. Warren and Price (1961) used a numerical model to investigate steady state and transient flow through heterogeneous porous media and examined the influence of several frequency distributions for hydraulic conductivity on the resulting solutions. Freeze (1975) extended the approach of Warren and Price by examining the multivariate problem in which porosity and compressibility, as well as hydraulic conductivity, are described by frequency distributions. He studied the effects of the statistical parameter distributions on predicted hydraulic head with the aid of a large number of Monte Carlo simulations for two one-dimensional saturated flow problems: steady state flow between two specified heads and transient consolidation of a clay layer. Numerical

simulation of groundwater basins was carried out by McMillan (1966) to evaluate the relationship between the hydraulic conductivity fluctuation and the resulting variation in the potential field (or hydraulic head) for one-, two-, and three-dimensional flows. Freeze (1972) discussed different aspects of regionalization of the hydrologic parameters of an aquifer due to the scarcity of data. He considered layered systems and emphasized the importance of treating the conductivity as an independent statistical variable. Meanwhile, Heller (1972) examined the effects of permeability heterogeneity on dispersion phenomenon in porous media using a numerical model. Lippmann (1973) and Wu et al. (1973) have analyzed flow through media with statistically characterized block units but without statistically distributed parameter values. Bibby and Sunada (1971) utilized Monte Carlo simulation to investigate the effects of normally distributed measurement errors in the initial head, boundary heads, pumping rate, aquifer thickness, hydraulic conductivity, and storage coefficient on solutions to the transient flow to a well in a confined aquifer. In the above and earlier statistical studies of flow models the spatial correlation structure of parameters such as the hydraulic conductivity was neglected.

In addition to the statistical studies on the determination of the hydraulic conductivity of aquifer materials, there exist in the literature deterministic flow models addressing the same problem. Nelson (1968) and Nelson and McCollum (1969) applied analysis of the energy dissipation in the flow system in order to obtain the permeability distributions in heterogeneous porous materials. Their approach, however, is another method of solving the inverse problem in which we seek to find distributions of the hydrologic properties of a certain

aquifer when the distribution of hydraulic head over the area of interest is given, as discussed by Emsellem and DeMarsily (1971). The effects on the discharge and travel time due to variations of the hydraulic conductivity, which were either linear or some power of the distance, were reported by Butler and Gundlach (1974). Prats (1972) discussed the influence of oriented arrays of thin impermeable shale lenses or of highly conductive natural fractures on the apparent permeability anisotropy of a reservoir, while Asfari and Witherspoon (1973) used a finite element method to simulate the permeability of naturally fractured reservoirs. Theis (1967) discussed the role of permeability variations in subsurface flows.

Trend surface analysis of geologic parameters has been widely applied (Krumbein and Graybill, 1965; Koch and Link, 1972; and Agterberg, 1974) and it has been noted that some properties of natural deposits can be described in terms of Markov models (Krumbein and Dacey, 1969; Lippmann, 1973; and Vistelius, 1967). Moreover, the use of spatial covariance functions and spectral analysis to describe the spatial variability of geologic parameters has been suggested (see Agterberg and Tukey, respectively, in Merriam ed., 1970) but is largely untried. Large-scale variations of the porosity were treated as a random function of position by Buyevich et al., (1969). Spatial variability of unsaturated hydraulic conductivity was briefly discussed by Stockton and Warrick (1971) while the spatial variability of soil moisture, saturated conductivity, bulk density, and the particle size distribution were examined in detail by Nielsen et al. (1973) and Coelho (1974).

Stochastic analysis of groundwater systems has been quite limited

and has emphasized the temporal variability through time series analysis and frequency spectra (e.g. Eriksson, 1970a). Yevjevich (1971) discussed sources of the stochastic behavior of most hydrologic variables. The use of time series analysis in the study of groundwater fluctuations was suggested by Julian (1967). Eriksson (1970b) used cross-spectrum analysis to study a 30-year record of precipitation, river water stage, and groundwater levels in the esker area of south Uppsala, Sweden. Jackson and others (1973) employed the technique of time series analysis to examine climatological and hydrogeological variables associated with a groundwater discharge area in Manitoba, Canada. Analytical models were developed by Gelhar (1974) and Gelhar et al. (1974) to describe the spectral response characteristics of phreatic aquifers subject to time variable accretion and fluctuations in adjacent stream stage. The effects of introducing spatial covariance structure characterizing hydraulic conductivity variations of aquifer materials on the flow in a sloping phreatic aquifer is analyzed in one and two dimensions by Gelhar (1976).

Previous studies of medium variability have generally assumed statistical independence in space or, as in the case of Sagar and Kisiel (1972), taken the medium properties to be uncertain, but constant with respect to space. One of the main features of the analysis developed here is the statistical representation of the medium in terms of spatial correlation structure, a feature which is inherent to the description of a porous medium flow as a continuum. Though it is recognized that the spatial covariance functions characterizing variations in hydraulic conductivity of the medium examined in this study are chosen for mathematical convenience, we will show later that these

functions do represent covariances of porosity and permeability field data reasonably well.

2.5 The Hydraulic Conductivity as a Stochastic Process

The continuum approach adopted in this study for solving the problem of groundwater flow in one and in three dimensions is applicable for large scale natural flow systems wherein the hydraulic conductivity together with the other hydrologic parameters may vary drastically from point to point throughout the flow system. The variation of the hydraulic conductivity of aquifer materials is complex and not feasibly observable in detail; hence conductivity is most appropriately thought of as a random variable. Traditionally, however, groundwater flow equations are solved as deterministic equations, usually with constant (nonrandom) coefficients, and the results used for parameter determination and prediction.

The complex variation of hydraulic conductivity in aquifer materials can be thought of in the continuum sense as a random field which is characterized by spatial covariance functions and spectral density functions in the wave-number domain (Gelhar, 1976). Most previous studies of the effects of medium variability in groundwater flow have ignored this spatial statistical structure, assuming that the medium consists of discrete zones of constant conductivity which are statistically independent. In this section we examine the reasons behind the need for treating the hydraulic conductivity of aquifer materials as a stochastic process or a random field and also discuss the mathematical justification for such a representation.

As indicated earlier, the hydraulic conductivity of clastic sediments is one of its most variable properties. In order to predict

groundwater movement in a given basin or to determine the travel time of pollutants and/or other substances in groundwater systems, to cite only two examples, a very large number of hydraulic conductivity measurements would have to be made throughout the basin. Yet, the effort and expense required to perform such a formidable task makes this prohibitive if not impossible. An alternative approach to the problem of characterizing hydraulic conductivity variation within a geologic unit is provided by assuming that the conductivity can be viewed as a random variable or a stochastic process. We then seek methods through which, given a reasonable number of conductivity determinations within a unit (called a realization in statistical terminology), we can use a single realization of conductivity variations to derive certain statistical properties which would enable us to describe the conductivity variations throughout the whole geologic unit.

So far, we have reduced the problem of describing, in detail, the conductivity variation in a geologic formation from having to measure the conductivity in a sufficiently large number of points in the unit to the problem of working with a record of limited number of measurements which is labelled a realization. Now a question arises as to under which conditions can a single realization of conductivity measurements represent variation of the conductivity over the whole unit. We require that the available record represent a statistically homogeneous process, which corresponds to a stationary process if we are working with a time series. By this we mean that the average properties of the process (in this case conductivity measurements) remain roughly the same during the interval; i.e. no systematic changes in the process occur with distance. A spatially-homogeneous record, by

definition, has statistical properties that are the same for all parts of the recorded interval. The statistical properties in this case refer to the various long-run spatial averages associated with the record, such as the mean, variance, and autocovariance (Breiman, 1969, p. 313). If all spatial records (sometimes called the ensemble) having the same properties as the given record are considered, then we are working with a probabilistic model.

Another way of presenting the above statement is as follows. As indicated in Lumley and Panofsky (1964, p. 37), "We wish to achieve the same results by averaging a single realization as we would achieve by averaging the whole ensemble. For this to be true, a single realization must of itself be an ensemble, that is different sections of the record must asymptotically be regarded as independent experiments. This is achieved by requiring the integral scales to exist, as discussed in detail in later chapters. By requiring all scales to exist, we are actually requiring the process to have a finite memory so that by waiting a sufficient time a given record can be regarded as a new experiment, independent of what went before...".

However, for the above discussion to hold, we need to examine the relation between the space average over our sample record and the ensemble average, that of all hypothetical similar records. The assumption most commonly made (Lumley and Panofsky, 1964) relating the various kinds of averages is that they are equivalent. In other words, if we encountered a situation in which more than one kind of average is available, the results obtained does not depend on which one was used in our calculations. This assumption relating an ensemble average to another type of average, space or time average, is called an ergodic

hypothesis. It is the validity of this assumption (see Monin and Yaglom, 1971 for its proof in certain cases) that enables us to regard the sample record of conductivity measurements as representing an ensemble of such records all having the same statistical properties as the given one. In fact, it is the statistical homogeneity assumed for the conductivity fluctuations, and the resulting ergodicity of these fluctuations that make it possible for us to use the stochastic Fourier-Stieltjes integral representation to describe variations in hydraulic conductivity and hydraulic head in the equations governing groundwater flow as discussed in Chapters 3 and 4, thus allowing for the spatial variations of conductivity and head to be incorporated and examined.

CHAPTER 3

STOCHASTIC ANALYSIS IN ONE DIMENSION

3.1 Introduction

In studies of groundwater flow based on mathematical solutions to deterministic models of flow through porous media, geologic units are assumed to be homogeneous and isotropic. Investigations of regional flow involving complex hydrogeologic systems (e.g. Freeze, 1966; Toth, 1963) are restricted to large scale heterogeneity among neighboring units, and homogeneity within any single unit. However, geologic formations seldom display the degree of homogeneity implied in these descriptions.

Though it is widely recognized that properties such as permeability are spatially variable, the effects of the variability on subsurface flow are largely unexplored. In this chapter the statistical structure of spatially variable flow properties (e.g. porosity, and hydraulic conductivity) of geologic formations will be established and used to describe variations in steady, saturated flow in one dimension. In particular, the effect on hydraulic head of random variations in hydraulic conductivity of a porous medium will be examined. In order to obtain the variance in hydraulic head, Darcy's equation will be solved considering fluctuations both in head and conductivity as random variables.

To account for the randomness encountered in hydrologic variables, Freeze (1975) analyzed one-dimensional groundwater flow in heterogeneous media in which the variables (e.g. porosity and permeability) are defined by frequency distributions. His Monte Carlo simulations

showed that the number of layers included in the model had a definite effect on the magnitude of the standard deviation of predicted hydraulic head; the errors in head decreased as the number of layers increased. This raises a question as to the appropriate number of layers needed to characterize a flow system. Furthermore, correlation of parameters from one layer to another was not accounted for in his study. Bennion and Hope (1974) utilized spectral analysis of core data to classify reservoir rock properties into three groups: Random, stratified correlated and stratified non-correlated. However, they looked at discrete points, i. e. from one well to another, neglecting spatial variations of the properties between the wells.

A major limitation of the approaches mentioned above is that the spatial statistical structure of medium properties (e.g. permeability) is completely ignored. In using random number generators to assign values of hydrologic parameters the authors assumed that these values are statistically independent of position. However, the mode of deposition of most clastic geologic formations suggests the existence of correlation patterns for properties within a given deposit. Therefore, statistical techniques are needed which incorporate the spatial variability of a given flow property.

Spectral analysis techniques discussed in the previous chapter (see also Appendix-A) will enable us to describe both the spatial variability of medium flow properties and the hydraulic head. The utility of the results obtained will be demonstrated through two hypothetical problems: estimation of the optimum well spacing required for achieving a specified degree of accuracy in hydraulic conductivity and the problem of the errors in specific discharge between two points

in an aquitard.

3.2 Perturbed Forms of the Flow Equation

In this section perturbed forms to the problem of steady flow in one dimension are discussed in relation to a possible exact formulation. Since flow of fluids in porous media is generally a multidimensional phenomenon, the applicability of one-dimensional solutions may be limited. Yet, any exact analytical solution in three dimensions is intractable thus making the approximate approach a necessity. The method of small perturbations adopted in this chapter serves as an illustrative example to a more general solution to be developed in the next chapter and also as a basis for examining the limitations of the one-dimensional results.

The equation for one-dimensional, steady state, saturated flow in the x direction through a heterogeneous isotropic porous medium is

$$q = -K(x)\frac{d\phi}{dx} \tag{3.1}$$

where ϕ is the hydraulic head, K(x) is the hydraulic conductivity at any point x, and q is the specific discharge, a constant. It is also possible to express the relationship between q and J, where J is the hydraulic gradient and equals $-\frac{d\phi}{dx}$, in terms of the hydraulic resistivity W(x) (Bear, 1972, p. 140). Hence, (3.1) becomes

$$\frac{d\phi}{dx} = -qW(x) \tag{3.2}$$

where

$$W \equiv \frac{1}{K}$$

This form of the flow equation has an advantage in that it allows for treating large fluctuations in conductivity exactly. Consequently, a solution to the problem of one-dimensional flow in the form of (3.2) will be called "the exact solution" and will serve as basis of comparison for the approximate solutions discussed below.

Another solution to the flow equation is obtained through a linear approximation of the hydraulic conductivity. A perturbed form of (3.1) can be solved by expressing both conductivity and head in terms of their means and fluctuations about the mean. Note, however, that the perturbed solution to (3.1) requires that the fluctuation about the mean be small compared to the mean. This requirement may not be satisfied readily since the conductivity is known to vary by several orders of magnitude in a given formation. (Freeze, 1975; and Todd, 1959, p. 53).

In addition to solving the perturbed form of the flow equation in terms of the hydraulic conductivity itself, a third solution will be obtained by perturbing in terms of the natural logarithm of the hydraulic conductivity (ln K). In order to carry out this analysis the differential form of the flow equation will be needed, i.e.

$$\frac{d}{dx}\left[K(x)\,\frac{d\phi}{dx}\right] = 0 \qquad (3.3)$$

The approximate solution of (3.3) in terms of ln K has the advantage that ln K will be considerably less variable than K itself, hence implying more accuracy when using the method of perturbation. Therefore,

it would be of interest to examine the range of validity of results from the approximate solutions in light of those obtained from the exact analysis. This will be considered in Chapter 6, Comparisons Among the Models. Furthermore, this linearized approach will be adopted in studying the three-dimensional flow problem, permitting estimation of the magnitude of the errors in one-dimensional flow.

3.3 Solution of the Flow Equation via Spectral Analysis Techniques

As already noted, the macroscopic steady state flow of water through most porous media can be represented by (3.3) or its integrated version, (3.1). Equation (3.3) results from an averaging of the microscopic flow within pores over a volume which encompasses many pores (a representative elementary volume (rev); Bear; 1972, p. 19). Physically this rev may be a few cm^3 in a fine granular material (i.e. the usual size of cored soil samples) and a few m^3 in the case of fractured rock. The continuum approach of (3.3) is applicable to large scale three-dimensional natural flow systems wherein the flow parameters may vary drastically from point to point throughout the flow system. The variation of these parameters is complex and not practically observable in detail; hence the parameters are most appropriately thought of as spatial stochastic random variables.

The problem described by either of (3.1) or (3.3) relates to interpretation of permeameter tests when the hydraulic conductivity varies in the direction of flow and the interpretation of field piezometer observations used to estimate discharge or hydraulic conductivity in a one-dimensional sense.

The different solutions to the one-dimensional flow problem are

developed in the following sections. Stochastic Fourier-Stieltjes integrals are used to represent fluctuations in hydraulic conductivity and hydraulic head. Expressions relating the spectra of these fluctuations are derived and thus the forms of the covariance functions describing their spatial variations will be established.

3.3.1 Exact Solution of the Flow Equation

We analyze the flow in one dimension (e.g. permeameter experiment) governed by

$$\frac{d\phi}{dx} = -qW(x) \tag{3.2}$$

Introducing the following quantities in terms of a mean part and a fluctuation part about the mean

$$\phi = \overline{\phi} + \phi' \quad , \quad E(\phi') = 0$$

$$W = \overline{W} + W' \quad , \quad E(W') = 0$$

and substituting them in (3.2) gives

$$\frac{d\overline{\phi}}{dx} + \frac{d\phi'}{dx} = -q\overline{W} - qW' \tag{3.4}$$

Note that the mean of (3.2) is

$$\frac{d\overline{\phi}}{dx} = -q\overline{W}(x)$$

and upon subtracting the mean part, (3.4) reduces to

$$\frac{d\phi'}{dx} = -qW' \tag{3.5}$$

which is the differential equation relating fluctuations in conductivity and head.

Consider the case of statistically homogeneous input perturbation, which is represented by Fourier-Stieltjes integrals in wave number k (see Appendix-A), as follows:

$$W' = \int_{-\infty}^{\infty} e^{ikx}\, dZ_w(k) \tag{3.6}$$

Similarly, the hydraulic head perturbation (or output) is represented by

$$\phi' = \int_{-\infty}^{\infty} e^{ikx}\, dZ_\phi(k) \tag{3.7}$$

Substituting (3.6) and (3.7) in (3.5), we obtain

$$\frac{d}{dx}\int_{-\infty}^{\infty} d^{ikx}\, dZ_\phi(k) = -q\int_{-\infty}^{\infty} e^{ikx}\, dZ_w(k)$$

which reduces to

$$\int_{-\infty}^{\infty} \left(ikdZ_\phi(k) + qdZ_w(k)\right)\, e^{ikx} = 0$$

For this expression to be true the quantity in brackets must be equal to zero identically for every value of x. Hence,

$$ikdZ_\phi(k) + qdZ_w(k) = 0$$

from which we obtain the following relationship between the complex Fourier amplitudes of head and resistivity:

$$dZ_{\phi}(k) = - \frac{q}{ik} \, dZ_{w}(k) \tag{3.8}$$

The wave number spectrum $\Phi_{\phi\phi}(k)$ of the hydraulic head in terms of the spectrum of the input perturbation $\Phi_{ww}(k)$ of the hydraulic resistivity can be constructed from (3.8) by multiplying each side by its complex conjugate and averaging (see Appendix-A). The resulting expression is

$$\Phi_{\phi\phi}(k) = \frac{q^2}{k^2} \, \Phi_{ww}(k) \tag{3.9}$$

Equation (3.9) is unbounded at the origin, i.e. it has a singularity at $k = 0$. However, the spectrum $\Phi_{\phi\phi}$ should integrate to a finite value so that the variance of hydraulic head is finite and hence its Fourier transform, representing the autocovariance function for head fluctuations, would exist. Therefore, the spectrum Φ_{ww} of hydraulic resistivity fluctuations would have to be proportional to k^2, permitting cancellation of the k^2 in the denominator.

A form of the resistivity autocovariance function whose inverse Fourier transform gives rise to a spectrum that is proportional to k^2 is (Erdelyi, 1954, p. 9)

$$R_{ww}(\xi) = \overline{W'^2} \, (1 - a\xi) \, e^{-a\xi} \qquad \text{if } \xi > 0 \tag{3.10}$$

where $\overline{W'^2}$ is the variance of W', ξ is the separation or lag, and a is

a correlation parameter having L^{-1} dimension. In addition to removing the singularity of (3.9) at the origin, the form (3.10) for R_{ww} is a physically realistic way of characterizing correlations between neighboring values of a property in a given medium. One would expect the correlation to drop off with increased spacing (or lag) and the negative exponential is a natural choice of functions which has this property (e.g. see Gelhar et al. 1974).

The spectrum Φ_{ww} is obtained by taking the inverse Fourier transform of R_{ww} defined by (3.10), i.e.

$$\Phi_{ww}(k) = \frac{1}{2\pi} \int_{-\infty}^{\infty} e^{-ik\xi} R_{ww}(\xi)\, d\xi = \frac{2ak^2\overline{W'^2}}{\pi(a^2 + k^2)^2} \tag{3.11}$$

The spectrum $\Phi_{\phi\phi}$ of hydraulic head fluctuations is then found by substituting (3.11) into (3.9)

$$\Phi_{\phi\phi}(k) = \frac{2aq^2\overline{W'^2}}{\pi(a^2 + k^2)^2} \tag{3.12}$$

To get the autocovariance function $R_{\phi\phi}$ of the hydraulic head we take the Fourier transform of (3.12), i.e.

$$R_{\phi\phi}(\xi) = \int_{-\infty}^{\infty} e^{ik\xi} \Phi_{\phi\phi}(k)\, dk$$

$$= \frac{q^2\overline{W'^2}}{a^2} (1 + a\xi)\, e^{-a\xi} \qquad \text{if } \xi > 0 \tag{3.13}$$

The variance of ϕ' is then given by

$$\overline{\phi'^2} = R_{\phi\phi}(0) = \int_{-\infty}^{\infty} \Phi_{\phi\phi}(k)\, dk$$

$$= \frac{q^2 \overline{W'^2}}{a^2} \qquad (3.14)$$

The autocorrelation function of hydraulic head obtained by dividing (3.13) by (3.14) is evaluated and presented in figure 3-1. Note that neighboring values of hydraulic head are highly correlated and that the correlation decreases as the separation increases.

The results of this analysis will be applied in a later section to establish the piezometer spacing required for achieving a given degree of accuracy in W in a permeameter type experiment. They will also serve as a basis for later comparisons with approximate solutions to the flow equation developed in the next two sections.

3.3.2 Linearized Solution in terms of K

The method of small perturbations is used to solve the one-dimensional flow equation in the form of (3.1). If the parameters are expressed in terms of a mean part and a small perturbation

$$K = \overline{K} + K'$$

$$\phi = \overline{\phi} + \phi'$$

equation (3.1) takes the form

$$(\overline{K} + K') \frac{d}{dx} (\overline{\phi} + \phi') = -q$$

We linearize by neglecting products of primed quantities to obtain

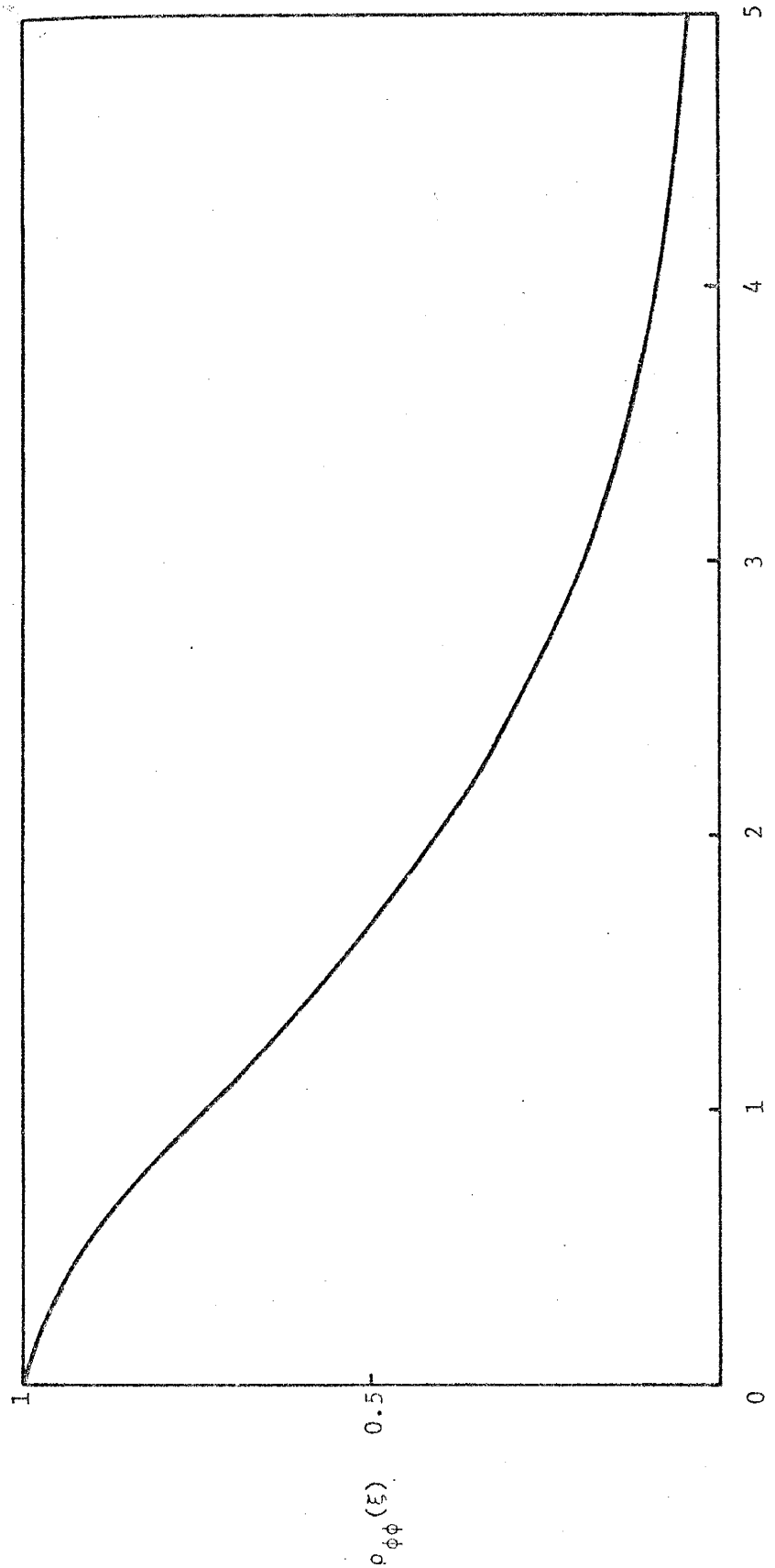

Fig. 3-1: Autocorrelation function, $\rho_{\phi\phi}(\xi)$, of hydraulic head fluctuations versus the dimensionless lag ξ/ℓ.

$$\bar{K}\frac{d\bar{\phi}}{dx} + K'\frac{d\bar{\phi}}{dx} + \bar{K}\frac{d\phi'}{dx} = -q \tag{3.15}$$

For a stationary random process the mean part of (3.15) is given by

$$\overline{\bar{K}\frac{d\bar{\phi}}{dx}} + \overline{K'\frac{d\bar{\phi}}{dx}} + \overline{\bar{K}\frac{d\phi'}{dx}} = -\bar{q} \tag{3.16}$$

Since by definition the mean of any primed quantity is zero, (3.16) reduces to

$$\bar{K}\frac{d\bar{\phi}}{dx} = -\bar{q}$$

Hence, (3.15) becomes

$$K'\frac{d\bar{\phi}}{dx} + \bar{K}\frac{d\phi'}{dx} = 0 \quad , \quad \text{or}$$

$$-K'J_o + \bar{K}\frac{d\phi'}{dx} = 0 \tag{3.17}$$

To the degree of approximation achieved by this perturbed solution we can write

$$q = J_o\bar{K},$$

which substituted in (3.17) yields

$$\frac{d\phi'}{dx} = q\frac{K'}{\bar{K}^2} \tag{3.18}$$

Note that $\frac{K'}{\bar{K}^2}$ corresponds to $-W'$ in the exact solution (compare with

(3.5)).

Assuming statistical homogeneity, the stochastic Fourier-Stieltjes integrals are used to represent the fluctuations as

$$K' = \int_{-\infty}^{\infty} e^{ikx}\, dZ_K(k) \tag{3.19}$$

with the head perturbations represented by (3.7). Substituting (3.7) and (3.19) in (3.18) and proceeding as in section 3.3.1, the following relationship between the Fourier amplitudes of head and conductivity is obtained:

$$ikdZ_\phi(k) = \frac{q}{\overline{K}^2}\, dZ_K(k) \tag{3.20}$$

Using (3.20) the spectrum $\Phi_{\phi\phi}$ of the hydraulic head fluctuations in terms of the spectrum of the input perturbation Φ_{KK} of the hydraulic conductivity is given by

$$\Phi_{\phi\phi}(k) = \frac{q^2}{\overline{K}^4\, k^2}\, \Phi_{KK}(k) \tag{3.21}$$

Equation (3.21) is singular at the origin and the discussion following (3.9) applies here also. Consequently, the form of the autocovariance R_{KK} of hydraulic conductivity is analogous to (3.10)

$$R_{KK}(\xi) = \overline{K'^2}\, (1 - a\xi)\, e^{-a\xi} \qquad \text{if } \xi > 0 \tag{3.22}$$

where $\overline{K'^2}$ is the variance of K' and the other symbols are as defined

earlier. The spectrum Φ_{KK} of the hydraulic conductivity fluctuations is obtained by taking the inverse Fourier transform of R_{KK} (see (3.11)); upon integration we get

$$\Phi_{KK}(k) = \frac{4ak^2\overline{K'^2}}{\pi(a^2 + k^2)^2} \tag{3.23}$$

The spectrum $\Phi_{\phi\phi}$ of the hydraulic head fluctuations is obtained by substituting (3.23) into (3.21)

$$\Phi_{\phi\phi}(k) = \frac{2aq^2}{\pi(a^2 + k^2)^2} \cdot \frac{\overline{K'^2}}{\overline{K}^4} \tag{3.24}$$

Note that $\overline{K'^2}/\overline{K}^4$ in the above expression corresponds to $\overline{W'^2}$ in the exact solution (compare with (3.12)). The Fourier transform of (3.24) gives the autocovariance $R_{\phi\phi}$ of the hydraulic head fluctuations (see (3.13)), and upon integrating we get

$$R_{\phi\phi}(\xi) = \frac{\overline{K'^2}}{\overline{K}^4} \cdot \frac{q^2}{a^2} (1 + a\xi)\, e^{-a\xi} \qquad \text{if } \xi > 0 \tag{3.25}$$

The variance of hydraulic head fluctuations would then be given by

$$\overline{\phi'^2} = R_{\phi\phi}(0) = \int_{-\infty}^{\infty} \Phi_{\phi\phi}(k)\, dk$$

which upon substituting $\Phi_{\phi\phi}$ from (3.24) and carrying the integration over wave number space or evaluating (3.25) at $\xi = 0$ becomes

$$\overline{\phi'^2} = \frac{\overline{K'^2}}{\overline{K}^4} \cdot \frac{q^2}{a^2} \tag{3.26}$$

The results of this analysis will be compared in a later chapter with the results from both the exact solution and the linearized solution developed next.

3.3.3 Linearized Solution in terms of ln K

The solution of differential equations by the method of perturbation requires that the fluctuation of the perturbed parameter should be small compared to its mean part. Thus, the results of the perturbed solution to the flow equation in terms of the conductivity, K, may not be appropriate in many cases since K may vary by several orders of magnitude. In an effort to relax this limitation, the flow equation is solved by perturbing in terms of the logarithm of the conductivity since the variability of ln K is considerably smaller than that of K itself.

We use (3.3) to describe the steady, saturated flow of water through a porous medium i.e.

$$\frac{d}{dx}\left[K(x)\ \frac{d\phi}{dx}\right] = 0 \tag{3.3}$$

Differentiating (3.3) and rearranging terms produces

$$\frac{d^2\phi}{dx^2} + \frac{d\ \ln\ K}{dx}\quad\frac{d\phi}{dx} = 0 \tag{3.27}$$

Linearize (3.27) by introducing the following quantities in terms of a mean part and a small perturbation

$$\phi = \bar{\phi} + \phi' + \ldots$$

$$\ln K = \bar{f} + f' = \overline{\ln K} + f'$$

$$= \ln K_g + f' \quad , \quad \text{or}$$

$$\ln \left(\frac{K}{K_g} \right) = f' \tag{3.28}$$

Substituting (3.28) into (3.27) gives

$$\frac{d^2\bar{\phi}}{dx^2} + \frac{d^2\phi'}{dx^2} + \frac{df'}{dx} \left[\frac{d\bar{\phi}}{dx} + \frac{d\phi'}{dx} + \ldots \right] = 0 \tag{3.29}$$

For the mean problem, neglecting products of fluctuations, (3.29) reduces to

$$\frac{d^2\bar{\phi}}{dx^2} = 0$$

The general solution for $\bar{\phi}$ is of the form

$$\bar{\phi} = Ax + B \quad , \tag{3.30}$$

where A and B are constants to be determined from the boundary conditions. To evaluate the constants we write Darcy's equation as

$$q_o = -K \frac{d\phi}{dx} \qquad \text{at } x = 0 \tag{3.31}$$

From the last member of (3.28) we can write

$$\frac{K}{K_g} = e^{f'} \quad ;$$

expanding the exponential term in a Taylor series gives

$$\frac{K}{K_\ell} = 1 + f' + \frac{f'^2}{2!} + \ldots \quad ,$$

from which the following expression for the conductivity is obtained by neglecting terms beyond the first order:

$$K = K_\ell (1 + f')$$

Hence, (3.31) becomes

$$q_o = -K_\ell (1 + f') \left(\frac{d\bar{\phi}}{dx} + \frac{d\phi'}{dx} + \ldots \right)$$

For the mean flow, again neglecting products of fluctuation, this reduces to

$$q_o = -K_\ell \frac{d\bar{\phi}}{dx} \tag{3.32}$$

However, differentiating (3.30) with respect to x and comparing with (3.32) we find that

$$\frac{d\bar{\phi}}{dx} = A = -\frac{q_o}{K_\ell} \tag{3.33}$$

The perturbation problem is formulated from (3.29) with the help of (3.33) as follows (again products of primed quantities are neglected):

$$\frac{d^2\phi'}{dx^2} - \frac{q_o}{K_\ell} \frac{df'}{dx} = 0 \tag{3.34}$$

The stochastic Fourier-Stieltjes integral representation of a

stationary process is used to solve (3.34) for the fluctuation f' in terms of ϕ'. Note that the fluctuations in the logarithm of the conductivity, f', are assumed to be normally distributed with standard deviation of $\sigma_{\ln K}$ (for references on lognormality of K or normality of ln K, see section 2.3). We assume statistical homogeneity of the fluctuations and write

$$f' = \int_{-\infty}^{\infty} e^{ikx}\, dZ_f(k)$$
$$\phi' = \int_{-\infty}^{\infty} e^{ikx}\, dZ_\phi(k) \tag{3.35}$$

Upon substituting (3.35) into (3.34) and manipulating, the following relationship between the complex Fourier amplitudes of the fluctuations is obtained

$$dZ_\phi(k) = -\frac{iq_o}{K_\ell k}\, dZ_f(k) \tag{3.36}$$

Multiplying each side of (3.36) by its complex conjugate and then averaging leads to (see Appendix-A)

$$E\,[dZ_\phi(k)\; dZ_\phi^*(k)] = \frac{q^2}{K_\ell^2 k^2}\, E\,[dZ_f(k)\; dZ_f^*(k)] \tag{3.37}$$

where the asterisk denotes the complex conjugate. From properties of the products of Fourier amplitudes appearing in (3.37), the spectrum $\Phi_{\phi\phi}$ of hydraulic head can be expressed in terms of the spectrum Φ_{ff} of ln K as

$$\Phi_{\phi\phi}(k) = \frac{q^2}{K_\ell^2 k^2} \Phi_{ff}(k) \tag{3.38}$$

Equation (3.38) is also singular at k = 0, as were equations (3.9) and (3.21) of the earlier analysis.

The autocovariance R_{ff} of the natural logarithm of K should be analogous to that of (3.10) since the spectra in both cases have the same properties, i.e.

$$R_{ff}(\xi) = \overline{f'^2}\,(1 - a\xi)\, e^{-a\xi} \qquad \text{if } \xi > 0 \tag{3.39}$$

Here $\overline{f'^2}$ is the variance of f' and the remaining symbols are as defined in earlier sections. The inverse Fourier transform of (3.39) yields the spectrum $\Phi_{ff}(k)$ of ln K, i.e.

$$\Phi_{ff}(k) = \frac{1}{2\pi} \int_{-\infty}^{\infty} e^{-ik\xi} R_{ff}(\xi)\, d\xi \quad ,$$

and upon substituting by (3.39) and integrating one obtains

$$\Phi_{ff}(k) = \frac{2ak^2\overline{f'^2}}{\pi(a^2 + k^2)^2} \tag{3.40}$$

Substituting Φ_{ff} from (3.40) into (3.38), the spectrum $\Phi_{\phi\phi}$ is given by

$$\Phi_{\phi\phi}(k) = \frac{2aq_o^2\overline{f'^2}}{\pi K_\ell^2(a^2 + k^2)^2} \tag{3.41}$$

The Fourier transform of $\Phi_{\phi\phi}$ leads to the autocovariance $R_{\phi\phi}$ of hydraulic head fluctuations

$$R_{\phi\phi}(\xi) = \int_{-\infty}^{\infty} e^{ik\xi}\, \Phi_{\phi\phi}(k)\, dk$$

$$= \frac{q_o^2 \overline{f'^2}}{a^2 K_\ell^2} (1 + a\xi)\, e^{-a\xi} \qquad \text{if } \xi > 0 \tag{3.42}$$

The variance $\overline{\phi'^2}$ of the hydraulic head fluctuations is then given by

$$\overline{\phi'^2} = R_{\phi\phi}(0) = \int_{-\infty}^{\infty} \Phi_{\phi\phi}(k)\, dk$$

$$= \frac{q_o^2 \overline{f'^2}}{a^2 K_\ell^2} = \frac{J_o^2 \overline{f'^2}}{a^2} \tag{3.43}$$

This concludes the details of the different solutions to the one-dimensional problem of steady, saturated flow through a porous medium. In the following section the form of the input spectrum of the hydraulic conductivity and the resulting autocovariance function will be discussed.

3.3.4 Theoretical Spectrum and Covariance Function of Hydraulic Conductivity

The stochastic analysis of the one-dimensional flow problem developed in section 3.3 implies a singularity at the origin for the expression relating the output spectrum $\Phi_{\phi\phi}$ of the hydraulic head to the input spectrum of the hydraulic conductivity (see equations (3.9), (3.21), and (3.38)). This singularity restricts our choice of the covariance function characterizing the spatial variability of the conductivity and hence the form of its spectrum. The factor k^2 appearing in (3.9), (3.21), and (3.38) suggests that the input fluctuations should have an autocovariance function whose inverse Fourier transform yields a spectrum proportional to k^2.

Figure 3-2 shows the form of the autocorrelation function $\rho(\xi)$ of hydraulic conductivity fluctuations represented by either of (3.10), (3.22) or (3.39) after dividing by the variance of the fluctuations. Note that the conductivity fluctuations are positively correlated up to the point where $a\xi$ equals one; here the correlation crosses the x axis and is negative thereafter. In other words, the conductivity fluctuations become consistently negatively correlated beyond the point $a\xi = 1$. The inverse of the parameter a, which we will now call the correlation length, is a characteristic length of the porous medium indicating the distance over which neighboring conductivity fluctuations are positively correlated. This parameter would be estimated from the statistical analysis of field data as discussed further in Chapter 5, where spectral calculations on hydraulic conductivity and porosity field data are performed.

The spectrum of the hydraulic conductivity fluctuations expressed by either of (3.11), (3.23), or (3.40) is depicted in figure 3-3. It represents a well-behaved function, finite at the origin and vanishing at infinity which it must in order for its Fourier transform to exist (which is the autocovariance function discussed above). Most of the energy is localized at small wave numbers as evidenced by the well-defined peak corresponding to conductivity fluctuations of large wave length. This aspect of the spectrum will be utilized later to identify the occurrence of periodicity or cyclicity patterns in data from different types of sediments.

3.4 Examples of Simple Network Design Problems

The results of the analysis developed in section 3.3 are applied

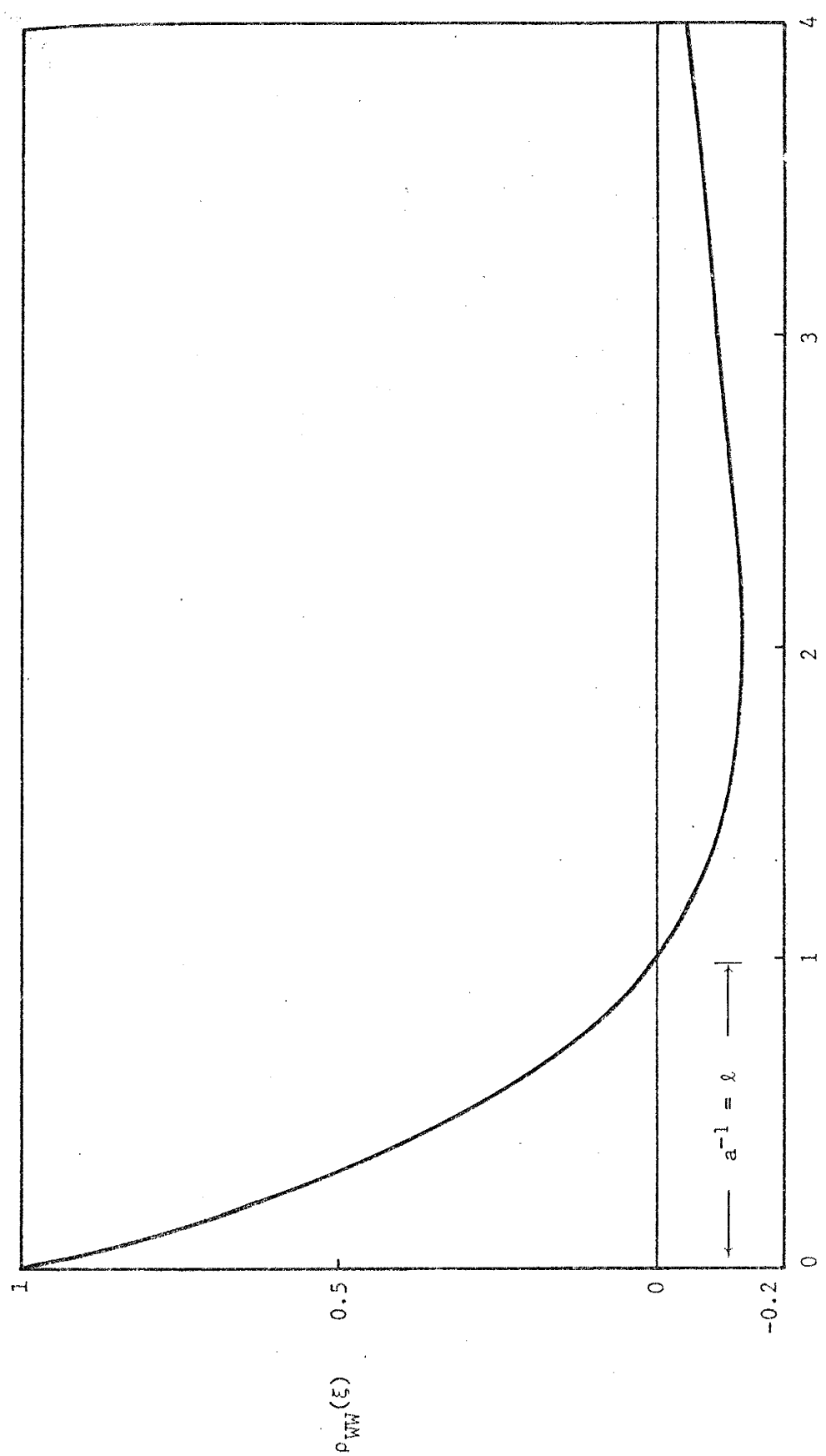

Fig. 3-2: Theoretical autocorrelation function of hydraulic resistivity versus dimensionless lag ξ/ℓ.

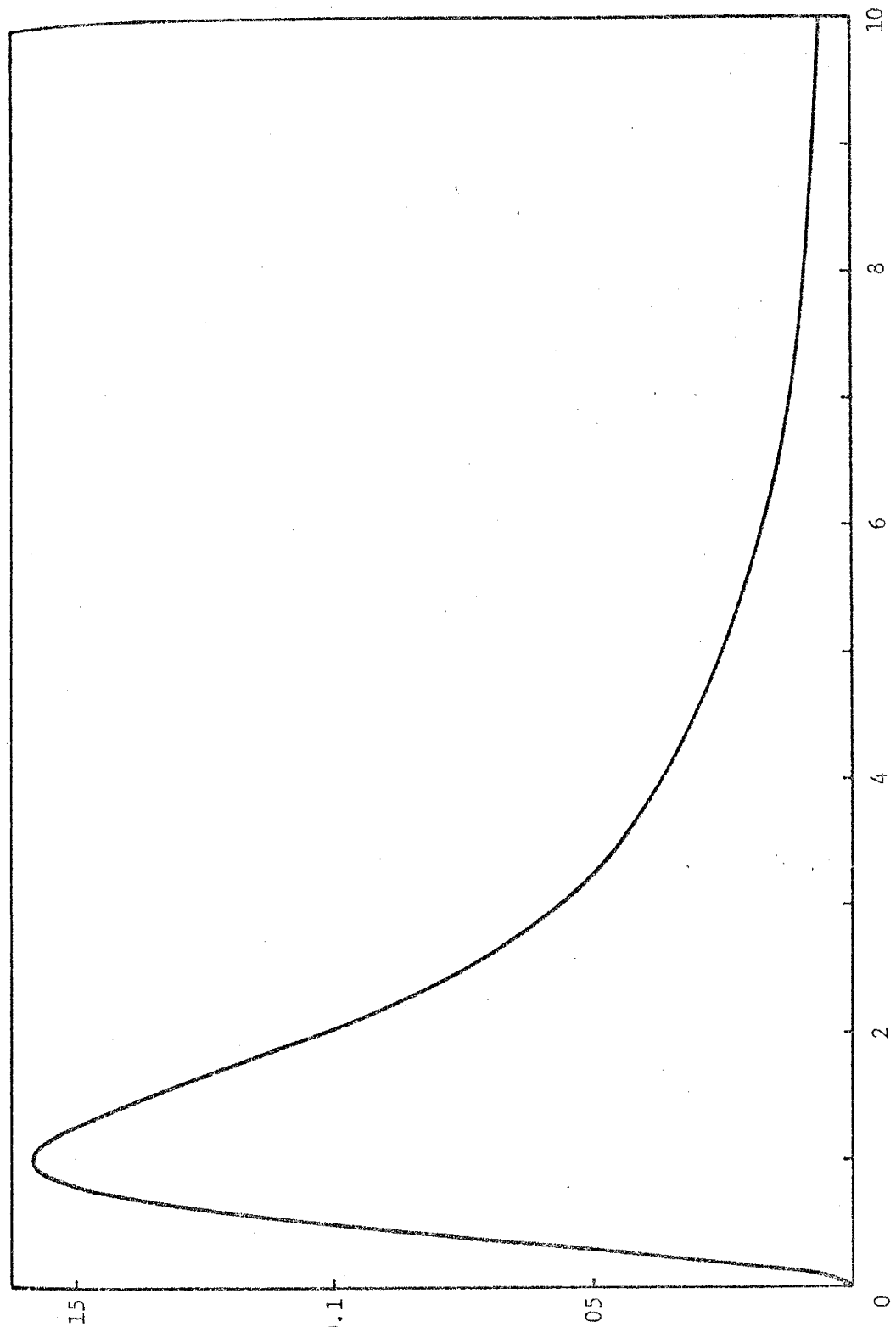

Fig. 3-3: Normalized theoretical spectrum of hydraulic resistivity versus dimensionless wave number.

to two network design problems. In the permeameter example, we evaluate the effect of spacing between two hydraulic head measurements on the accuracy attainable in a hydraulic conductivity estimate at an intermediate point. The second problem deals with evaluating errors in flow across an aquitard in relation to the spatial variability of hydraulic conductivity. Several graphs are constructed to indicate the utility of the analysis in prediction purposes. Both problems illustrate the importance of the correlation length, ℓ, of the medium in one-dimensional flow analysis.

3.4.1 Permeameter Example

Now we will answer the question: In a permeameter type flow (see Fig. 3-4), what would be the error in a hydraulic resistivity estimate made between two head measurements when the specific discharge is measured with absolute certainty? We proceed by using Darcy's relationship to express the resistivity estimate as follows

$$\hat{W}(x) = \frac{\hat{\phi}_1 - \hat{\phi}_2}{qL} \tag{3.44}$$

The mean of the resistivity $\overline{W}$ is also obtained from averaging Darcy's equation

$$q = -K(x) \frac{d\phi}{dx}$$

which may be written in the form

$$-\int_{\phi_1}^{\phi_2} d\phi = q \int_{x_1}^{x_2} \frac{dx}{K(x)} = q \int_{x_1}^{x_2} W(x)\, dx$$

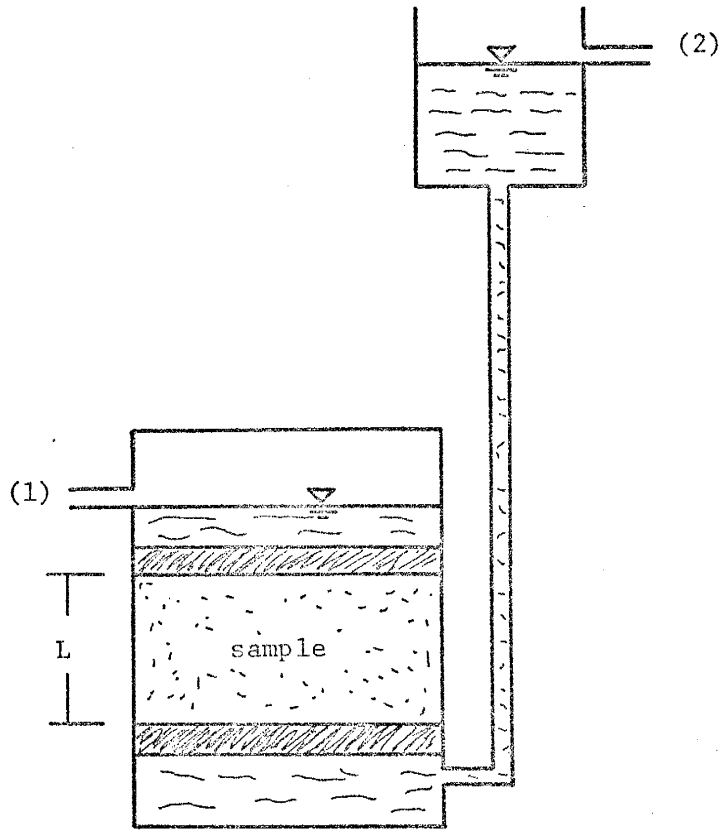

Fig. 3-4: Schematic diagram of a permeameter set up.

$$\phi_1 - \phi_2 = q\bar{W}L \qquad \text{or}$$

$$\bar{W} = \frac{\phi_1 - \phi_2}{qL}$$

The error in the resistivity estimate $\hat{W}$ relative to the mean is then given by

$$\hat{W} - \bar{W} = \frac{1}{qL} \left[(\hat{\phi}_1 - \phi_1) - (\hat{\phi}_2 - \phi_2)\right]$$

$$= \frac{1}{qL} (\phi'_1 - \phi'_2) \tag{3.45}$$

Squaring (3.45) and taking the expected value on both sides results in

$$\overline{(\hat{W} - \bar{W})^2} = \frac{1}{q^2L^2} \overline{(\phi'_1 - \phi'_2)^2}$$

$$= \frac{1}{q^2L^2} (\overline{\phi'^2_1} - 2\overline{\phi'_1\phi'_2} + \overline{\phi'^2_2}) \tag{3.46}$$

Assuming statistical homogeneity of the fluctuations yields $\overline{\phi'^2_1} = \overline{\phi'^2_2} \equiv \overline{\phi'^2}$ and hence (3.46) becomes

$$\overline{(\hat{W} - \bar{W})^2} = \frac{2}{q^2L^2} (\overline{\phi'^2} - \overline{\phi'_1\phi'_2}) \tag{3.47}$$

Dividing both sides of (3.47) by $\bar{W}^2$ and noting that

$$\overline{\phi'(x_1)\ \phi(x_2)} = \overline{\phi'(x_1)\ \phi(x_1 + \xi)} \equiv R_{\phi\phi}(\xi)$$

(3.47) becomes

$$\overline{\left(\frac{\hat{W} - \overline{W}}{\overline{W}}\right)^2} = \frac{2}{q^2 L^2 \overline{W}^2} \left(\overline{\phi'^2} - \overline{\phi'_1 \phi'_2}\right) \tag{3.48}$$

Substituting (3.13) and (3.14) in (3.48) and rearranging, we get

$$\overline{\left(\frac{\hat{W} - \overline{W}}{\overline{W}}\right)^2} = \frac{2}{(aL)^2} \overline{\left(\frac{W'}{\overline{W}}\right)^2} \left[1 - (1 + a\xi)\, e^{-a\xi}\right] \tag{3.49}$$

where ξ is equal to the spacing L between the head measurements, $\overline{\left(\frac{W'}{\overline{W}}\right)^2}$ is the theoretical relative variance of resistivity fluctuations while the left hand side of (3.49) represents its observed counterpart. Making use of the fact that a is the inverse of ℓ and $\xi \equiv L$, (3.49) takes the following nondimensional form:

$$\overline{\left(\frac{\hat{W} - \overline{W}}{\overline{W}}\right)^2} \Bigg/ \overline{\left(\frac{W'}{\overline{W}}\right)^2} = 2\left(\frac{\ell}{L}\right)^2 \left[1 - (1 + L/\ell)\, e^{-L/\ell}\right] \tag{3.50}$$

Note that $\left[\overline{\left(\frac{\hat{W} - \overline{W}}{\overline{W}}\right)^2}\right]^{1/2}$ represents the standard deviation of errors to be tolerated in the estimated resistivity value. The theoretical variance ratio is obtained from the properties of the lognormal distribution (Aitchison and Brown, 1957, p. 8) as follows:

$$\frac{W'^2}{\overline{W}^2} = \frac{\text{Var}\ (W)}{(E(W))^2} = e^{\sigma^2} - 1 \equiv \frac{K'^2}{\overline{K}^2} \quad ;$$

here σ is the standard deviation of ln K. In other words (3.50) is equally valid if W is replaced by K, or

$$\overline{\left(\frac{\hat{W} - \overline{W}}{\overline{W}}\right)^2} \Bigg/ \overline{\left(\frac{W'}{\overline{W}}\right)^2} \equiv \overline{\left(\frac{\hat{K} - \overline{K}}{\overline{K}}\right)^2} \Bigg/ \overline{\left(\frac{K'}{\overline{K}}\right)^2}$$

Equation (3.50) is evaluated for different values of the ratio L/ℓ and the results are shown in figure 3-5. As the spacing L between hydraulic head measurements decreases with respect to the correlation length, ℓ, the observed resistivity (or conductivity) variance ratio becomes identical to the theoretical value. The departure of the observed variance from its theoretical value increases as the spacing increases.

Since the theoretical variance ratio depends primarily on the standard deviation of ln K, $\sigma_{\ln K}$, another way of presenting (3.50) would be to look at the effects of $\sigma_{\ln K}$ on the ratio L/ℓ. Such a presentation is given in figure 3-6 for two values of the percent error in conductivity. Note the required proportionality between spacing, L, of the hydraulic head observations and standard deviation, σ of ln K. Except for the first few points, the ratio L/ℓ for the 10% error level is approximately twice its corresponding value for the 20% error curve for all values of σ greater than 0.15.

One way of using the results of the one-dimensional analysis in light of the above discussion is related to determining core properties in the laboratory. An estimate of the length, L, of core material that would be required to measure the conductivity within a certain degree of accuracy can be made from results of the type shown in figure 3-6. Note, however, that as σ the standard deviation of the conductivity of the formation under consideration becomes larger, longer core lengths are required, making the determination of resistivity impractical or unfeasible to perform. Finally, it probably is worth mentioning that σ has a smaller effect on the spacing L of head measurements if larger errors in the conductivity (e.g. > 50%) are tolerable, whereas it is the controlling factor if smaller errors are sought.

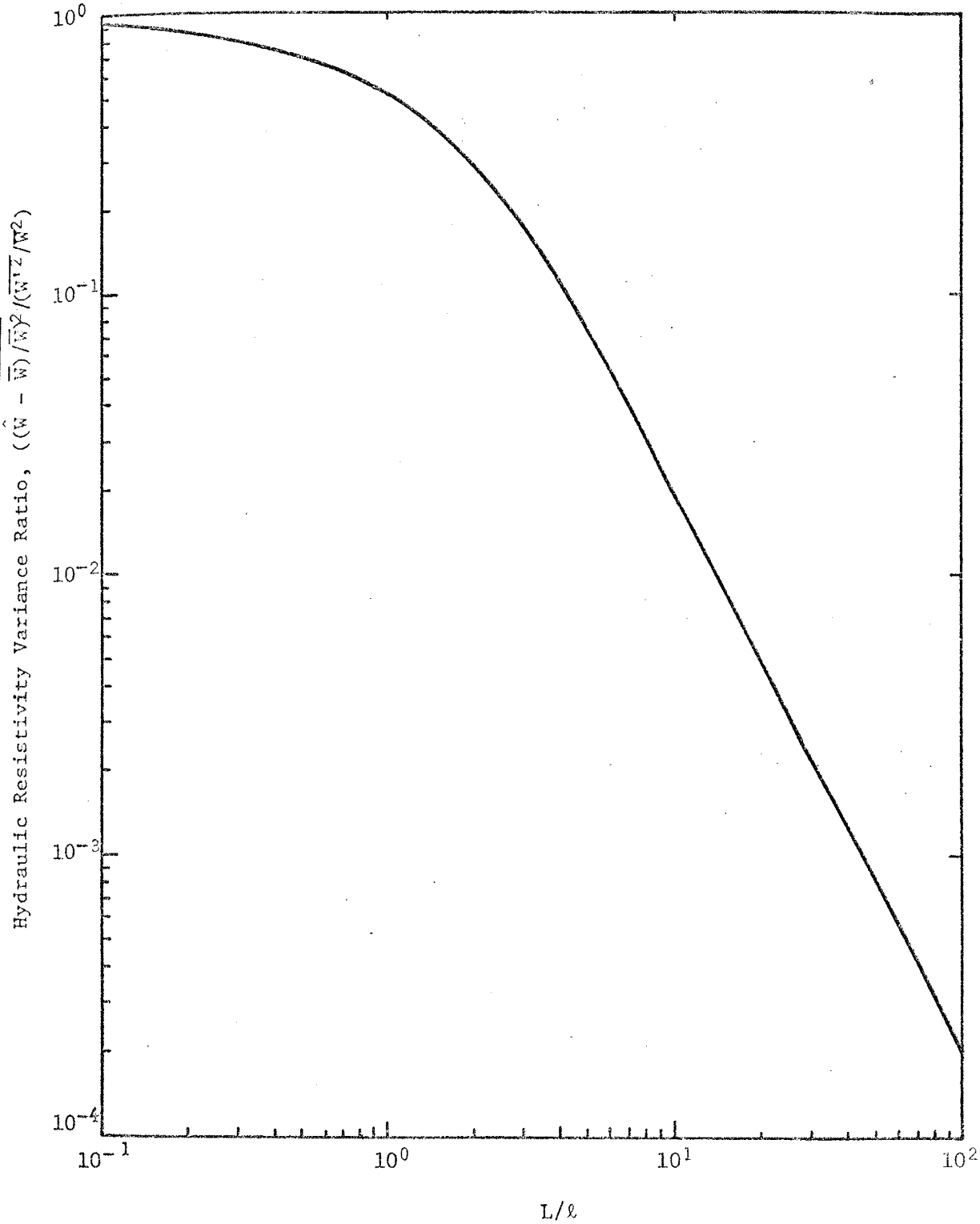

Fig. 3-5: Ratio of variance of estimated hydraulic resistivity to its theoretical value versus dimensionless spacing between head measurements.

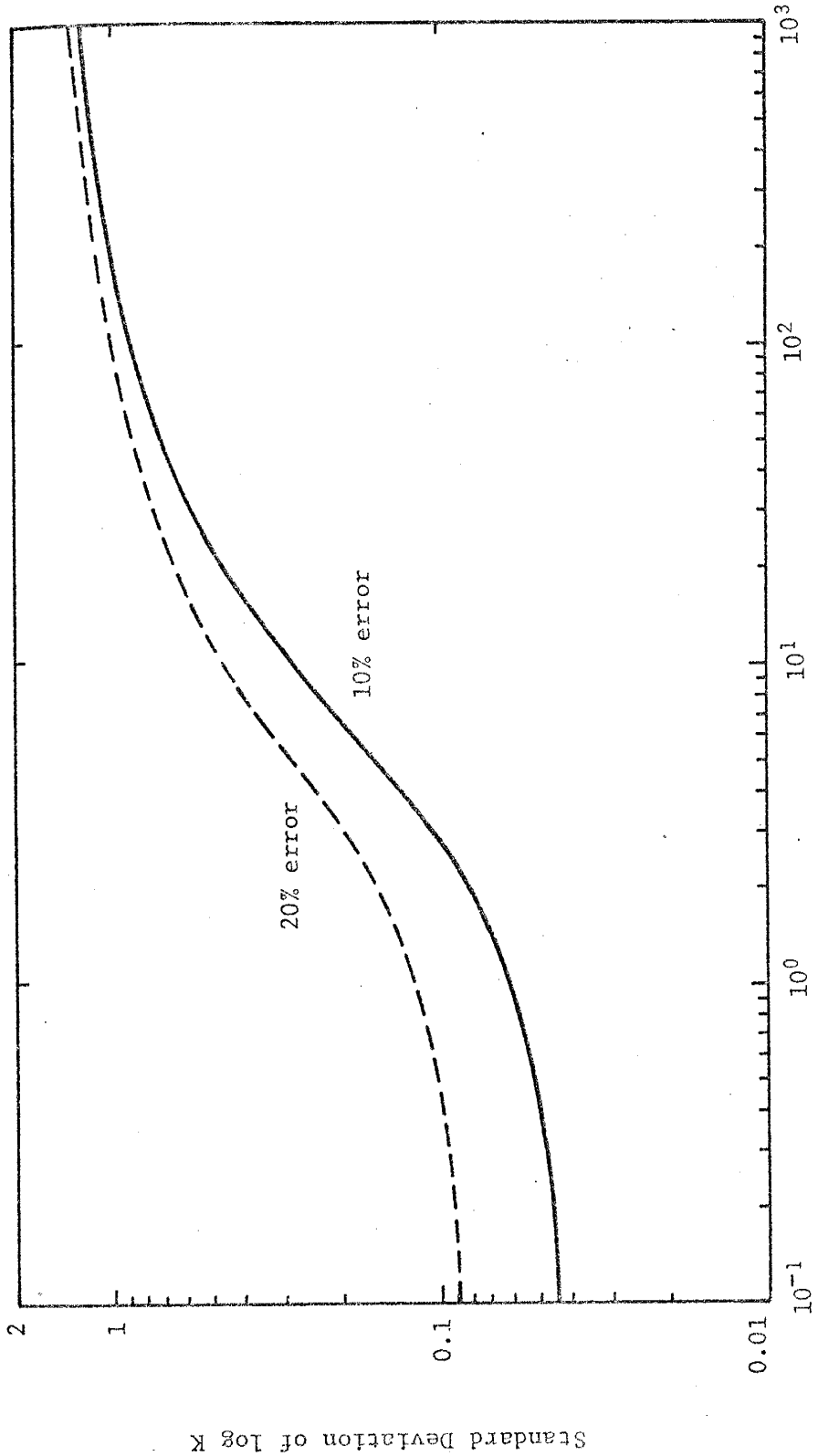

Fig. 3-6: Piezometer spacing in terms of the correlation length versus the standard deviation of log K.

3.4.2 Errors in Estimates of Flow across an Aquitard

Given the driving force (hydraulic head difference) between two points in an aquitard, shown in figure 3-7a, we seek expressions for statistical error estimates of the flow across the aquitard. The hydraulic resistivity is also known at some intermediate point. Both the resistivity and the hydraulic head are considered to have spatial variability characterized by their covariance functions (e.g. see (3.10) and (3.13), section 3.3.1).

An estimate of the specific discharge $\hat{q}$ between L_1 and L_2 is obtained from Darcy's relationship as

$$\hat{q} = K_3 \frac{\phi_1 - \phi_2}{L_1 - L_2} \tag{3.51}$$

where ϕ_1 is the potentiometric surface elevation in the phreatic aquifer, and ϕ_2 is the piezometric surface elevation in the confined aquifer. To obtain an expression for the average change of head $\bar{\phi}$ over some distance L, we write Darcy's equation in the form

$$q = K \frac{d\phi}{dx}$$

from which

$$\frac{q}{K} = Wq = \frac{d\phi}{dx}$$

where q is the true specific discharge and is a constant. Taking expected values on both sides of the above expression results in

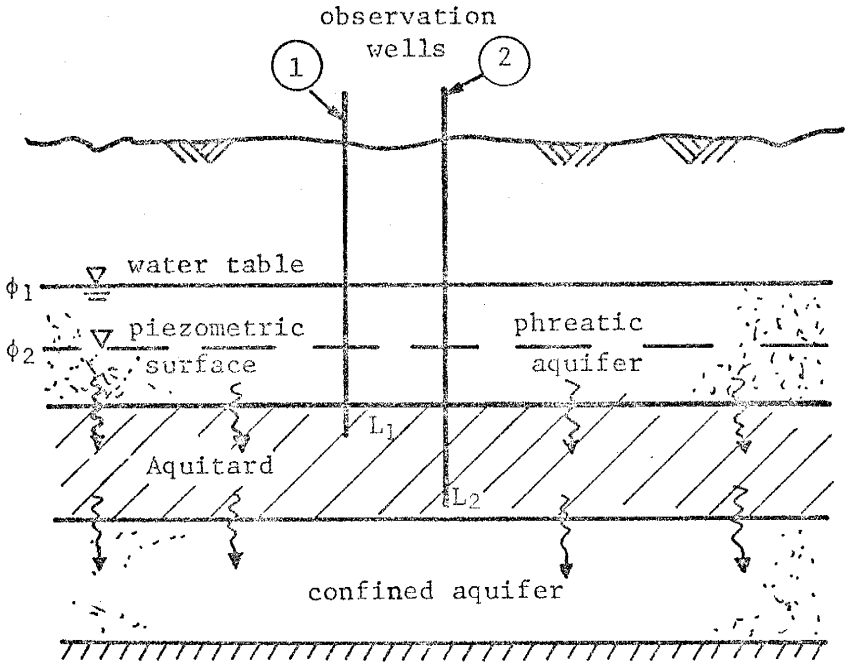

Fig. 3-7a: Diagramatic representation of the aquitard problem.

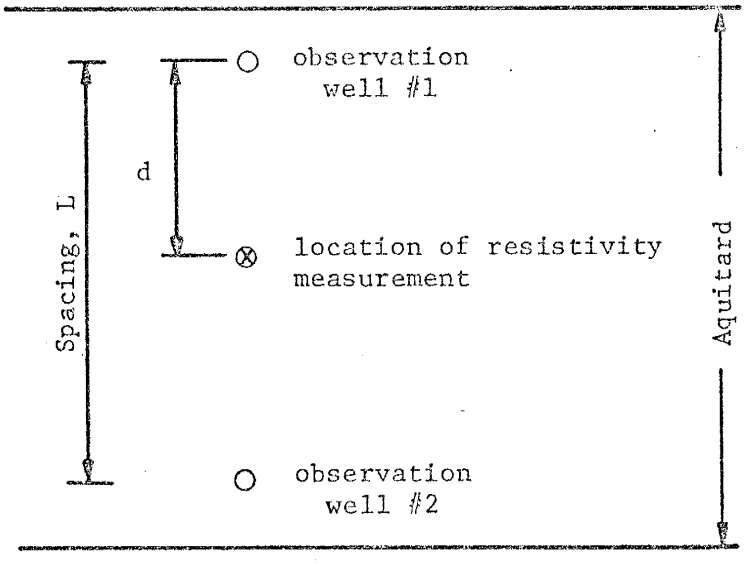

Fig. 3-7b: Details of the geometry of the discharge and resistivity measurements in the aquitard.

$$\overline{Wq} = \overline{\frac{d\phi}{dx}} = \frac{d}{dx}\,\overline{\phi}$$

or

$$\overline{q} = \frac{\overline{\phi}_1 - \overline{\phi}_2}{\overline{W}L} \tag{3.52}$$

We now write the following quantities in terms of a mean part and a fluctuation part about the mean:

$$W = \overline{W} + W'_3$$

$$\phi_1 = \overline{\phi}_1 + \phi'_1$$

$$\phi_2 = \overline{\phi}_2 + \phi'_2 \quad ;$$

W'_3 indicates the fluctuation part of resistivity measurement somewhere between the points L_1 and L_2. Substituting these quantities in (3.51) and replacing the difference $L_2 - L_1$ by L, we get

$$\hat{q} = \frac{1}{\overline{W} + W'_3}\left[\frac{(\overline{\phi}_1 + \phi'_1) - (\overline{\phi}_2 + \phi'_2)}{L}\right]$$

Subtracting $\overline{q}$ (given by (3.52)) from both sides of this equation yields

$$\hat{q} - \overline{q} = \frac{1}{\overline{W} + W'_3}\left[\frac{\overline{\phi}_1 - \overline{\phi}_2}{L} + \frac{\phi'_1 - \phi'_2}{L}\right] - \frac{\overline{\phi}_1 - \overline{\phi}_2}{\overline{W}L}$$

which can be rewritten as

$$\hat{q} - \overline{q} = \frac{\overline{\phi}_1 - \overline{\phi}_2}{\overline{W}L}\left[\frac{1}{1 + (W'_3/\overline{W})} - 1\right] + \frac{\phi'_1 - \phi'_2}{L(\overline{W} + W'_3)}$$

Rearranging of this equation results in

$$\hat{\bar{q}} - \bar{q} = - \left[\frac{(W'_3/\bar{W})}{1 + (W'_3/\bar{W})} \right] \bar{q} + \frac{(\phi'_1 - \phi'_2)\bar{q}}{\Delta\bar{\phi}(1 + W'_3/\bar{W})}$$

Dividing both sides by $\bar{q}$ gives

$$e \equiv \frac{\hat{\bar{q}} - \bar{q}}{\bar{q}} \cong - \frac{W'_3}{\bar{W}} \left(1 - \frac{W'_3}{\bar{W}} \right) + \frac{\phi'_1 - \phi'_2}{\Delta\bar{\phi}} \left(1 - \frac{W'_3}{\bar{W}} \right) \tag{3.53}$$

where only the second order term in fluctuations has been retained. Taking the expected value of both sides of the above expression and noting that the average of primed quantities is zero, we obtain

$$\bar{e} \equiv \overline{\left(\frac{\hat{\bar{q}} - \bar{q}}{\bar{q}} \right)} = \overline{\left(\frac{W'_3}{\bar{W}} \right)^2} - \overline{\left(\frac{\phi'_1 W'_3}{\bar{W}\Delta\bar{\Phi}} \right)} + \overline{\left(\frac{\phi'_2 W'_3}{\bar{W}\Delta\bar{\Phi}} \right)} \tag{3.54}$$

The fluctuation part e' of the discharge estimate is defined as

$$e' = e - \bar{e}$$

Hence, by subtracting (3.54) from (3.53) and reducing, we arrive at the following expression for e' (after neglecting higher order terms):

$$e' = \frac{\phi'_1}{\Delta\bar{\phi}} - \frac{\phi'_2}{\Delta\bar{\phi}} - \frac{W'_3}{\bar{W}} \tag{3.55}$$

The variance $\overline{e'^2}$ of the fluctuations e' of the discharge errors is found by squaring (3.55)

$$\overline{e'^2} = \overline{\left(\frac{W'_3}{\bar{W}} \right)^2} + 2\overline{\left(\frac{\phi'}{\Delta\bar{\phi}} \right)^2} - 2\frac{\overline{W'_3\phi'_1}}{\bar{W}\Delta\bar{\Phi}} + 2\frac{\overline{W'_3\phi'_2}}{\bar{W}\Delta\bar{\Phi}} - 2\frac{\overline{\phi'_1\phi'_2}}{(\Delta\bar{\Phi})^2} \tag{3.56}$$

in which $\overline{\phi_1'^2} = \overline{\phi_2'^2}$ is used.

In order to evaluate the cross-covariance terms appearing in (3.56), recall that (3.8) from the exact solution is given by

$$dZ_\phi = -\frac{q}{ik}\, dZ_w \tag{3.8}$$

Working with the complex conjugate of (3.8) and multiplying both sides by dZ_w and then taking expected values, we find

$$E[dZ_w\, dZ_\phi^*] = \frac{q}{ik}\, E[dZ_w\, dZ_w^*] \quad ,$$

which leads to the following expression relating the cross-spectrum $\Phi_{w\phi}$ between resistivity and head fluctuations to the spectrum Φ_{ww} of the resistivity:

$$\Phi_{w\phi}(k) = \frac{q}{ik}\, \Phi_{ww}(k) \tag{3.57}$$

Replacing Φ_{ww} by its value from (3.11) produces the following expression for the cross spectrum $\Phi_{w\phi}$:

$$\Phi_{w\phi}(k) = \frac{aqk\overline{W'^2}}{i\pi(a^2 + k^2)^2} \tag{3.58}$$

The cross-covariance between W and ϕ is defined as

$$R_{w\phi}(\xi) = E[W(x + \xi)\, \phi(x)] = \int_{-\infty}^{\infty} e^{ik\xi}\, \Phi_{w\phi}(k)\, dk$$

We can express the exponential function in terms of trigonometric

functions in the above integral as

$$R_{w\phi}(\xi) = \int_{-\infty}^{\infty} (\cos k\xi + i \sin k\xi) \frac{2aqk\overline{W'^2}}{i\pi(a^2 + k^2)^2} \, dk$$

But, since the integral of an odd function over a symmetric interval is equal to zero, the expression for $R_{w\phi}$ reduces to

$$R_{w\phi}(\xi) = \frac{2aq\overline{W'^2}}{\pi} \int_{-\infty}^{\infty} \frac{k \sin k\xi}{(a^2 + k^2)^2} \, dk$$

In order to evaluate this integral (which is a Fourier sine transform type integral) we write it in the form

$$\int_{-\infty}^{\infty} \frac{k \sin k\xi}{(a^2 + k^2)^2} \, dk = 2 \int_{0}^{\infty} \frac{k \sin k\xi}{(a^2 + k^2)^2} \, dk$$

since the integrand is an even function of k. Hence,

$$\int_{-\infty}^{\infty} \frac{k \sin k\xi}{(a^2 + k^2)^2} \, dk = \begin{cases} \frac{\pi\xi}{2a} e^{-a\xi} & \text{for } \xi > 0 \\ \frac{\pi\xi}{2a} e^{a\xi} & \text{for } \xi < 0 \end{cases}$$

Consequently, the cross-covariance $R_{w\phi}$ becomes

$$R_{w\phi}(\xi) = \begin{cases} q\xi\overline{W_3'^2} \, e^{-a\xi} & , \quad \xi > 0 \\ q\xi\overline{W_3'^2} \, e^{a\xi} & , \quad \xi \leq 0 \end{cases}$$

Also, note that

$$\overline{W'_3\phi'_1} = R_{w\phi}(\xi) = R_{w\phi}(d) \quad , \quad d > 0 \qquad (3.59)$$

and

$$\overline{W'_3\phi'_2} \equiv \overline{\phi'_2 W'_3} = R_{\phi w}(L - d) = R_{w\phi}(d - L) \quad , \quad d - L \leq 0 \quad (3.60)$$

We are now in a position to evaluate the different discharge error estimates represented by (3.54) and (3.56). Substituting (3.59) and (3.60) into (3.54) and making use of (3.52), the mean or average error $\bar{e}$ in specific discharge is found to be

$$\frac{\bar{e}}{(W'_3/\bar{W})^2} = \left[1 - \frac{d}{L} e^{-ad} + \frac{(d - L)}{L} e^{a(d-L)} \right] \quad (3.61)$$

Equation (3.61) shows that our average discharge estimate is determined by two parameters, namely d/L and aL. Similarly, upon substituting (3.59) and (3.60) into (3.56) and manipulating (see Appendix-B for the details), the variance $\overline{e'^2}$ of discharge fluctuations becomes

$$\frac{\overline{e'^2}}{(W'_3/\bar{W})^2} = \left\{ 1 + \frac{2}{(aL)^2} [1 - (1 + aL) e^{-aL}] + 2\left(\frac{d}{L} - 1\right) e^{a(d-L)} - 2 \frac{d}{L} e^{-ad} \right\} \quad (3.62)$$

Both (3.61) and (3.62) were normalized by the variance ratio of the resistivity fluctuation. A mean square error (MSE) in discharge was also obtained by adding the square of (3.61) to (3.62). To examine the applicability and significance of the above results, several graphs were constructed for the various error expressions against aL and d/L, where a is a correlation parameter characteristic of the porous medium and d and L are as defined in figure 3-7 b.

Figures 3-8 through 3-10, in which the errors in discharge are plotted against d/L for different values of aL, all show a minimum in the error estimate at d/L = 0.5, i.e. when the hydraulic conductivity is measured at the midpoint between the two observation wells. Maximum errors occur at d/L values of zero and 1, indicating that the conductivity was measured at the location of either of the two observation wells. Note that the various errors are directly proportional to aL; minimum error occurs at smaller spacing between observations. When the discharge errors are plotted versus aL for different values of d/L we observe the following (see figures 3-11 through 3-13): first, the errors start at a minimum for small aL values and increase with increasing aL until they asymptotically reach a maximum at aL values from 10 to 15 (larger values correspond to larger d/L). Secondly, for d/L = 0.5, the errors are approximately 30 to 50% less than those for d/L equal to zero.

In summary, the stochastic analysis of the aquitard problem shows two points. First, the minimum error in discharge occurs if the hydraulic resistivity is measured at the midpoint between the two observation wells, and the errors increase as the point of measurement of the resistivity is moved closer to either one of the two piezometers. Secondly, the errors in discharge decrease as the vertical spacing between the two piezometers decreases.

3.5 Summary and Limitations of the One-Dimensional Approach

3.5.1 Summary

A number of points arrived at in the course of the analysis of one-dimensional steady groundwater flow problem are summarized below.

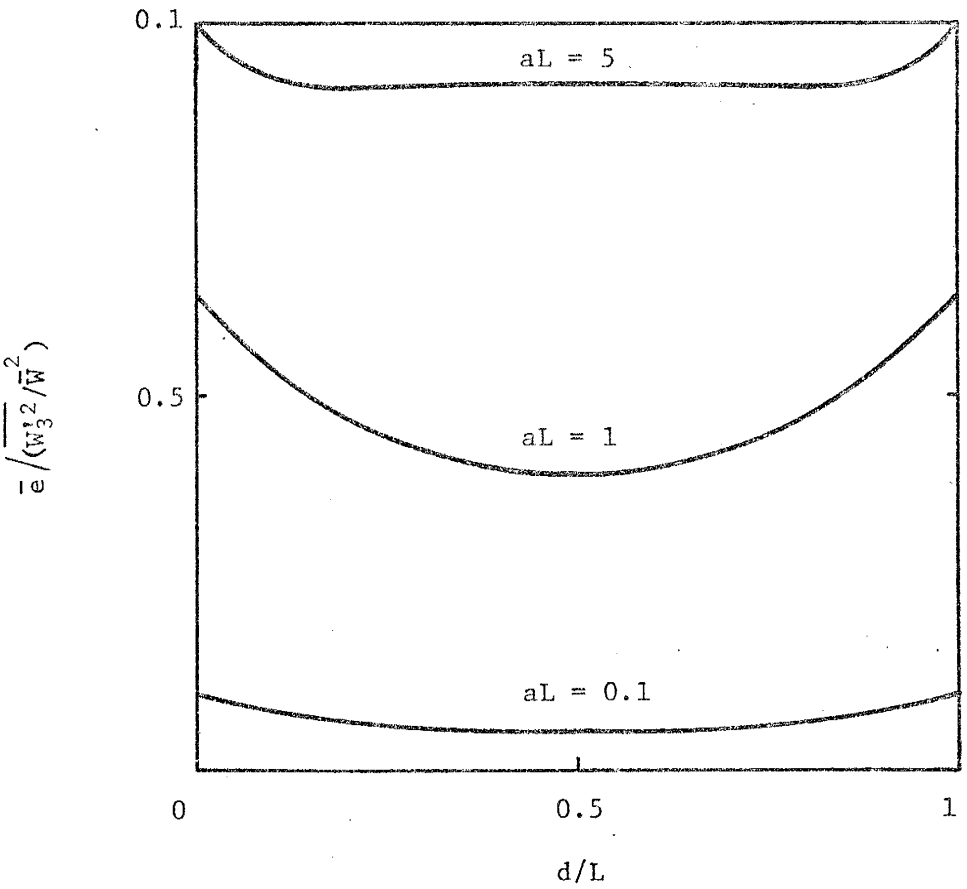

Fig. 3-8: Normalized mean specific discharge errors, $\bar{e}$, versus the ratio d/L for different values of aL (see text for definition of symbols).

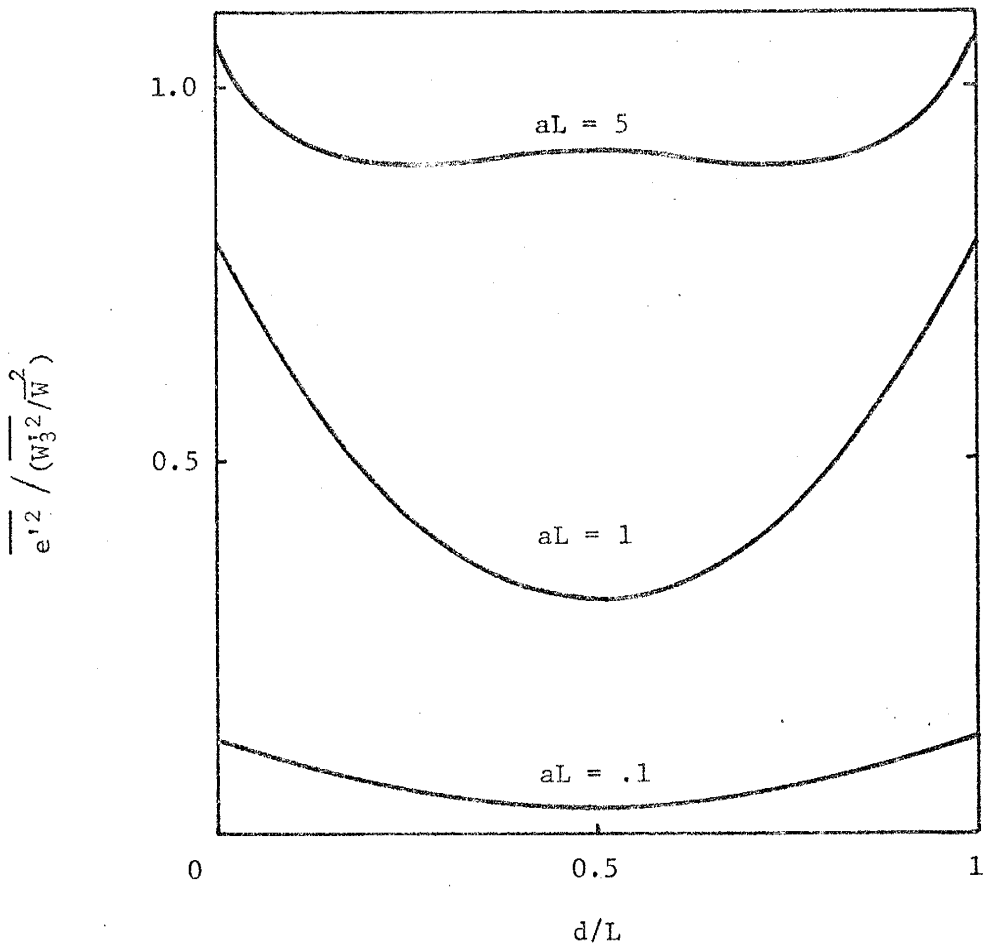

Fig. 3-9: Normalized variance of specific discharge estimates versus d/L for different values of aL (see text for definition of symbols).

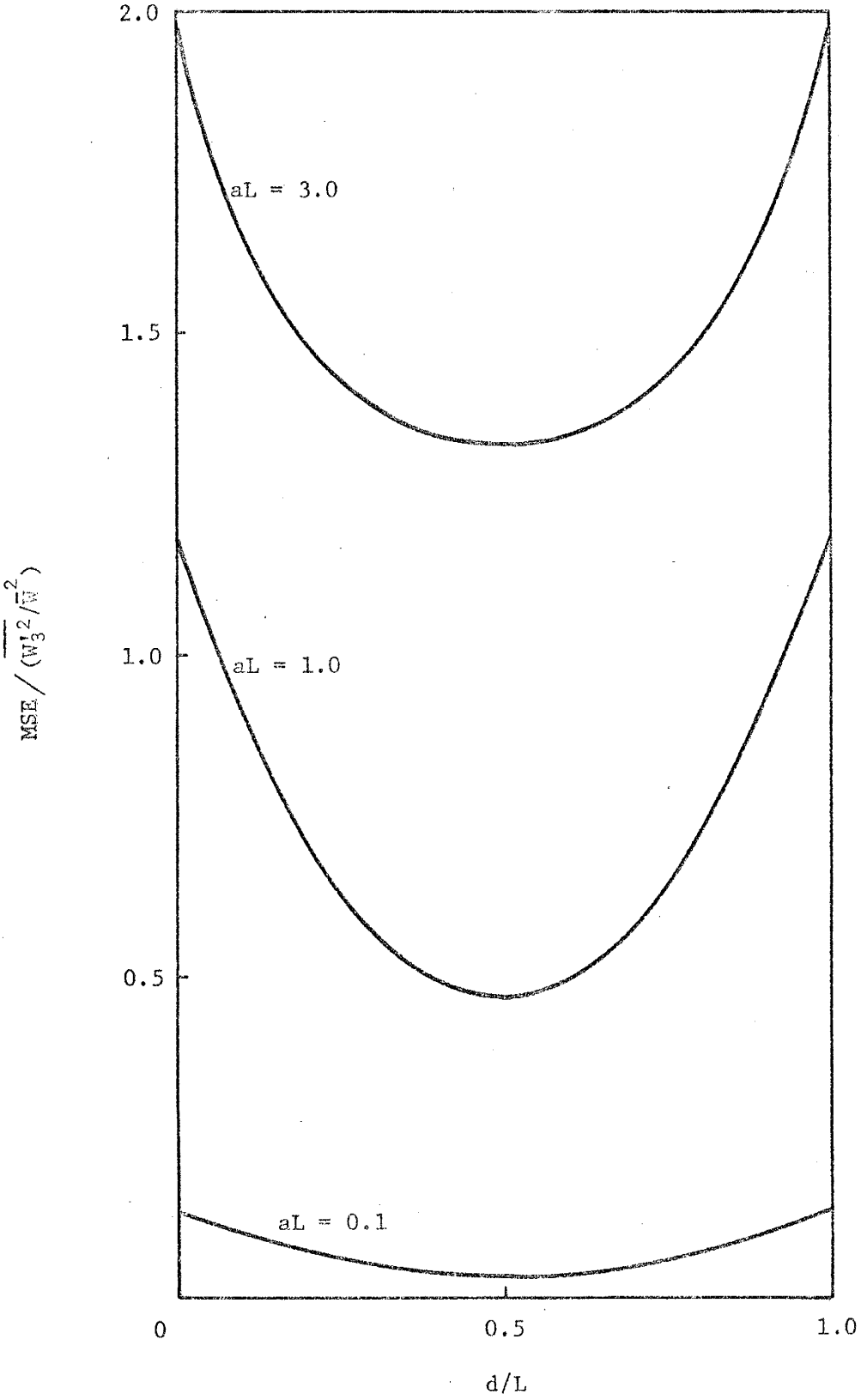

Fig. 3-10: Normalized mean square error (MSE) in specific discharge versus d/L for different values of aL (see text for definition of symbols).

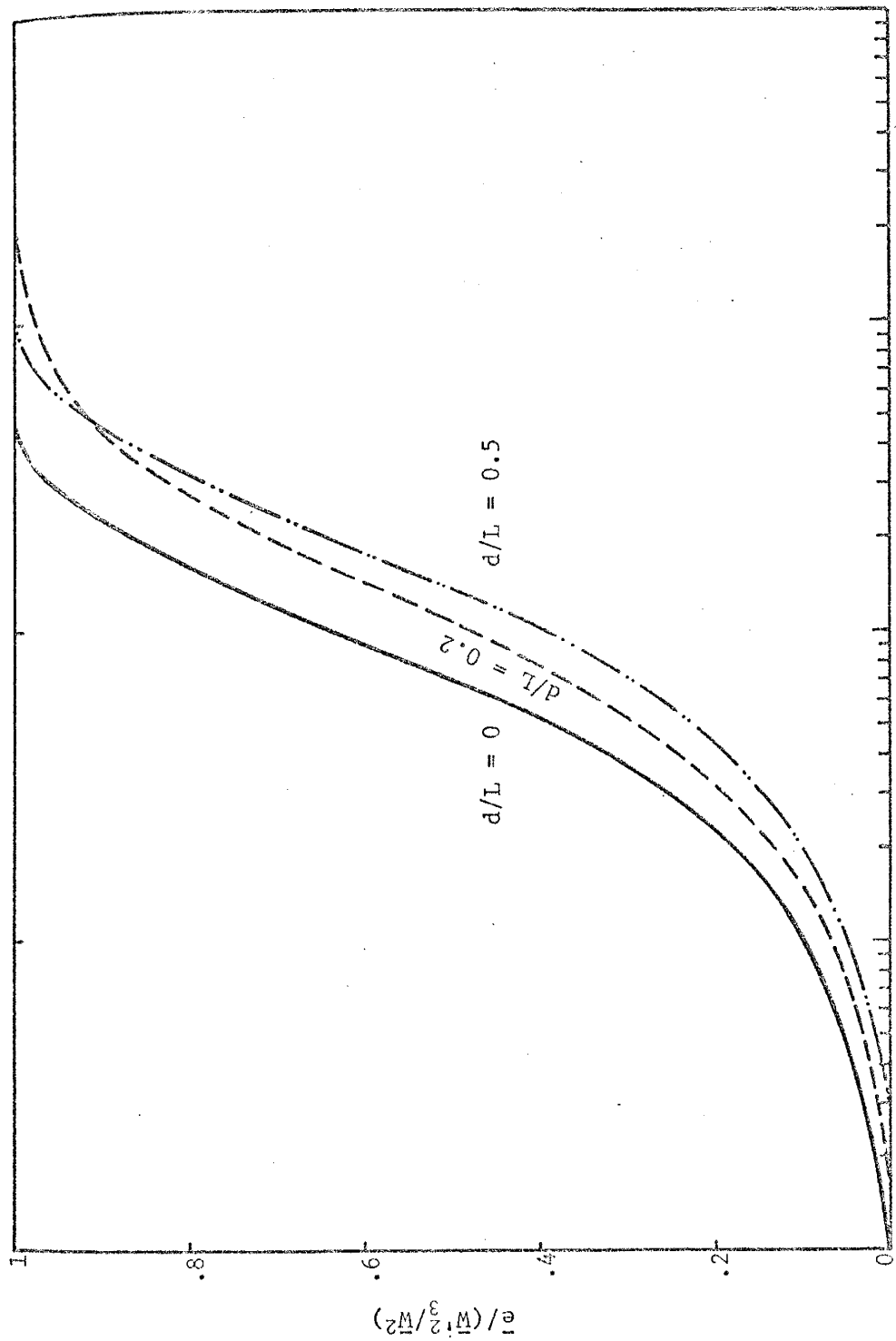

Fig. 3-11: A semi-logarithmic plot of the normalized mean error in specific discharge versus aL for different values of d/L.

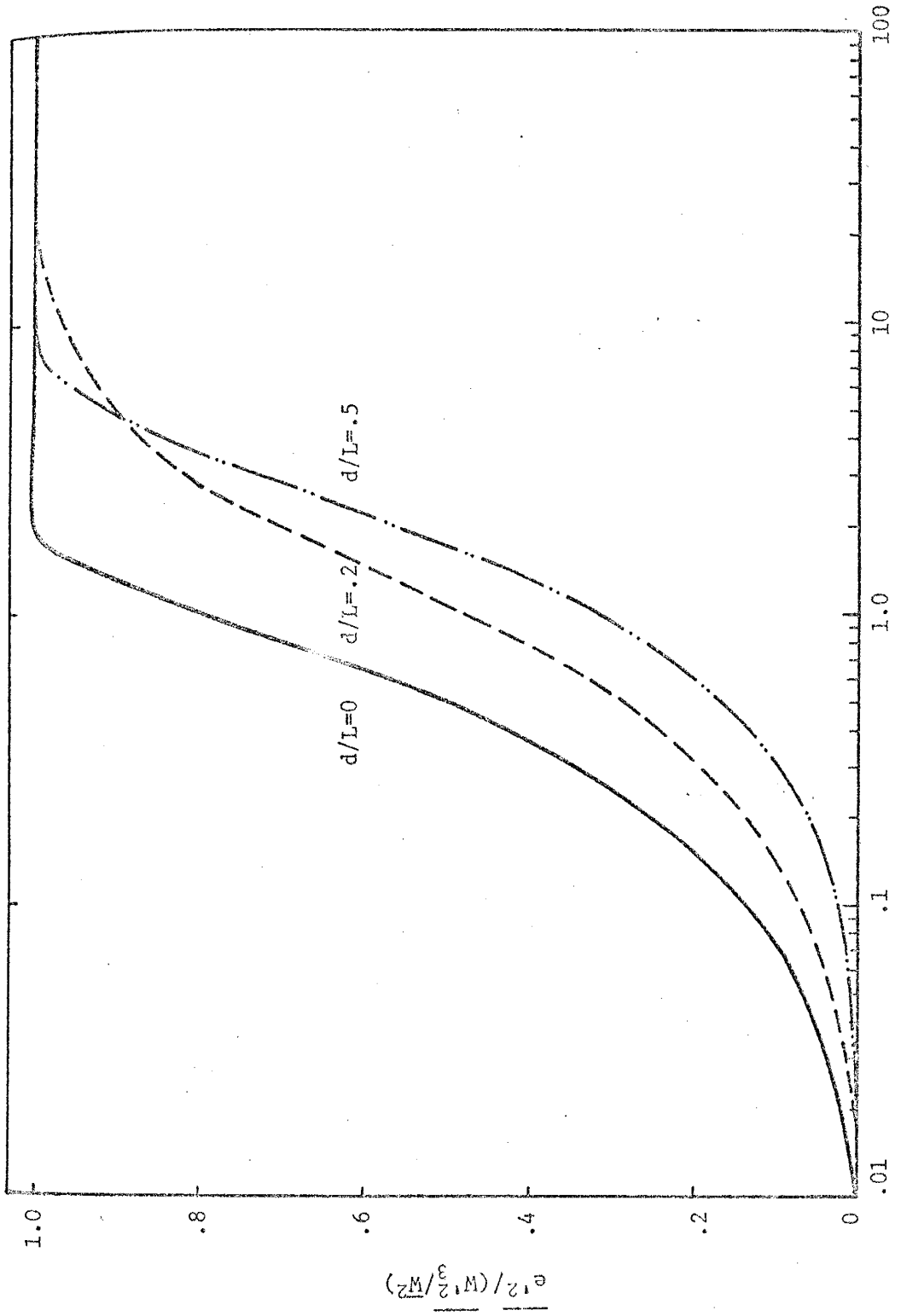

Fig. 3-12: Normalized variance of specific discharge versus aL on logarithmic scale for different values of d/L.

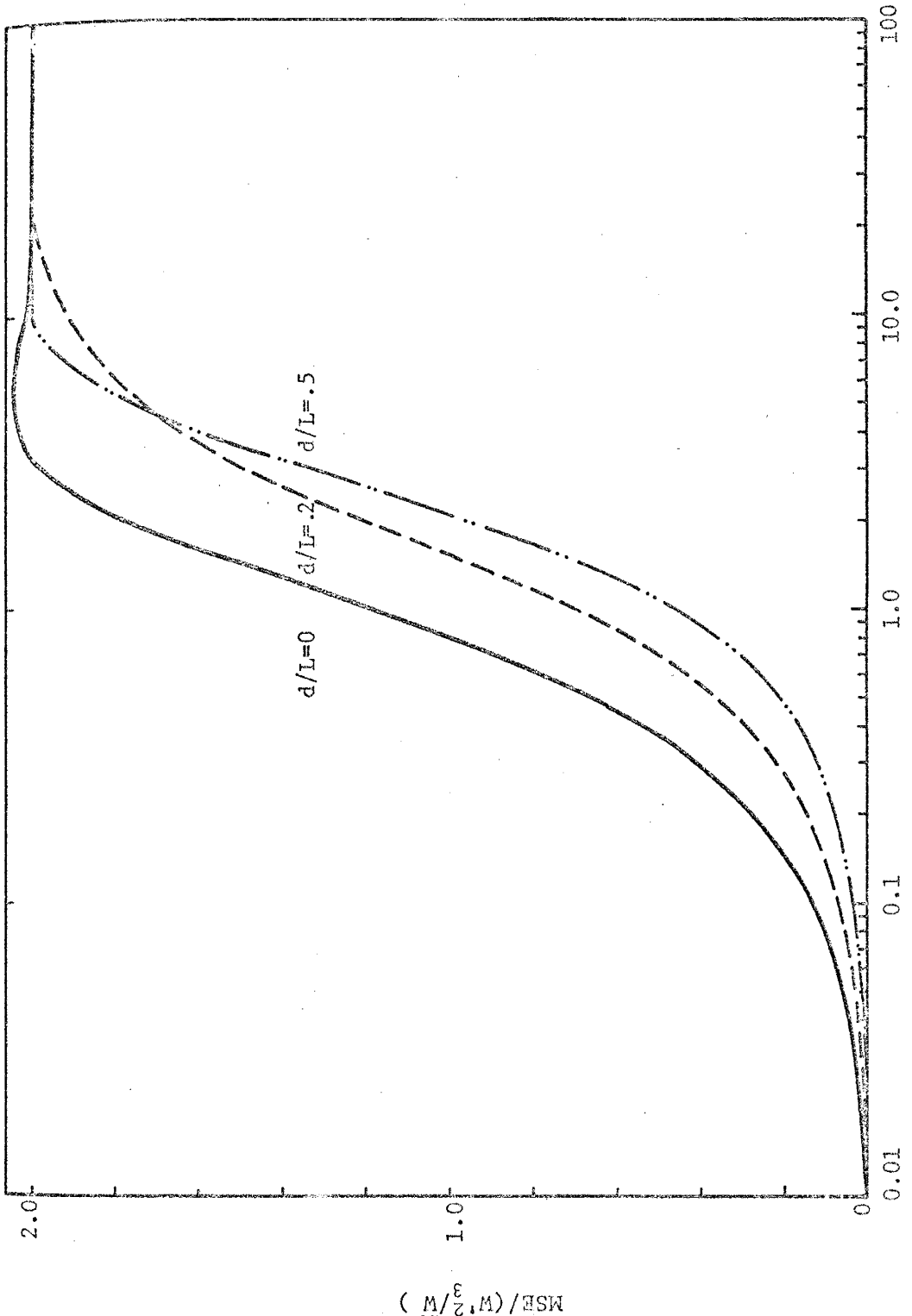

Fig. 3-13: A semi-logarithmic plot of the normalized mean square error (MSE) in specific discharge versus aL for different values of d/L.

1. The one-dimensional flow is a two parameter problem, namely, the standard deviation of ln K and the correlation length, ℓ, of the medium.

2. The exact analysis in terms of W(x) is valid for any value of W' since we can express any function in terms of its mean and a fluctuation about the mean with no limitation on the size or amplitude of the W' fluctuations.

3. In estimating flow quantities in one dimension using Darcy's law one would have to work with the hydraulic resistivity W, and not the conductivity K. That is because the hydraulic conductivity varies drastically even in a supposedly homogeneous medium. This is also due to the fact that the amount of fluid flow in one dimension is governed mainly by the resistance to the flow characterized by W.

4. The analysis of the permeameter example proved useful in establishing the spacing between two hydraulic head measurements required to estimate the hydraulic resistivity with a given degree of accuracy.

5. The results of the permeameter example may be of use in estimating the length of core material that would be required to measure the conductivity with a certain degree of accuracy.

6. The aquitard problem led to two conclusions. First, the minimum error in specific discharge across an aquitard occurs if the hydraulic resistivity is measured midway between the two hydraulic head measurements; the error increases as the point of measurement of the resistivity is placed closer to either one of the two observation wells. Secondly, the errors in discharge decrease as the vertical spacing between the two piezometers decreases.

7. It is interesting to note the contrast between results of the permeameter problem to those from the aquitard example. The minimum

error in a hydraulic resistivity measurement occurs at large spacing between the hydraulic head measurements in the permeameter case, whereas in the aquitard example the minimum error in specific discharge measurements occur at small vertical spacing between the hydraulic head measurements.

8. The analysis developed in this chapter serves as a pilot example before addressing the three-dimensional problem since it demonstrated, for instance, a possible form for theoretical autocovariance functions to be used in characterizing spatial variation in conductivity. It also showed the benefits derived from using the perturbation approach in terms of ln K compared with the exact analysis in terms of W since an exact solution in three dimensions would be intractable.

3.5.2 Limitations of One-Dimensional Analysis

The validity of results obtained from the analyses of flow in one dimension should now be put in their proper perspective. It is more likely that the variance of hydraulic head fluctuations might be smaller if the analyses were carried out in a multidimensional system. The one-dimensional flow is illusive and unrealistic in the sense that it is a simplified description of a truly two- or three-dimensional phenomenon. Water flowing through a two-dimensional system moves along paths offering the least resistance to the flow. This would not be feasible in a one-dimensional system and hence the increased variance in head results. Therefore, it is of importance to study the flow with more realistic three-dimensional spatial variations of the hydrologic parameters to examine the extent of their influence on flow properties such as fluctuations in predicted hydraulic head. This analysis will be performed in the following chapter.

In the approximate solutions to the problem of groundwater flow in one dimension developed in section 3.3, it was assumed that the autocovariance functions of hydraulic conductivity, K, and of log K are identical. However, it should be emphasized that this will not be exactly the case. This approximation may affect results, e.g. variance of predicted hydraulic head, obtained from the linearized solutions in relation to those of the exact case. Consequently, the above assumption deserves careful examination in future research.

CHAPTER 4

STOCHASTIC ANALYSIS IN THREE DIMENSIONS

4.1 Introduction

As mentioned in the previous chapter, the implicit limitations of one-dimensional analysis of flow problems indicate the need to consider flow in a more realistic multidimensional sense. In this chapter, three-dimensional spatial variations in hydraulic conductivity are introduced and their effects on hydraulic head variations are examined. A negative exponential function is assumed to characterize correlation in conductivity of neighboring points in the medium. It was reasoned that, because of the nature of inhomogeneity of porous materials, correlation between values of a property would decrease as the spacing (or lag) between successive points increased.

The analysis to be developed here is somewhat related to earlier work by Buyevich et al. (1969), though major differences exist. Buyevich et al. (1969) investigated the problem of variations in filtration velocity induced by spatial variations in local porosity of the medium. Rather than dealing directly with spatial variations in hydraulic conductivity (the main property influencing flow), they incorporated permeability variations indirectly in terms of porosity variations. In their study, a Gaussian function was the form assumed for the correlation function of porosity fluctuations. In the stochastic approach developed here, however, a negative exponential is used to describe the autocovariance of conductivity fluctuations. It will be shown later that the negative exponential function provides a suitable fit of field data for porosity and permeability. This form has also

been used by several other authors (e.g. Agterberg, 1974; Gelhar et al., 1974; Rodriguez-Iturbe and Mejia, 1974).

In solving the three-dimensional flow problem we linearize the flow equation in terms of the natural logarithm of the hydraulic conductivity rather than in terms of porosity, the approach of Buyevich et al. (1969). Based on the large magnitude of conductivity variations in subsurface materials, it is frequently appropriate to work with ln K since the logarithm of a quantity is less variable than the quantity itself. It is implicit in the subsequent analysis that fluctuations in ln K are small compared to their mean. Thus linearizing in terms of ln K instead of K itself implies a less severe limitation when using the method of small perturbations.

4.2 Form of the Perturbed Flow Equation and Assumptions Necessary for Its Solution

Consider the case where the main flow component is in a particular direction (e.g. the horizontal x-axis) with perturbations to both flow and hydraulic conductivity in three dimensions. In the subsequent analysis we assume the medium to be isotropic on the local scale (i.e. on the scale of cores). This is a reasonable assumption since the geologic literature (e.g. Pettijohn et al., 1972, p. 529) indicates that local anisotropy of the medium with respect to permeability is generally small; the ratio of maximum to minimum permeability within single core samples does not exceed 4 in most sediments. The form of Darcy's equation in three dimensions is

$$\vec{q} = -K\nabla\phi \tag{4.1}$$

where $\vec{q}$ is the specific discharge vector and ∇ is the differential operator defined by

$$\nabla = \vec{i}\,\frac{\partial}{\partial x} + \vec{j}\,\frac{\partial}{\partial y} + \vec{k}\,\frac{\partial}{\partial z}$$

The equation stating conservation of mass for three-dimensional, steady state, saturated flow of a constant density fluid through a heterogeneous porous medium is

$$\nabla \cdot \vec{q} = 0 \tag{4.2}$$

Substituting (4.1) in (4.2) and carrying the indicated operation results in

$$\nabla^2\phi + \frac{\nabla K}{K} \cdot \nabla\phi = 0 \tag{4.3}$$

Since

$$\frac{\nabla K}{K} = \nabla \ln K \quad ,$$

(4.3) becomes

$$\nabla^2\phi + \nabla \ln K \cdot \nabla\phi = 0 \tag{4.4}$$

The hydraulic head ϕ is defined in terms of a mean and a three-dimensional fluctuation as

$$\phi = -J_o x + \phi'(x, y, z) \tag{4.5}$$

where J_o is the mean hydraulic gradient. Using (4.5), the form of (4.4) becomes

$$\nabla^2\phi' + \nabla \ln K \cdot \nabla [-J_o x + \phi'(x, y, z)] = 0 \tag{4.6}$$

and assuming that

$$\frac{\partial\phi'}{\partial x} << \frac{d}{dx}(-J_o x) \quad ,$$

(4.6) reduces to

$$\nabla^2\phi' - J_o \frac{d}{dx}(\ln K) = 0 \tag{4.7}$$

This is the governing equation for output fluctuations in hydraulic head in terms of variations in input ln K, where both fluctuations in head and in ln K are thought of as spatial random variables or stochastic processes. Spectral analysis techniques will be utilized to obtain a solution of (4.7), assuming the hydraulic conductivity field to be statistically isotropic. Before proceeding with the details of the solution, however, it is appropriate to briefly discuss the assumption of statistical isotropy of the medium, and its implications.

Statistical isotropy of the medium is a useful assumption often made to simplify analysis of problems in several dimensions. A statistically isotropic medium with regard to some property is one in which the value of that property does not depend on the direction in

which it is measured. Therefore, the covariance function R (ξ) of the hydraulic conductivity for example that is statistically isotropic can be a function only of the length of the separation vector $\vec{\xi}$, since the length is the only property characterizing $\vec{\xi}$ which does not change under a rotation of the coordinate system (Lumley and Panofsky, 1964, p. 25). Hence, the autocovariance function of the conductivity, in this example, is spherically symmetric, i.e. all one-dimensional autocovariance functions are the same (Lumley, 1970, p. 100). The symmetry thus introduced into the problem results in, as will be seen in the next section, considerable simplifications especially in evaluating certain integrals arising in the analysis.

Another assumption that is made in order to solve (4.7) is that of the statistical homogeneity of the medium. A statistically homogeneous medium with regard to some property is one in which the statistical properties (e.g. the mean, the variance and the covariance) characterizing that property do not depend on the location at which it is measured. This assumption is made to simplify the analysis.

We now examine the implications and limitations of the two assumptions made above, namely, that of the statistical homogeneity and the statistical isotropy of the medium. Consider an identifiable unit or geologic formation consisting of sands, for example, that were deposited under more or less the same physical conditions. If we examine a geophysical well log recorded over the total thickness of such a unit, we would expect fluctuations in the property recorded to reflect similar patterns of variation. A more precise way of expressing the above statement is feasible through defining an autocovariance function R(ξ) describing correlation among neighboring values of some property in the

formation as

$$R(\xi) = E[f(x + \xi)\, f(x)]$$

where f could represent the hydraulic conductivity for instance. The geologic unit would be statistically homogeneous if values of $R(\xi)$ of some property depend on the distance ξ and not on the location in the unit. Though it is recognized that such a unit is heterogeneous in the deterministic sense, it is convenient to assume it to be statistically homogeneous. A different situation arises when statistical isotropy is examined. Geologic formations commonly exhibit some form of layering or stratification. If the autocovariance function defined above is estimated for some distance ξ in the direction parallel to bedding and the estimates are repeated at a large number of points in the formation, then we would find that the average of such horizontal determinations is different from that obtained by repeating the same process at the same distance in the vertical direction perpendicular to bedding. This behavior is caused mainly by the presence of these layers. Due to the nature of geologic deposits it is expected that statistical anisotropy is the rule rather than the exception. However, since this work represents an initial step in the stochastic study of the effects of spatial variations of medium properties on groundwater flow, it was deemed necessary to assume statistical isotropy of the medium for the purpose of isolating the stochastic effects in the clearest possible way.

4.3 Development of Solution to the Three-Dimensional Flow Problem

Spectral analysis techniques are used in this section to develop a solution to (4.7). Since the problem considered is a more realistic and general representation of flow in porous media, the results to be derived are expected to help in critically examining the one-dimensional analysis of Chapter 3.

Assuming statistical homogeneity of the fluctuations, we use the stochastic Fourier-Stieltjes integrals to express the fluctuations in three dimensions as follows:

$$\left.\begin{aligned} \phi'(x, y, z) &= \int_{-\infty}^{\infty} e^{i\vec{k}\cdot\vec{x}}\, dZ_{\phi}(\vec{k}) \\ \ln K \equiv f(x, y, z) &= \int_{-\infty}^{\infty} e^{i\vec{k}\cdot\vec{x}}\, dZ_{f}(\vec{k}) \end{aligned}\right] \qquad (4.8)$$

Substituting (4.8) in (4.7) and manipulating we obtain

$$\int_{-\infty}^{\infty} \left[\left(-k_x^2 - k_y^2 - k_z^2\right)\, dZ_{\phi}(\vec{k}) - iJ_o k_x dZ_f(\vec{k})\right] e^{i\vec{k}\cdot\vec{x}} = 0$$

This equation holds only if the quantity in brackets is identically equal to zero, i.e.

$$\left(-k_x^2 - k_y^2 - k_z^2\right)\, dZ_{\phi}(\vec{k}) - iJ_o k_x dZ_f(\vec{k}) = 0$$

from which we obtain the following expression relating the complex Fourier amplitudes of head and ln K fluctuations respectively:

$$dZ_\phi(\vec{k}) = -\frac{iJ_o k_x}{\left(k_x^2 + k_y^2 + k_z^2\right)} dZ_f(\vec{k}) \tag{4.9}$$

The spectrum $\Phi_{\phi\phi}$ of head fluctuations in terms of that of conductivity fluctuations is obtained by multiplying each side of (4.9) by its complex conjugate and taking expected values,

$$\Phi_{\phi\phi}(\vec{k}) = \frac{J_o^2 k_x^2}{k^4} \Phi_{ff}(\vec{k}) \tag{4.10}$$

in which $k = \left(k_x^2 + k_y^2 + k_z^2\right)^{\frac{1}{2}}$ represents the magnitude of the wave number vector $\vec{k}$.

In order to evaluate (4.10) explicitly the spectrum $\Phi_{ff}(k)$ must be specified. For this analysis we will assume a simple exponential form for the autocovariance function of ln K (see for example Agterberg, 1974, p. 341; Gelhar et al., 1974, p. 78), namely

$$R_{ff}(\vec{\xi}) = \overline{f'^2}\, e^{-\gamma|\vec{\xi}|} \tag{4.11}$$

in which $\overline{f'^2}$ is the variance of ln K, $\vec{\xi}$ is the separation or lag vector, and γ is a correlation parameter characterizing the porous medium. The inverse of this parameter is the integral scale

$$\lambda = \int_o^\infty \left(\frac{R_{ff}(\vec{\xi})}{\overline{f'^2}}\right) d\xi \tag{4.12}$$

The integral scale indicates the average distance over which the conductivity is correlated.

We can now proceed to evaluate the spectrum Φ_{ff} of fluctuations in ln K by taking the inverse Fourier transform of (4.11)

$$\Phi_{ff}(\vec{k}) = \frac{1}{(2\pi)^3} \iiint_{-\infty}^{\infty} e^{-i\vec{k}\cdot\vec{\xi}} R_{ff}(\vec{\xi})\, d\vec{\xi} \tag{4.13}$$

Taking advantage of the symmetry obtained in the problem after introducing the assumption of statistical isotropy we change from a rectangular to a spherical coordinate system. The scalar product of the vectors $\vec{k}$ and $\vec{\xi}$ (see Fig. 4-1a) is given by

$$\vec{k}\cdot\vec{\xi} = k\xi \cos\theta$$

The rectangular elemental volume $d\vec{\xi}$ can be written in spherical coordinates (see Appendix-C) as

$$d\vec{\xi} = d\xi_1\, d\xi_2\, d\xi_3 = \xi^2 \sin\theta\, d\alpha d\theta d\xi$$

Hence, (4.13) becomes

$$\Phi_{ff}(\vec{k}) = \frac{1}{(2\pi)^3} \int_{\xi=0}^{\infty} \int_{\theta=0}^{\pi} \int_{\alpha=0}^{2\pi} \overline{f'^2}\, e^{-\gamma|\xi|}\, e^{-ik\xi\cos\theta} \sin(\theta)\, \xi^2 d\alpha d\theta d\xi \tag{4.14}$$

Let us first integrate (4.14) over θ by making a change of variables. Setting $u = \cos\theta$ and rewriting the θ-dependent part of (4.14), we obtain

$$I = \int_{\theta=0}^{\pi} e^{-ik\xi\cos\theta} \sin\theta d\theta = -\int_{1}^{-1} e^{-ik\xi u}\, du$$

$$= \int_{-1}^{1} e^{-ik\xi u}\, du = -\left.\frac{e^{-ik\xi u}}{ik\xi}\right|_{-1}^{1}$$

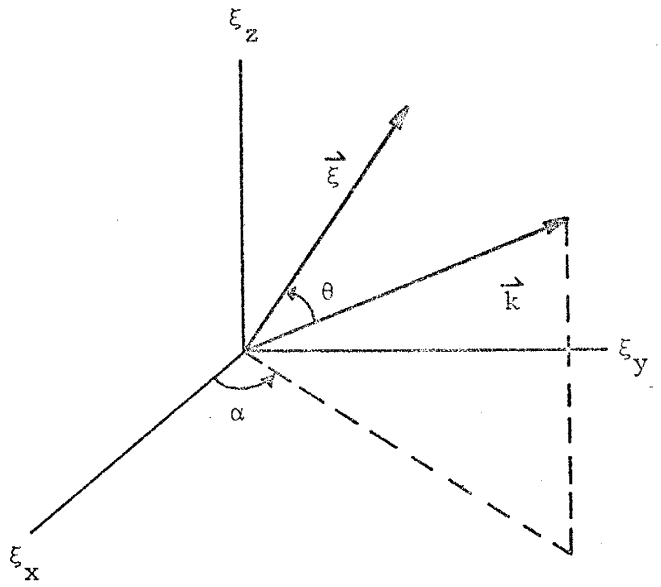

Fig. 4-1a: Geometry of the wave number vector relative to the separation vector.

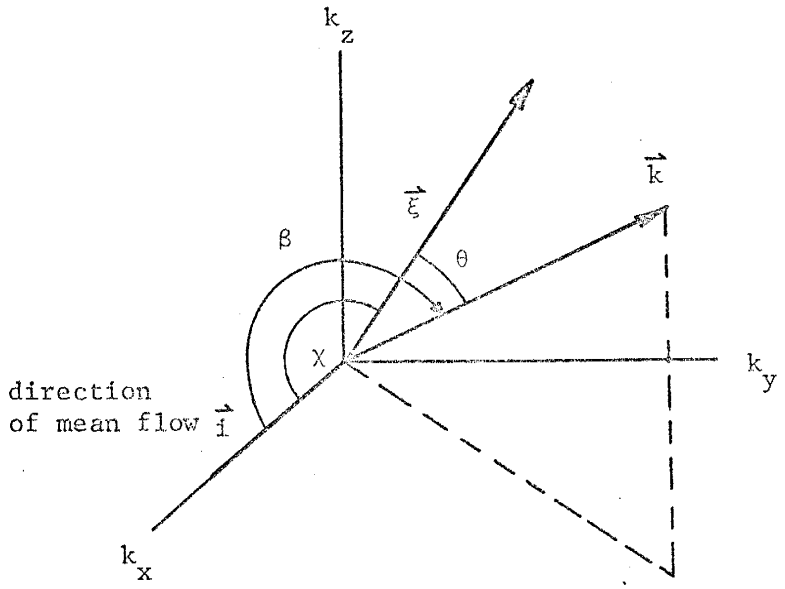

Fig. 4-1b: Geometry of the wave number and separation vector relative to the direction of mean flow.

$$= \frac{2 \sin k\xi}{k\xi}$$

The integral of (4.14) over α is equal to 2π. Thus (4.14) reduces to

$$\Phi_{ff}(\vec{k}) = \frac{2\overline{f'^2}}{k(2\pi)^2} \int_0^\infty \xi \, e^{-\gamma|\xi|} \sin k\xi \, d\xi$$

The value of the above integral (see Gradshteyn and Ryzhik, 1965, p. 198) is

$$\int_0^\infty \xi \, e^{-\gamma|\xi|} \sin k\xi d\xi = \frac{e^{-\gamma|\xi|}}{(\gamma^2 + k^2)} \left[\left[-\gamma\xi - \frac{\gamma^2 - k^2}{\gamma^2 + k^2} \right] \sin k\xi - \left(k\xi + \frac{2\gamma k}{\gamma^2 + k^2} \right) \cos k\xi \right] \Bigg|_0^\infty$$

This expression vanishes when evaluated at the upper limit and we are left with its value at the lower limit, i.e.

$$\Phi_{ff}(\vec{k}) = \frac{\gamma \overline{f'^2}}{\pi^2(\gamma^2 + k^2)^2} \tag{4.15}$$

The spectrum $\Phi_{\phi\phi}$ of hydraulic head fluctuations is obtained by substituting (4.15) in (4.10)

$$\Phi_{\phi\phi}(\vec{k}) = \frac{\gamma J_o^2 \, \overline{f'^2} \, k_x^2}{\pi^2 k^4 (\gamma^2 + k^2)^2} \tag{4.16}$$

Taking the Fourier transform of $\Phi_{\phi\phi}$ given by (4.16), one obtains the autocovariance $R_{\phi\phi}$ of hydraulic head fluctuations,

$$R_{\phi\phi}(\vec{\xi}) = \iiint_{-\infty}^{\infty} e^{i\vec{k}\cdot\vec{\xi}}\, \Phi_{\phi\phi}(\vec{k})\, d\vec{k} \qquad (4.17)$$

Change to spherical coordinates, as shown in Appendix-C, and define the following relationships (see Fig. 4-1b):

$$\vec{k}\cdot\vec{i} = k\cos\beta = k\eta \quad , \quad \text{or}$$

$$k_x = k\cos\theta\cos\chi + k\sin\theta\sin\chi\cos\alpha \quad ,$$

where χ is the angle between the separation vector $\vec{\xi}$ and the direction of mean flow represented by the vector $\vec{i}$. The above expression can be rewritten as

$$\frac{k_x}{k} = \cos\theta\cos\chi + \sin\theta\sin\chi\cos\alpha \qquad (4.18)$$

where ξ and χ represent coordinates of the autocovariance function whereas k, θ, and α are integration variables. Writing $d\vec{k}$ in spherical coordinates and substituting (4.18) into the expression for $R_{\phi\phi}$ results in

$$R_{\phi\phi}(\xi,\chi) = \int_{k,\alpha,\theta=0}^{\infty\ 2\pi\ \pi} \frac{\gamma J_o^2\ \overline{f'^2}\ k_x^2}{\pi^2 k^4(\gamma^2+k^2)^2}\, k^2\, e^{i\vec{k}\cdot\vec{\xi}}\sin\theta\, dk d\alpha d\theta$$

$$= \frac{\gamma J_o^2\ \overline{f'^2}}{\pi^2} \int_{k,\alpha,\theta=0}^{\infty\ 2\pi\ \pi} \frac{\eta^2\sin\theta}{(\gamma^2+k^2)^2}\, e^{i\vec{k}\cdot\vec{\xi}}\, dk d\alpha d\theta$$

$$= C \int_{k,\alpha,\theta=0}^{\infty\ 2\pi\ \pi} \frac{(\cos\theta\cos\chi + \sin\theta\sin\chi\cos\alpha)^2}{(\gamma^2+k^2)^2}\,(\sin\theta)\, x$$

$$e^{ik\xi\cos\theta}\, dk d\alpha d\theta \qquad (4.19)$$

in which $C = \frac{\gamma J_o^2 \overline{f'^2}}{\pi^2}$

Make a change of variables by setting $y = \cos\theta$, from which $dy = -\sin\theta\, d\theta$; hence (4.19) becomes

$$R_{\phi\phi}(\xi,\chi) = C \int_{k=0}^{\infty} \int_{\alpha=0}^{2\pi} \int_{y=-1}^{1} \frac{(y\cos\chi + \sqrt{1-y^2}\cos\alpha\sin\chi)^2}{(\gamma^2+k^2)^2} \times e^{ik\xi y}\, dy d\alpha dk$$

Writing the exponential function in terms of its trigonometric expansion leads to

$$R_{\phi\phi} = C \int_{k=0}^{\infty} \int_{\alpha=0}^{2\pi} \int_{y=-1}^{1} \frac{[y^2\cos^2\chi + (1-y^2)\sin^2\chi\cos^2\alpha](\cos k\xi y + i\sin k\xi y)}{(\gamma^2+k^2)^2} \times dy d\alpha dk$$

$$+ 2C \int_{k=0}^{\infty} \int_{\alpha=0}^{2\pi} \int_{y=-1}^{1} \frac{y\sqrt{1-y^2}\sin\chi\cos\chi\cos\alpha\,(\cos k\xi y + i\sin k\xi y)}{(\gamma^2+k^2)^2} \times dy d\alpha dk \qquad (4.20)$$

Let us first evaluate the second integral of (4.20). The integral of the real part vanishes because the integrand is an odd function of y integrated over a symmetric interval. Thus, we are left with the imaginary part which also vanishes when integrated over α because:

$$\int_o^{2\pi} \cos\phi\, d\phi = \sin\phi \Big|_o^{2\pi} = 0$$

Hence, the second integral of (4.20) vanishes. Now, the imaginary part

of the first integral of (4.20) is an odd function of y and thus also vanishes when integrated over a symmetric interval about the origin. The only part of the integral remaining in (4.20), therefore, is the real part of the first integral, i.e.

$$R_{\phi\phi} = C \int_{k=0}^{\infty} \int_{\alpha=0}^{2\pi} \int_{y=-1}^{1} \frac{(y^2 \cos^2\chi + \sin^2\chi \cos^2\alpha - y^2 \sin^2\chi \sin^2\alpha) \cos k\xi y}{(\gamma^2 + k^2)^2} \times$$

$$dy d\alpha dk \qquad (4.21)$$

Evaluating (4.21), the following expression for the autocovariance $R_{\phi\phi}$ of hydraulic head fluctuations is obtained (see Appendix-D):

$$R_{\phi\phi}(\xi,\chi) = \frac{J_o^2 \overline{f'^2}}{2\gamma^2}\left\{(\cos^2\chi - 1)\left[e^{-\gamma\xi} + \frac{2(e^{-\gamma\xi} - 1)}{\gamma\xi}\right]\right.$$

$$\left. + (3\cos^2\chi - 1)\left[(1 - e^{-\gamma\xi})\frac{8}{(\gamma\xi)^3} - e^{-\gamma\xi}\left(1 + \frac{4}{\gamma\xi} + \frac{8}{(\gamma\xi)^2}\right)\right]\right\} \qquad (4.22)$$

Taking the limit of (4.22) as $\xi \to 0$ we obtain (see Appendix-E) an expression for the variance of head fluctuations,

$$R_{\phi\phi}(o,\chi) = \overline{\phi'^2} = \frac{J_o^2 \overline{f'^2}}{3\gamma^2} \qquad (4.23)$$

Equation (4.23) represents a significant result of three-dimensional analysis which will be elaborated upon briefly in the next section and in more detail together with other features of three-dimensional results in Chapter 6.

4.4 Significance and Limitations of Three-Dimensional Results

In this section, the significance of the three-dimensional results obtained in section 4.3 is briefly discussed in relation to the one-dimensional analysis developed in Chapter 3. We also comment on questions raised by Freeze (1975) concerning the validity of deterministic models used in groundwater hydrology in light of the more general results of this chapter. Finally, limitations of the approach followed in the study of the three-dimensional, steady, saturated flow problem are pointed out.

One of the most significant and indeed encouraging results obtained from the general solution is the reduction of variance of predicted hydraulic head relative to that of the one-dimensional case. It is interesting to compare (4.23), representing the variance in head in three-dimensional sense, with its one-dimensional counterpart (see (3.43) of Chapter 3). At a first glance, it is apparent that the variance resulting from three-dimensional analysis is one-third that of the corresponding variance in one dimension. However, as will be shown in Chapter 6, the reduction in variance is even greater than that indicated above since the value of the correlation parameter, γ, turns out to be more than twice the value of a, the corresponding parameter in one dimension.

Based on high variance of predicted head for simple one-dimensional problems in which a statistical description of properties of the porous medium was adopted, Freeze (1975) raised doubts about the accuracy of the deterministic models widely used in groundwater hydrology. Our results, however, show an order of magnitude reduction

in the variance of predicted hydraulic head relative to that of the one-dimensional case when the three-dimensional nature of the flow system is considered. As indicated in section 3.5.2, the one-dimensional description of the flow is an oversimplification of a generally multidimensional phenomenon. Hence, results obtained from such restricted representation of the flow tend to be misleading unless interpreted with considerable caution. Equation (4.23) in comparison to (3.43) demonstrates the serious errors that would be incurred if results from one-dimensional analysis are used to draw conclusions concerning the effect of heterogeneities which are naturally three-dimensional.

The analyses developed in this chapter were restricted to the problem of steady state flow in a statistically isotropic medium. Although we expect that most aquifer materials will exhibit statistical anisotropy, it was felt that important initial insight could be obtained by assuming isotropy. The consideration of anisotropy and unsteadiness will complicate the mathematical procedure, but the effects of anisotropy and unsteadiness should be analyzed in future research.

CHAPTER 5

SPECTRAL ANALYSES OF PERMEABILITY AND POROSITY FIELD DATA

5.1 Introduction

In this chapter, spectral analyses of permeability and porosity from field data is carried out. Two types of data were available: Core analysis data of samples from aquifer materials and data from some Holocene (or Recent) sand bodies, including river bars, beaches, and dunes. The purpose in performing these analyses is threefold. The first objective of this chapter is to illustrate typical spatial statistical structures of permeability and porosity data.

In the previous analyses of the problem of groundwater flow in one and in three dimensions we assumed certain forms for the auto-covariance functions describing correlation of neighboring conductivity fluctuations. The second objective is, therefore, to examine the validity of these models utilizing actual data. Earlier examples of simple network design problems gave rise to a length scale, which is characteristic of the medium. This parameter would be obtained, as indicated in Chapter 3, from statistical analysis of field data. Estimation of this correlation parameter together with a discussion of its significance represent the third objective of the spectral analysis of field data performed in this chapter.

Practical considerations in the estimation of spectra from discrete data, e.g. length of record, are discussed in section 5-2. Results of the spectral analysis of core data are presented in section 5.3 with a list of the type and source of data used and a brief description of their lithology. Also considered in section 5.3

is the spectral analysis of porosity and log permeability of published field data for a number of Recent sand bodies. In section 5.4 we examine the autocorrelation functions of field data in light of the assumed form for the covariance between neighboring points. The question of the integral scale, its definition, estimation, and its significance are also discussed in section 5.4. Comparison between spectra of log permeability of field data and the spectra of the theoretical models assumed in Chapters 3 and 4 are carried out in section 5.5.

5.2 Spectral Analysis of Discrete Data

The subsequent discussion follows essentially Jenkins and Watts (1968). We deal with observations $f(x)$ which are a function of one space coordinate (e.g. the log of the hydraulic conductivity of a subsurface material). In this case consecutive values of $f(x)$ are correlated so that in addition to the mean μ and variance σ^2, we need to specify the covariances, $R(\xi)$, between the values of $f(x)$ at different distances or separations, ξ. If a single observed series is to give meaningful information about the ensemble properties (e.g. σ^2 and $R(\xi)$), it is necessary to assume statistical homogeneity, i.e. that all statistical properties depend on differences $x_i - x_j$ rather than on the x_i and x_j themselves. This reduces the covariances to be estimated to the autocovariances, namely

$$\hat{R}(\xi) = \frac{1}{N-\xi} \sum_{i=1}^{N-\xi} \{(X_i - \overline{X})(X_{i+\xi} - \overline{X})\} \qquad (5.1)$$

where the hat indicates an estimate, and $\overline{X} = \frac{1}{N} \sum_{i=1}^{N} X_i$.

The observations f(x) are also characterized by their spectral density function which is the inverse Fourier transform of the autocovariance

$$\Phi(k) = \frac{1}{2\pi} \int_{-\infty}^{\infty} R(\xi) \cos k\xi d\xi \qquad (5.2)$$

We are interested in evaluating estimates of (5.2) from a sample record consisting of a limited number of observations of discrete sampling points. In the estimation of spectra from records of finite length, certain practical questions arise; these include:

1) sampling interval or frequency of sampling,

2) length of record and the resulting variance of the spectral estimates, and

3) number of lags of the autocovariance function and the bandwidth used in calculating the spectral density.

These items will be briefly discussed in the remainder of this section.

One of the uses of spectral analysis is to detect periodicities or length scales characterizing patterns of variations of a given property. Consequently, the frequency of sampling or the sampling interval should be chosen such that these scales can be determined. If we sample every Δ units, the highest unambiguous frequency detectable is the Nyquist frequency, $F_N = \frac{1}{2\Delta}$, i. e., the sampling interval determines the maximum frequency which can be distinguished (see Jenkins and Watts, 1968, p. 53). Thus if F_{max} is the highest frequency thought to be significant then the spacing between the samples, Δ, should be selected such that $\frac{1}{2\Delta} > F_{max}$, i. e. say $\Delta = \frac{1}{3F_{max}}$.

The length of the record, meanwhile, determines the extent to which peaks in the spectrum may be distinguished. It also controls the number

of degrees of freedom of the power spectral estimates which in turn gives a measure of the uncertainty in the spectral estimates as discussed later in this section.

For a limited amount of data, the spectral density $\Phi(k)$ is estimated by the discrete analogue of (5.2), given by

$$\hat{\Phi}(k) = \frac{1}{2\pi} \left[\hat{R}(o) + 2 \sum_{\xi=1}^{M} \hat{R}(\xi) \cos (\xi k)\right] \qquad (5.3)$$

where the hats denote estimators. To obtain a consistent estimate of $\Phi(k)$ it is customary to smooth this estimate by a set of weighting factors which is usually called a "spectral window". The spectral window corresponds to a slit of width $\frac{1}{N}$ where N is the total length of record, so that for large N it is reasonable to assume that the spectral estimates are constant over the slit (Jenkins and Watts, 1968, p. 243). The Rectangular, Bartlett, Tukey, and Parzen windows are among the most commonly used spectral windows (see for example p. 244 of Jenkins and Watts, 1968).

The "width" of the spectral window is often called the bandwidth in the terminology of electrical engineering. The bandwidth, b, gives the width over which smoothing occurs in the spectral domain, and peaks less than this width apart are fused together into one peak. In other words, in order to obtain a good estimate of a peak in a spectrum, the width of the spectral window must be of the same order as the width of the peak (Jenkins and Watts, 1968, p. 256).

Note that the variance of the spectral estimator is inversely proportional to the bandwidth of the spectral window. Hence, small variance of the spectral estimate is associated with large bandwidth and vice versa.

The variance of the smoothed spectral estimator can be reduced by making the total number of lags M small. However, the narrower the base width of the lag window, the less biased is the smoothed spectrum of $\hat{\Phi}(k)$; conversely, a narrow spectral window gives larger variance to the spectral estimates. In other words, reducing M increases the bias and causes more distortion of the theoretical spectrum, since then the spectral window is wider. The foregoing discussion demonstrates the necessity to compromise between the variance and the bias of the estimator when selecting the spectral window.

The number of degrees of freedom, ν, of the smoothed estimator is given by

$$\nu = 2\left(\frac{N}{M}\right)b \tag{5.4}$$

The degrees of freedom gives a measure of the uncertainty in the spectral estimates and are used to construct confidence intervals for those estimates in the following sections. It is evident from (5.4) that a large bandwidth implies that the number of degrees of freedom of the smoothed estimator is large and the variance is small, whereas a small bandwidth is indicative of few degrees of freedom and hence large variance. Since it was indicated above that the bias is reduced by making the width of the lag windows large, it follows that small bias is associated with small bandwidth.

5.3 Spectral Analysis of Field Data

In this section we present and discuss graphs illustrating results of the spectral analysis of permeability and porosity field data. The graphs consist of two types: those showing autocorrelation between neighboring values of porosity and permeability versus the separation

distance or lag, while the other group of figures depict the spectral density for the same sets of data versus the frequency. In all of these figures the logarithm to the base 10 of permeability data is used in the various calculations. We use log permeability in these analyses since the results will be utilized in a later section for comparison with the theoretical models based on the spectrum of ln K. Furthermore, to insure statistical homogeneity of the input series, linear trends (e.g. systematic changes in the mean with distance) were removed from the original data. These and the spectral calculations were performed using program BMD 02T (Biomedical Computer Program, Autocovariance and Power Spectral Analysis, W. J. Dixon (Ed.), 1974). Part of the output of this program consists of graphs of autocovariance function and spectra of the input series which are discussed in this chapter.

5.3.1 Spectral Analysis of Core Data

We analyse a number of sets of permeability and porosity measurements from core data of samples from the Mt. Simon aquifer in northeastern Illinois. This data was obtained from the files of the Illinois State Water Survey (Visocky, 1975). The data sets have both horizontal and vertical permeability in addition to porosity determinations; all at one foot intervals. Also studied is a 190m segment of published porosity and permeability values discretized at one meter intervals from core data obtained from a site near Venice, Italy (Gambolati et al. 1974). Table 5.1 lists pertinent information on the data discussed in this section. Actual values of the Illinois porosity and permeability data are included in Appendix-F. Examples of input series of porosity and log

Table 5.1 Summary of Pertinent Information on Core Data

Set #[1]	Length of Record (ft)[2]	No. of lags[3]	Log K[4] var.	Log K[4] mean	Porosity var.	Porosity mean	Integral Scale (ft)[5]
Gambolati et al. (1974)	190 m	20	2.03	-3.91	16.00	43.34	5.35
IL036H	193	19	0.90	0.89	11.70	10.91	3.34
IL036V	193	19	0.76	0.63	-	-	2.04
IL040H	233	23	0.53	1.21	8.03	11.33	1.74
IL040V	233	23	0.60	1.02	-	-	1.74
IL042H	213	21	0.60	1.38	9.88	11.76	1.30
IL042V	213	21	0.61	1.22	-	-	1.09
IL052H	164	16	0.47	1.22	14.38	12.89	1.26
IL052V	164	16	0.45	0.97	-	-	1.60
IL056H	303	30	0.67	0.79	7.22	10.94	1.57
IL056V	303	30	0.63	0.61	-	-	1.30
IL062H	161	16	0.77	0.52	5.87	9.99	1.52
IL062V	161	16	0.59	0.11	-	-	2.00
IL064H	149	14	0.81	0.67	6.85	9.56	1.69
IL064V	149	14	0.64	0.33	-	-	2.13
IL066H	217	21	0.71	0.63	7.21	10.41	2.13
IL066V	217	21	0.72	0.33	-	-	2.56

Remarks

1) Set IL036H, or IL036V, for instance, consist of a serial number while H and V refer to horizontal and vertical permeability respectively.

2) All sets were sampled at one foot intervals except Gambolati et al. (1974) were discretized at one meter intervals.

3) No. of lags indicates the maximum distance used to compute the auto-correlation of neighboring values.

4) The log of the hydraulic conductivity in cm/sec. for Gambolati et al. (1974) is given whereas the permeability of the data from Illinois are in millidarcys.

5) Details of the integral scale for log K are presented in section 5.4.

6) Gambolati et al. (1974) data are from Pleistocene sediments of Po River at Venice, Italy, while all Illinois data are from the Mt. Simon aquifer in northeastern Illinois consisting of Late Cambrian orthoquartzite.

permeability are shown in figures 5-1 and 5-2 respectively.

Figures 5-3 through 5-8 show the autocorrelation functions while figures 5-9 through 5-14 illustrate the spectral density functions for the porosity and permeability data used in this work. Note that the correlation among neighboring values of porosity or permeability is high at small lags and decreases for larger lags. Most of the data sets shown in figures 5-3 through 5-8 are characterized by an autocorrelation function which becomes negative for large separation. Exceptions are the porosity and both horizontal and vertical permeability data of IL066 and the vertical permeability of IL053V where the autocorrelation between neighboring values remains positive for all lags; the correlation decreases however for large separations. Also, the horizontal permeability of IL052H and IL064H are positively correlated for all except at one point where they are slightly negatively correlated. Finally, note that the change in sign of the autocorrelation functions shown in the figures discussed above reflects what is possibly a quasi-periodic nature of the original series (Jenkins and Watts, 1968, p. 218).

As seen from Table 5.1, the variance of log K for the Illinois data changes from 0.45 to 0.9. This variation is well within the range of variation of log K for core data summarized in Freeze (1975, Table 1). For the porosity of the Illinois data the variance changes from 5.87 to 14.38 while the mean varies between 9.56% and 12.89%. The exception is the data from Gambolati et al. (1974) where the variance of log K is 2.03 and the mean of the porosity data is 43.34. This high porosity indicates the presence of significant amounts of clay. Note that this data is obtained from a geologic section consisting of sand and silt

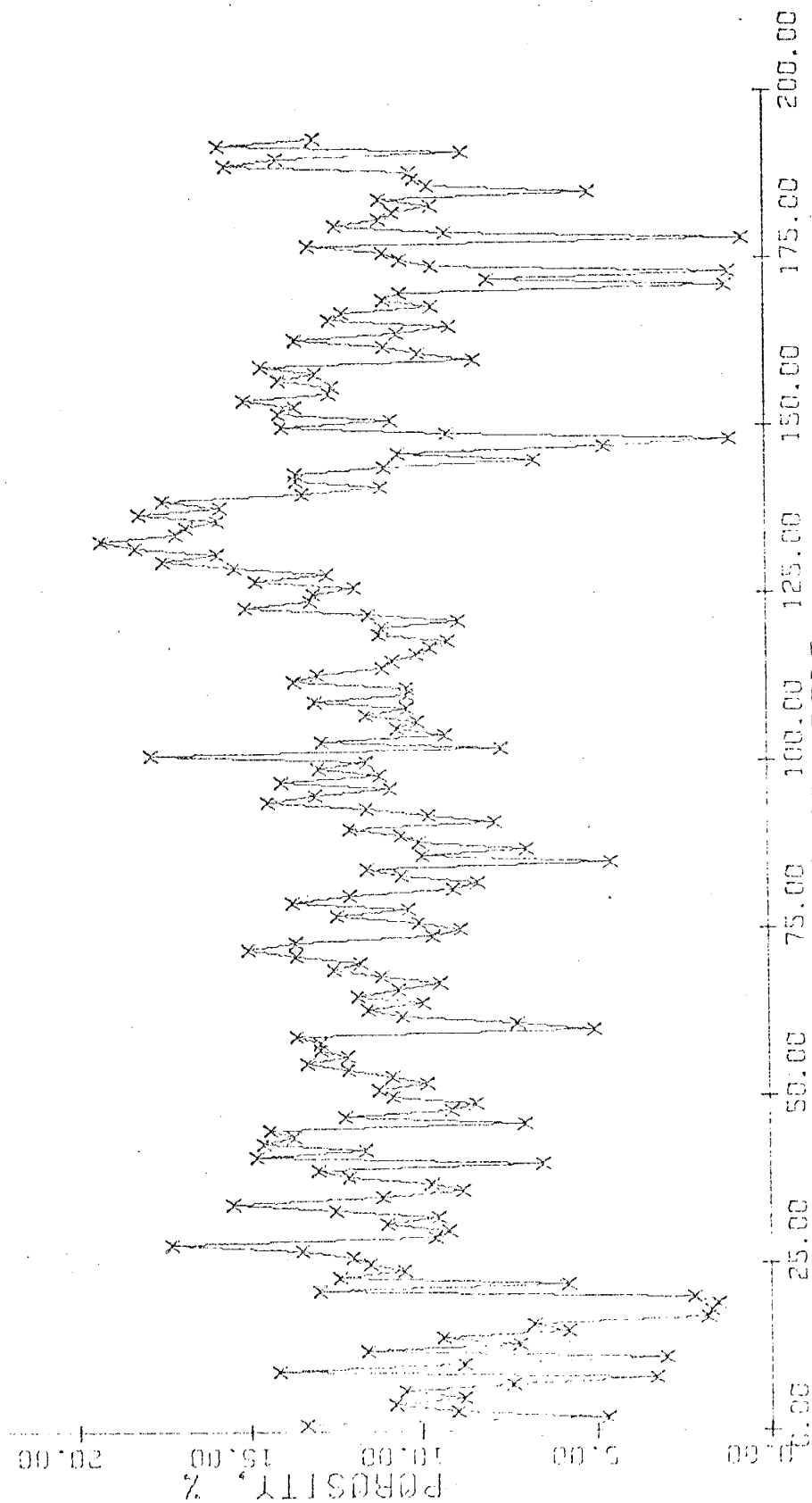

Fig. 5-1: Original series of porosity data versus spacing between samples for IL036.

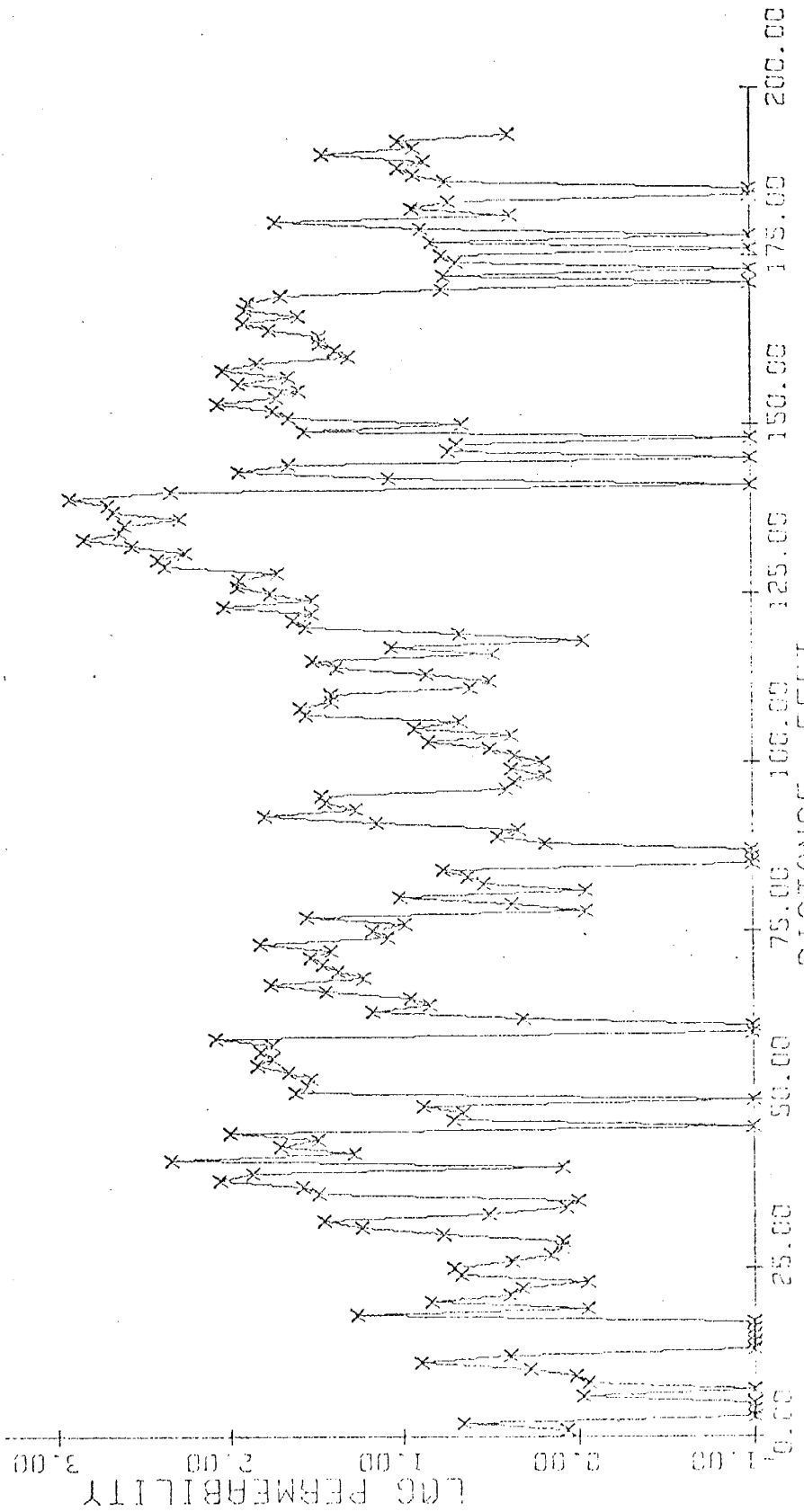

Fig. 5-2: Original series of log permeability data versus spacing between samples for IL036H.

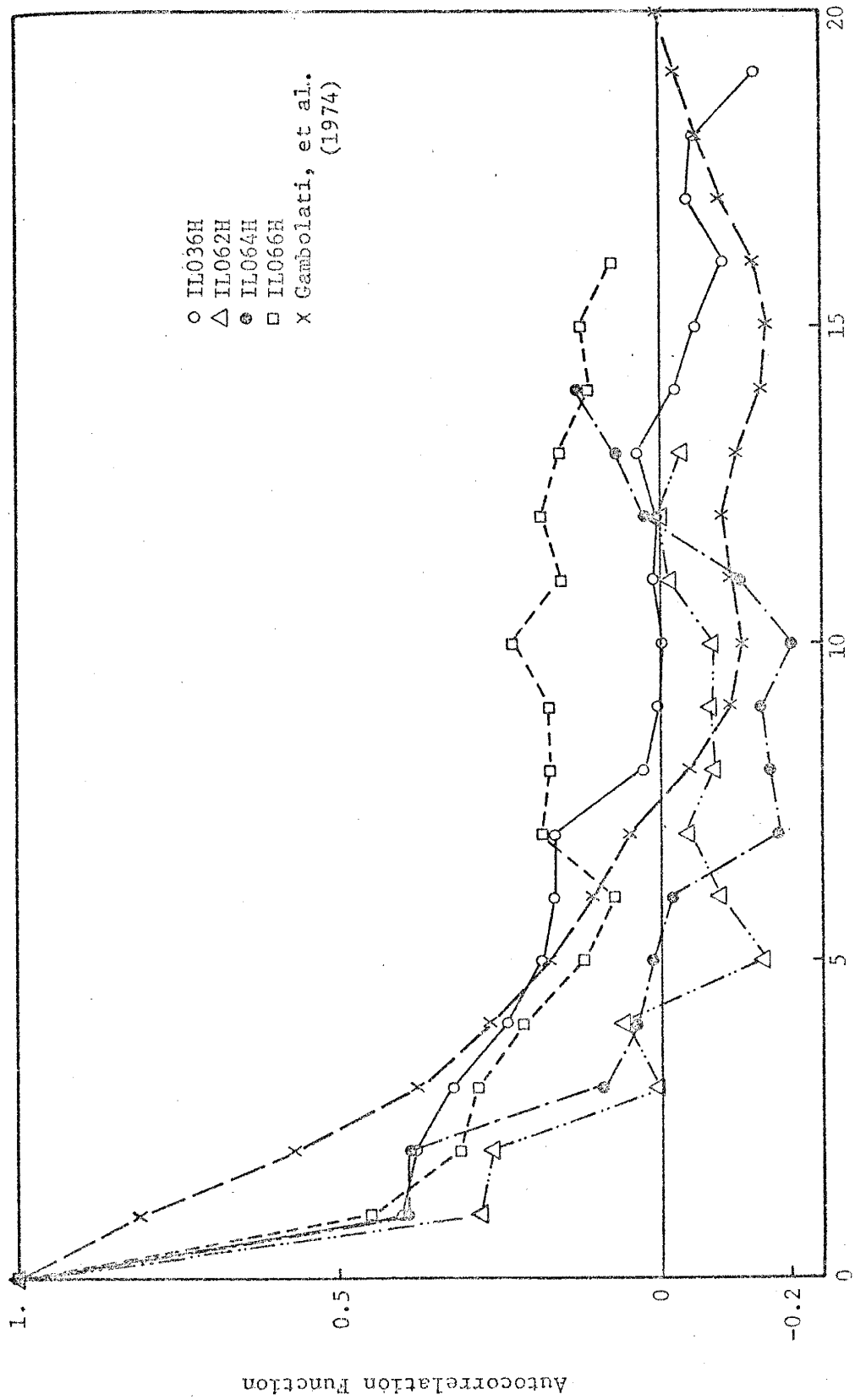

Fig. 5-3: Autocorrelation function of porosity data versus the lag in feet (except Gambolati's data, the lag is in meters).

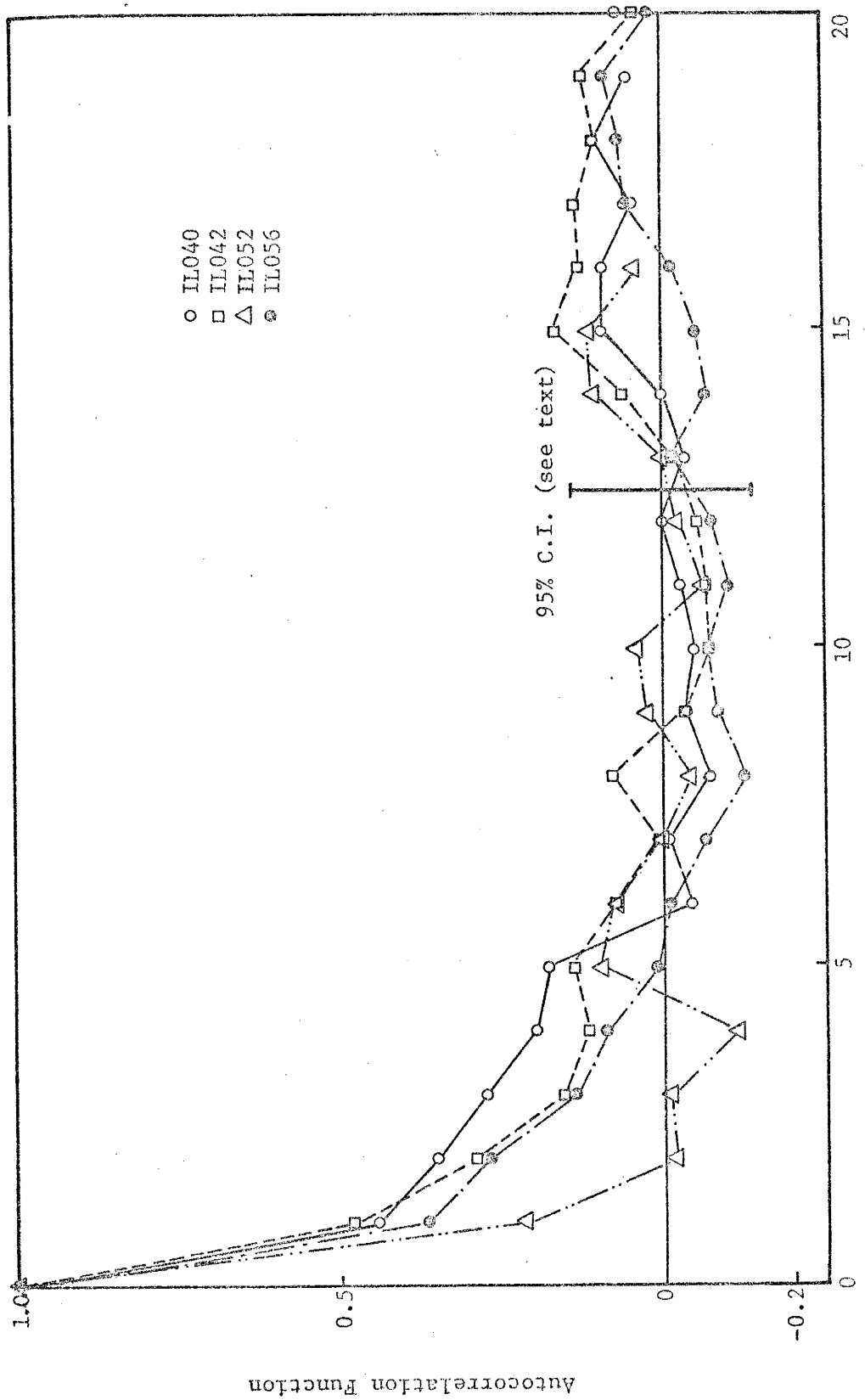

Fig. 5-4: Autocorrelation of porosity data versus the lag in feet. Confidence interval at 95% level is shown.

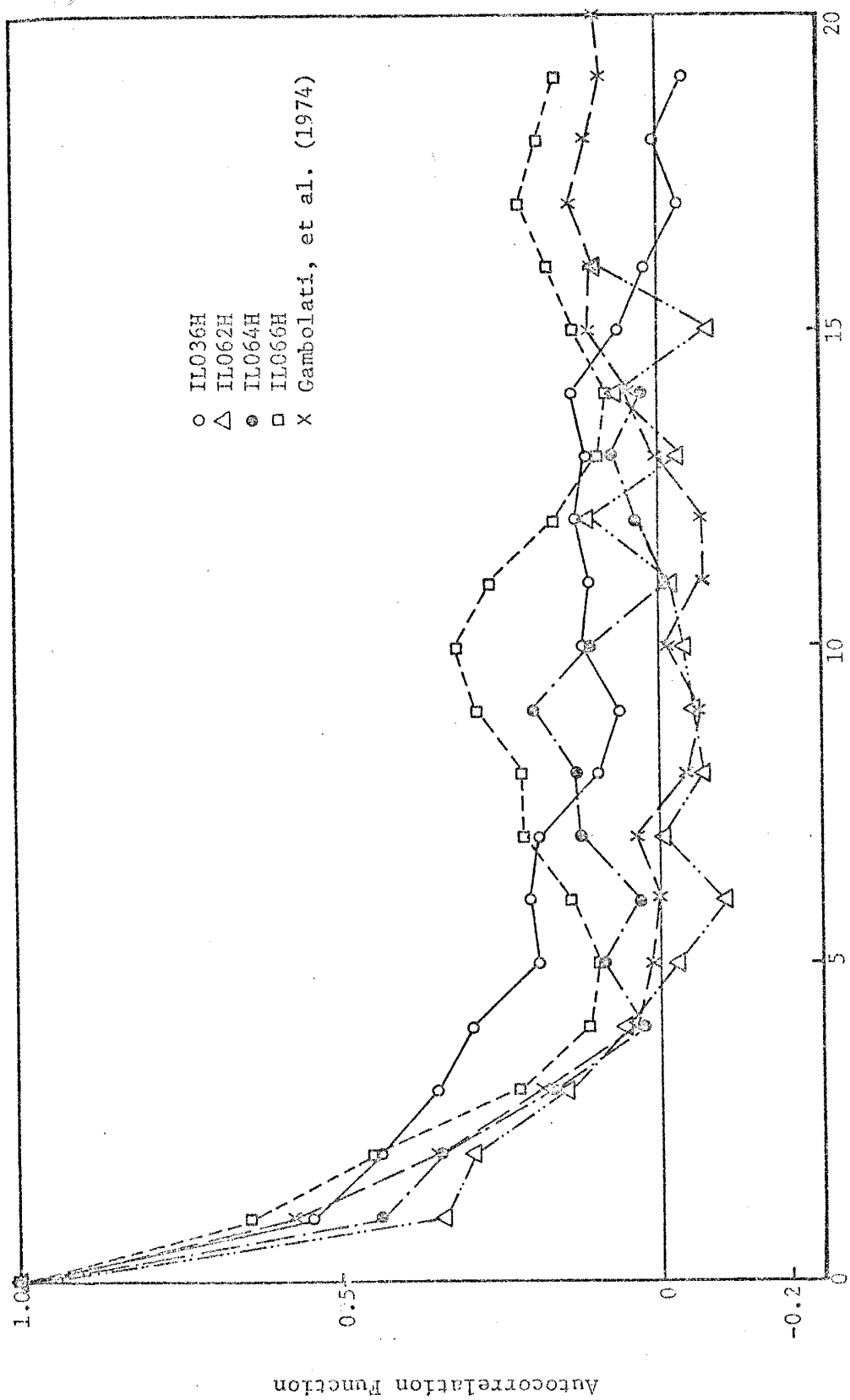

Fig. 5-5: Autocorrelation function of the log of horizontal permeability data versus the lag in feet (For Gambolati's data, the lag is in meters).

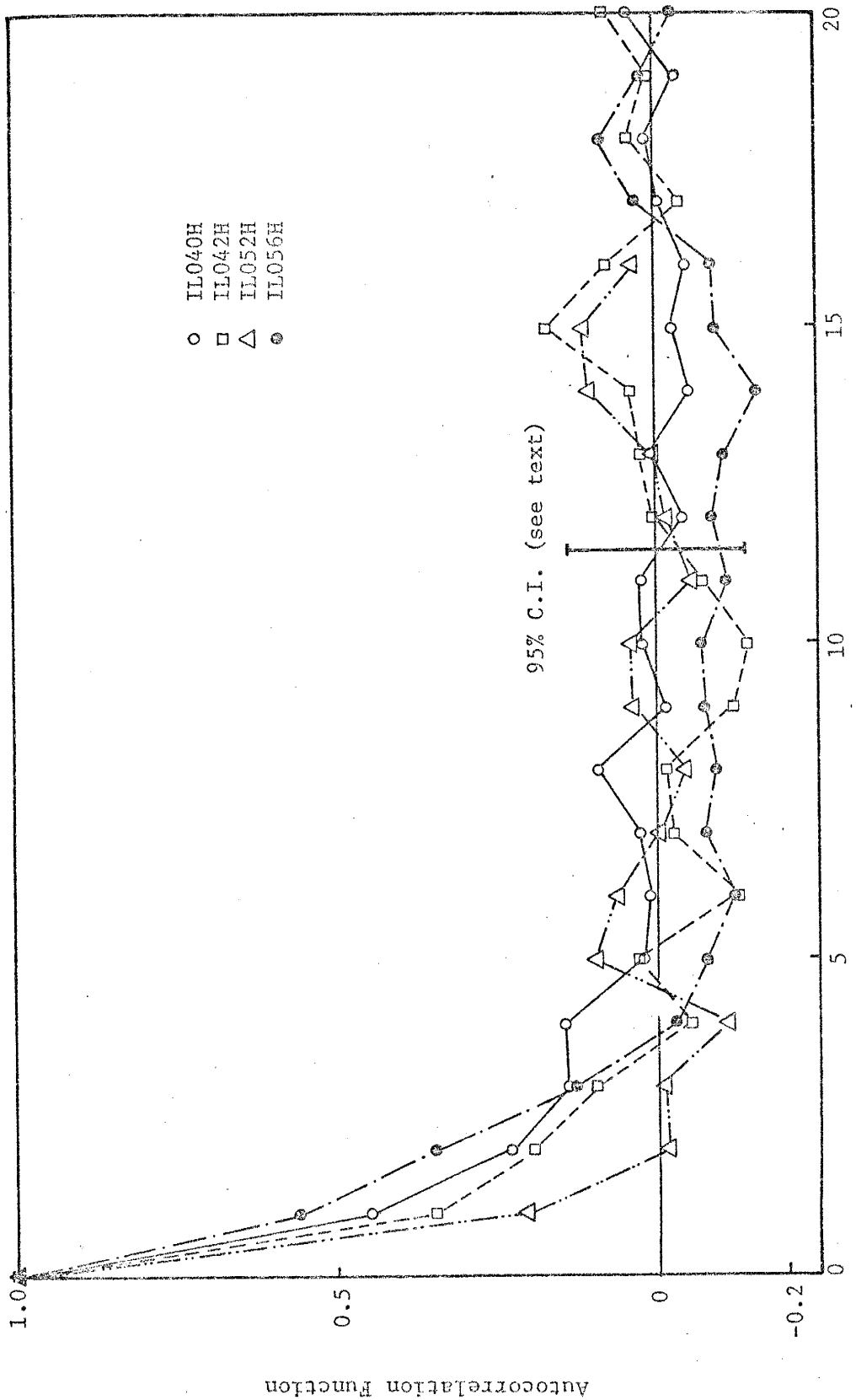

Fig. 5-6: Autocorrelation function of the log of horizontal permeability data versus the lag in feet. Confidence interval at the 95% level is shown.

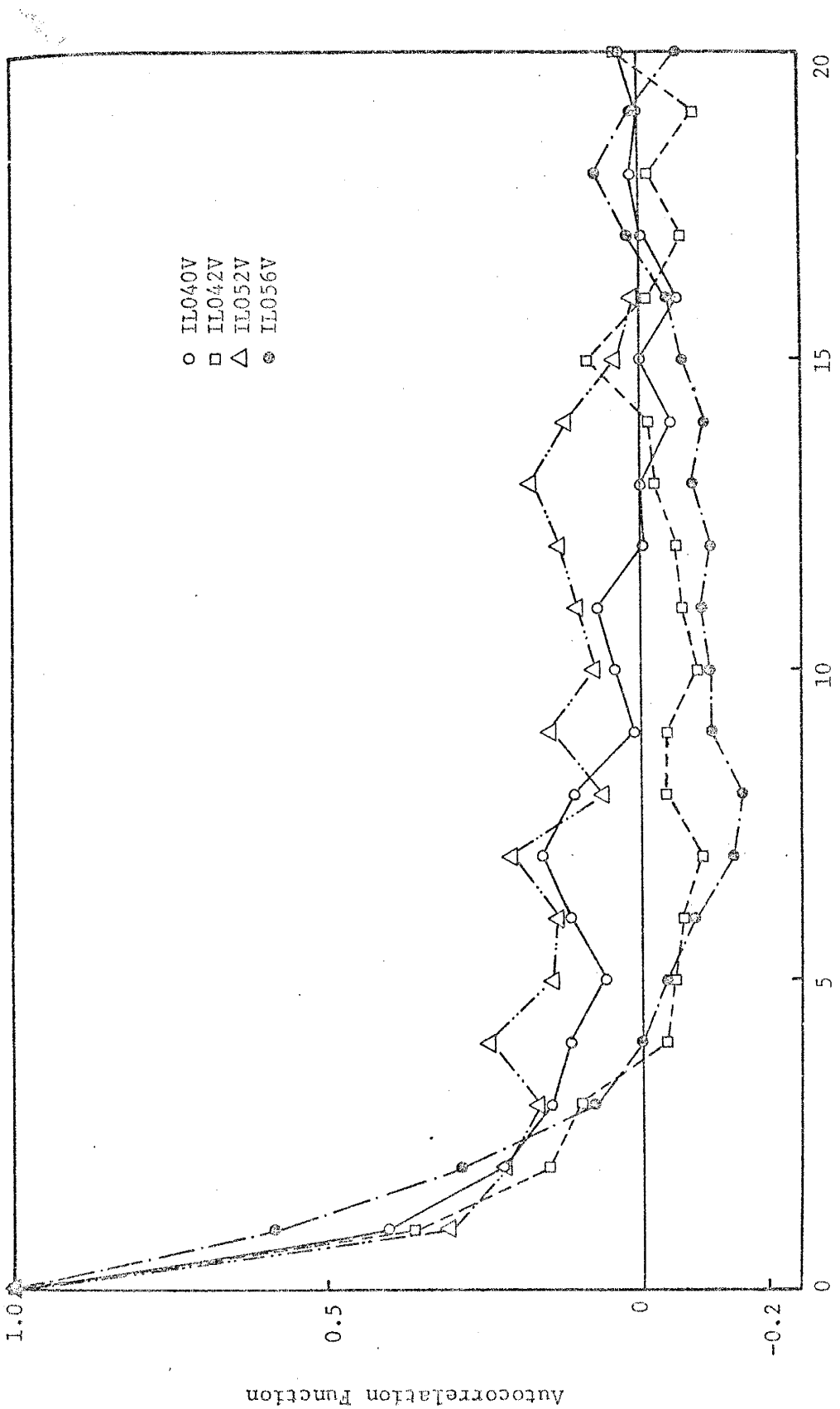

Fig. 5-8: Autocorrelation function of the log of vertical permeability data versus the lag in feet.

with interbedded clay units which may explain this high value of the variance of log K.

The corresponding spectra for above data (see figures 5-9 through 5-14) have a peak at small frequency, i.e. most of the contribution to the variance is found at small frequency. Exception is the porosity spectrum of IL052 which consists of two peaks that extend over a wider range of frequencies than the peaks of the other spectra. The inverse of the frequency at which a peak in the spectrum occurs indicates a length scale at which a possible pattern of variation in porosity or permeability repeats itself. The spectra discussed above for the Illinois data reveal length scales on the order of a few tens of feet while data from Gambolati et al. (1974) give rise to length scales on the order of several meters.

In order to indicate the range of variation in the power spectral estimates of the spectra discussed above, two confidence intervals computed (see Appendix-J) at 80% and 95% levels are shown in figure 5-15. The reason for plotting the spectra on a logarithmic scale is that confidence intervals for the spectrum can be represented by a constant interval about the spectral estimates for all wave numbers; whereas if the spectrum was plotted on linear scale, confidence intervals would have to be computed for each wave number (Jenkins and Watts, 1968, p. 255).

Confidence intervals for the autocovariance estimates are difficult to estimate since neighboring values are correlated. However, if we assume that neighboring points of the autocovariance function are uncorrelated (as for the case of a purely random series or white noise), confidence intervals can then be constructed as indicated in Jenkins

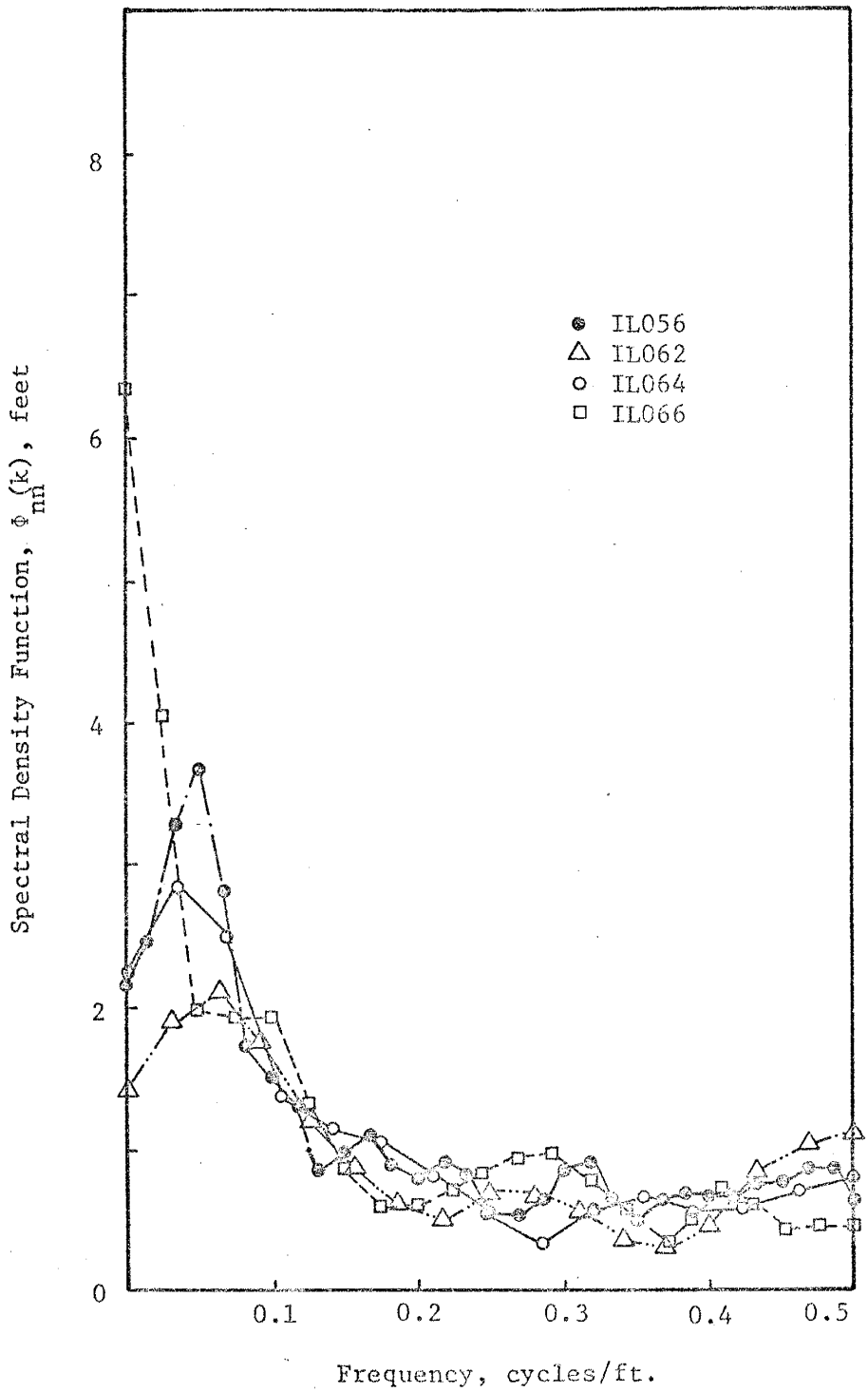

Fig. 5-9: Spectral density function of porosity data versus the frequency in cycles per foot.

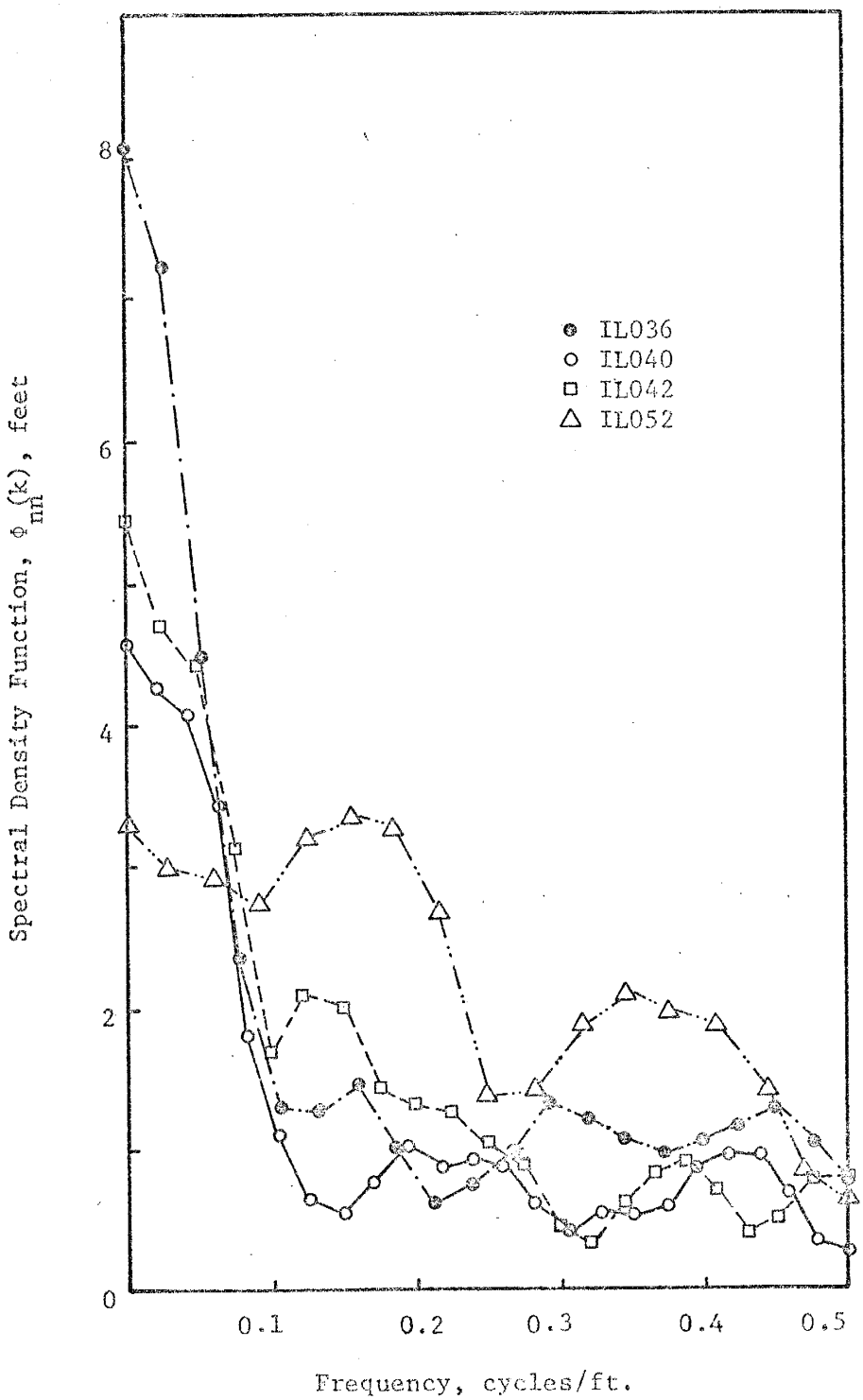

Fig. 5-10: Spectral density function of porosity data versus the frequency in cycles per foot.

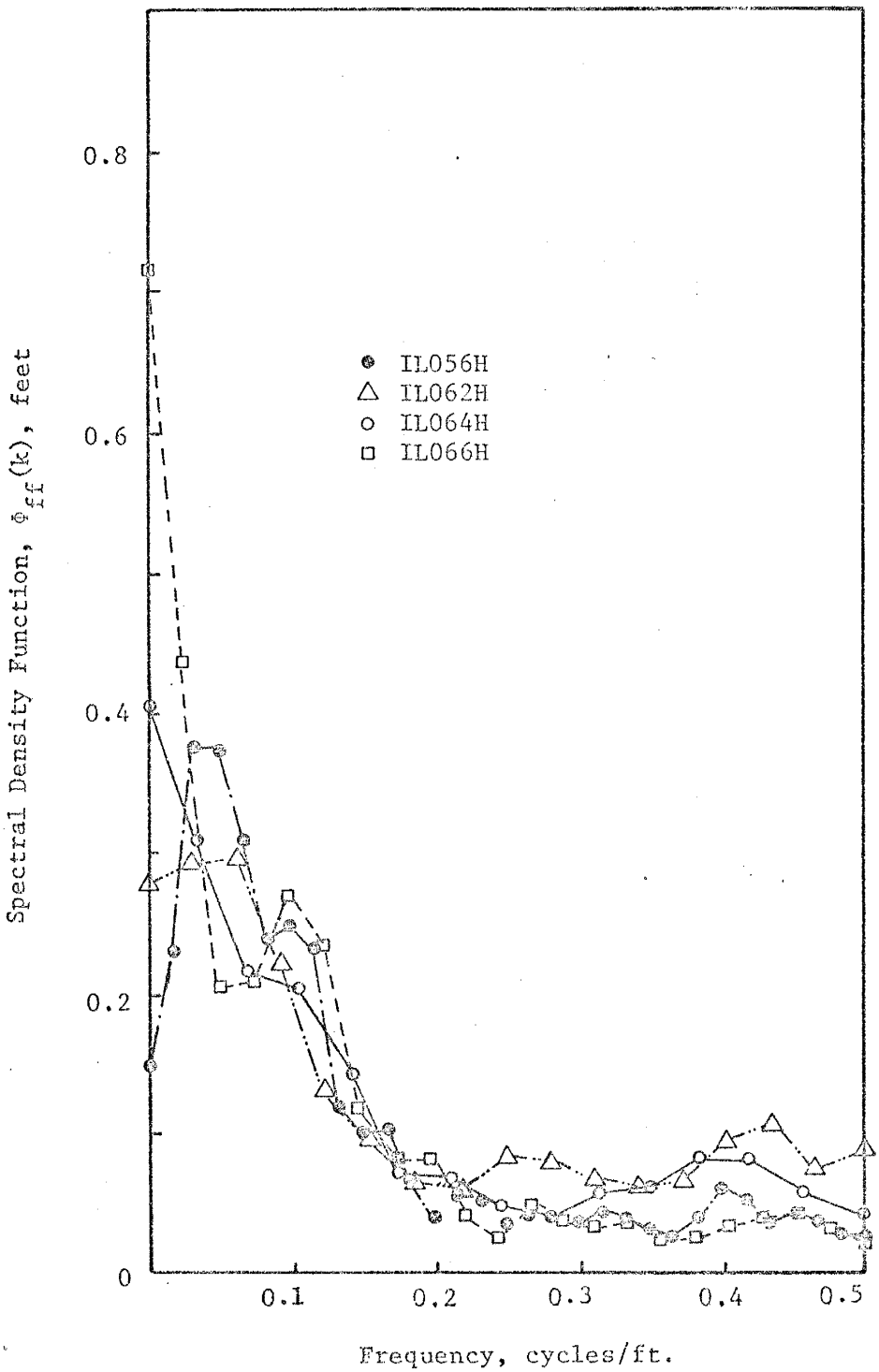

Fig. 5-11: Spectral density function of the log of horizontal permeability data versus the frequency in cycles per foot.

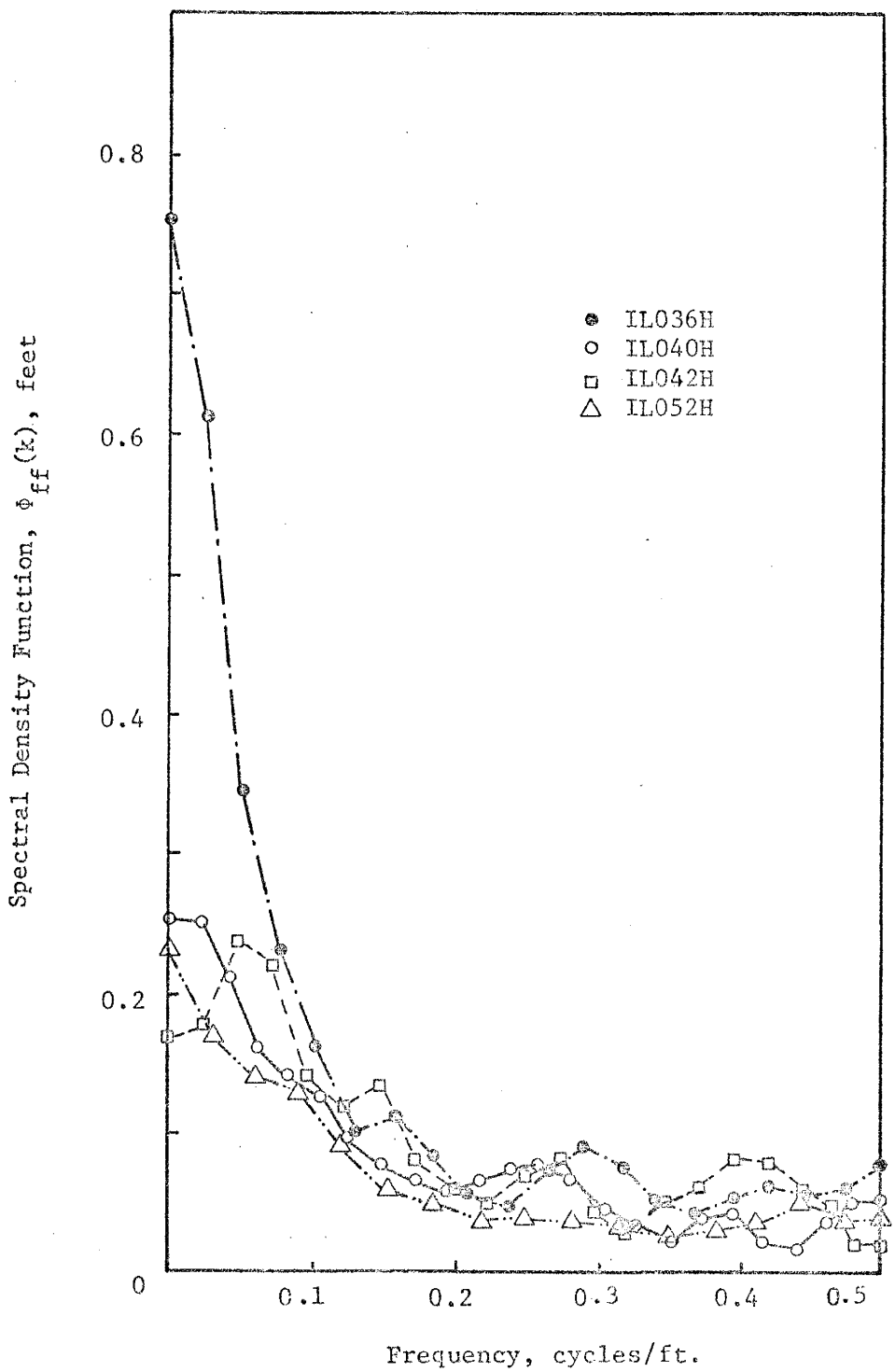

Fig. 5-12: Spectral density function of the log of horizontal permeability data versus the frequency in cycles per foot.

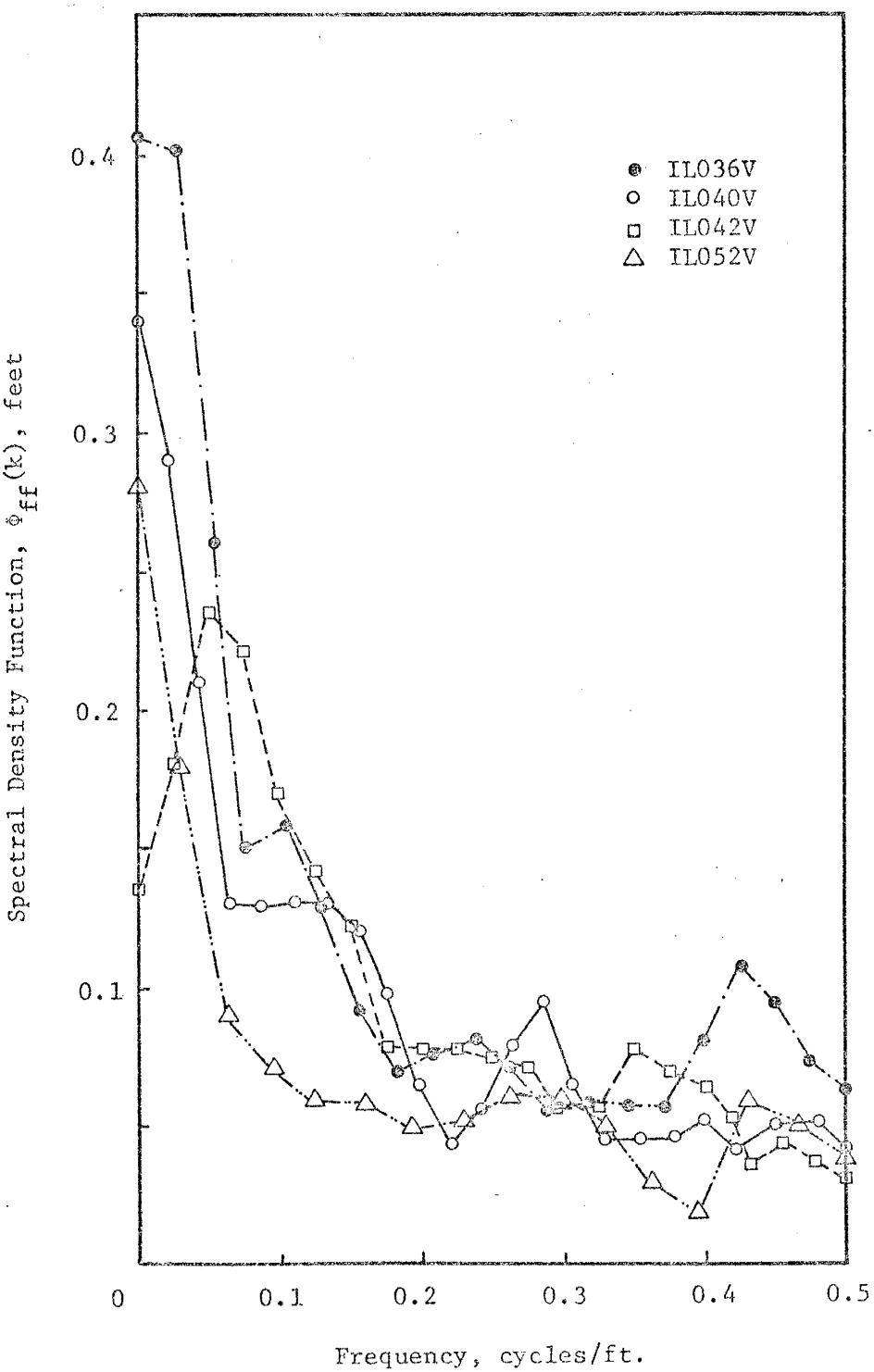

Fig. 5-13: Spectral density function of the log of vertical permeability data versus the frequency in cycles per foot.

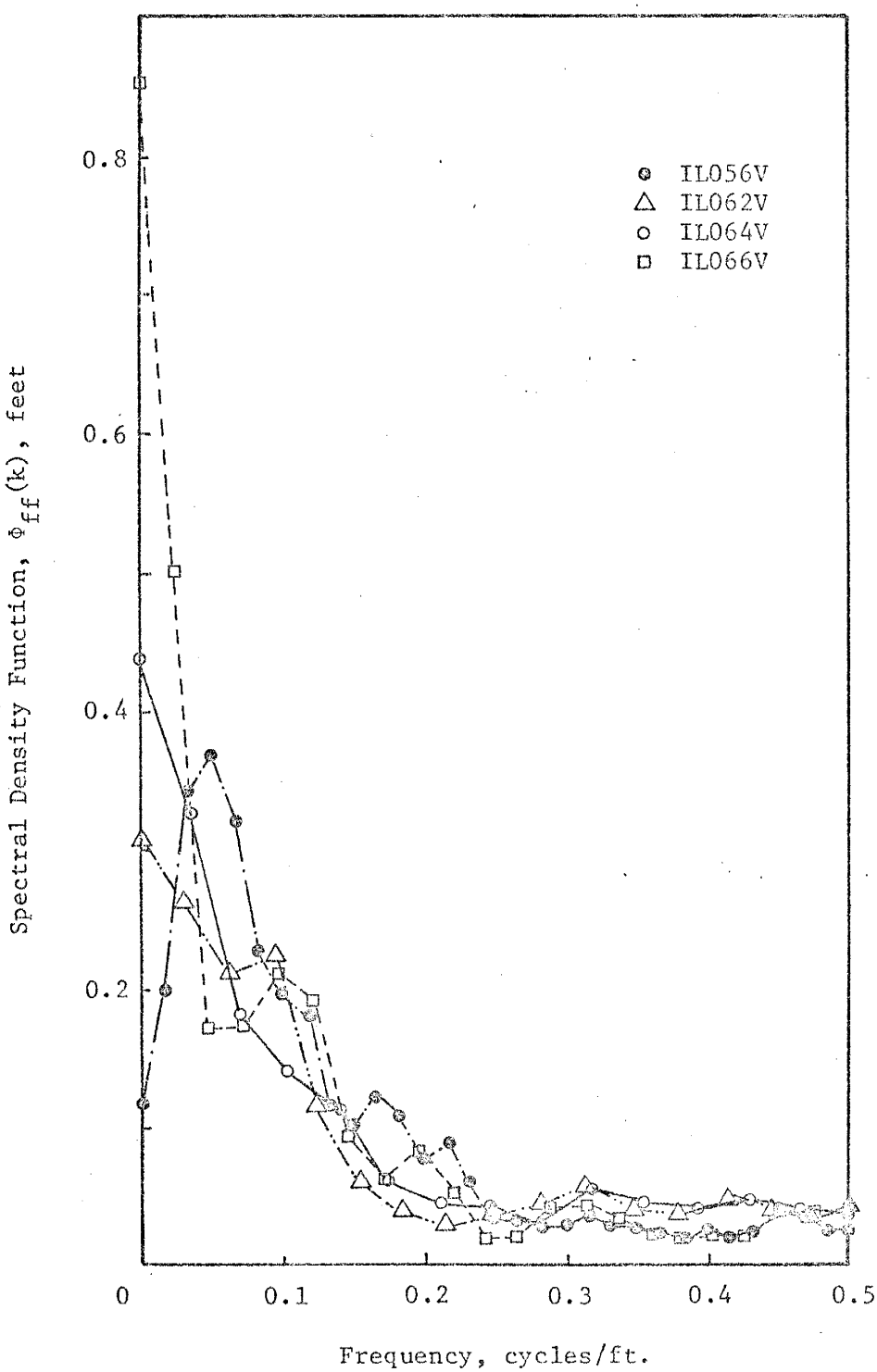

Fig. 5-14: Spectral density function of the log of vertical permeability data versus the frequency in cycles per foot.

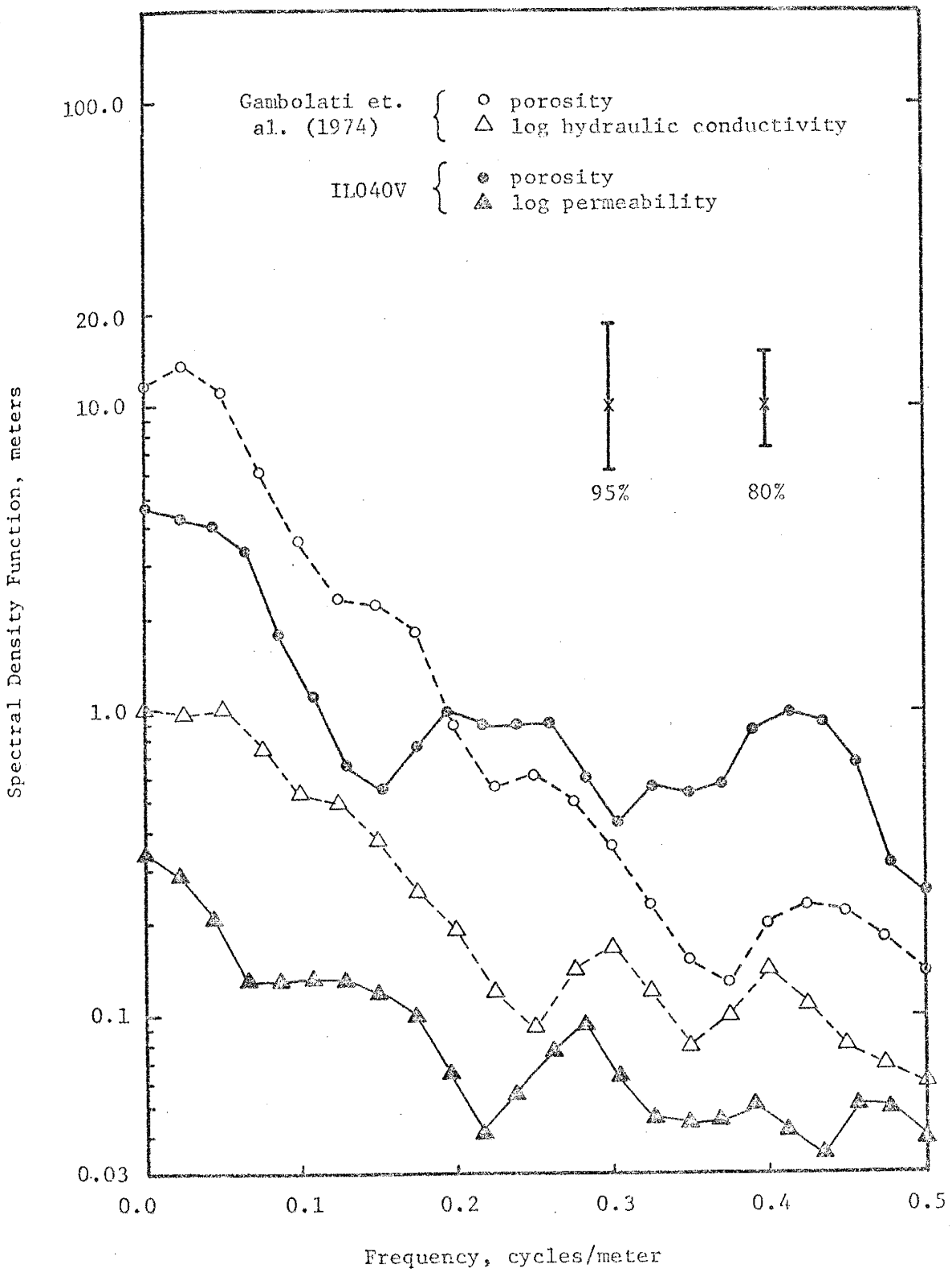

Fig. 5-15: Confidence intervals at 80% and 95% levels for the spectra of porosity and log K. (The dimensions of the vertical and horizontal axes for IL040V are feet and cycles/ft respectively).

and Watts (1968), p. 187). Though such confidence intervals are not the proper ones to use in our case, they do serve the purpose of giving an order of magnitude for the possible variations in our covariance estimates. Such a confidence interval at the 95% level for the autocorrelation function of data from the Mt. Simon aquifer is shown in figures 5-4, 5-6 and 5-7. The width of this confidence interval implies that the indicated fluctuations in the autocorrelation estimates at large separations are insignificant statistically.

5.3.2 Spectral Analysis of Data From Recent Sand Bodies

So far we have discussed spectral results of porosity and permeability data along a vertical line in a given formation, i.e. core data. It is equally important, however, to examine spectral results from porosity and permeability data measured along a horizontal section. Several sets of such data, though consisting of a small number of samples, were available for a few Holocene sand bodies (Pryor, 1973). These samples were obtained from river bars, beaches, and dunes undergoing active sedimentation. Hence all data reflected high values of permeability and porosity characteristic of loose sands.

Information regarding data sets used in this section is summarized in Table 5.2. Actual permeability and porosity values for these sets are published elsewhere (Pryor, 1973). The variance of log K for these data varies from 0.003 to 0.165; this range is very low compared to those of Table 5.1 and also to those summarized in Freeze (1975). The spacing or sampling interval ranged from 0.25 feet up to 400 feet. However, the total number of samples in each record is very small leading to increased variance in the spectral estimates as discussed in section

Table 5.2 Summary of Pertinent Information on Data From Pryor (1973)

Set No.	Total No. of Samples	Sampling interval (ft)	No. of lags	log K† var.	log K† mean	Porosity† var.	Porosity† mean	Description*
PR0001	15	1	6	.012	2.01	1.69	45.80	Fig. 5, Section A, horizontal perm., ⊥
PR0002	17	1	6	.008	1.70	1.64	44.24	Fig. 5, Section A, vertical data, ⊥
PR0006	18	0.25	6	.165	1.87	18.73	42.56	Fig. 6, Section I-1, ⊥
PR0010	15	1	6	.005	1.74	3.39	46.87	Fig. 11, Section A; Ship Isle Beach, ||
PR0021	11	2	5	.012	1.52	2.08	50.09	Fig. 13 & 14, St. Andrews dunes, vertical profile, ⊥
PR0022	9	2	4	.029	1.57	7.85	49.00	Same as above, but 3rd sample line, ⊥
PR0024	10	200	5	.005	1.78	2.85	45.60	Fig. 9 & 10, Ship Island beach, ||
PR0025	10	200	5	.018	1.79	2.13	47.60	Same as above, but middle profile, ||
PR0034	10	10	5	.016	1.72	5.17	48.09	Fig. 9 & 10, Samples vertical to shore-line, profile #4, ⊥
PR0035	10	10	5	.015	1.83	3.84	46.70	Same as above, profile #5, ⊥
PR0040	6	400	3	.007	1.51	1.61	49.17	Fig. 13 & 14, St. Andrews dunes, horizontal profile, ||
PR0042	6	400	3	.009	1.54	13.85	48.67	Same as above, 4th profile from bottom, ||

*Figure numbers in this column are those in Pryor (1973). †Permeability data are in millidarcys, while porosity data are in per cent. \|\| sampled parallel to bedding. ⊥ sampled perpendicular to bedding.

5-2. This also reduces the number of lags available for calculation of autocovariance functions and hence leads to smaller degrees of freedom and wider confidence intervals; this indicates a higher degree of variability of the spectral estimates as will be shown later.

The autocorrelation function of porosity and log permeability data of the trench section on Whitewater River bar (PR0006) are shown in figure 5-16. The permeability data are positively correlated up to a distance of approximately 0.7 foot and their autocorrelation function remains negative thereafter, whereas the porosity data are positively correlated up to a distance of 0.2 foot with an autocorrelation function that fluctuates in sign. The corresponding spectra for these data are depicted in figures 5-17 and 5-18 for log permeability and porosity respectively. Note that the log permeability spectrum is maximum at small frequency, i. e. most of the contribution to the variance is found at small frequency. The porosity spectrum, however, does not have a peak at small frequency but rises steadily to reach a maximum at high frequency.

Figure 5-19 demonstrates the autocorrelation functions of log permeability data for PR0001, PR0002, PR00010, PR0021, and PR0022. These data are positively correlated up to a distance of about 2 feet with the exception of PR0002 where neighboring points are positively correlated up to a distance of about 0.8 foot. All data have autocorrelation functions whose signs are fluctuating except for PR0010 where the autocorrelation remains negative once it becomes so. The autocovariance functions for the porosity data of the above sets are shown in figure 5-20. Only PR0010 and PR0021 have autocorrelation

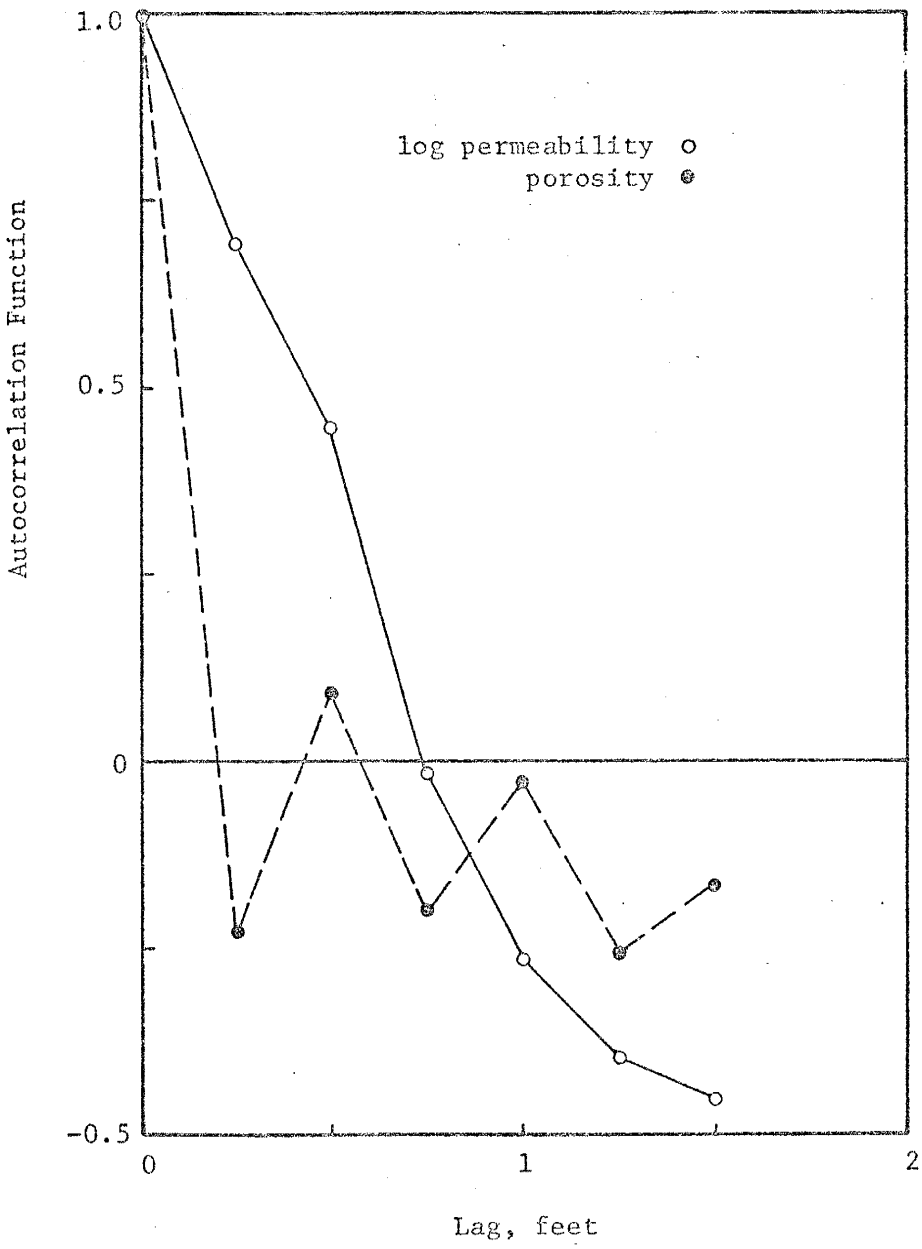

Fig. 5-16: Autocorrelation function of log permeability and porosity data versus the lag in feet for PR0006.

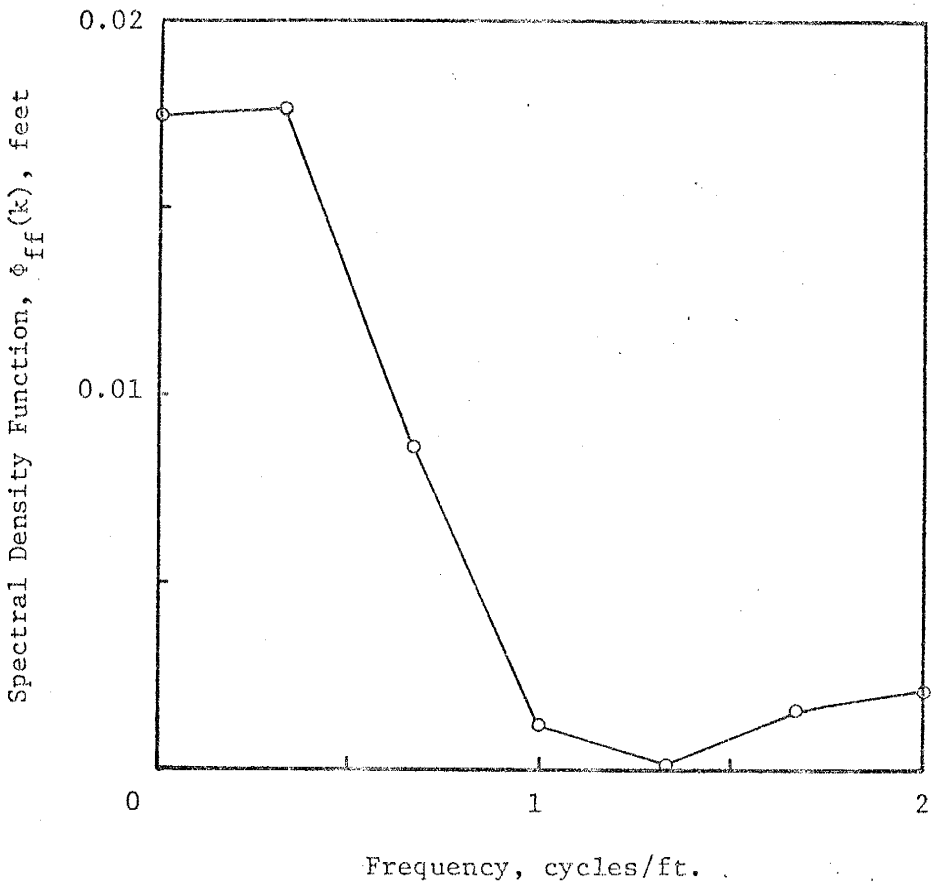

Fig. 5-17: Spectral density function of log permeability versus the frequency in cycles per foot for PR0006.

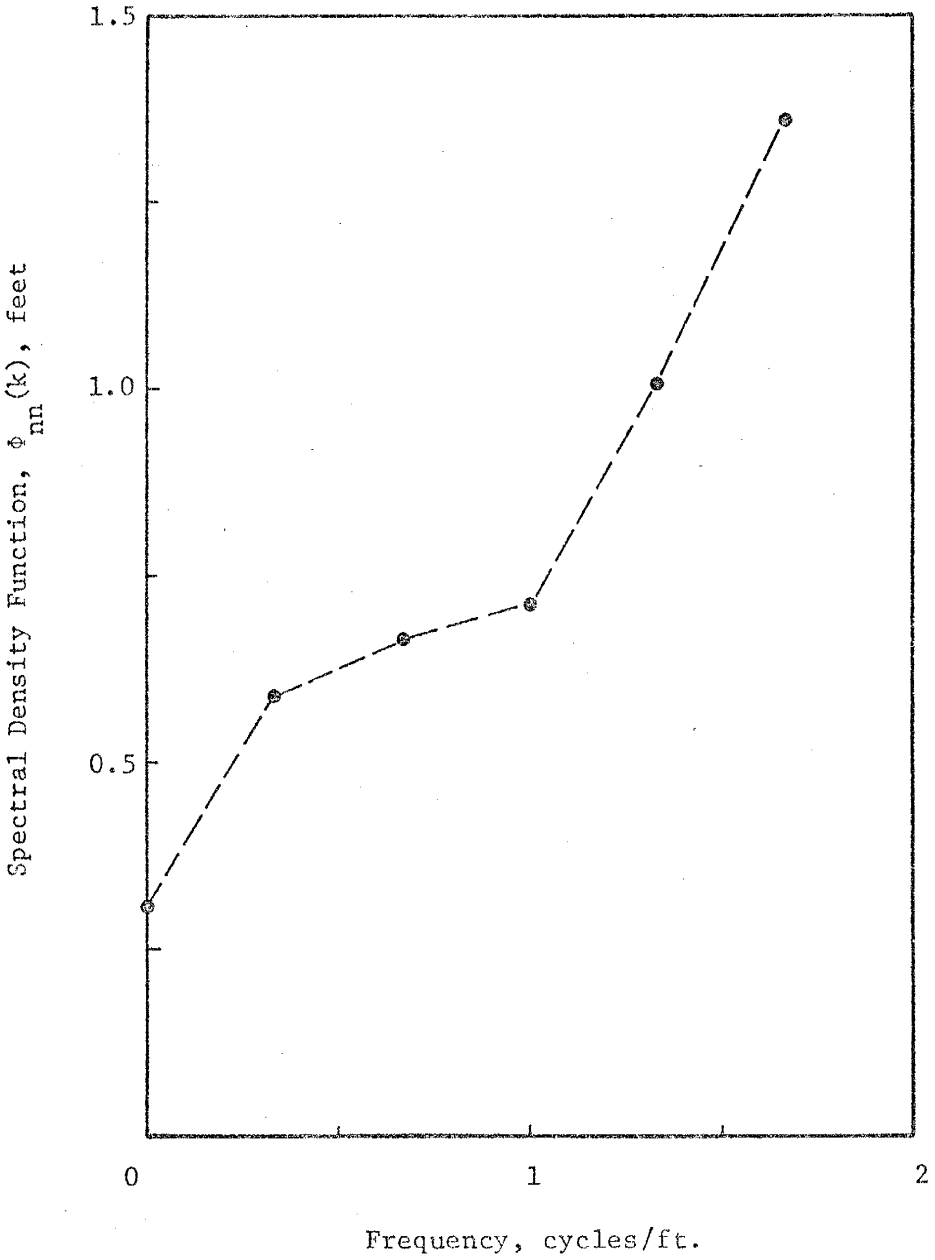

Fig. 5-18: Spectral density function of porosity versus the frequency in cycles per foot for PR0006.

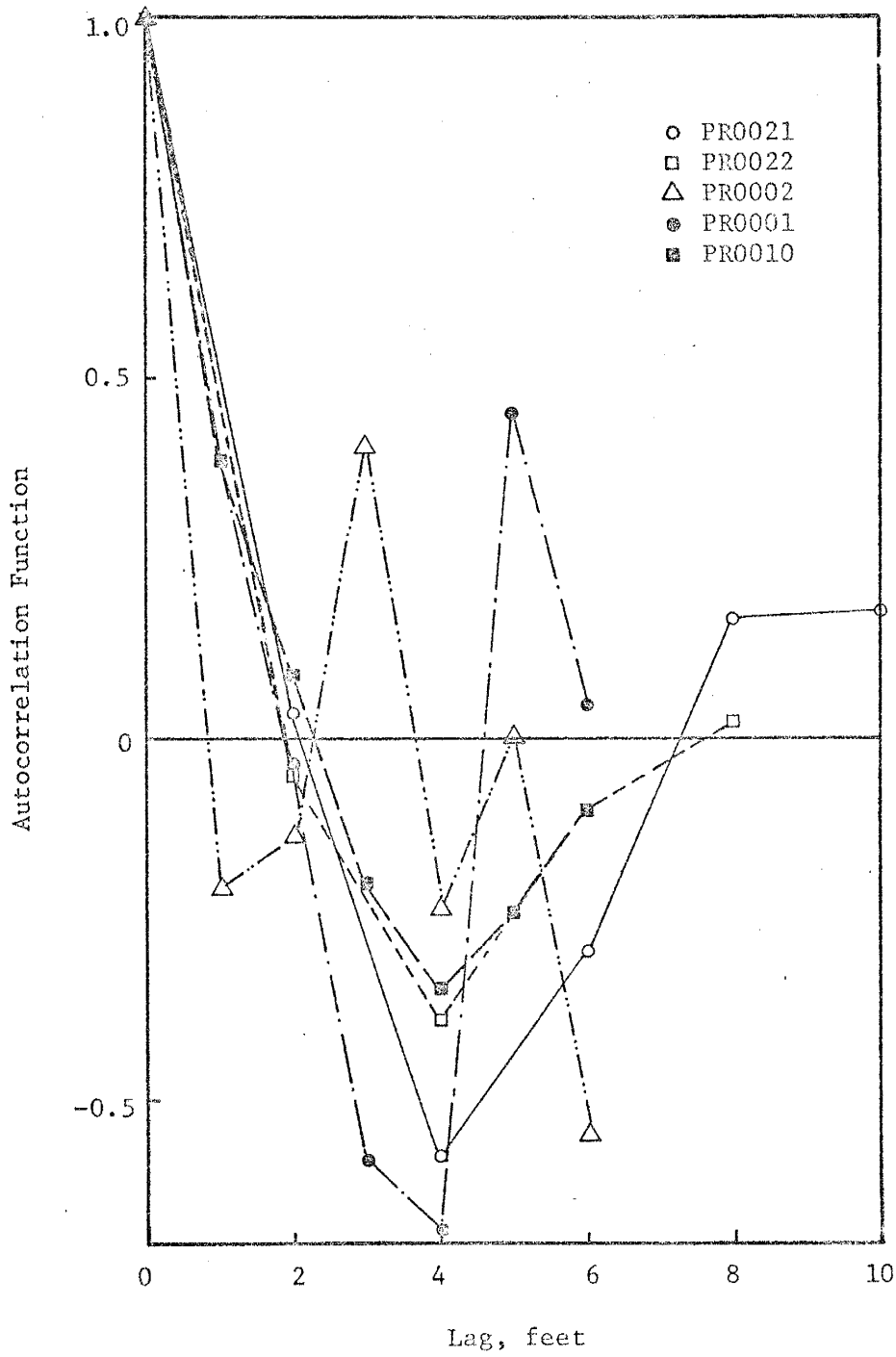

Fig. 5-19: Autocorrelation function of log permeability versus the lag in feet for a few data sets from Pryor (1973).

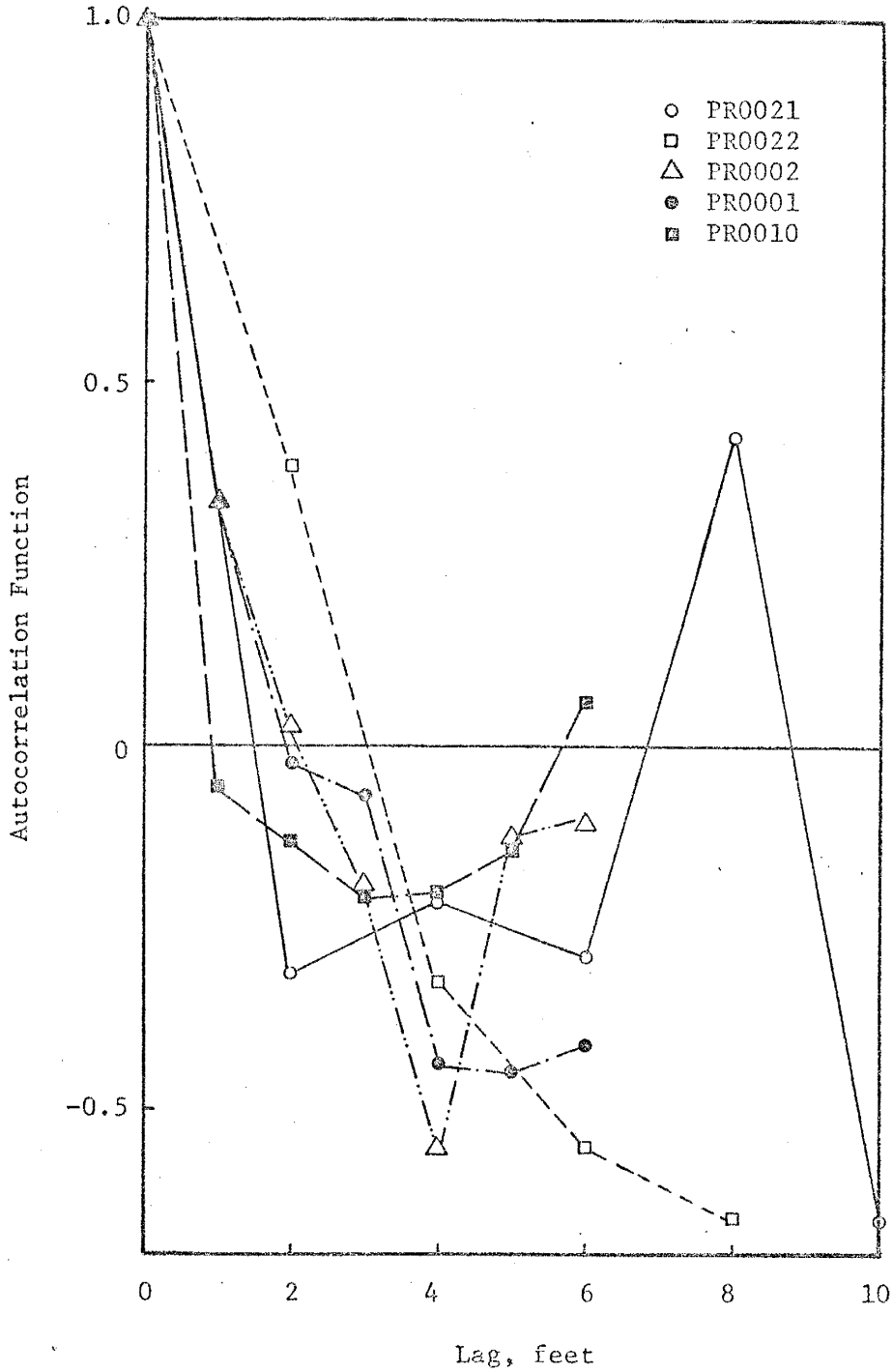

Fig. 5-20: Autocorrelation function of porosity versus the lag in feet for a few data sets from Pryor (1973).

functions that fluctuate in sign while the remaining data are positively correlated up to a distance ranging from about one to three feet and become negatively correlated thereafter. Spectral density functions of log permeability for the above data sets are depicted in figure 5-21 while figure 5-22 shows the spectral density functions of their porosity. Figure 5-21 indicates that all the log permeability spectra have a peak at small frequency with the exception of PR0002 where the peak is at large frequency. Similarly the porosity spectra all have peaks at low frequency except for PR0001 where the spectrum reaches a maximum at high frequency.

The sampling interval for the data discussed above was one foot for PR0001, PR0002, and PR0010 and two feet for PR0021 and PR0022. Figure 5-23 is a plot of the autocorrelation function for log permeability and porosity data from beaches (PR0034 and PR0035) sampled at 10 foot intervals. Neighboring permeability and porosity values are positively correlated up to a distance ranging from about eight feet up to about 22 feet. Only the autocorrelation function of porosity for PR0035 changes sign while the remaining data are characterized by autocorrelation functions that do not change sign once they became negative. The corresponding spectral density function for the above data sets are shown in figures 5-24 and 5-25 for log permeability and porosity data respectively. All spectra have a peak at low frequency indicating that the main contribution to the variance is found at low frequency.

Autocorrelation functions for log permeability of data from beaches (PR0024 and PR0025) sampled at 200 foot intervals and for data from dunes (PR0040 and PR0042) sampled at 400 foot intervals are shown in

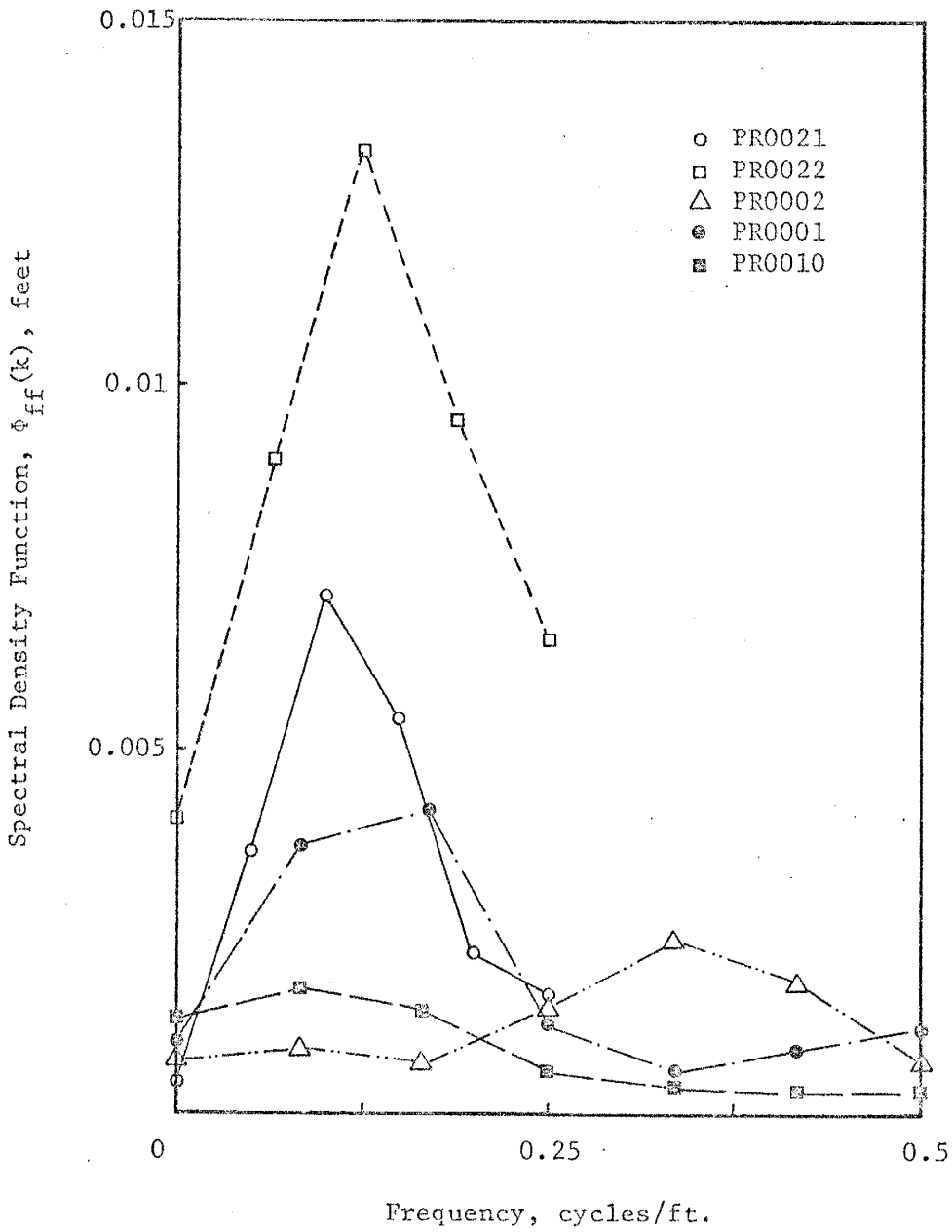

Fig. 5-21: Spectral density function of log permeability versus the frequency in cycles per foot for a few data sets from Pryor (1973).

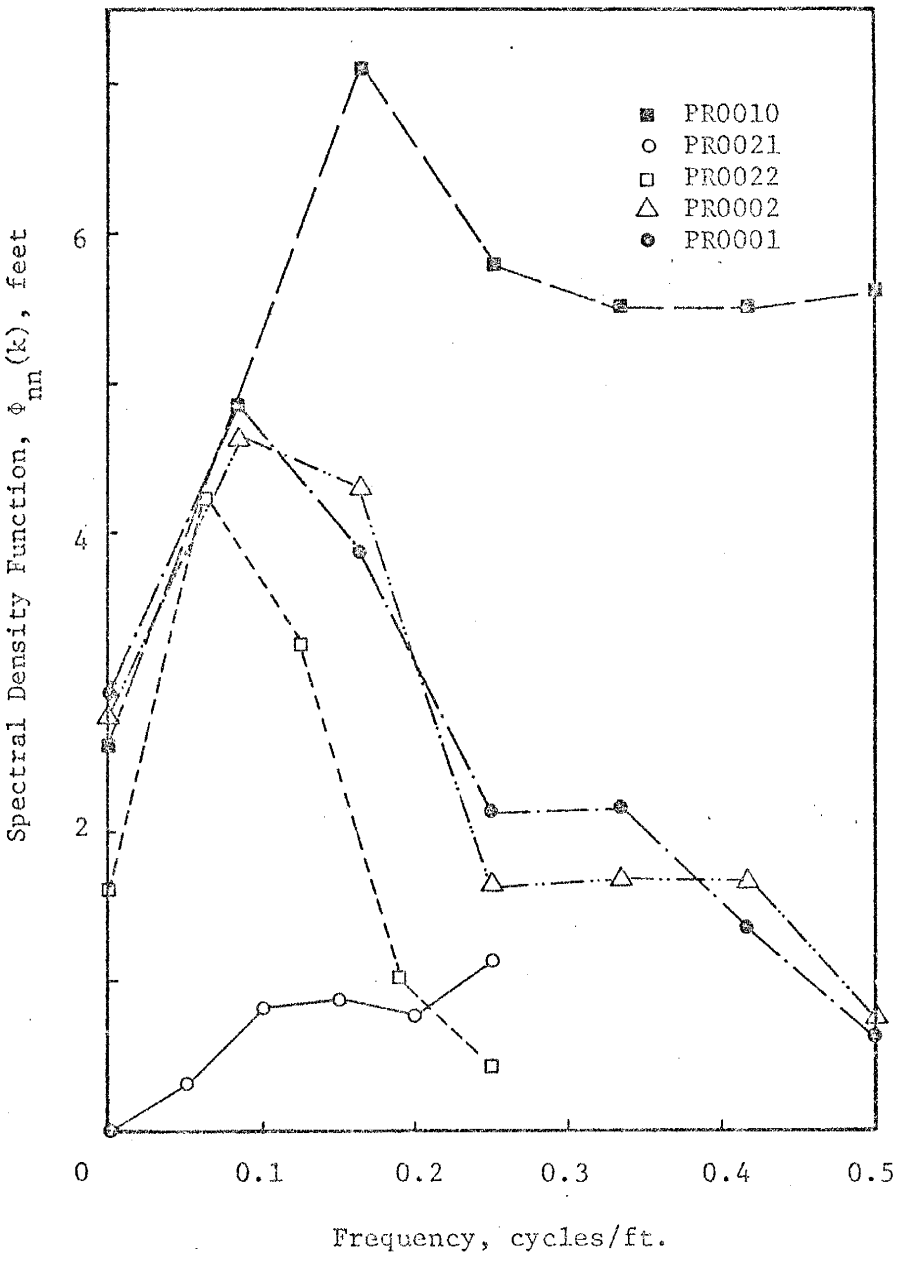

Fig. 5-22: Spectral density function of porosity versus the frequency in cycles per foot for a few data sets from Pryor (1973).

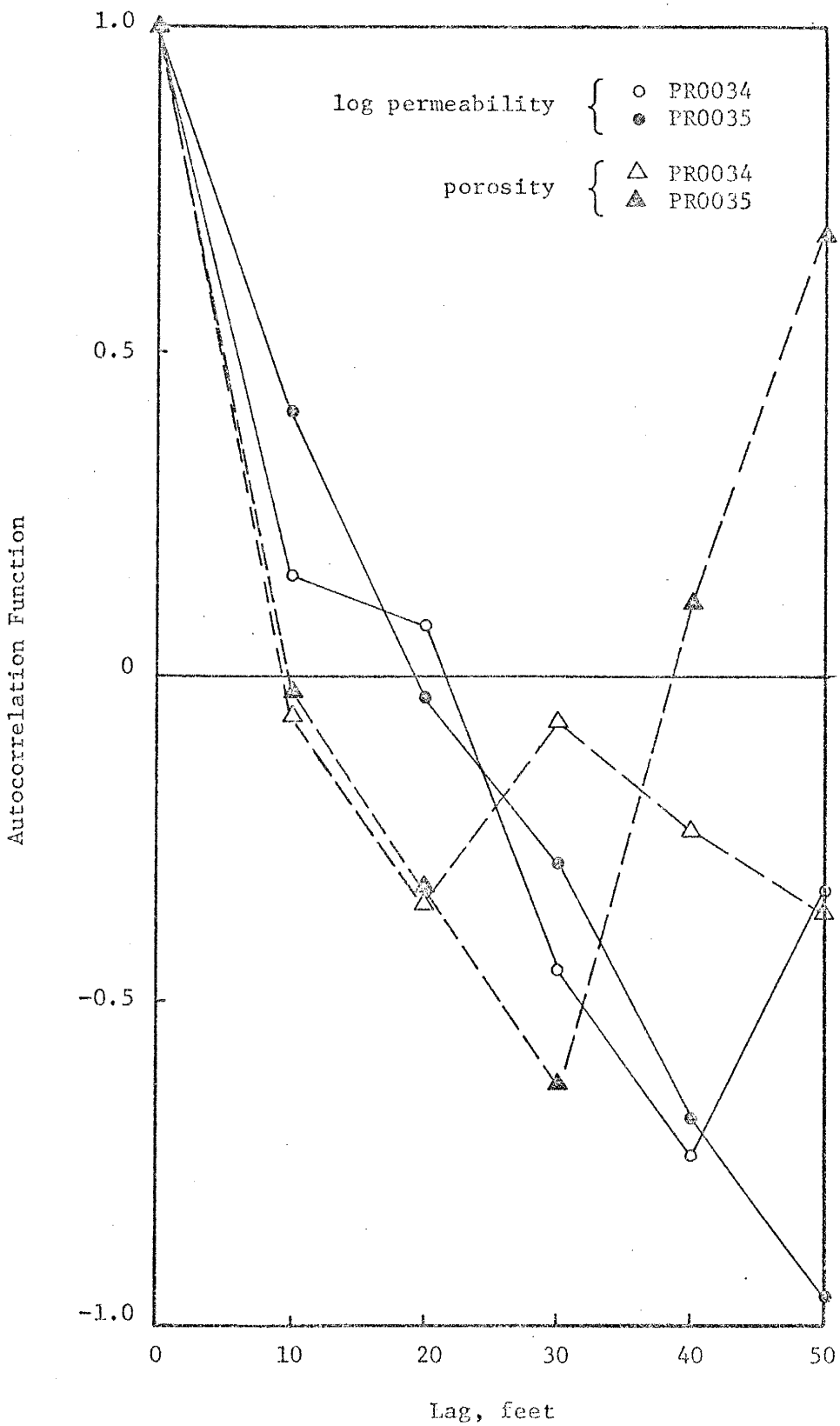

Fig. 5-23: Autocorrelation function of log permeability and porosity versus the lag in feet for PR0034 and PR0035.

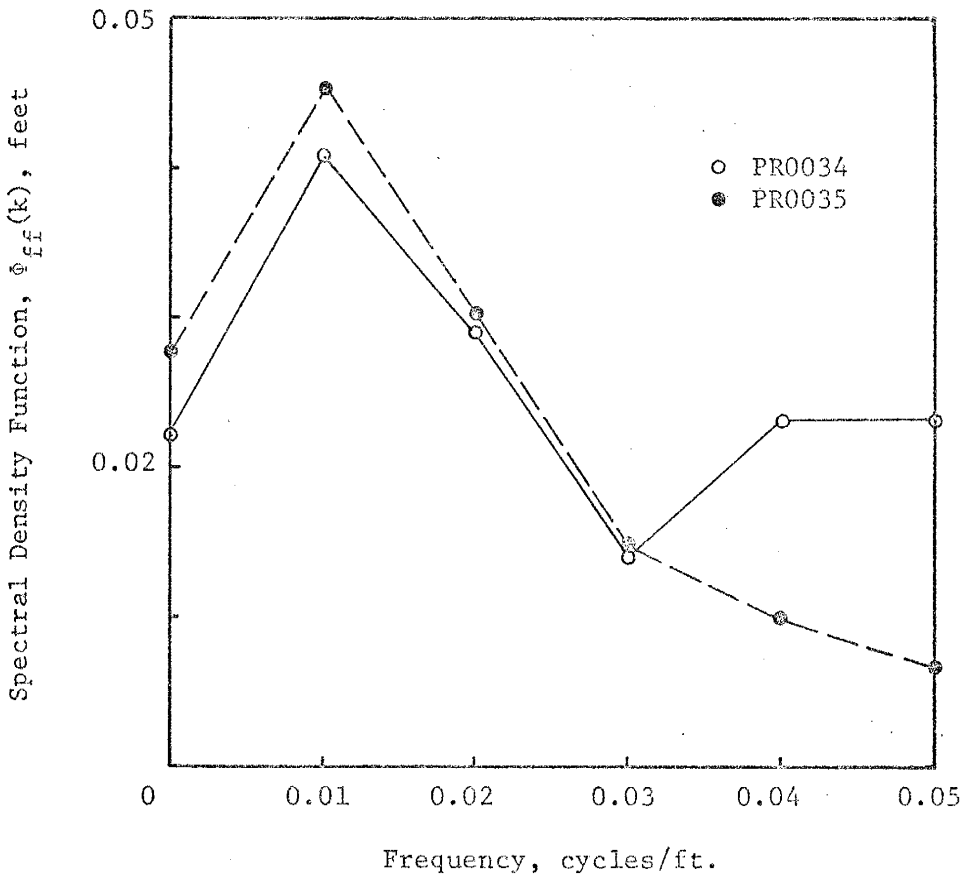

Fig. 5-24: Spectral density function of log permeability versus the frequency in cycles per foot for PR0034 and PR0035.

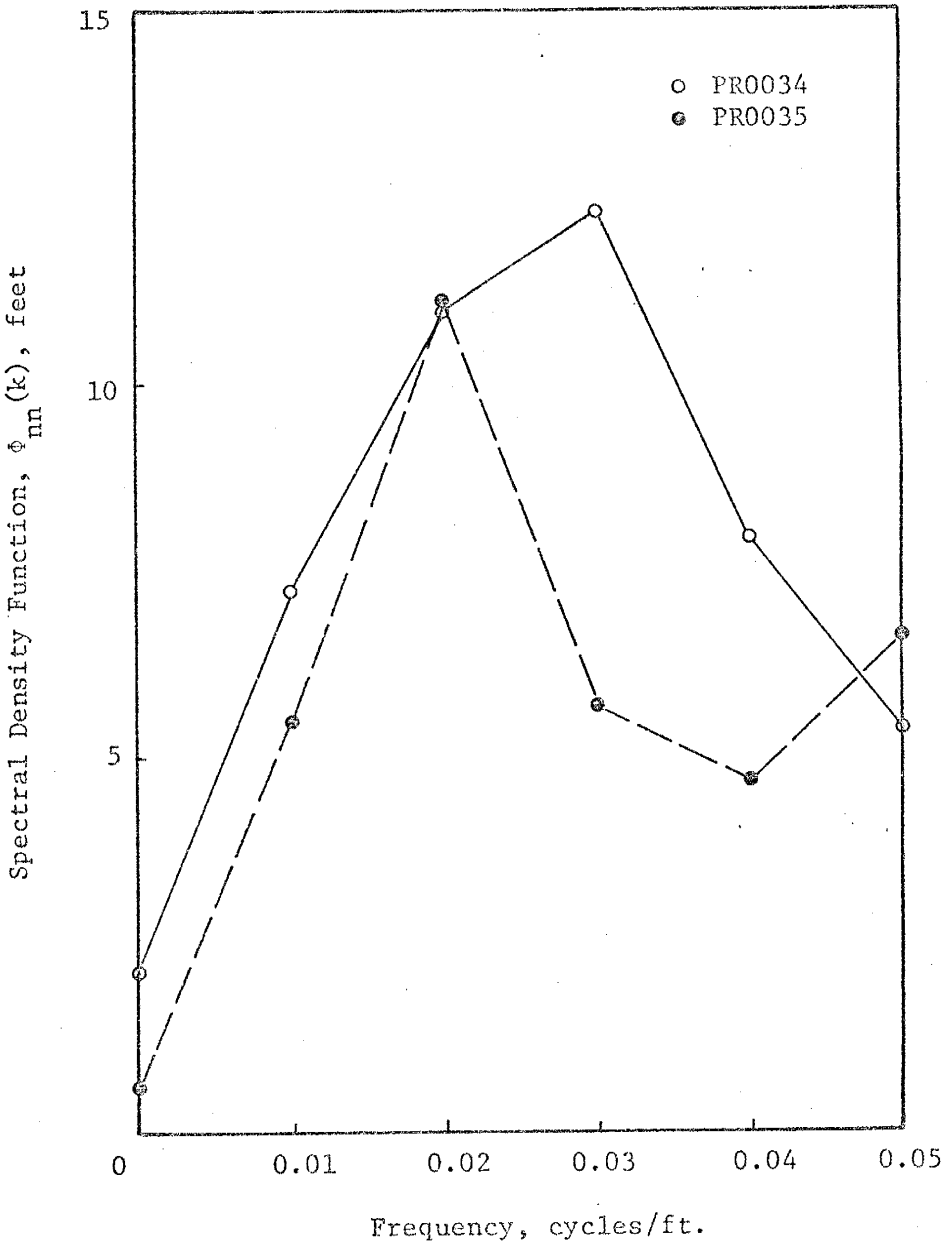

Fig. 5-25: Spectral density function of porosity versus the frequency in cycles per foot for PR0034 and PR0035.

figure 5-26. Neighboring permeability values are positively correlated up to a distance of about 150 feet for data from beaches and from 200 up to 600 feet for data from dunes. Only the autocorrelation function of PR0040 remains negative once it becomes so while the other data have correlation functions that fluctuate in sign. Figure 5-27 shows the autocorrelation functions of porosity for the data sets mentioned above. Porosity data from beaches and dunes are positively correlated up to a distance of about 300 feet.

Spectral density functions of log permeability for the data from beaches and dunes discussed above are presented in figure 5-28. Only the data of PR0040 are characterized by a spectrum that has a peak at small frequency while the remaining data have spectra that reach a maximum at large frequency. Figure 5-29 shows spectral density function of porosity for the same data sets appearing in figure 5-28. All spectra are characterized by a peak at small frequency with the exception of PR0042 whose spectrum reaches a maximum at large frequency.

In order to indicate the range of variation in the spectral estimates for the spectra discussed in this section, two confidence intervals computed (see Appendix-J) at 80% and 95% levels for two degrees of freedom are shown in figure 5-30. Note, however, that the statistical significance of these spectral results is quite limited due to the small number of data points used in the computations. It may be of interest to remark that the peak in the spectrum of log K, for instance, at the 95% level is not statistically different from the spectrum of white noise (which is constant over the whole frequency range) although the peak may be significant at the 80% level indicating some structure to the original series.

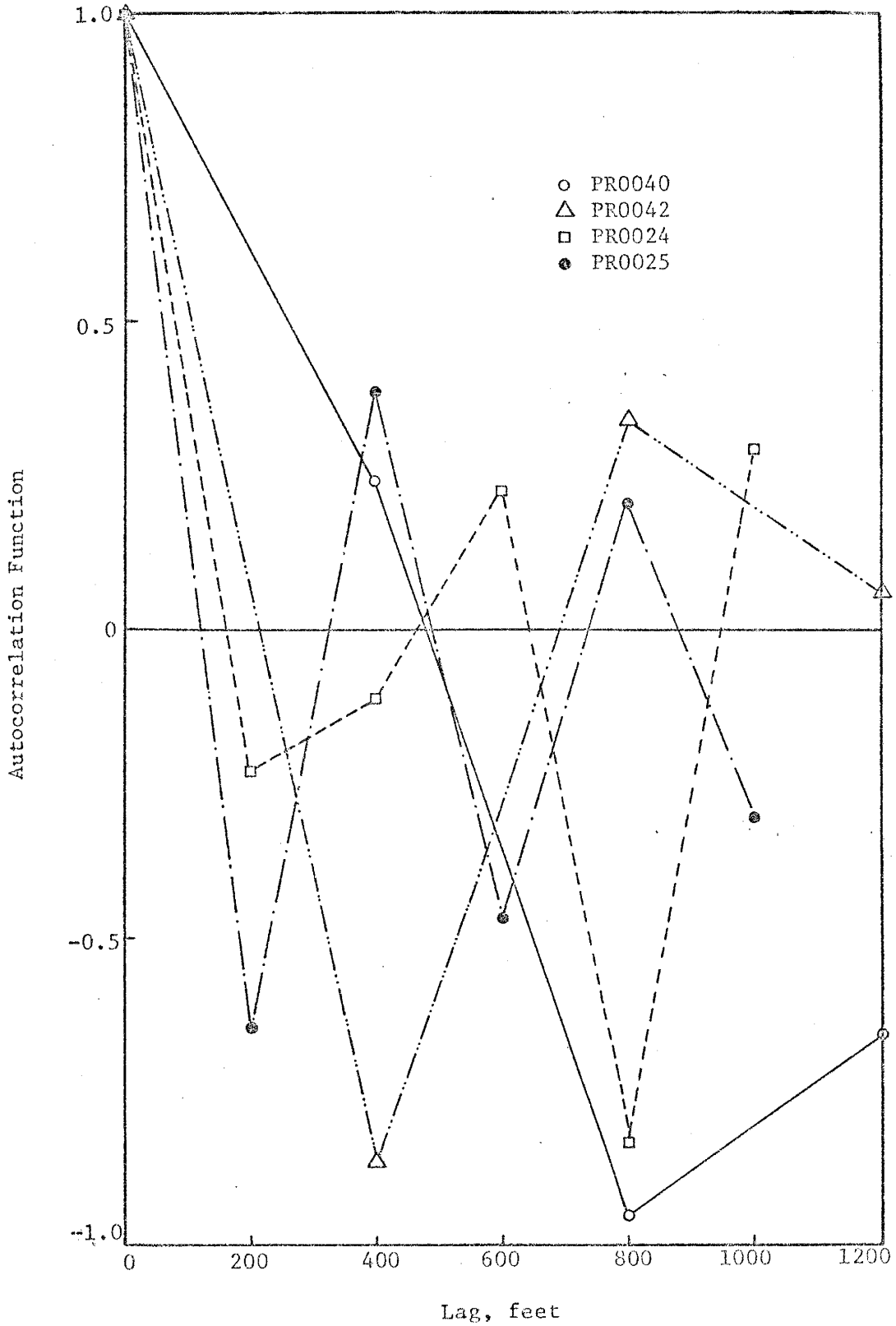

Fig. 5-26: Autocorrelation function of log permeability versus the lag in feet for a few data sets from Pryor (1973).

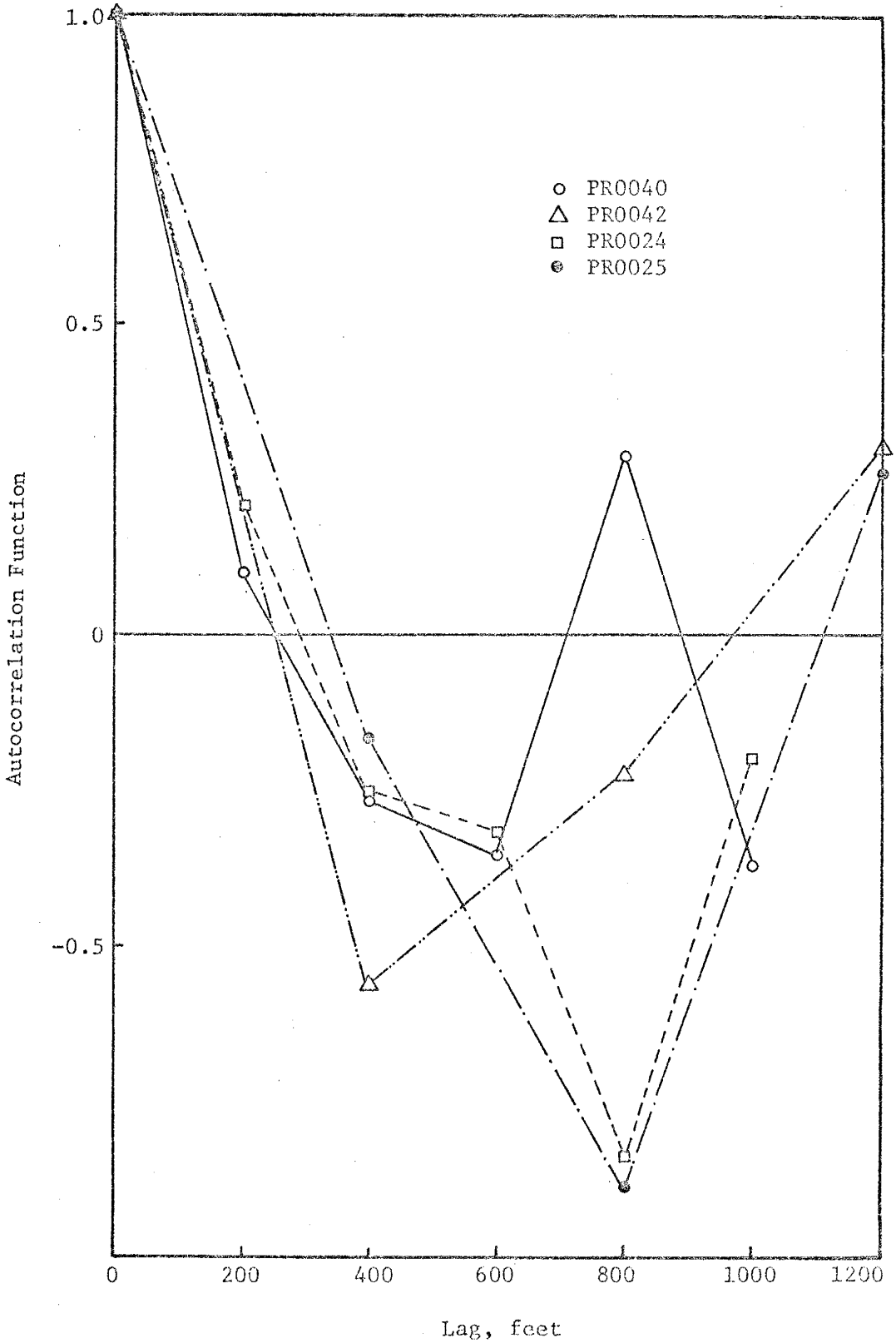

Fig. 5-27: Autocorrelation function of porosity versus the lag in feet for a few data sets from Pryor (1973).

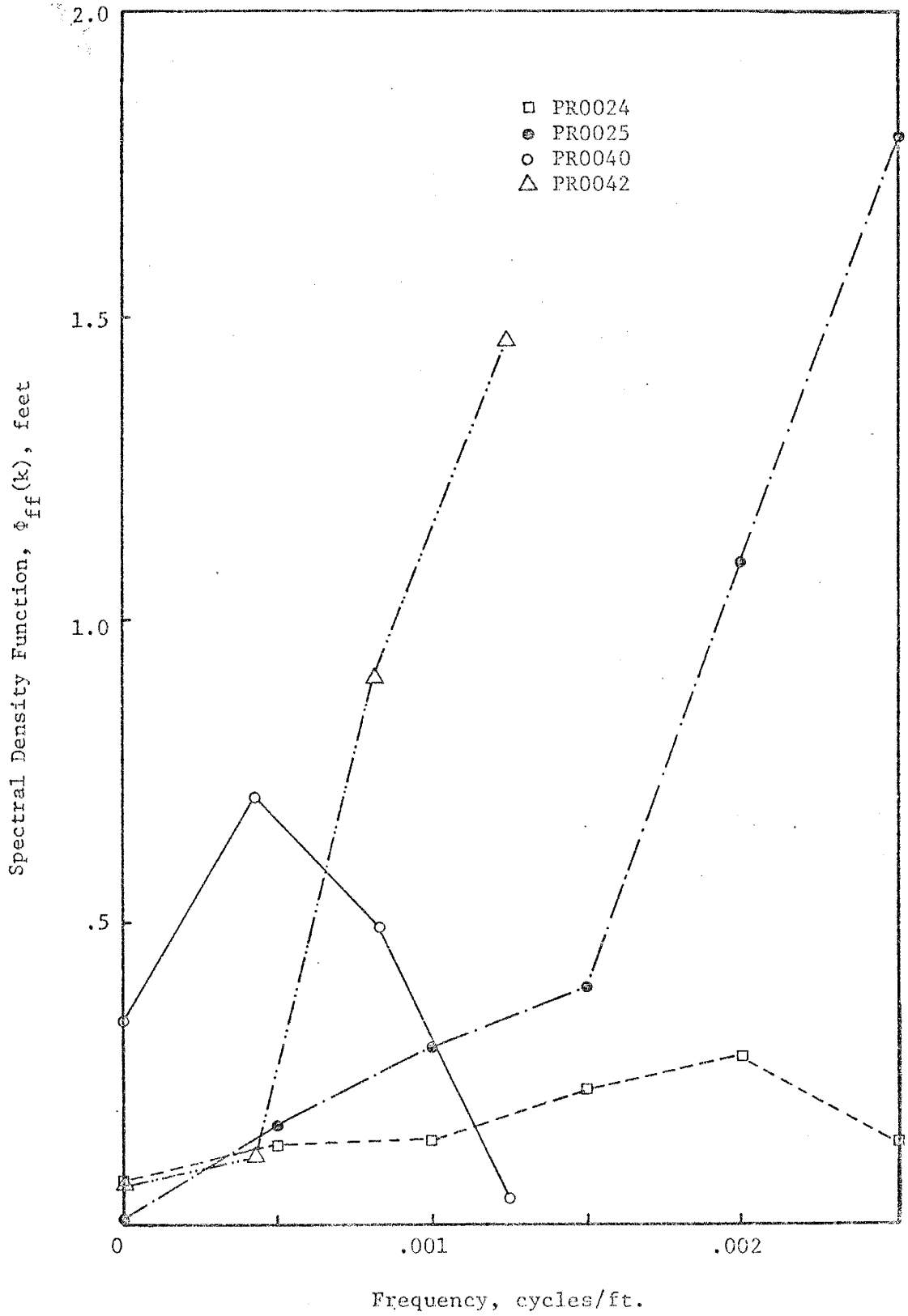

Fig. 5-28: Spectral density function of log permeability versus the frequency in cycles per foot for a few data sets from Pryor (1973).

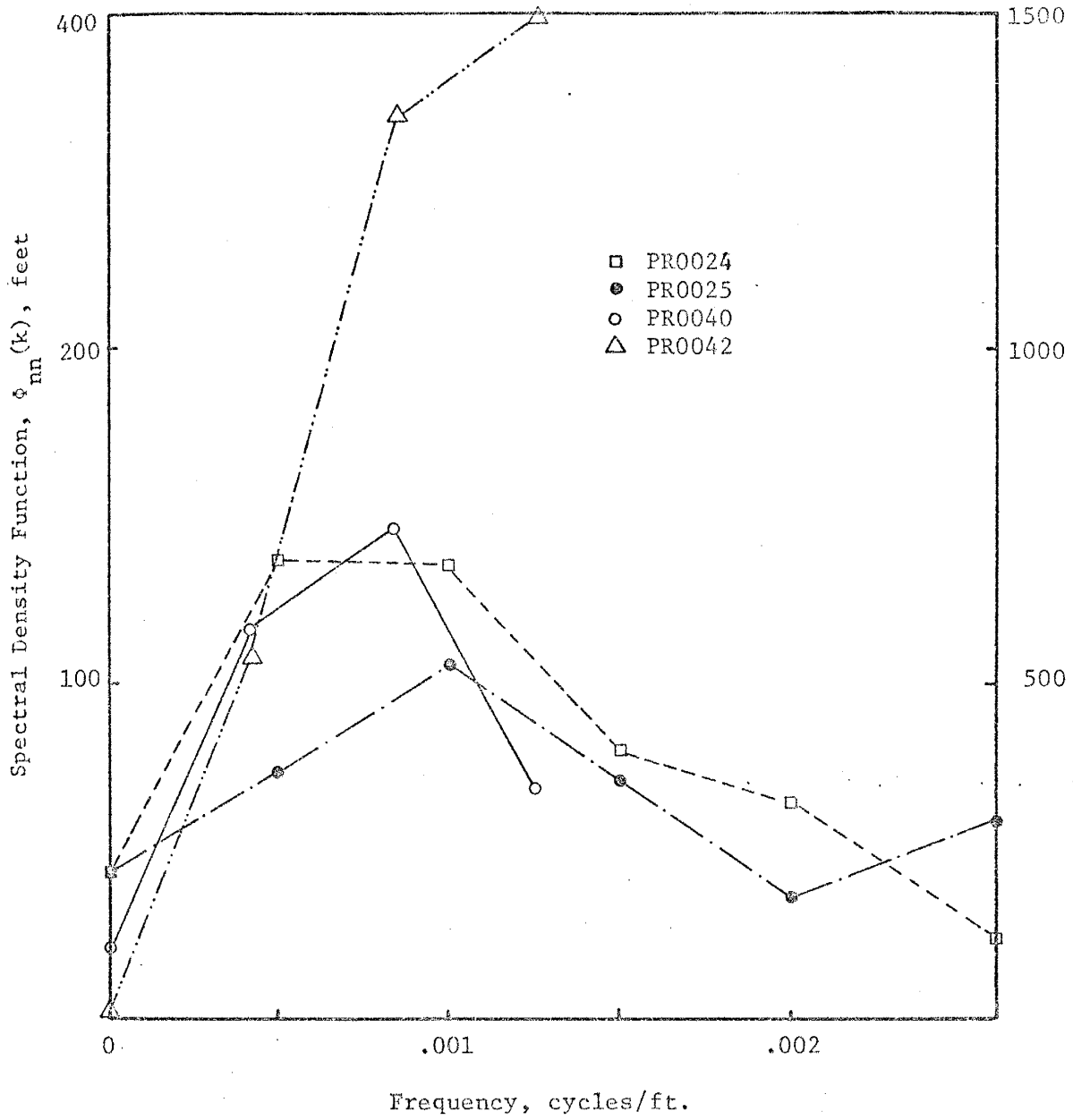

Fig. 5-29: Spectral density function of porosity versus the frequency in cycles per foot for a few data sets from Pryor (1973). The vertical scale to the right applies to PR0042.

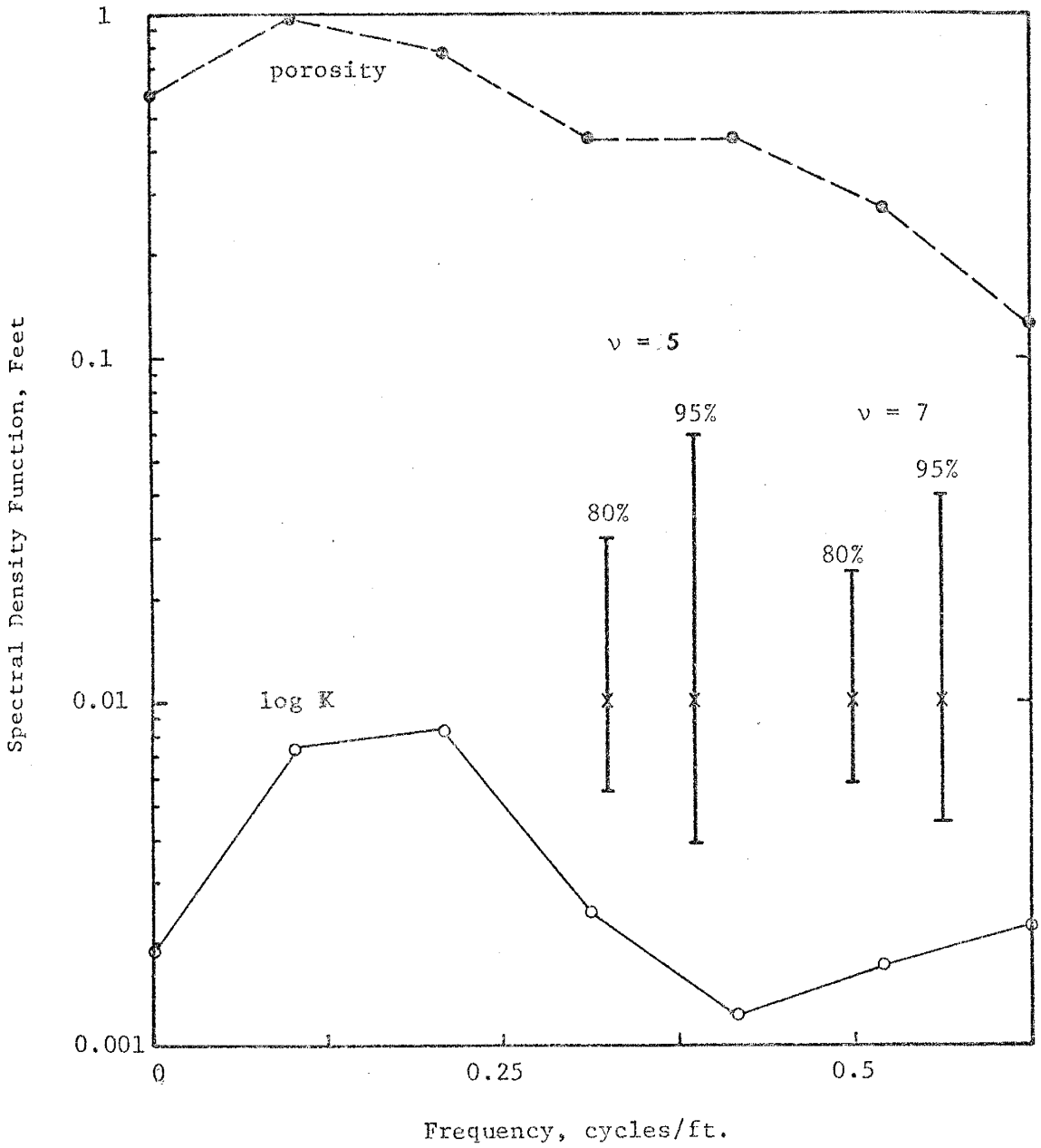

Fig. 5-30: Spectral density functions of log permeability and porosity of PR0001 and confidence intervals at 80% and 95% levels for two degrees of freedom are shown.

5.4 Comparison of the Autocorrelation Function of Field Data with the Theoretical Autocorrelation Functions

In this section we discuss the autocorrelation function of log permeability and porosity of core data from the Mt. Simon aquifer in northeastern Illinois in light of the theoretical autocorrelation function assumed to characterize correlation of neighboring fluctuations in ln K (see section 4.3). This is carried out using the integral scale discussed in section 2.5. In section 5.6 we discuss the significance and implications of the integral scale characterizing correlation between neighboring values of ln K.

It is of interest at this stage to examine how the assumed covariance function describing fluctuations in ln K fits estimated covariances for permeability and porosity field data. Assuming that the three-dimensional autocorrelation function is a reasonable model to fit such data, we proceed to evaluate their integral scales, λ. This autocorrelation function is obtained by dividing (4.11) from section 4.3 by the variance $\overline{f'^2}$, i. e.

$$\rho_{ff}(\xi) = e^{-\gamma\xi} \quad ; \quad \gamma = 1/\lambda$$

Taking the natural logarithm of both sides we obtain

$$\ln \rho = -\gamma\xi$$

or $2.3 \log_{10} \rho = -\gamma\xi$

which can be written as

$$\xi = -\frac{2.3}{\gamma} \log_{10} \rho$$

This represents an equation for a straight line of the form

$$Y = m \log x$$

where m is the slope. Plotting the autocorrelation on a logarithmic scale versus the separation ξ on a linear scale, a straight line is obtained whose slope determines the integral scale. This procedure is illustrated in figure 5-31 for a few data sets.

Values of the integral scale for several sets of porosity and log permeability (both horizontal and vertical) core data from the Mt. Simon aquifer in northeastern Illinois (see Appendix-G) were obtained following the method described above and are listed in Table 5.1. Figure 5-32 shows the autocorrelation of the log of horizontal permeability of Illinois data while figure 5-33 shows the autocorrelation of the log of vertical permeability of the same data; both are plotted against dimensionless lag ξ/λ. The solid curve on both figures is the negative exponential representing the autocorrelation function characterizing fluctuations in ln K. The agreement between the theory and field data is reasonable indicating that the negative exponential is an appropriate model to describe correlation of hydraulic conductivity of field data. Note that in section 6.3.1 it is shown that one way to compare the autocorrelation function of ln K in one dimension to its counterpart in three dimensions is to equate their slopes at the origin; this requires $\gamma = 2a$. However, graphical inspection of both autocorrelation functions showed that $\gamma = 2.5a$ offered a better fit between them. Consequently, the one-dimensional autocorrelation is evaluated using a value of $\gamma = 2.5a$ and is shown by the dashed curve in figures 5-32 and 5-33. However, the dashed curve does not fit the field data as well as the negative exponential. Figure 5-34 is a plot of the autocorrelation function of porosity versus ξ/λ for the samples used in

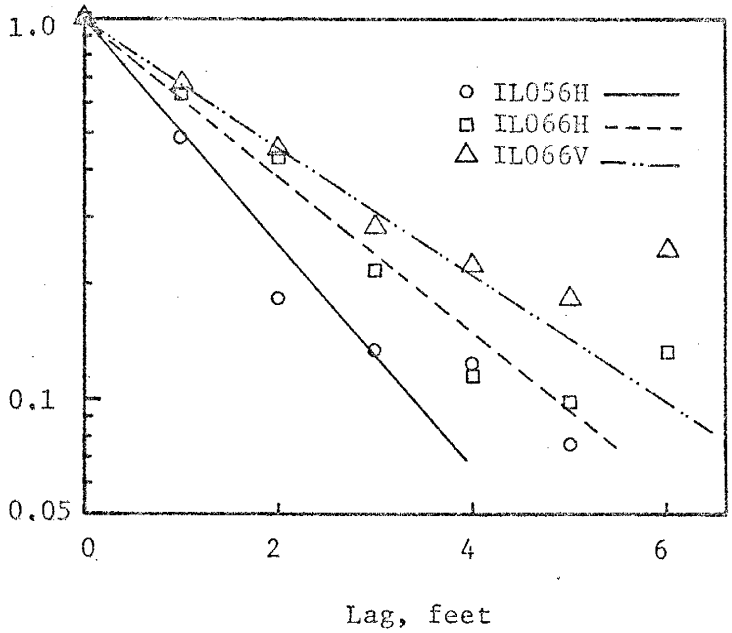

Fig. 5-31: A plot of the logarithm of the autocorrelation function of log permeability data from the Mt. Simon aquifer versus the lag in feet. The straight lines are based on visual fit. Autocorrelation values beyond 4 lags were ignored.

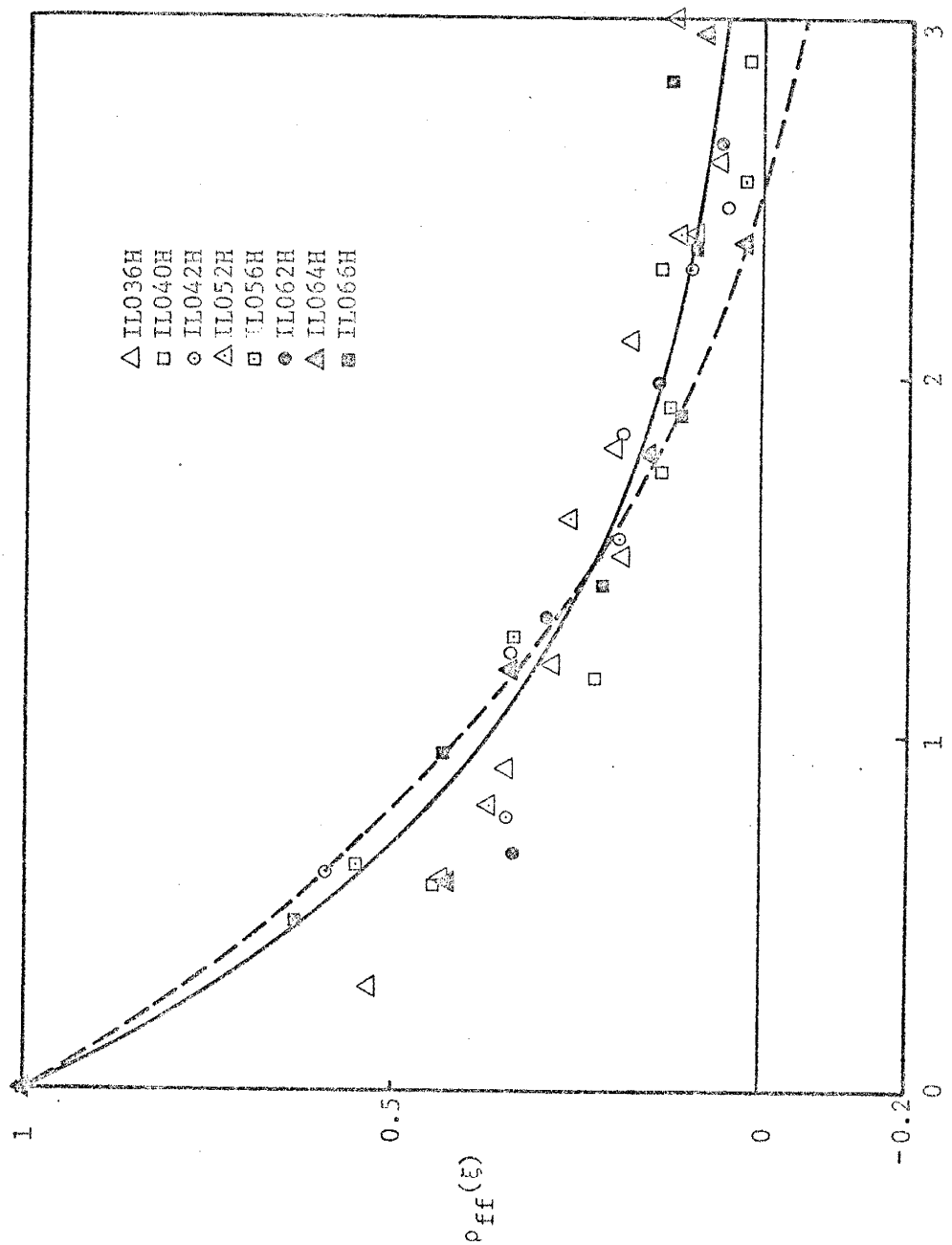

Fig. 5-32: Autocorrelation function of the log of horizontal permeability versus the dimensionless lag (the dashed and solid curves are the one- and three-dimensional theoretical autocorrelation functions respectively).

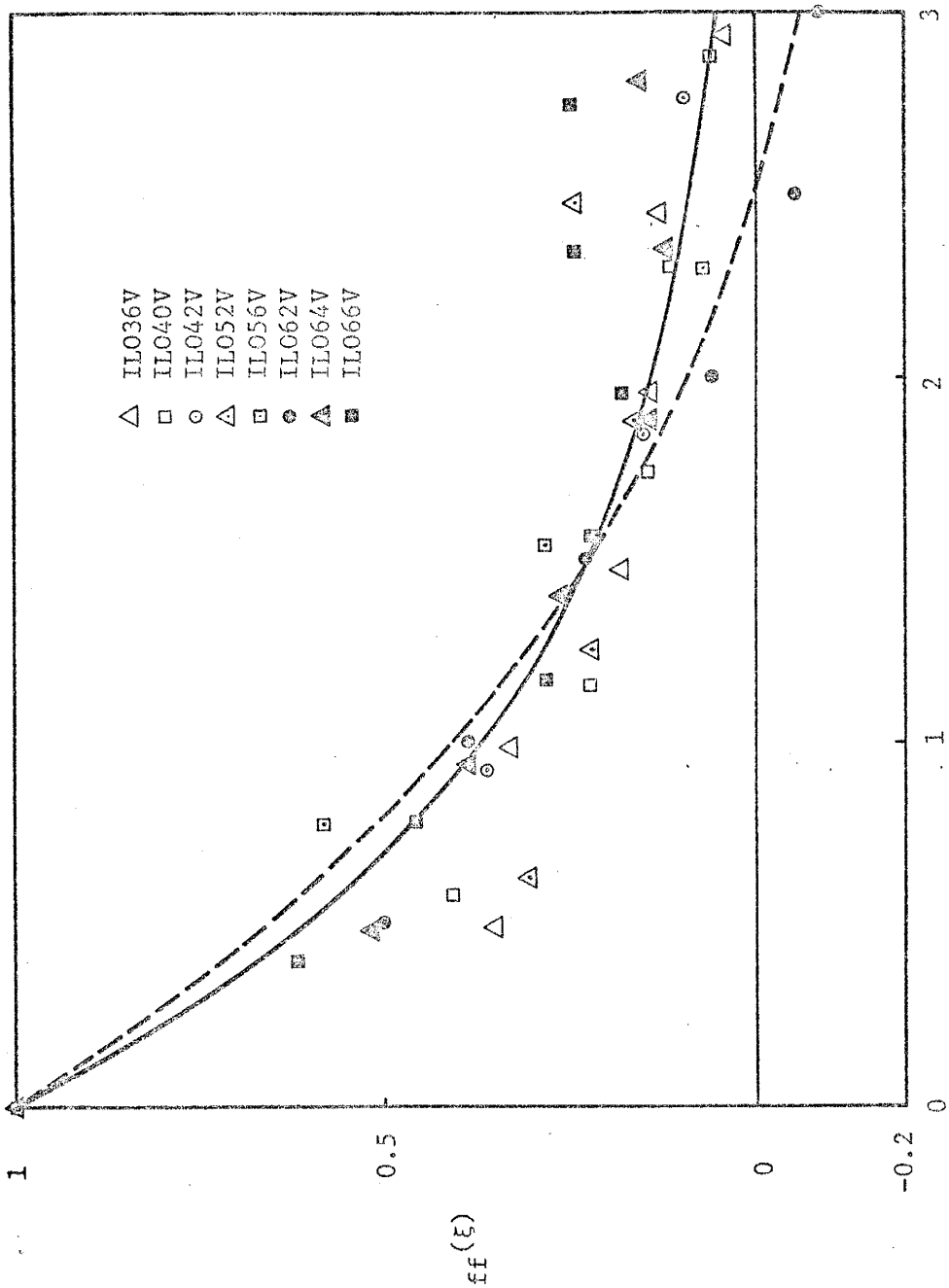

Fig. 5-33: Autocorrelation function of the log of vertical permeability versus the dimensionless lag (dashed and solid curves represent 1-D and 3-D theoretical autocorrelation functions respectively).

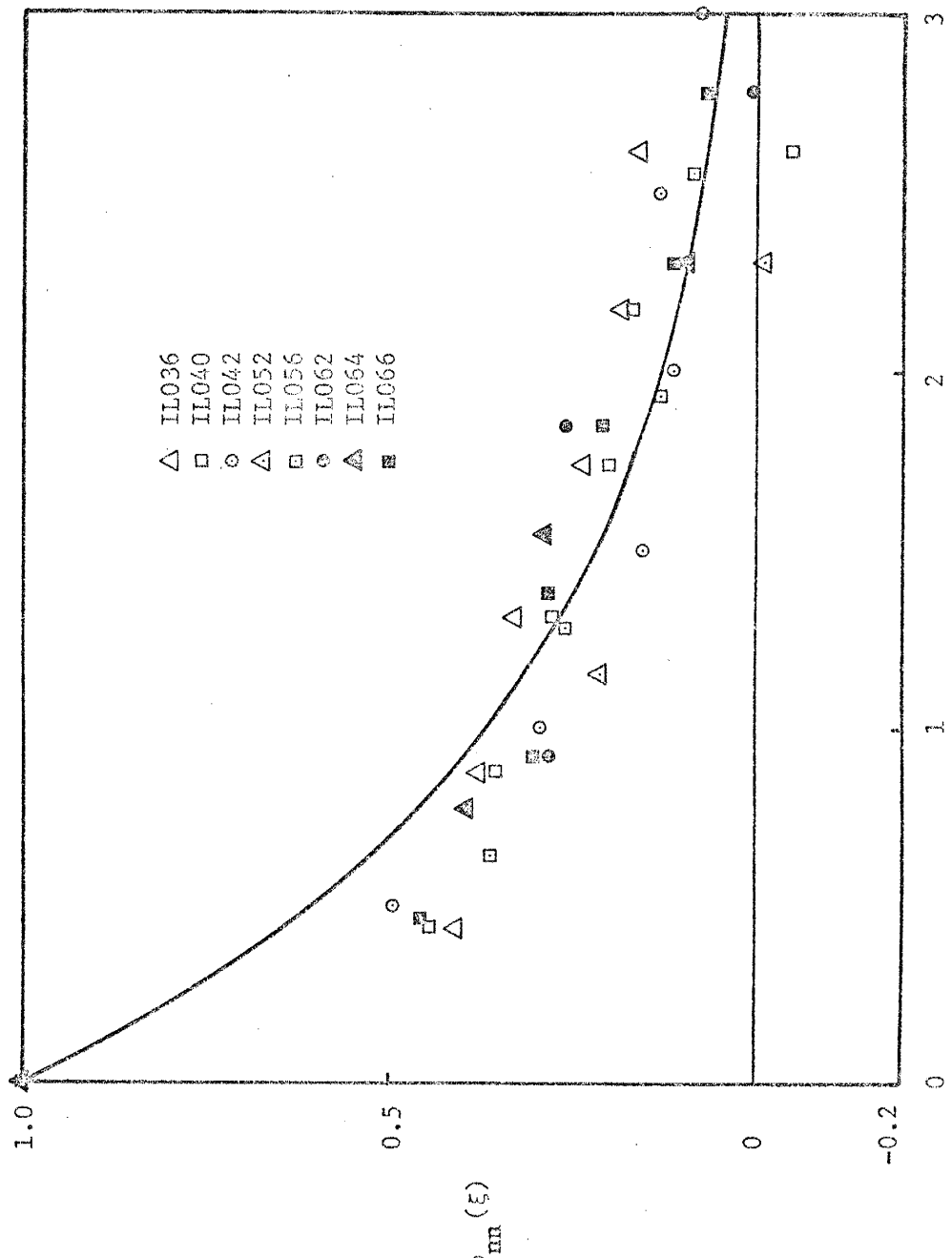

Fig. 5-34: Autocorrelation function of porosity versus the dimensionless lag (solid curve shows the theoretical three-dimensional autocorrelation function).

constructing figures 5-32 and 5-33. The agreement of the values of the autocorrelation function of porosity data with the theoretical values (solid curve) is also evident from figure 5-34. Porosity and permeability data used in constructing figures 5-32 through 5-34 are listed in Appendix-F.

The fact that the negative exponential requiring an integral scale for fluctuations of ln K fits field data reasonably well indicates that the integral scale is a valid concept, and that the negative exponential function is appropriate for the description of correlation of neighboring fluctuations in ln K. That the range of variation in the integral scale (see Table 5.1) of data obtained from different horizons of the same aquifer is small demonstrates the consistency of this parameter.

5.5 Comparison of the Spectra of Field Data with the Theoretical Spectra

In the previous section we compared the theoretical autocovariance with that of porosity and permeability field data. In this section we wish to examine the spectral estimates compared with the spectra from the assumed models representing fluctuations of porosity and permeability. The subsequent discussion and graphs are based on a few of the data sets though the remarks and conclusions we make here are pertinent to the remaining data.

Rewriting the expression for the spectrum $\Phi_{ff}(k)$ resulting from solving the problem of groundwater flow in one dimension and given by (3.40) from section 3.3.3, leads to

$$\Phi_{ff}(k) = \frac{2\,\overline{f'^2}\,(k/a)^2}{\pi a[1 + (k/a)^2]^2} \qquad (5.5)$$

Equation (5.5) is evaluated for different values of the dimensionless wave number k/a, where the relationship $\gamma = 2.5a$ mentioned in section 5.4 was used, and the results are shown in figure 5-35. Furthermore, the spectrum $\Phi_{ff}^{(1)}$ characterizing fluctuations in the log of permeability resulting from solving the problem of groundwater flow in three dimensions and given by (see (6.14) of section 6.3.1)

$$\Phi_{ff}^{(1)}(k_1) = \frac{\overline{f'^2}}{\pi\gamma[1 + (k_1/\gamma)^2]} \qquad (5.6)$$

is evaluated for different values of the variable k/γ and the results are illustrated in figure 5-36.

In order to compare the spectra of permeability field data to the theoretical spectra represented by (5.5) and (5.6) the spectra of field data are plotted on similar semi-logarithmic papers as depicted in figures 5-37 through 5-39. To determine the location of the peak of the spectrum of figure 5-35, we differentiate (5.5) with respect to the wave number and equate the resulting expression to zero. To obtain the match point for the spectrum of figure 5-36, (5.6) is evaluated at zero wave number. Table 5.3 gives a summary of the match points for the data used in this section.

Figures 5-37 and 5-38 indicate that the spectrum given by (5.6) fits the spectrum of field data slightly better than that given by (5.5). However, within the confidence band at the 80% level for the spectral estimates shown in these figures both curves of the different theoretical spectra can represent the spectrum of field data rather well especially at low frequency or wave number. Figure 5-39, however, shows that the spectrum given by (5.5) fits the spectrum of field data

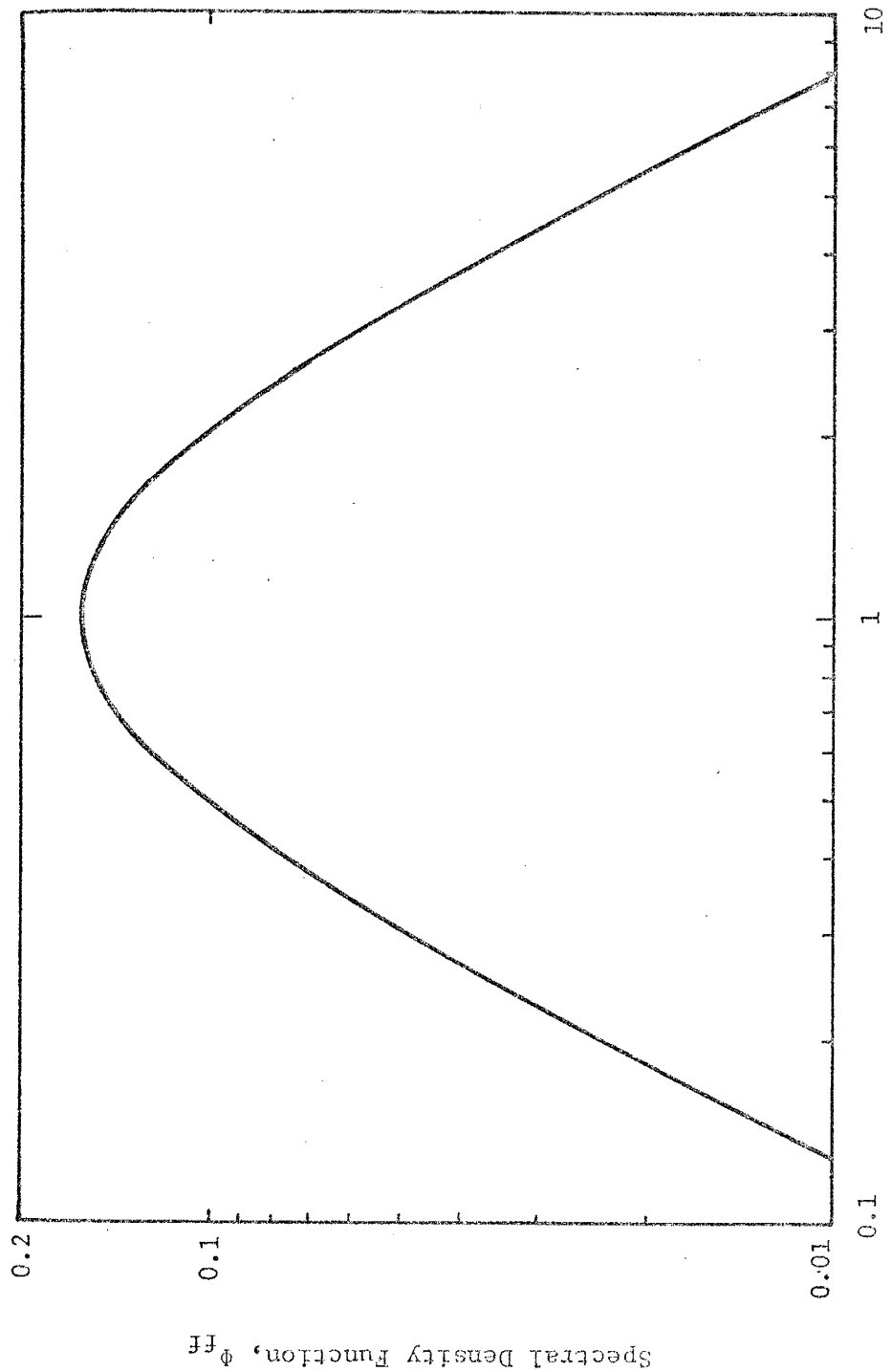

Fig. 5-35: Theoretical spectrum of fluctuations in log permeability resulting from the solution of the problem of flow in one dimension given by (5.5).

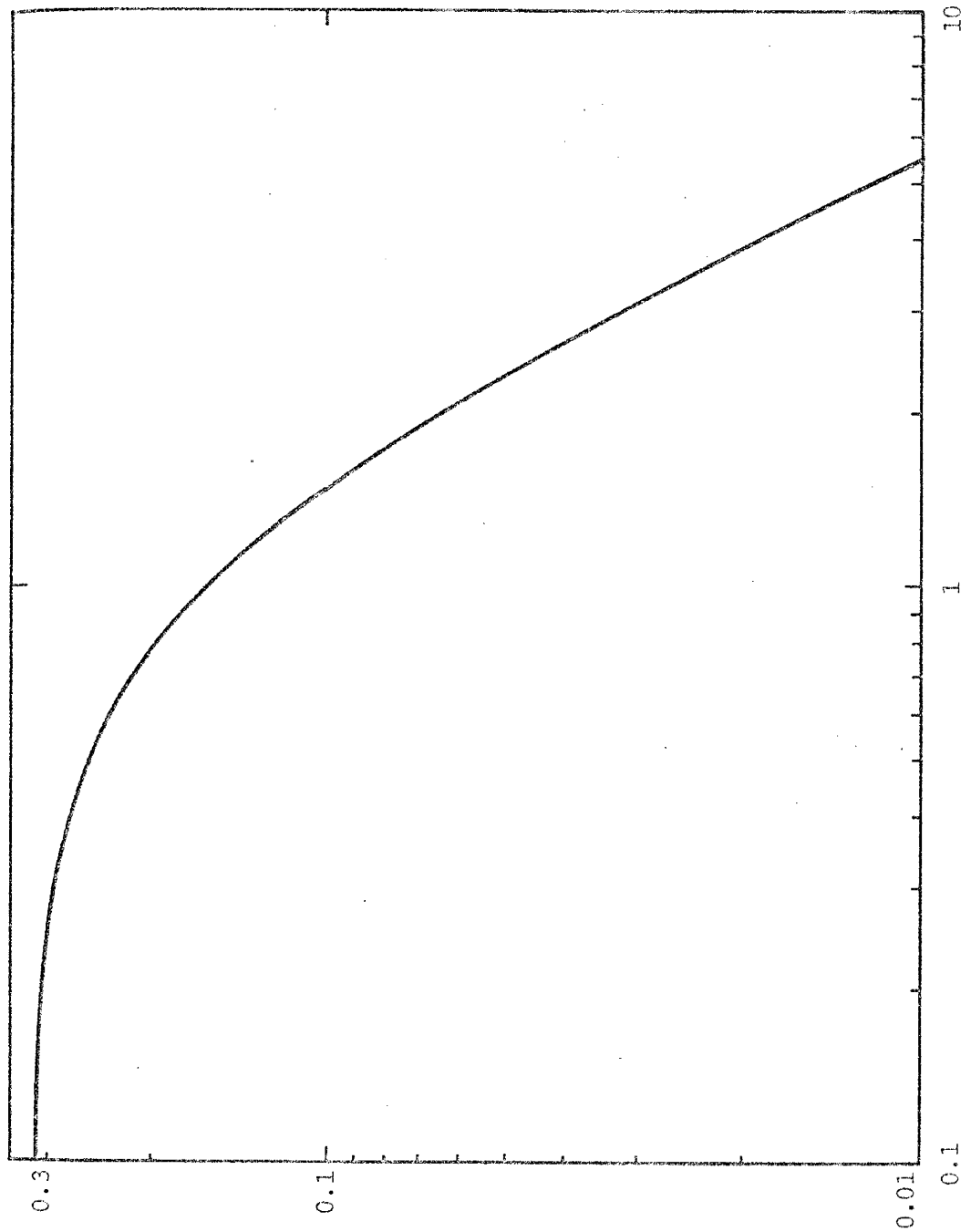

Fig. 5-36: Theoretical spectrum of fluctuations in log permeability resulting from the solution of the problem of flow in three dimensions given by (5.6).

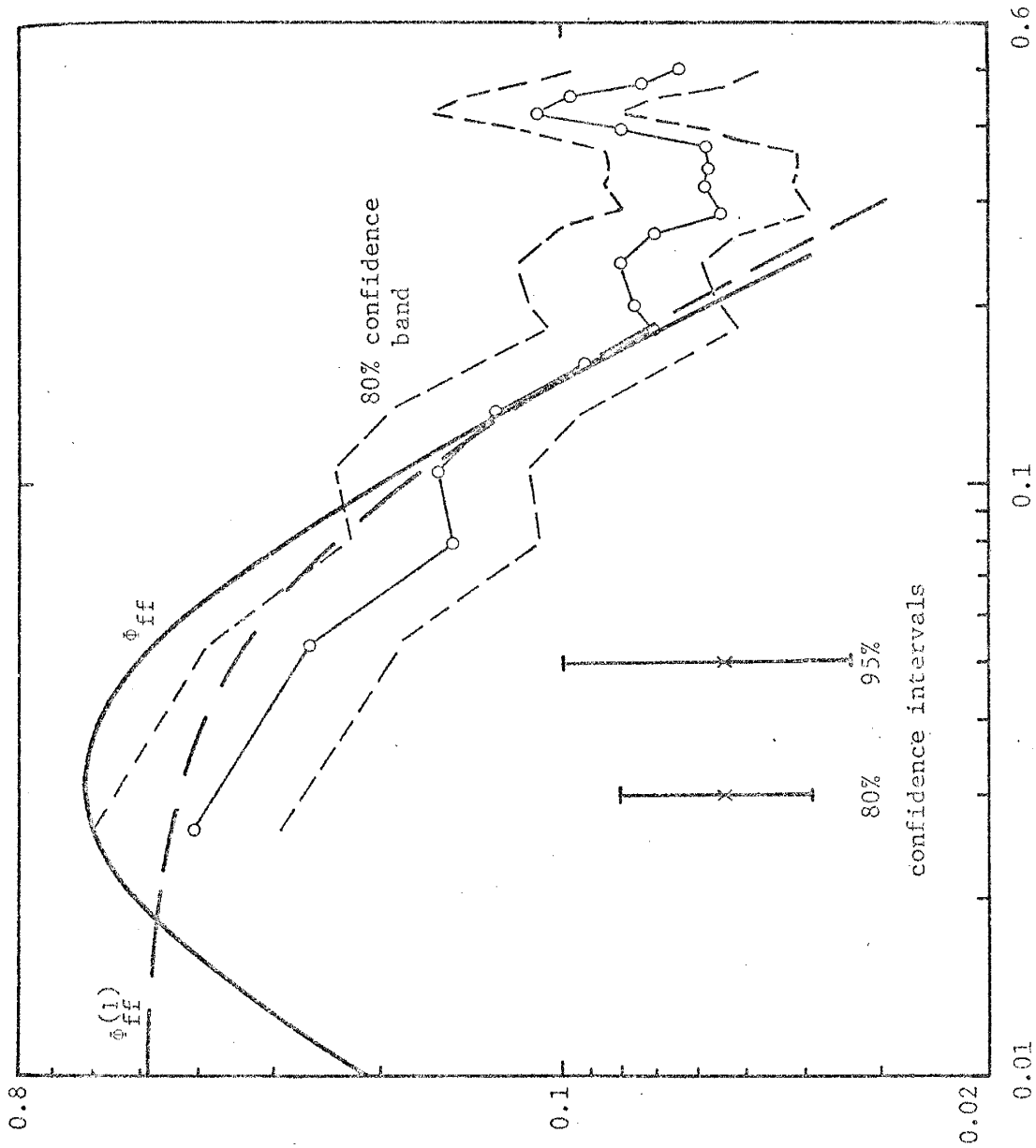

Fig. 5-37: Fit between theoretical spectra and the spectrum of log permeability of field data for set no. IL036V (represented by circles).

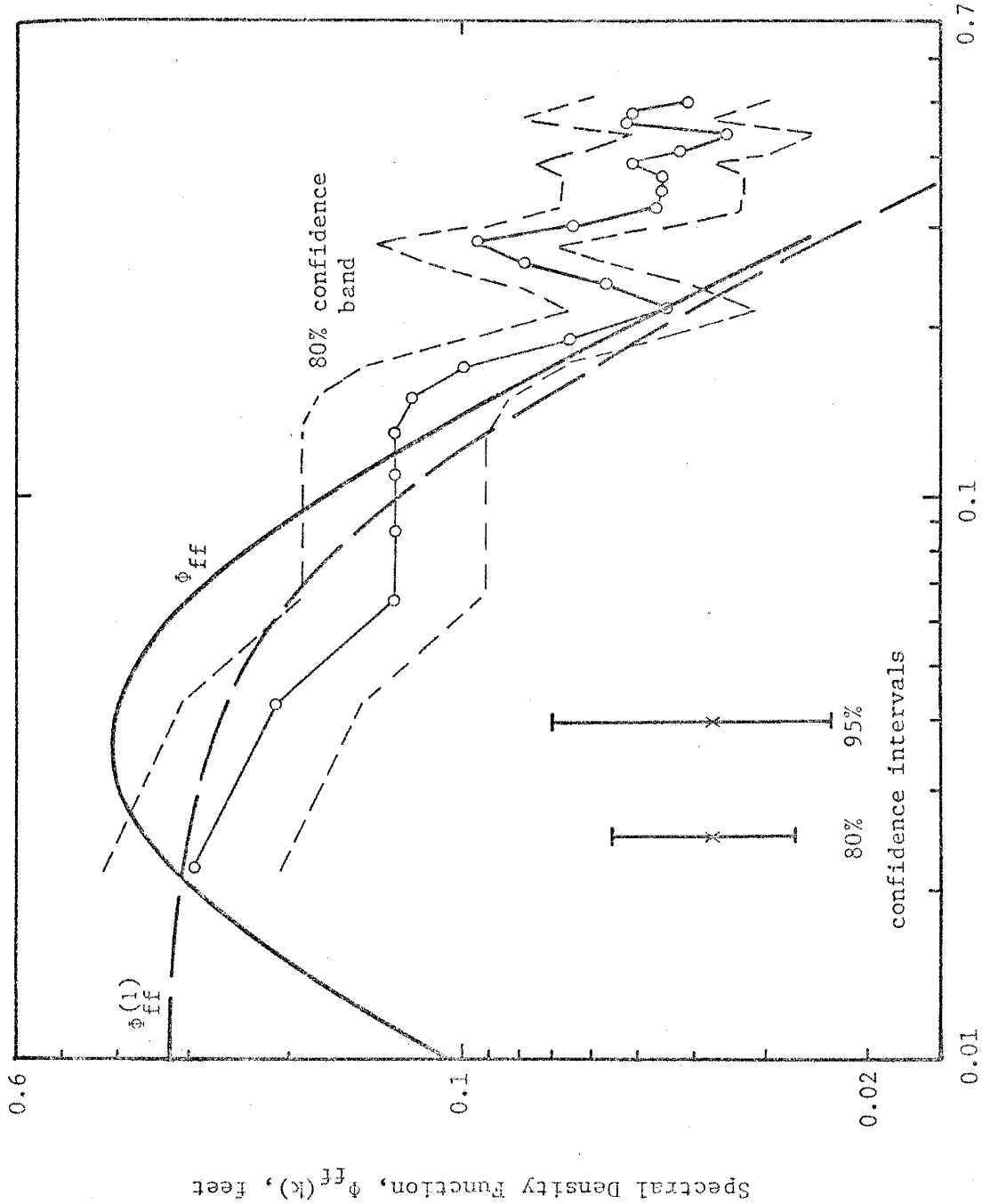

Fig. 5-38: Fit between theoretical spectra and the spectrum of log permeability of field data for set no. IL040V (represented by circles).

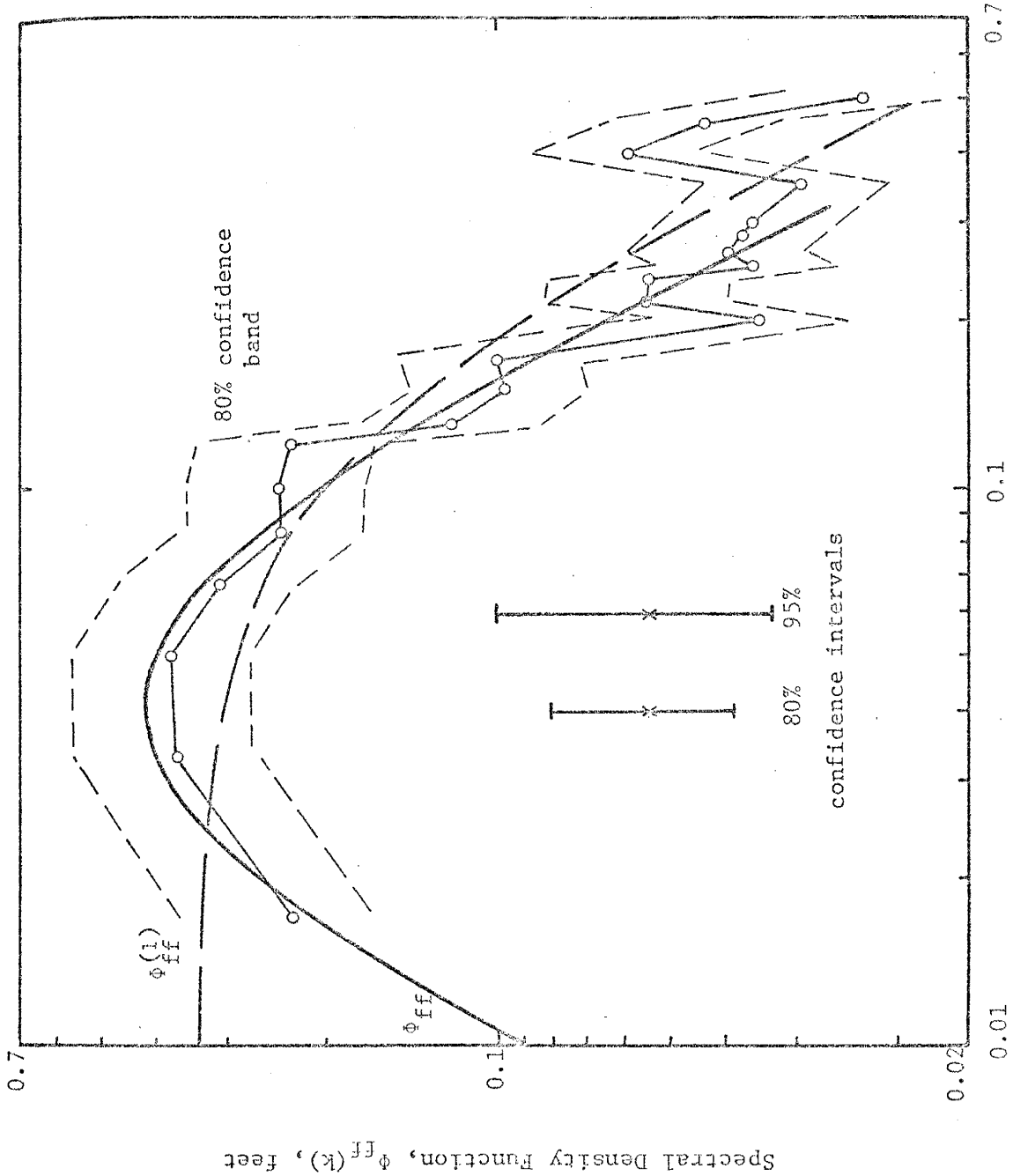

Fig. 5-39: Fit between theoretical spectra and the spectrum of log permeability of field data for set no. IL056H (represented by circles).

Table 5.3 Summary of Data Used in the Comparsion of Theoretical Spectra with Those of Field Data

Set No.	Correlation parameter in 3-D, γ	Correlation parameter in 1-D, a	Variance of log K, $\overline{f^{12}}$	Location[1] of intercept at vertical axis of $\Phi_{ff}^{(1)}$	Frequency[2] at match point for $\Phi_{ff}^{(1)}$	Location[3] of the peak of Φ_{ff}	Frequency[4] at match point for Φ_{ff}
IL036V	0.490	0.196	0.760	0.494	0.078	0.617	0.031
IL040V	0.575	0.230	0.596	0.327	0.091	0.412	0.036
IL056H	0.637	0.255	0.671	0.335	0.101	0.419	0.041

1) Location of intercept of the spectrum, $\Phi_{ff}^{(1)}$ at vertical axis is $\frac{\overline{f^{12}}}{\pi\gamma}$

2) Frequency of match point for $\Phi_{ff}^{(1)}$ is at $\gamma/2\pi$

3) Location of the peak of Φ_{ff} is at $\frac{\overline{f^{12}}}{2\pi a}$

4) Frequency of match point for Φ_{ff} is at $\frac{a}{2\pi}$

slightly better than the spectrum of (5.6). It should be mentioned that the spectra of field data shown in figures 5-37 and 5-38 are typical of the spectra of the remaining field data.

5.6 Summary of Results of Spectral Analysis of Permeability and Porosity Field Data

Spectral analysis of log permeability and porosity field data led to the following results:

1. The form of the autocovariance function assumed to characterize fluctuations in the log of hydraulic conductivity of aquifer materials appears to be appropriate as evidenced by the good agreement between it and the covariance of actual data as shown in figures 5-32 through 5-34.

2. Values of the integral scale determined from a large set of core analysis of samples from different parts of an aquifer in northeastern Illinois showed little variation. This observation lends support to the contention that the integral scale characterizing permeability fluctuations is a physical parameter.

3. The existence of the integral scale describing correlation of neighboring values of a hydrologic parameter enhances the applicability of the simple network design problems discussed in Chapter 3 since the analysis of these problems indicated the need for such a parameter.

4. The theoretical spectral density functions assumed for fluctuations in the log of the permeability reasonably fit corresponding spectra computed for log permeability of field data especially at low frequency.

CHAPTER 6

COMPARISONS AMONG THE MODELS

6.1 Introduction

In the previous chapters solutions to the one-dimensional, steady, saturated flow problem and its counterpart in three dimensions were derived via spectral analyses techniques. The applicability of these solutions to actual field data of porosity and permeability were discussed in the previous chapter. Here, we seek to develop quantitative expressions to facilitate comparisons among the results obtained.

It is of interest to examine the range of validity of the approximate solutions to the problem of one-dimensional, steady flow in reference to the exact analysis. This is carried out in section 6.2. Comparisons between one- and three-dimensional stochastic analyses of the flow problem are made in section 6.3. We examine the concept of one-dimensional spectrum (e.g. of conductivity variations) relative to the spectrum in three dimensions. Validity of other related descriptions to the problem of groundwater flow in one and three dimensions appearing in the literature is briefly considered in light of the stochastic approach developed here.

Finally, consequences of the results obtained on practical problems of observation network design are explored. One of the overall objectives of this study is the proper interpretation of groundwater field measurements. We wish to appraise the benefits derived from the analysis developed toward the achievement of this objective.

6.2 Comparison of the One-Dimensional Results

Recall that we obtained a solution to the problem of steady, saturated flow of groundwater in one dimension in which fluctuations in hydraulic conductivity were exactly incorporated (see section 3.3.1). Also derived were two approximate solutions to the same problem by perturbing the flow equation in terms of the conductivity and its logarithm (see sections 3.3.2 and 3.3.3 respectively). To compare the results obtained from these three methods of solution, we can compare the variance of predicted hydraulic head and the mean hydraulic gradient.

6.2.1 Variance of Predicted Hydraulic Head

The variance of predicted hydraulic head $\overline{\phi_W'^2}$, obtained from the exact analysis is given by (3.14) whereas the linearized solutions in terms of K and in terms of ln K are given by (3.26) and (3.43) respectively. Dividing (3.26) by (3.14), the following variance ratio results:

$$\frac{\overline{\phi_K'^2}}{\overline{\phi_W'^2}} = \frac{\overline{K'^2}}{\overline{K}^4\,\overline{W'^2}} \tag{6.1}$$

From the properties of the lognormal distribution (since K and hence W were assumed to be lognormally distributed) one can write

$$\left.\begin{aligned} \frac{\overline{K}}{K_\ell} \equiv \overline{W}K_\ell &= e^{\sigma^2/2} \\ \text{and} \\ \frac{\sigma_K^2}{\overline{K}^2} \equiv \frac{\sigma_W^2}{\overline{W}^2} &= e^{\sigma^2}-1 \end{aligned}\right\} \tag{6.2}$$

where μ, and σ^2 are the mean and variance of the natural logarithm of the hydraulic conductivity. Note that $\overline{f'^2} \equiv \sigma^2$ and that $K_\ell = e^{\mu}$. Substituting (6.2) into (6.1) results in

$$\frac{\overline{\phi_K'^2}}{\overline{\phi_W'^2}} = e^{-2\sigma^2} \tag{6.3}$$

Similarly, dividing (3.43) by (3.14) leads to

$$\frac{\overline{\phi_\ell'^2}}{\overline{\phi_W'^2}} = \frac{\overline{f'^2}}{K_\ell^2\,\overline{W'^2}} \tag{6.4}$$

Substituting the values of $\overline{f'^2}$ and K_ℓ^2 from above, (6.4) becomes

$$\frac{\overline{\phi_\ell{}^2}}{\overline{\phi_W'^2}} = \frac{\sigma^2}{e^{\sigma^2}(e^{\sigma^2}-1)} \tag{6.5}$$

Equations (6.3) and (6.5) reflect the behavior of predicted hydraulic head from the approximate solutions relative to that from the exact results. Values of σ in the range reported by Freeze (1975) were used to evaluate (6.3) and (6.5). It is evident from figure 6-1 that the standard deviation of hydraulic head from the linearized analyses are nearly equal to the corresponding standard deviation from the exact solution only for very small values of σ (less than .05). For σ values up to 0.15, the departure of the approximate solutions from the exact is negligible (about 5%). However, as σ increases to values frequently reflected by point measurements in natural deposits (e.g. > 0.2), the

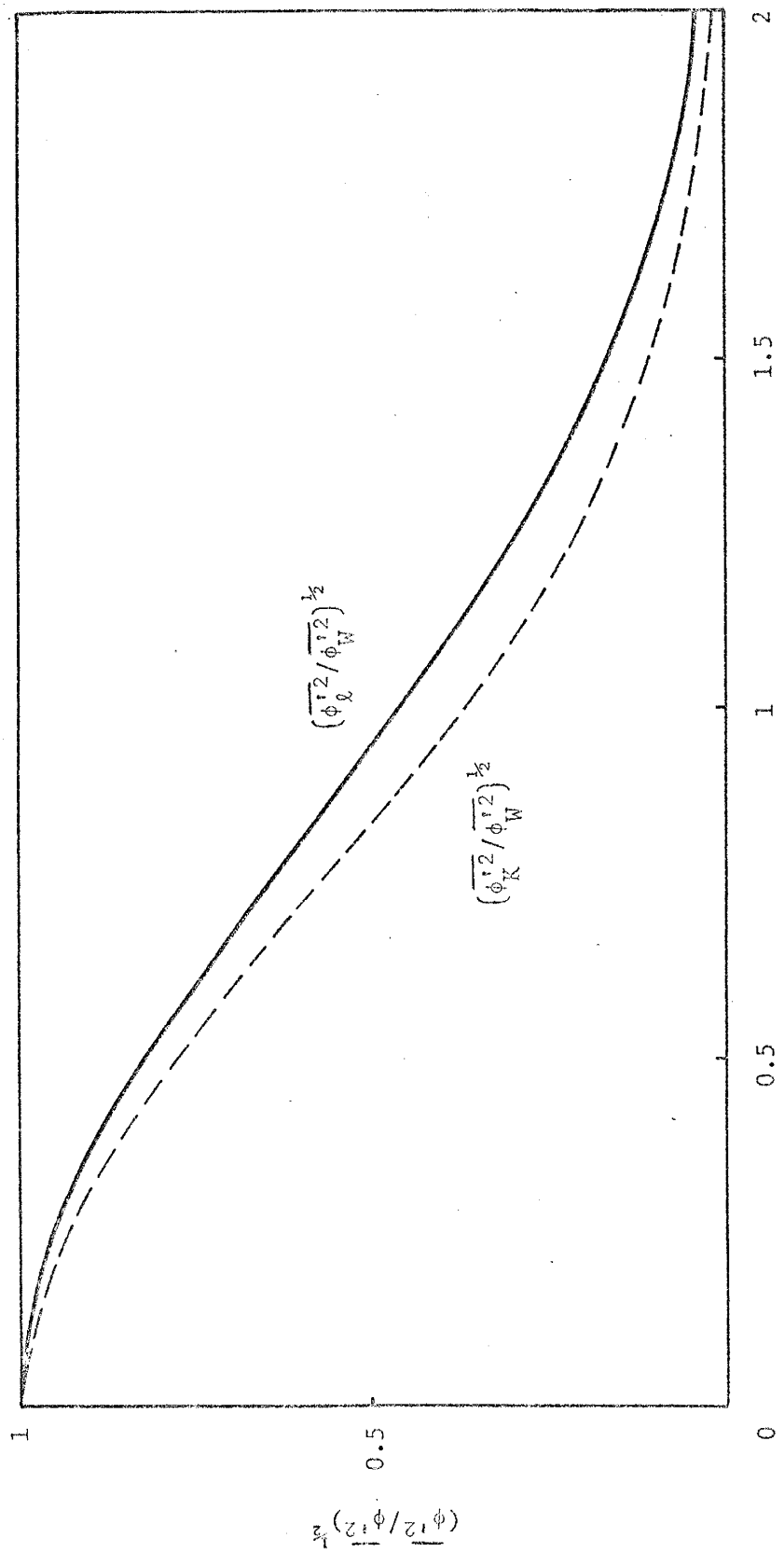

Fig. 6-1: Ratio of the standard deviation of the hydraulic head from approximate solutions to that of the exact versus the standard deviation of log K.

difference between the exact and the approximate solutions becomes significant. By linearizing in terms of K or ln K we tend to underestimate the standard deviation $\sqrt{\overline{\phi'^2}}$ of predicted hydraulic head. However, linearizing in terms of ln K gives consistently better results; it underestimates $\sqrt{\overline{\phi'^2}}$ the least. Thus whenever predictions of hydraulic head in a given one-dimensional groundwater system are needed, one is best advised to use the hydraulic resistivity to characterize the flow properties of the porous medium rather than the conductivity. Furthermore, the linearized solutions appear to be limited in comparison with the exact results (see figure 6-1) especially for natural flow systems where σ is commonly indicated to be greater than 0.2 (see Table 5.1). Note, however, that the field estimates of σ are based on point measurements (cores) whereas the one-dimensional flow description implies an average of conditions over a plane normal to the flow. Thus, the appropriate input variance for the one-dimensional flow model will be smaller than that based on point observations.

6.2.2 Mean Hydraulic Gradient

Another way to compare the results from the linearized methods of solution (in terms of K and in ln K) to those obtained from the exact approach is by examining the mean hydraulic gradients, J_K and J_ℓ in terms of J_W. Recall that

$$J_W = q\overline{W}$$

$$J_K = \frac{q}{\overline{K}} \quad , \text{ and}$$

$$J_\ell = \frac{q}{K_\ell}$$

from which the following ratios are obtained:

$$\frac{J_K}{J_W} = \frac{1}{\overline{K}\,\overline{W}} \tag{6.6}$$

and

$$\frac{J_\ell}{J_W} = \frac{1}{K_\ell \overline{W}} \tag{6.7}$$

Making use of (6.2) and the definition of K_ℓ, (6.6) and (6.7) take the form

$$\frac{J_K}{J_W} = e^{-\sigma^2} \tag{6.8}$$

and

$$\frac{J_\ell}{J_W} = e^{-\sigma^2/2} \tag{6.9}$$

Equations (6.8) and (6.9) are evaluated for different values of σ and the results are shown in figure 6-2. Both linearized solutions yield results that are identical and do not differ significantly from those of the exact analysis for σ values up to 0.1. However, as σ increases, both approximate results tend to underestimate the mean hydraulic gradient; the linearized approach in terms of K underestimates J the most.

We can also compare among the various one-dimensional results in terms of the standard deviation of head normalized by some typical change in mean head. The change in mean hydraulic head over some distance (taken

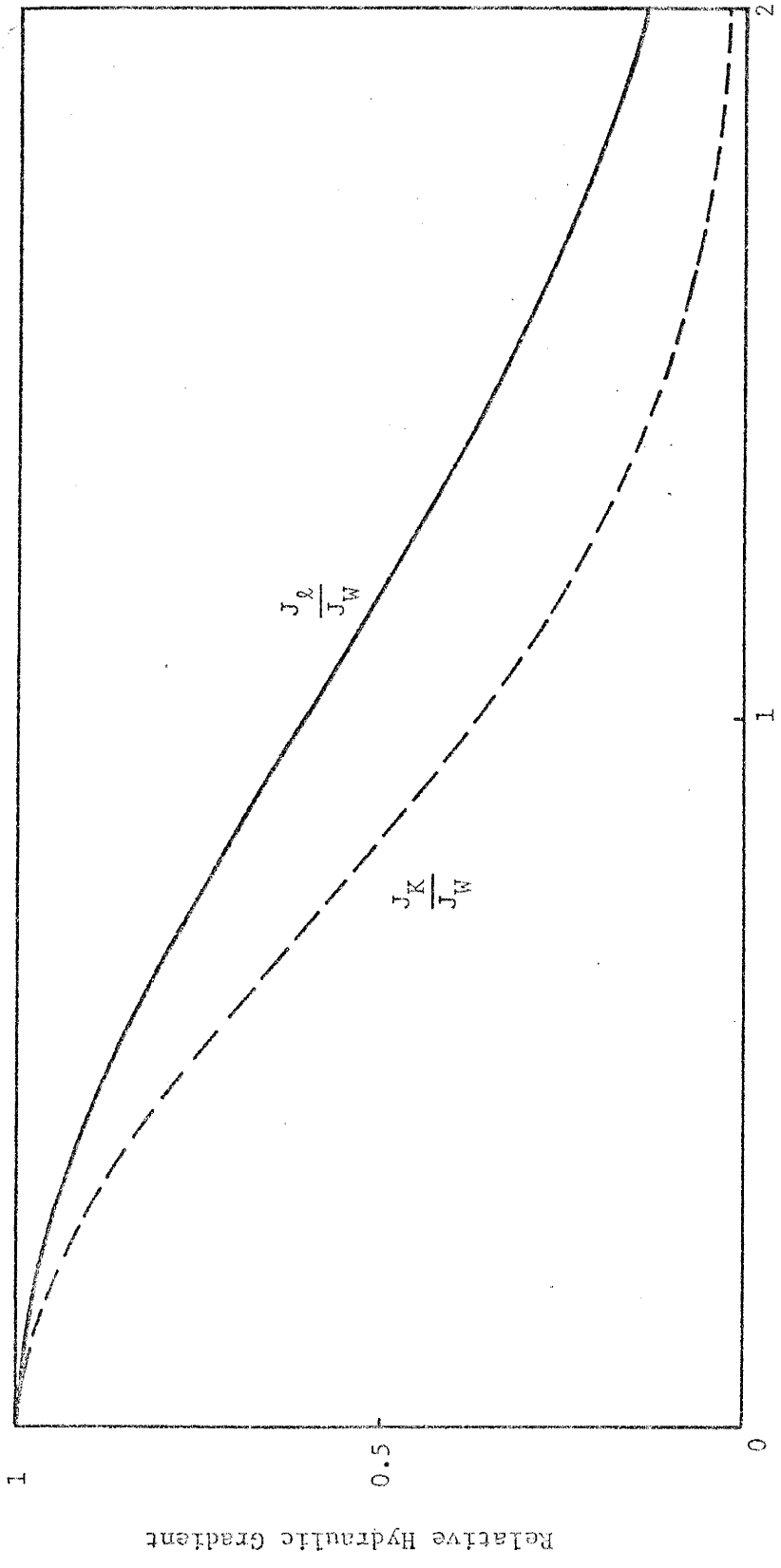

Fig. 6-2: Ratio of mean hydraulic gradient from approximate solutions to that of the exact versus the standard deviation of log K.

to be the correlation length, ℓ; the only length scale in the one-dimensional analysis) is used in this normalization. Thus, one obtains

$$\frac{\overline{\phi_K'^2}}{\ell^2 J_K^2} \Big/ \frac{\overline{\phi_W'^2}}{\ell^2 J_W^2} = \frac{\left(\overline{\phi_K'^2}/J_K^2\right)}{\left(\overline{\phi_W'^2}/J_W^2\right)} = 1 \tag{6.10}$$

and similarly

$$\frac{\left(\overline{\phi_\ell'^2}/J_\ell^2\right)}{\left(\overline{\phi_W'^2}/J_W^2\right)} = \frac{\sigma^2}{(e^{\sigma^2}-1)} \tag{6.11}$$

Equation (6.10) is rather surprising since it shows that the linearized approach in terms of K gives identical results to those of the exact solution, whereas earlier results (see figures 6-1 and 6-2) show that the linearization in terms of ln K is actually closer to the exact result. The square root of (6.11) is evaluated for different values of σ and is plotted in figure 6-3. This figure indicates that linearization in terms of ln K gives results that depart considerably from those of the exact solution for the relative variance.

Table 6.1 summarizes the equations used in the comparison of the different one-dimensional results.

6.3 One-Dimensional Versus Three-Dimensional Results

The results obtained from the various methods of solution to the flow problems considered herein are summarized in Table 6.2. Included are autocorrelation functions and spectra of hydraulic conductivity and hydraulic head and the variance of predicted hydraulic head. All

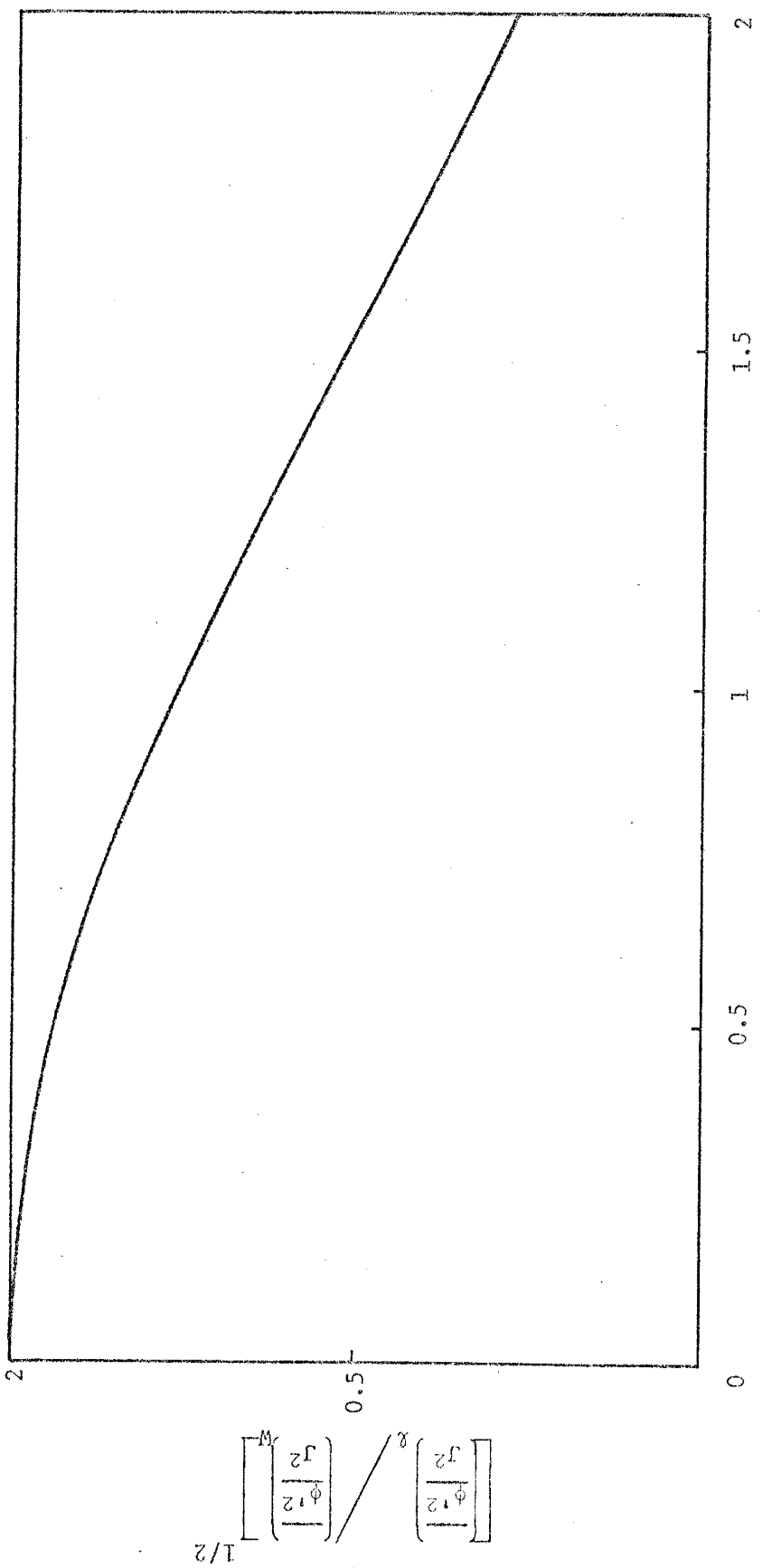

Fig. 6-3: Ratio of the standard deviation of hydraulic head over mean hydraulic gradient of the linearized solution in terms of ln K to that of the exact versus the standard deviation of log K.

Table 6.1 Comparisons Among One-Dimensional Results*

Method of solution of Flow Eq. / Property	EXACT $\frac{d\phi}{dx} = -qW(x)$	APPROXIMATE Linearized in terms of K	APPROXIMATE Linearized in terms of ln K
1. Variance of hydraulic head $(\overline{\phi'^2}) = [L^2]$	$\overline{\phi_W'^2} = \frac{q^2\overline{W'^2}}{a^2}$	$\overline{\phi_K'^2} = \frac{q^2\overline{K'^2}}{\bar{K}^4 a^2}$	$\overline{\phi_\ell'^2} = \frac{q^2\overline{f'^2}}{K_\ell^2 a^2}$
2. Hydraulic head variance ratio $(\overline{\phi'^2}/\overline{\phi_W'^2})$	1	$\frac{\overline{K'^2}}{\bar{K}^4\overline{W'^2}} = e^{2\sigma^2}$	$\frac{\overline{f'^2}}{K_\ell^2\overline{W'^2}} = \frac{\sigma^2 e^{\sigma^2}}{(e^{\sigma^2} - 1)}$
3. Mean hydraulic gradient $\left(-\frac{d\phi}{dx}\right)$	$J_W = q\bar{W}$	$J_K = \frac{q}{\bar{K}}$	$J_\ell = \frac{q}{K_\ell}$
4. Mean hydraulic gradient ratio relative to exact results	1	$\frac{J_K}{J_W} = \frac{1}{\bar{K}\bar{W}} = e^{\sigma^2}$	$\frac{J_\ell}{J_W} = \frac{1}{K_\ell\bar{W}} = e^{\sigma^2/2}$
5. $\left(\frac{\overline{\phi'^2}}{J^2\ell^2}\right)$ $\left(\frac{\overline{\phi_W'^2}}{J_W^2\ell^2}\right)$	1	1	$\frac{\sigma^2}{(e^{\sigma^2} - 1)}$

* Symbols used are defined in the text (also see List of Symbols)

Table 6.2 Results of Spectral Analyses in a Normalized (or Nondimensional) Form.

Form of the Solution	One-Dimensional Results					Three-Dimensional Results
Function Considered	Exact (W)	Approximate (K)	Approximate (ln K)	General Form	Derived from 3-D results	Approximate: Linearized in ln K
1. Autocorrelation of resistivity, conductivity, or log conductivity	$\rho_{WW}(\xi) = \frac{R_{WW}(\xi)}{\overline{W'^2}}$	$\rho_{WW}(\xi) = \frac{R_{KK}(\xi)}{\overline{K'^2}}$	$\rho_{ff}(\xi) = \frac{R_{ff}(\xi)}{\overline{f'^2}}$	$= (1-a\lvert\xi\rvert)e^{-a\lvert\xi\rvert}$	$\rho_{ff}^{(1)}(\xi_1) = e^{-\gamma\lvert\xi_1\rvert}$	$\rho_{ff}(\xi) = \frac{R_{ff}(\xi)}{\overline{f'^2}} = e^{-\gamma\lvert\xi\rvert}$
2. Spectrum of resistivity, conductivity, or log conductivity	$\frac{a\bar{\phi}_{WW}(k)}{\overline{W'^2}}$	$\frac{a\bar{\phi}_{KK}(k)}{\overline{K'^2}}$	$\frac{a\bar{\phi}_{ff}(k)}{\overline{f'^2}}$	$= \frac{2(k/a)^2}{\pi[1+(k/a)^2]^2}$	$\frac{\gamma\bar{\phi}_{ff}^{(1)}(k_1)}{\overline{f'^2}} = \frac{1}{\pi[1+(k_1/\gamma)^2]}$	$\frac{\gamma^3\bar{\phi}(\vec{k})}{\overline{f'^2}} = \frac{1}{\pi^2[1+(k/\gamma)^2]^2}$
3. Autocorrelation of hydraulic head	$\rho_{\phi\phi}(\xi) = \frac{R_{\phi\phi}(\xi)}{\overline{\phi'^2}}$	$\rho_{\phi\phi}(\xi)$	$\rho_{\phi\phi}(\xi)$	$= (1+a\lvert\xi\rvert)e^{-a\lvert\xi\rvert}$	$\frac{R_{\phi\phi}^{(1)}(\xi_1,0)}{\overline{\phi'^2}} = \left[\left(1-e^{-\gamma\lvert\xi_1\rvert}\right) \times \frac{8}{(\gamma\lvert\xi_1\rvert)^3} - e^{-\gamma\lvert\xi_1\rvert} \times \left(1+\frac{4}{\gamma\lvert\xi_1\rvert}+\frac{8}{(\gamma\xi_1)^2}\right)\right]$	$\frac{R_{\phi\phi}(\xi,\chi)}{\overline{\phi'^2}} = \frac{3\sin^2\chi}{2(\gamma\lvert\xi\rvert)}\left[(\gamma\lvert\xi\rvert+2)e^{-\gamma\lvert\xi\rvert}-2\right] + \frac{12(3\cos^2\chi-1)}{(\gamma\lvert\xi\rvert)^3} \times \left[1-\left\{1+\gamma\lvert\xi\rvert+\frac{(\gamma\xi)^2}{2}+\frac{(\gamma\lvert\xi\rvert)^3}{8}\right\}e^{-\gamma\lvert\xi\rvert}\right]$
4. Variance of hydraulic head	$\overline{\phi'^2} = \frac{q^2\overline{W'^2}}{a^2}$	$\frac{\overline{K'^2}q^2}{\overline{K}^2a^2}$	$\frac{J_o^2\overline{f'^2}}{a^2}$	$= \frac{q^2\cdot\mathrm{var}(W,K,\text{or } f)}{a^2}$	———	$\overline{\phi'^2} = \frac{J_o^2\overline{\xi'^2}}{3\gamma^2}$
5. Spectrum of hydraulic head	$\frac{a\bar{\phi}_{\phi\phi}(k)}{\overline{\rho'^2}}$	same	same	$= \frac{2}{\pi[1+(k/a)^2]^2}$	$\frac{\gamma\phi_{\phi\phi}^{(1)}(k_1)}{\overline{\phi'^2}} = \frac{3}{\pi}\left[\left(1+\frac{1}{1+(\gamma/k_1)^2}\right) - 2(k_1/\gamma)^2\ln(1+(\gamma/k_1)^2)\right]$	$\frac{\gamma^3\phi_{\phi\phi}(k)}{\overline{\phi'^2}} = \frac{3\cos^2\theta}{\pi^2(k/\gamma)^2[1+(k/\gamma)^2]^2}$

expressions are normalized to give nondimensional quantities which make the subsequent graphical comparisons independent of units. In order to insure compatibility of the comparisons between results from the three-dimensional approach to those from the one-dimensional analysis we reduce the three-dimensional equations to corresponding formulae in one dimension. In other words, in the subsequent discussion we are actually comparing the one-dimensional results obtained in section 3.3.3 to corresponding one-dimensional expressions derived from the analysis in three dimensions.

In this section we compare spectra and autocovariance functions representing fluctuations in ln K or the input to the problem of groundwater flow under investigation; this is carried out in section 6.3.1. The spectrum and autocovariance functions describing the output from the system or predicted hydraulic head are examined in section 6.3.2.

6.3.1 Spectrum and Autocovariance Function of Hydraulic Conductivity

Comparisons between spectra and autocovariance functions of fluctuations in ln K obtained from considering the flow of groundwater in one dimension and those resulting from analysing the flow in three dimensions is carred out in this section. Following Lumley and Panofsky (1964, p. 25), the one-dimensional spectrum, $\Phi^{(1)}$ can be obtained by integrating the three-dimensional spectrum, $\Phi(\vec{k})$ over the plane in wave number space which is normal to the wave number component of interest, i. e.

$$\Phi^{(1)}(k_1) = \int_{-\infty}^{\infty}\int \Phi(\vec{k})\, dk_2 dk_3 \qquad (6.12)$$

The one-dimensional spectrum $\Phi^{(1)}(k_1)$ represents the spectrum that would be found from observations along a sampling line in the X_1 direction as in the case of the core data analyzed in Chapter 5. Substituting the three-dimensional spectrum of ln K given by (4.15) into (6.12) yields

$$\Phi_{ff}^{(1)}(k_1) = \int_{-\infty}^{\infty}\int \frac{\overline{\gamma f'^2}}{\pi^2(\gamma^2 + k^2)^2}\, dk_2 dk_3 \qquad (6.13)$$

Changing to cyclindrical coordinates (see Lumley, 1970, p. 101) which are oriented along the k_1 axis as shown in figure 6-4 and noting that

$\tau^2 + k_1^2 = k^2$, and hence

$\tau d\tau = kdk$

where $\tau = 0$ at $k = k_1$, (6.13) takes the form

$$\Phi_{ff}^{(1)}(k_1) = \int_0^{2\pi}\int_0^{\infty} \frac{\overline{\gamma f'^2}}{\pi^2(\gamma^2 + k^2)^2}\, \tau d\tau d\zeta$$

$$= \int_0^{2\pi}\int_{k_1}^{\infty} \frac{\overline{\gamma f'^2}}{\pi^2(\gamma^2 + k^2)^2}\, kdkd\zeta$$

As integrating over ζ gives 2π, the above integral becomes

$$\Phi_{ff}^{(1)}(k_1) = \frac{2\overline{\gamma f'^2}}{\pi} \int_{k_1}^{\infty} \frac{kdk}{(\gamma^2 + k^2)^2}$$

which yields the following expression for the one-dimensional spectrum of ln K:

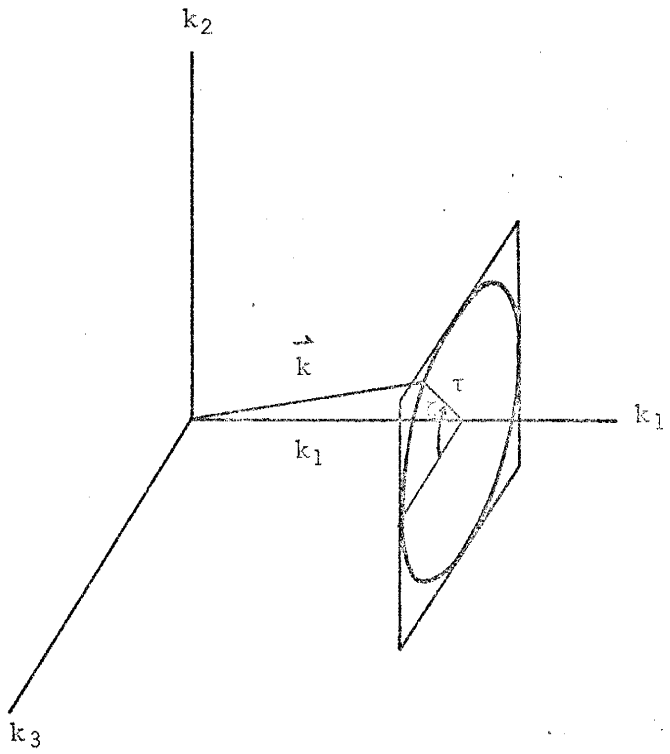

Fig. 6-4: Geometry of the wave number vector in cylindrical coordinates (after Lumley, 1970).

$$\Phi_{ff}^{(1)}(k_1) = \frac{\overline{\gamma f'^2}}{\pi(\gamma^2 + k_1^2)} \tag{6.14}$$

This expression differs from the corresponding result given by (3.40) for the one-dimensional analysis of section 3.3.3 in that it does not have k^2 in the numerator and that the bracketed quantity in the denominator is not squared as in (3.40). Both results will be compared graphically later in this section.

The spectrum $\Phi_{ff}^{(1)}(k_1)$ of the conductivity fluctuations can also be obtained from the autocovariance, $R_{ff}(\xi)$, as follows:

$$\Phi_{ff}^{(1)}(k_1) = \frac{1}{2\pi} \int_{-\infty}^{\infty} e^{-ik_1\xi_1} R_{ff}^{(1)}(\xi_1) d\xi_1$$

where $R_{ff}^{(1)}(\xi_1) = R_{ff}(\xi_1, 0, 0)$. Substituting the value of $R_{ff}^{(1)}$ from Table 6.2 into the above expression yields

$$\Phi_{ff}^{(1)}(k_1) = \frac{\overline{f'^2}}{2\pi} \int_{-\infty}^{\infty} e^{-\gamma|\xi_1|} e^{-ik_1\xi_1} d\xi_1 \tag{6.15}$$

Since $e^{-\gamma|\xi_1|}$ is an even function, we can write (6.15) in terms of the Fourier cosine transform as

$$\Phi_{ff}^{(1)}(k_1) = \frac{\overline{f'^2}}{\pi} \int_{0}^{\infty} e^{-\gamma\xi_1} \cos k_1\xi_1 d\xi_1 \tag{6.16}$$

From tables of integrals (Erdelyi, 1954, p. 14) the value of (6.16) is

$$\Phi_{ff}^{(1)}(k_1) = \frac{\overline{\gamma f'^2}}{\pi(\gamma^2 + k_1^2)}$$

which is identical to (6.14).

Let us now compare between the autocorrelation functions characterizing fluctuations in ln K in one and three dimensions. One way to do so is to examine their slopes at the origin, i. e. at $\xi = 0$. The slopes are obtained by differentiating their expressions, given in Table 6.2, and evaluating the result at $\xi = 0$, or

$$\frac{d\rho_{ff}(\xi)}{d\xi} = (1 - a\xi)(-a)\, e^{-a\xi} - a\, e^{-a\xi}\Big|_{\xi=0} = -2a$$

while

$$\frac{d\rho_{ff}(\xi)}{d\xi} = -\gamma\, e^{-\gamma|\vec{\xi}|} = -\gamma$$

for the autocorrelation functions in one and three dimensions respectively. This comparison is facilitated by requiring that the slopes of the two autocorrelation functions are equal at the origin, i. e. that

$$\gamma = 2\, a \tag{6.17}$$

where a, and γ are the correlation parameters in one and three dimensions respectively. Equation (6.17) is used to evaluate $\rho(\xi)$ which is shown together with the autocorrelation in one dimension in figure 6-5. Note the strong negative correlation reflected in the one-dimensional case. Recall that autocovariances of most porosity and permeability field data examined in the previous chapter also had a negative part for larger separations. However, for field data the length of record is usually not adequate for significant estimates of covariances for

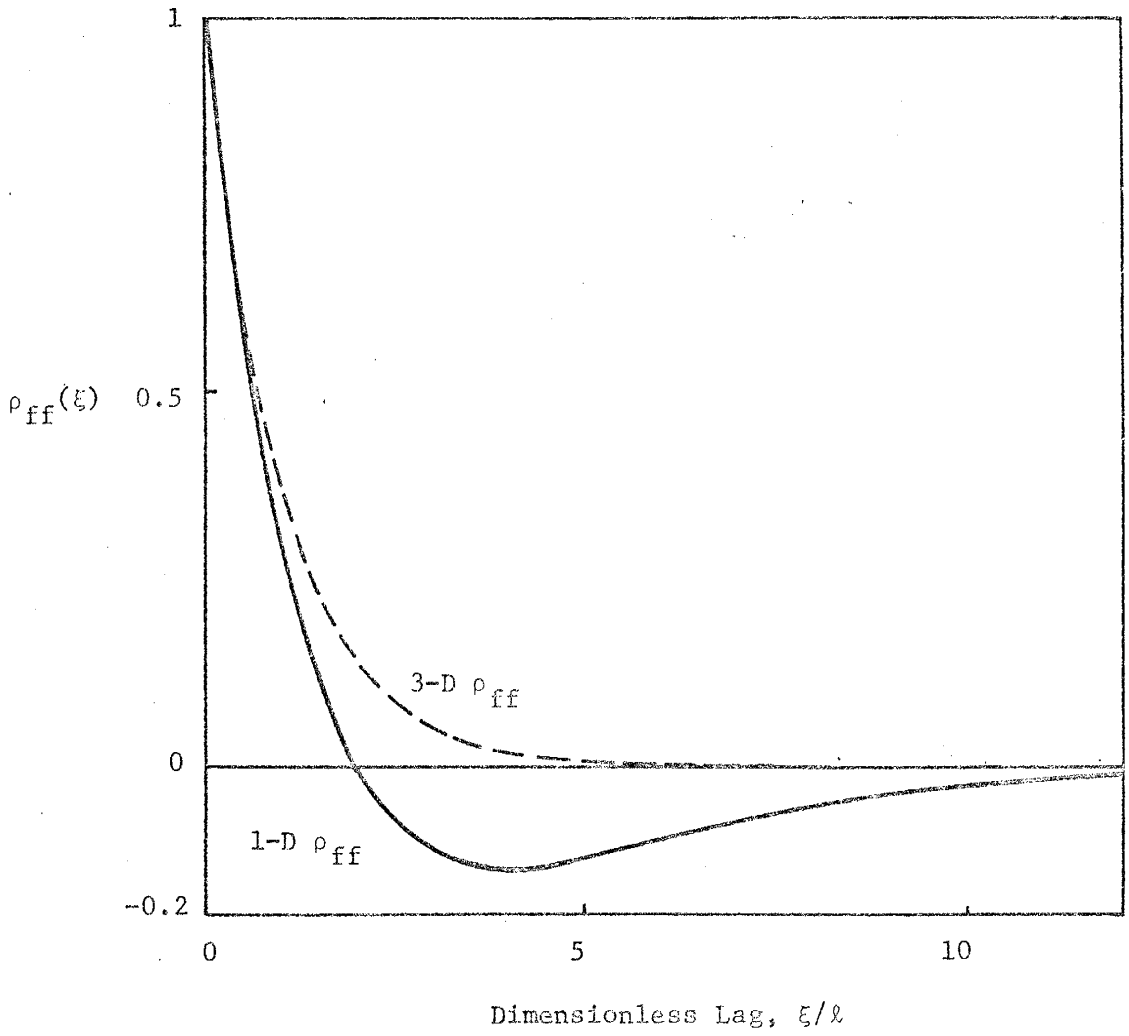

Fig. 6-5: Comparison between the autocorrelation functions of log K in one and three dimensions.

large separation. Therefore, it is of interest to examine the two autocorrelation functions for small separations. Figure 6-6 presents both autocorrelation functions for small values of the dimensionless quantity ξ/ℓ. It is evident that the two functions do not differ appreciably from each other. However, as demonstrated in the previous chapter, the exponential autocorrelation function was found to fit actual field data better. Finally, we note that when the autocorrelation function for conductivity was evaluated for different values of the parameter a in terms of γ, it was found that $\gamma = 2.5a$ gives a better fit (see figures 5-32 through 5-34), which is also evident from figure 6-6.

We now consider the question of scale of spatial correlation of conductivity fluctuations, referred to as the integral scale, λ, and defined by (Lumley & Panofsky, 1964),

$$\lambda = \int_0^\infty \rho_{ff}(\xi)d\xi \tag{6.18}$$

As indicated by Lumley and Panofsky (1964, p. 37), in order for experimental measurements of a process to be interpreted meaningfully, the existence of integral scales must be assumed. The necessity for the existence of an integral scale is discussed in section 2.5.

Using (6-18) let us find the integral scale for fluctuations in ln K in three dimensions

$$\lambda = \int_0^\infty e^{-\gamma|\xi|}d\xi \text{ , or}$$

$$\lambda = \frac{1}{\gamma} \tag{6.19}$$

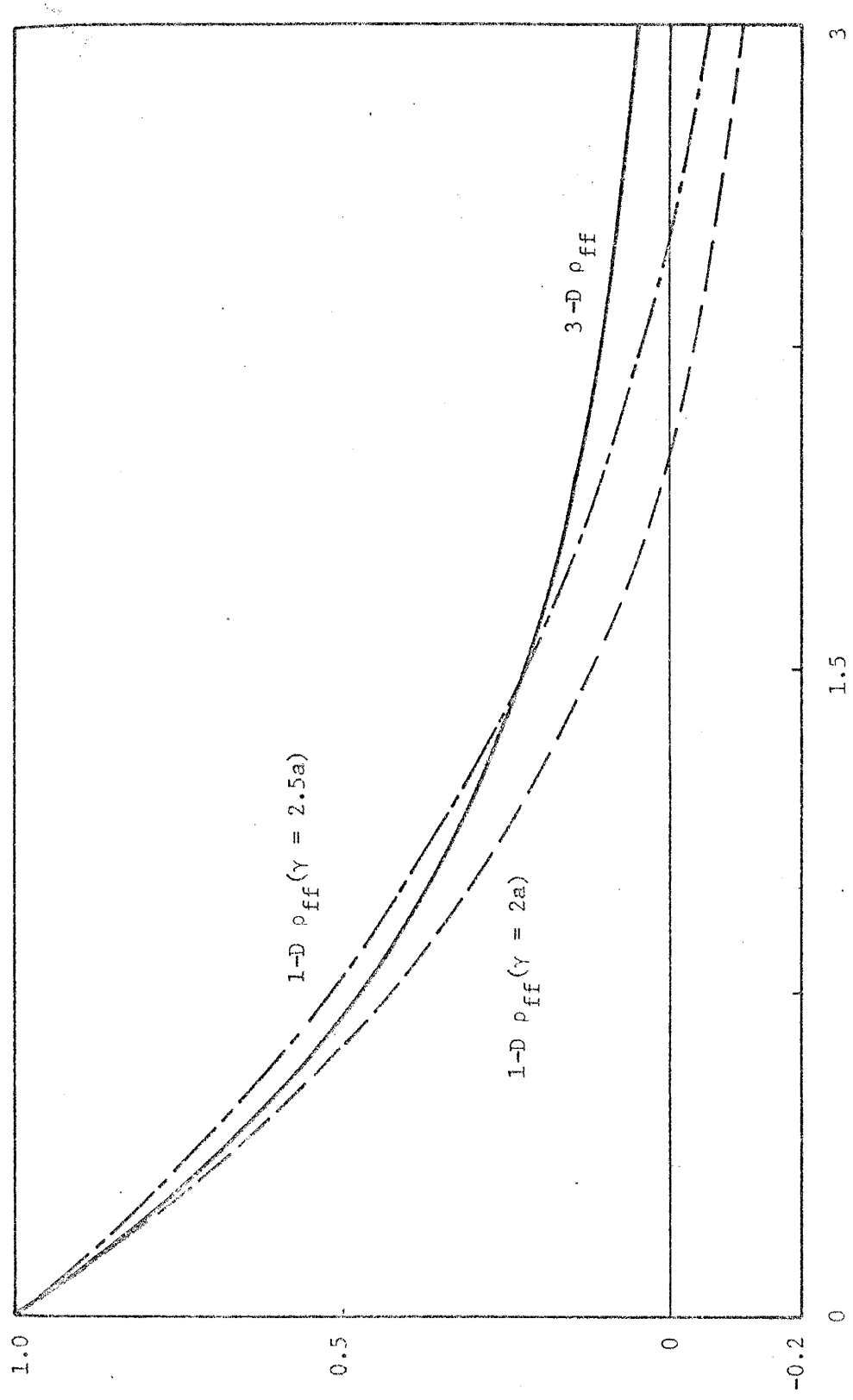

Fig. 6-6: Comparison between the one-dimensional autocorreiation function of log K (for the cases of $\gamma = 2$ and 2.5a) and that of three-dimensional autocorrelation.

which indicates that an integral scale exists for the three-dimensional case. Thus, the inverse of the correlation parameter, γ, represents the average distance over which fluctuations in ln K are correlated. However, an integral scale in the sense of (6.18) is identically zero for the conductivity covariance used in the one-dimensional flow analysis (see (3.39)). This situation arises (Lumley, 1970, p. 79) when the process is the derivative of another process; the conductivity in this case is the derivative of hydraulic head in Darcy's equation. However, a length scale for this case can be defined through the spectrum (see Lumley, 1970, p. 79). Analysis of porosity and permeability field data (see Chapter 5) demonstrated that fluctuations in these hydrologic properties were positively correlated up to a certain distance, the inverse of which is the correlation parameter, a, defined earlier.

Let us now examine spectra of fluctuations in hydraulic conductivity in one and three dimensions. In the comparisons to be made below we are assuming that $\gamma = 2.5a$. One way of presenting the spectra is a linear plot of the spectral density function against the wave number as shown in figure 6-7. This figure shows that the one-dimensional spectrum, $\Phi_{ff}^{(1)}$, obtained by reducing the three-dimensional results has a peak at the origin while the spectrum arrived at from considering the flow problem in one dimension vanishes at the origin.

However, a linear plot tends to obscure details of the spectra if wide ranges of spectra and wave numbers are of interest. A logarithmic plot is another way of presenting spectra, i. e., the logarithm of the spectral density versus the logarithm of the wave number. Both spectra, $\Phi_{ff}^{(1)}$ and Φ_{ff} of fluctuations in ln K are depicted using this method in

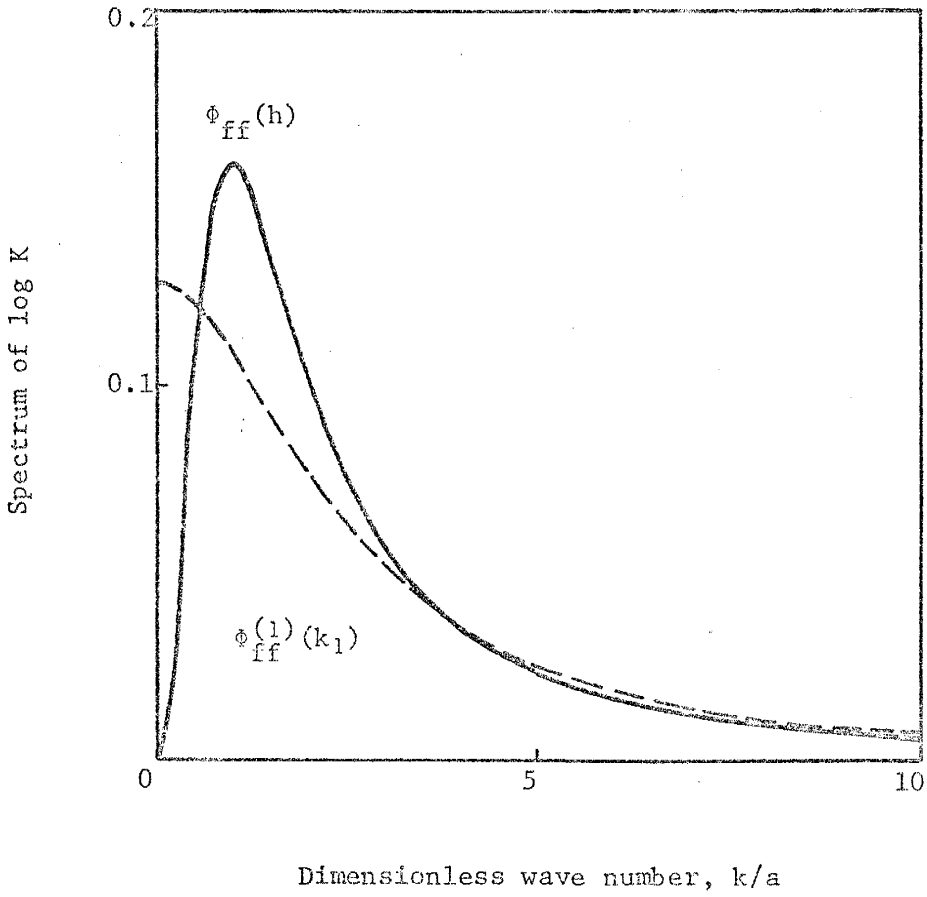

Fig. 6-7: Spectral density function of log K plotted against the dimensionless wave number, k/a (for the case of $\gamma = 2.5a$)

figure 6-8. The logarithmic presentation has the advantage of showing constant powers of the wave number as straight lines with a slope corresponding to the powers. However, this method does not give realistic weight to high wave numbers.

A graphical presentation commonly used in meteorology (Lumley and Panofsky, 1964, p. 19) is a plot of $k\Phi(k)$ versus log k. This procedure has the advantage of collapsing the wave number scale while preserving area under the curves. A plot of $k\Phi_{ff}(k)/\overline{f'^2}$ versus log (k/a) is shown in figure 6-9 for both one-dimensional spectra, $\Phi_{ff}^{(1)}$ and Φ_{ff}. This normalization of Φ_{ff} produces the same area under each of the curves and thus graphically represents the relative distribution of variance over wave number. Note that $\Phi_{ff}^{(1)}$ reflects a broader range of wave numbers for conductivity fluctuations compared to Φ_{ff}.

We summarize the results of this section in the following statements. First, the one-dimensional spectrum $\Phi_{ff}^{(1)}$ of fluctuations in ln K was obtained from its three-dimensional counterpart. Comparison of $\Phi_{ff}^{(1)}$ and the spectrum Φ_{ff} obtained from solving the problem of groundwater in one dimension was then carried out. Secondly, the autocovariance functions characterizing fluctuations in ln K in one and three dimensions were compared and it was graphically shown that $\gamma = 2.5a$ gives a better fit between the two functions. Finally, the integral scale characterizing variations in ln K was obtained and discussed.

6.3.2 Spectrum and Autocovariance Function of Hydraulic Head

In this section we derive an expression for $R_{\phi\phi}^{(1)}$ of hydraulic head from its three-dimensional counterpart, $R_{\phi\phi}$. We then use $R_{\phi\phi}^{(1)}$ to obtain

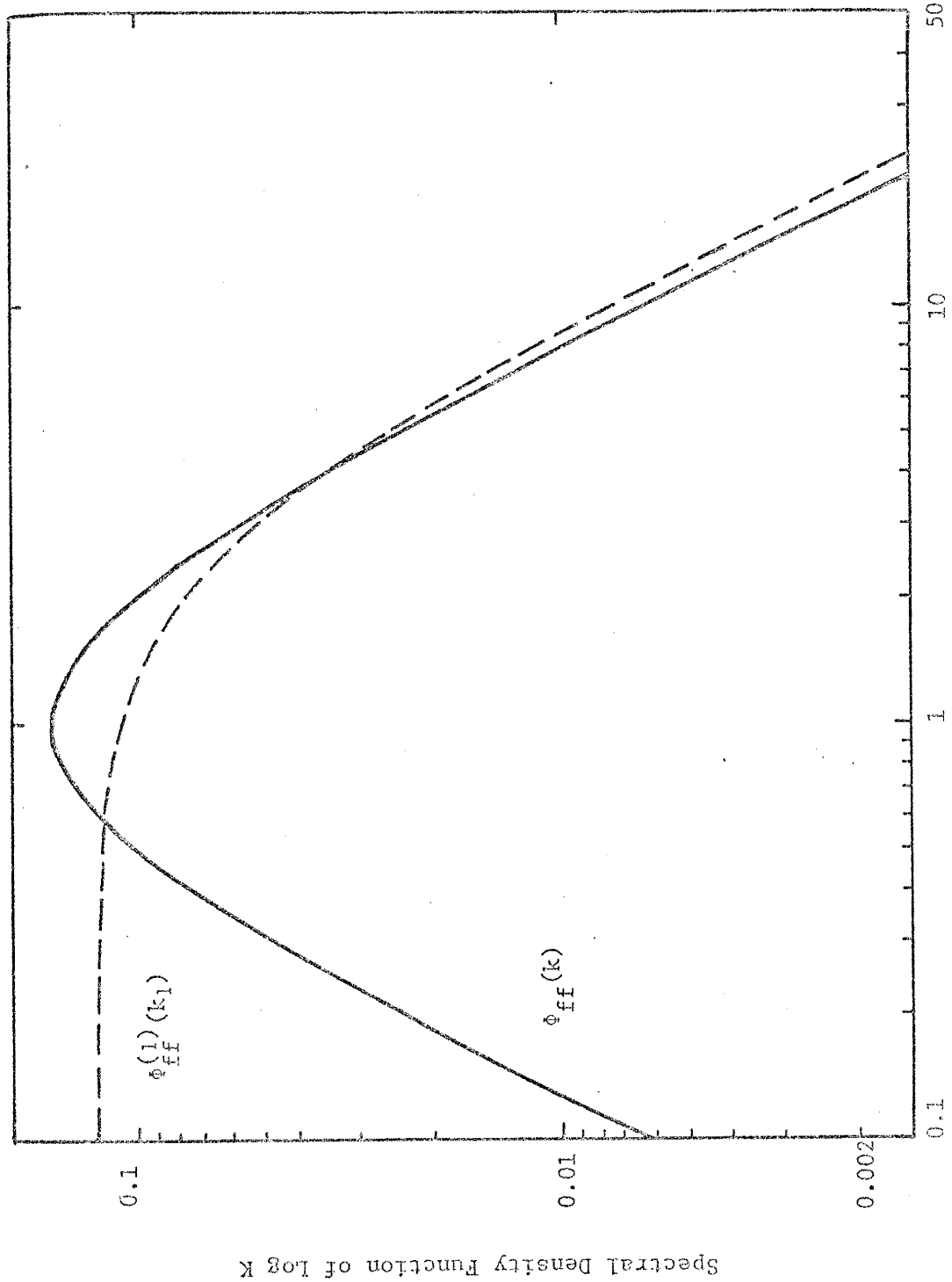

Fig. 6-8: Normalized spectral density functions of log K versus the dimensionless wave number, k/a (for the case of γ = 2.5a)

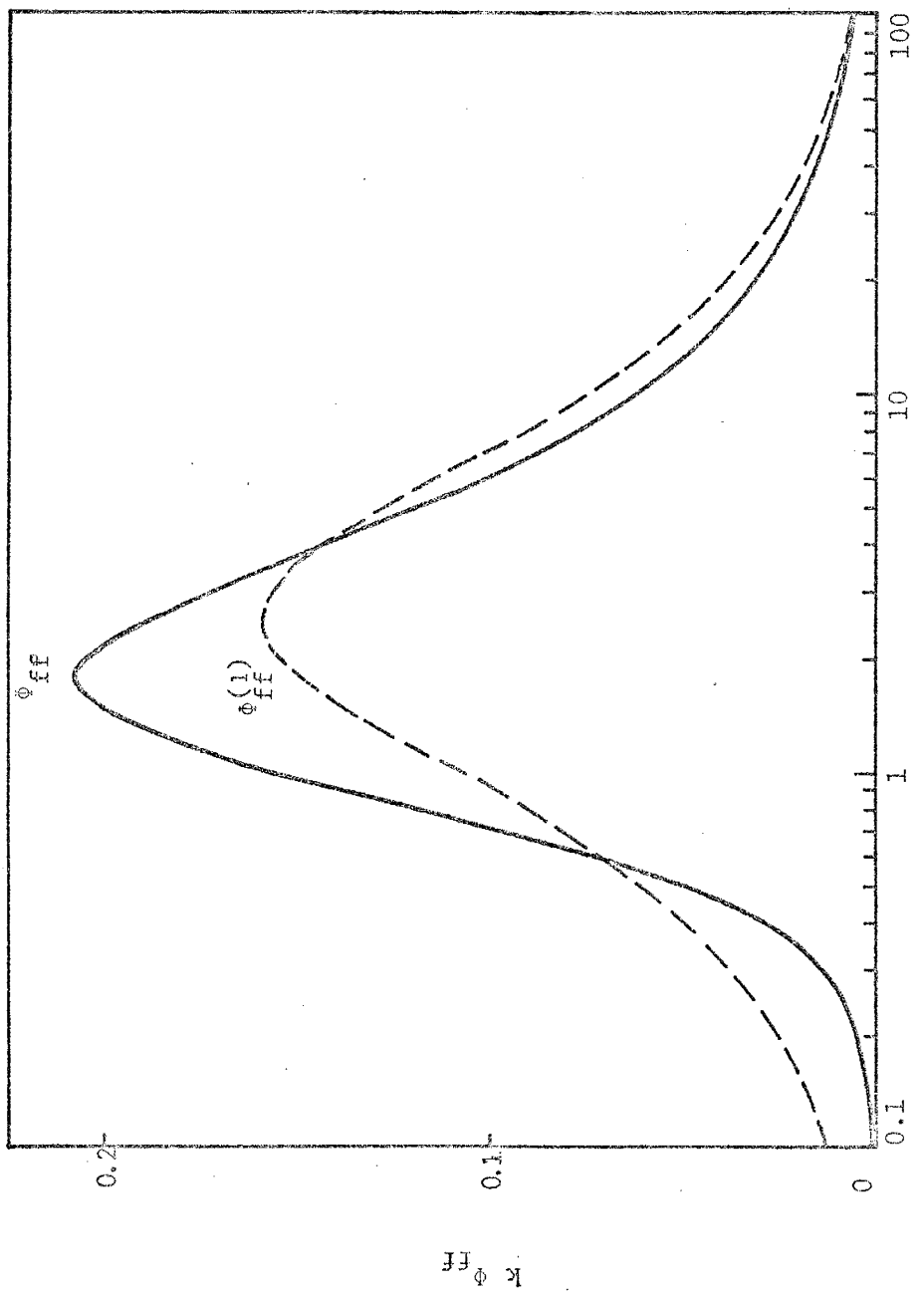

Fig. 6-9: Normalized spectral density functions of log K versus the dimensionless wave number, k/a (for the case of $\gamma = 2.5a$).

the spectrum $\Phi^{(1)}_{\phi\phi}$ of hydraulic head fluctuations in one dimension. The spectrum $\Phi^{(1)}_{\phi\phi}$ is also obtained by integration of the three-dimensional spectrum $\Phi_{\phi\phi}$ over the plane. Finally, several graphical results are presented to facilitate comparison between spectra and autocovariance functions of hydraulic head obtained from the analyses of the flow in one and three dimensions.

Starting with the expression for $R_{\phi\phi}(\xi,\chi)$ representing the autocovariance function for fluctuations in hydraulic head in three dimensions, we obtain the spectrum, $\Phi^{(1)}_{\phi\phi}(k_1)$, of fluctuations in head in one dimension. Recall that $R_{\phi\phi}(\xi,\chi)$ is given by (4.22) and since $R^{(1)}_{\phi\phi}(\xi_1) = R_{\phi\phi}(\xi_1, 0, 0) = R_{\phi\phi}(\xi,0)$, we write

$$\Phi^{(1)}_{\phi\phi}(k_1) = \frac{1}{2\pi} \int_{-\infty}^{\infty} R_{\phi\phi}(\xi_1,0)\, e^{-ik_1\xi_1} d\xi_1$$

To obtain the autocovariance $R^{(1)}_{\phi\phi}(\xi_1)$ of fluctuations in hydraulic head in the direction of the mean flow, we make use of the geometry of the problem as sketched in figure 6-10a. In this case, the angle χ which the displacement vector $\vec{\xi}$ makes with respect to the direction of the mean flow is equal to zero. Hence, (4.22) reduces to

$$R^{(1)}_{\phi\phi}(\xi_1) \equiv R_{\phi\phi}\Big|_{\substack{\xi=\xi_1 \\ \chi=0}} = \frac{J_o^2 \overline{f'^2}}{\gamma^2} \left[\left(1-e^{-\gamma\xi}\right)\frac{8}{(\gamma\xi)^3} - e^{-\gamma\xi}\left(1+\frac{4}{\gamma\xi}+\frac{8}{(\gamma\xi)^2}\right) \right] \tag{6.20}$$

To examine the autocovariance function of fluctuations in hydraulic head in the direction perpendicular to the principal flow direction we substitute the value of $\chi = \pi/2$ in (4.22) to obtain, after some manipulation,

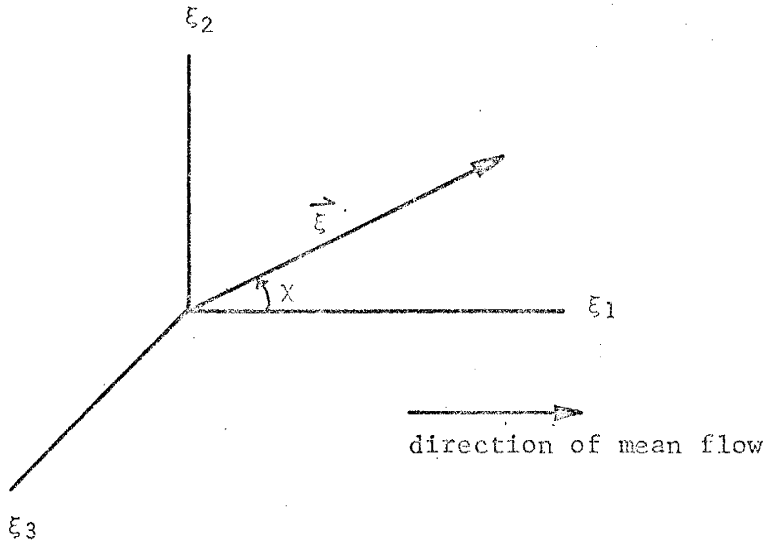

Fig. 6-10a: Geometry of the separation vector, $\vec{\xi}$, and the direction of mean flow.

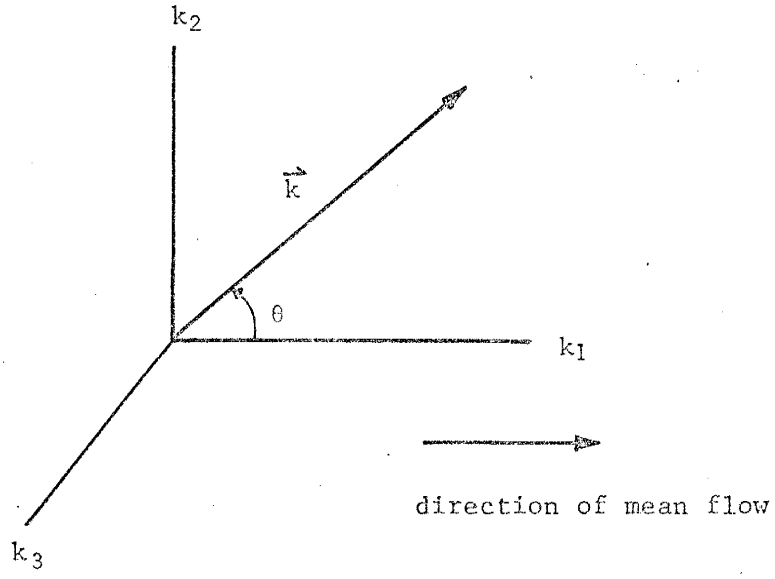

Fig. 6-10b: Geometry of the wave number vector, k, and the direction of mean flow.

the following expression:

$$R^{(2)}_{\phi\phi}(\xi_2) \equiv R_{\phi\phi}\Big|_{\substack{\xi=\xi_2 \\ \chi=\pi/2}} = \frac{J_o^2 \overline{f'^2}}{\gamma^2}\left[\frac{1}{\gamma\xi}\left(1 - \frac{4}{(\gamma\xi)^3}\right) + \frac{e^{-\gamma\xi}}{\gamma\xi}\left(1 + \frac{4}{\gamma\xi} + \frac{4}{(\gamma\xi)^2}\right)\right] \tag{6.21}$$

Normalizing (4.22), we obtain the autocorrelation function characterizing hydraulic head fluctuations, i. e.

$$\rho_{\phi\phi} \equiv \frac{R_{\phi\phi}(\xi,\chi)}{\overline{\phi'^2}} = 3\left\{-\frac{\sin^2\chi}{2\eta}\left[(\eta+2)e^{-\eta}-2\right] + \frac{4(3\cos^2\chi-1)}{\eta^3}\left[1-(1+\eta+\frac{\eta^2}{2}+\frac{\eta^3}{8})e^{-\eta}\right]\right\} \tag{6.22}$$

where $\eta = \gamma\xi$.

Equation (6.22) is evaluated for different values of χ and the results are shown in figure 6-11. Fluctuations in hydraulic head are highly correlated for small values of the parameter ξ/λ, which expresses the lag in terms of the integral scale discussed earlier, while the correlation decreases as ξ/λ increases. Figure 6-11 shows that the fluctuations in hydraulic head in the direction perpendicular to the direction of the mean flow (i.e. $\chi = \pi/2$) have consistently higher correlation values than in any other direction, for the same values of ξ/λ; the hydraulic head fluctuations in the direction of the mean flow ($\chi=0$) having the least correlation values. It is interesting to note that although

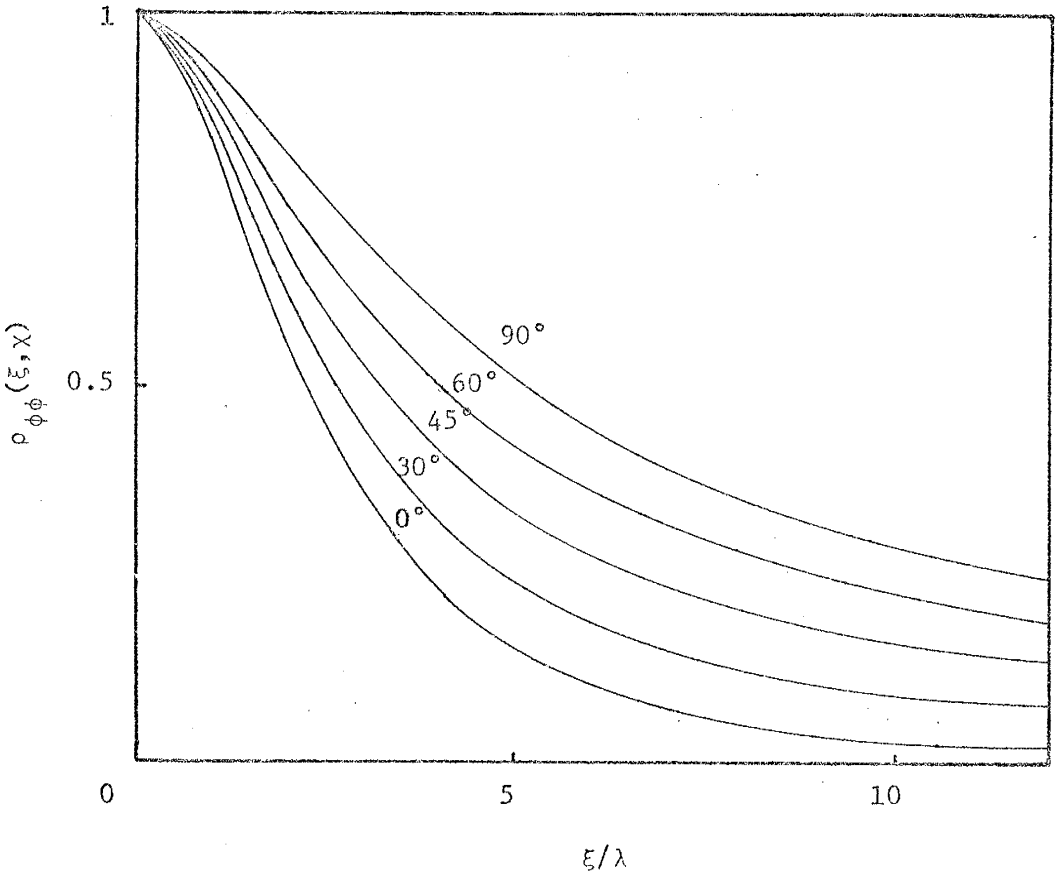

Fig. 6-11: Dimensionless plot of the three-dimensional autocorrelation function of hydraulic head versus the lag.

we assumed the input (hydraulic conductivity) to be isotropic, figure 6-11 indicates that the output (hydraulic head) is anisotropic since $\rho_{\phi\phi}$ depends on the angle χ.

In order to examine the spectrum characterizing fluctuations of hydraulic head in three dimensions we introduce, following Lumley and Panofsky (1964, p. 26), the spectrum $E_{\phi\phi}(k)$ which gives the energy content regardless of the direction of $\vec{k}$ unlike the spectrum $\Phi_{\phi\phi}(\vec{k})$ which depends on the direction of $\vec{k}$. The spectrum $E_{\phi\phi}(k)$ is defined as the integral of $\Phi_{\phi\phi}(k)$ over a spherical shell of radius $k = |k|$

$$E_{\phi\phi}(k) = 2\pi k^2 \int_0^{\pi} \Phi_{\phi\phi}(k,\theta) \sin\theta d\theta \tag{6.23}$$

Substituting (4.16) after replacing k_x^2 by $k^2 \cos^2\theta$, where θ is the angle that the wave number vector $\vec{k}$ makes with the direction of the mean flow, in (6.23) gives

$$E_{\phi\phi}(k) = 2\pi k^2 \int_0^{\pi} \frac{\overline{J_o^2 f'^2} \cos^2\theta}{\pi^2 \gamma^3 k^2 [1 + (k/\gamma)^2]^2} \sin\theta \, d\theta \tag{6.24}$$

Noting that $d \cos\theta = -\sin\theta \, d\theta$, (6.24) takes the form

$$E_{\phi\phi}(k) = -\frac{2 \overline{J_o^2 f'^2}}{\pi\gamma^3 [1 + (k/\gamma)^2]^2} \int_0^{\pi} \cos^2\theta \, d \cos\theta$$

Performing the above integration leads to the following expression for $E_{\phi\phi}(k)$:

$$E_{\phi\phi}(k) = \frac{4\, J_o^2 \overline{f'^2}}{3\pi\gamma^3} \cdot \frac{1}{[1 + (k/\gamma)^2]^2} \tag{6.25}$$

We now normalize (6.25) to make the resulting expression independent of units and also multiply both sides by k/γ to obtain

$$\frac{k\, E_{\phi\phi}(k)}{\overline{\phi'^2}} = \frac{4(k/\gamma)}{\pi[1 + (k/\gamma)^2]^2} \tag{6.26}$$

where the variance of hydraulic head $\overline{\phi'^2} = \frac{J_o^2 \overline{f'^2}}{3\gamma^2}$. Equation (6.26) is evaluated for different values of the dimensionless wave number, k/γ , and the results are shown in figure 6-12.

Similarly, we introduce the spectrum of the input (log conductivity), $E_{ff}(k)$, and since the hydraulic conductivity field was assumed to be isotropic we can write (Lumley and Panofsky, 1964)

$$E_{ff}(k) = 4\pi k^2\, \Phi_{ff}(\vec{k}) \tag{6.27}$$

Substituting by $\Phi_{ff}(\vec{k})$ from (4.15) in (6.27) results in

$$E_{ff}(k) = \frac{4\, \overline{f'^2}(k/\gamma)^2}{\pi\gamma[1 + (k/\gamma)^2]^2} \tag{6.28}$$

Multiplying both side of (6.28) by k/γ leads to

$$\frac{k\, E_{ff}(k)}{\overline{f'^2}} = \frac{4\, (k/\gamma)^3}{\pi[1 + (k/\gamma)^2]^2} \tag{6.29}$$

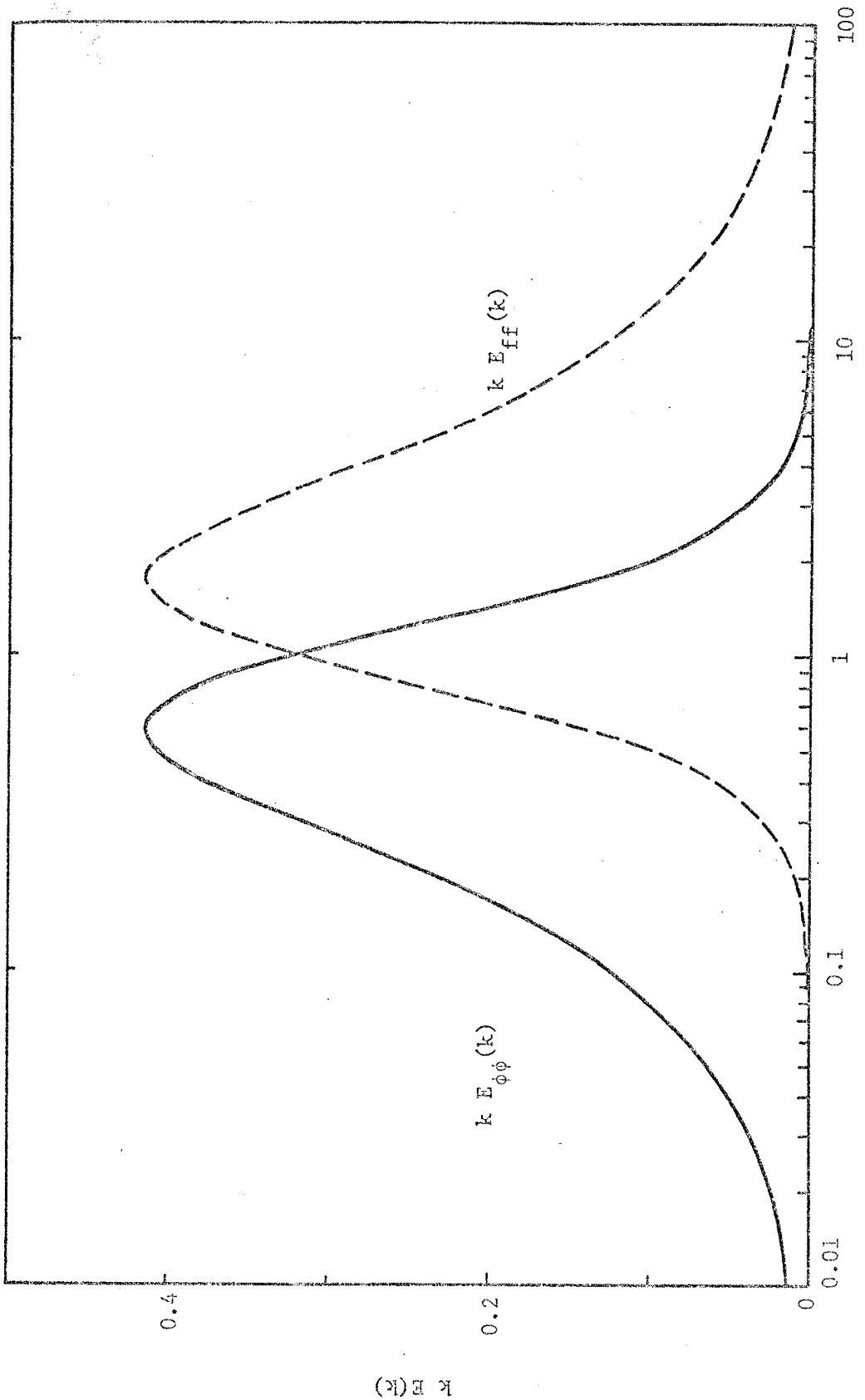

Fig. 6-12: Normalized spectra of log K and hydraulic head versus the dimensionless wave number.

Figure 6-12 also shows the results of evaluating (6.29) for different values of k/γ . This figure illustrates the filtering effect of the flow system. The main contributions to the head variance appear at lower wave numbers than those contributing to the input variance (the hydraulic conductivity). The flow fluctuations are influenced mainly by the low wave number conductivity perturbation.

We now proceed to obtain the one-dimensional spectrum, $\Phi^{(1)}_{\phi\phi}(k_1)$, of hydraulic head fluctuations from its three-dimensional counterpart, $\Phi_{\phi\phi}(\vec{k})$, following the method of integration utilized in section 6.3.1 in connection with the hydraulic conductivity spectrum. The resulting one-dimensional spectrum, $\Phi^{(1)}_{\phi\phi}$, will be compared to the spectrum of hydraulic head fluctuations obtained from the analysis of groundwater flow in one dimension. The one-dimensional spectrum, $\Phi^{(1)}_{\phi\phi}(k_1)$, is defined by (6.12) and the three-dimensional spectrum $\Phi_{\phi\phi}(\vec{k})$ from (4.16) as follows:

$$\Phi^{(1)}_{\phi\phi}(k_1) = \int_{-\infty}^{\infty}\int \frac{J_o \overline{f'^2} \gamma k_1^2}{\pi^2 k^4 (\gamma^2 + k^2)^2} \, dk_2 dk_3 \qquad (6.30)$$

Making use of the axial symmetry of the problem and changing to cylindrical coordinates about the k_1 axis (see figures 6-4), the following expressions result:

$$\tau^2 + k_1^2 = k^2 \ , \quad \text{hence}$$

$$\tau d\tau = k dk$$

where $\tau = 0$ when $k = k_1$. Thus (6.30) becomes

$$\Phi^{(1)}_{\phi\phi}(k_1) = \frac{\overline{J_o^2 f'^2}}{\pi^2} \int_{\zeta=0}^{2\pi} \int_{\tau=0}^{\infty} \frac{\gamma k_1^2 \, \tau d\tau d\zeta}{(\tau^2 + k_1^2)^2 \, (\gamma^2 + k_1^2 + \tau^2)^2}$$

Integration over ζ gives a factor of 2π, i. e.

$$\Phi^{(1)}_{\phi\phi}(k_1) = \frac{\overline{J_o^2 f'^2}}{\pi} \int_{0}^{\infty} \frac{\gamma k_1^2 \, d\tau^2}{(\tau^2 + k_1^2)^2 \, (\tau^2 + k_1^2 + \gamma^2)^2} \tag{6.31}$$

in which the integral is rewritten in terms of τ^2 to simplify its evaluation. Evaluation of (6.31), as shown in Appendix-H, leads to

$$\Phi^{(1)}_{\phi\phi}(k_1) = \frac{\overline{J_o^2 f'^2}}{\pi\gamma^3} \left[\left(1 + \frac{1}{1 + (\gamma/k_1)^2} \right) - 2\left(\frac{k_1}{\gamma}\right)^2 \ln \left[1 + (\gamma/k_1)^2 \right] \right] \tag{6.32}$$

Equation (6.32) represents the one-dimensional spectrum of hydraulic head fluctuations that we set out to derive from the three-dimensional expression. Rewriting (6.32) in a nondimensional form and making use of the variance of hydraulic head fluctuations given by (4.23) we obtain

$$\frac{\gamma \Phi^{(1)}_{\phi\phi}(k_1)}{\overline{\phi'^2}} = \frac{3}{\pi} \left[\left(1 + \frac{1}{1 + (\gamma/k_1)^2} \right) - 2\left(\frac{k_1}{\gamma}\right)^2 \ln \left[1 + (\gamma/k_1)^2 \right] \right] \tag{6.33}$$

As a check on our calculations we can use (6.32) to arrive at an expression for the variance, $\overline{\phi'^2}$, of predicted hydraulic head, defined as

$$\overline{\phi'^2} = \int_{-\infty}^{\infty} \Phi^{(1)}_{\phi\phi}(k_1) \, dk_1 \tag{6.34}$$

This is carried out in Appendix-I, where it is shown that we do arrive at the same expression for $\overline{\phi'^2}$ as shown in Table 6.2.

Figure 6-13 is a plot of the product $k\Phi^{(1)}_{\phi\phi}(k_1)/\overline{\phi'^2}$ (obtained from (6.33)) and the product $k\Phi_{\phi\phi}(k)/\overline{\phi'^2}$ obtained from the one-dimensional analysis of the flow on linear scale versus the logarithm of $\frac{k}{a}$ which has the advantage of collapsing the wave number scale while preserving the area under the spectra. The two spectra are generally similar in shape. The one-dimensional spectrum derived from the three-dimensional flow shows that the peak is located at a slightly higher wave number and is a slightly broader spectrum. The difference in the location of the peaks may be in part due to that difference of the input (see figure 6-9).

Finally, another way to examine the spectrum $\Phi_{\phi\phi}(k)$ of hydraulic head in one dimension in light of the corresponding spectrum $\Phi_{\phi\phi}(\vec{k})$ resulting from the analysis of groundwater flow in three dimensions is to compare their respective variance of hydraulic head. The variance of predicted hydraulic head in one dimension is given by (3.43) as shown in section 3.3.3 while (4.23) from section 4.3 gives the corresponding result in three dimensions. Recall that in section 5.4, it was indicated that a better comparison of results in one and three dimensions required that $\gamma = 2.5a$, where a and γ are the correlation parameters in one and three dimensions respectively. Substituting this expression in (4.23) gives

$$\overline{\phi'^2} = \frac{J_o^2 \overline{f'^2}}{18.7\ a^2} \tag{6.35}$$

for the variance of hydraulic head in three dimensions while the corresponding expression in one dimension is

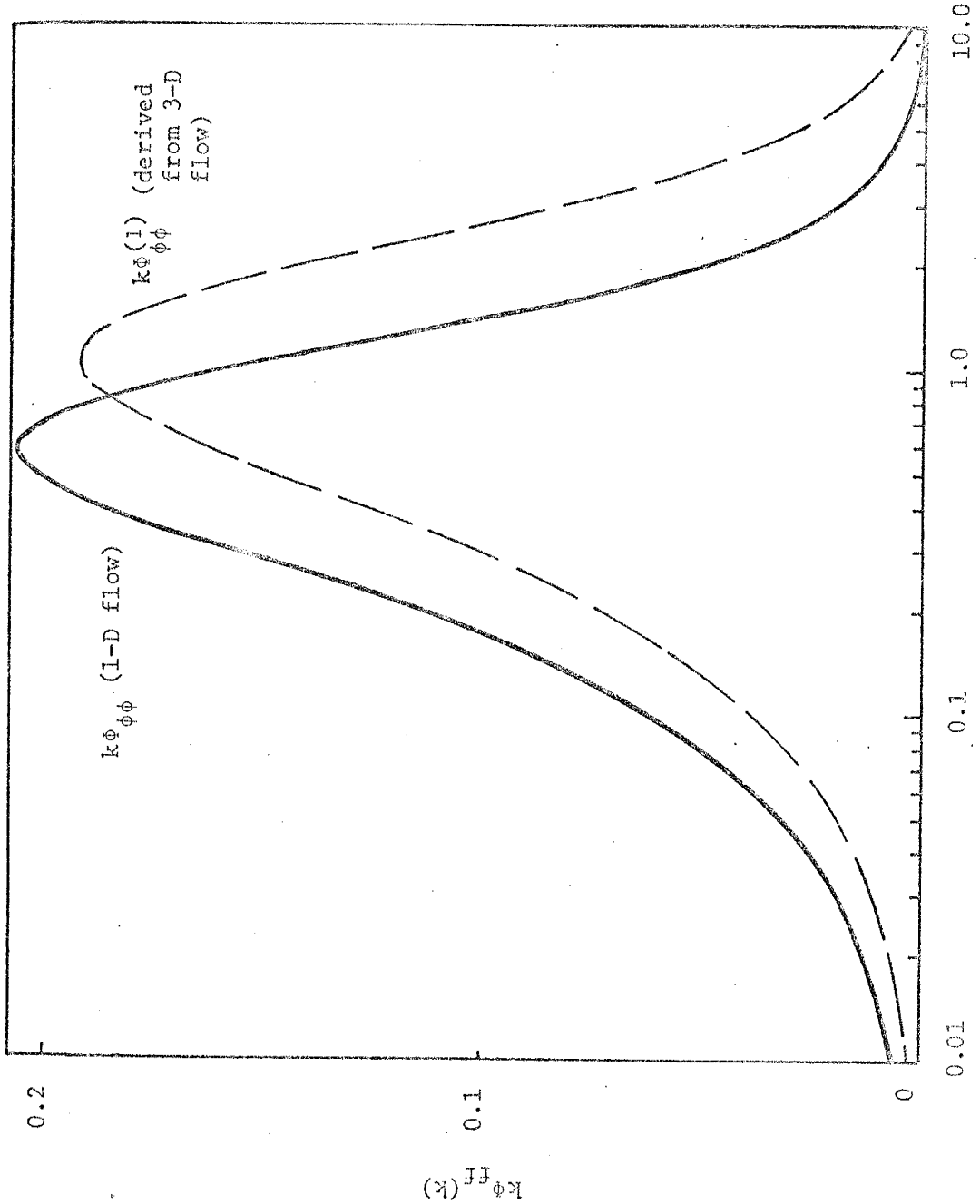

Fig. 6-13: Comparison between the normalized spectra of hydraulic head from one-dimensional flow (for the case of $\gamma = 2.5a$) and that derived from the three-dimensional results.

$$\overline{\phi'^2} = \frac{J_o^2 \overline{f'^2}}{a^2} \tag{3.43}$$

Equation (6.35) reflects an order of magnitude reduction in the variance of predicted hydraulic head in three dimensions relative to that of the one-dimensional case. The above observation indicates the serious errors that would be introduced if results from one-dimensional analysis are used to draw conclusions concerning the effect of heterogeneities which are inherently three-dimensional.

6.4 Discussion of Results

In this section we discuss the results obtained in the previous sections and comment on their implication and significance. We also comment on previous statistical analysis of groundwater flow (e.g. Warren and Price, 1961; McMillan, 1966; Heller, 1972; and Freeze, 1975) in light of the results presented in this and in the previous chapter.

Comparison of the one-dimensional results was carried out in section 6.2. It is indicated therein that the linearized solutions (in terms of K and ln K) to the analysis of groundwater flow in one dimension yield results that depart considerably from that of the exact solution. This observation demonstrates that the linearized solutions are of limited accuracy in comparison with that from the exact for natural flow systems if the standard deviation of ln K is greater than 0.2.

An expression of the spectrum $\phi_{ff}^{(1)}(k_1)$ of fluctuations in ln K was obtained in section 6.3.1 (given by (6.14)) from its three-dimensional counterpart. Equation (6.14) is different from the

corresponding result given by (3.40) for the spectrum $\Phi_{ff}(k)$ arising from the one-dimensional flow analysis of section 3.3.3 in two respects. First, (6.14) does not have k^2 in the numerator and secondly, the bracketed quantity in the denominator is not squared. Graphical comparison of these two spectra (see figure 6-7) showed that while Φ_{ff} has a maximum at $k/a = 1$, the spectrum $\Phi_{ff}^{(1)}$ is a maximum at $k/a = 0$. In figure 6-8 the part of these spectra starting at $k/a = 4$ is a straight line. Figure 6-9, however, shows that $\Phi_{ff}^{(1)}$ has a broader range of wave numbers for conductivity fluctuations in comparison to Φ_{ff}.

The autocorrelation functions of ln K in one and three dimensions were also examined in section 6.3.1. Both functions are quite similar for small lags and as the lag increases they differ from each other; while $\rho_{ff}(\vec{\xi})$ goes to zero the autocorrelation function ρ_{ff} in one dimension becomes negative. However, as indicated in section 5.3.1 the fluctuations in the autocorrelation estimates at large separations are statistically insignificant. Furthermore, in field situations we seldom have enough data to enable the computation of autocorrelation estimates beyond a few lags. Recall, however, that in section 5.4 it is shown that the theoretical autocorrelation function of ln K in three dimensions fits that of field data better than its equivalent in one dimension.

In section 6.3.2, comparison of the autocorrelation functions and spectra characterizing fluctuations in hydraulic head in one and three dimensions was carried out. The autocorrelation of head in three dimensions is anisotropic since it depends on the angle χ that the separation distance makes with the direction of mean flow. It is also of interest to note how the spectrum $E_{\phi\phi}$ of hydraulic head is attenuated with respect to the spectrum E_{ff} of ln K for larger values of the wave number. Finally,

results of the stochastic analysis of the problem of groundwater in three dimensions lead to variance of predicted hydraulic head that is an order of magnitude smaller than the corresponding result for the one-dimensional flow. In other words, serious errors would be involved if results from one-dimensional analysis are used to draw conclusions about natural flow systems in which the conductivity perturbations are inherently three-dimensional.

We now comment on statistical studies of groundwater flow referred to in the beginning of this section. In all of these investigations, the flow systems are assumed to consist of a number of blocks or layers each of constant conductivity. Random number generators are used to assign conductivity values to each unit according to some frequency distribution. However, neighboring conductivity values are assumed to be independent of each other and thus spatial correlation of the hydrologic parameters are not accounted for, rendering these representations incomplete. In this work the analysis of groundwater flow in one dimension developed in Chapter 3 and those of the more general three-dimensional approach presented in Chapter 4 are both based on the theory of flow in a stochastic conductivity continuum with specific covariance structure (see (3.10) and 4.11) in sections 3.3.1 and 4.2 respectively). Spectral analyses of several core data of porosity and permeability from an aquifer in northeastern Illinois demonstrated that the assumed covariance function of hydraulic conductivity fluctuations, though adopted for mathematical convenience, fits the covariance of field data reasonably (see figures 5-31 through 5-33 in section 5.4).

In the Monte Carlo simulations of flow in heterogeneous media carried out by Warren and Price (1961) it was observed that the most

probable value for the permeability of the elements of the model was almost identical to the geometric mean. This observation indicates that the mean conditions for their simulations were consistent with the mean conditions of the analysis developed in section 3.3.3 in which linearization in ln K was used. This is because the log of the geometric mean is identical to the logarithmic mean.

Finally, in the three-dimensional simulation of groundwater flow performed by McMillan (1966), he obtained an empirical factor defined as

$$\text{Empirical factor} = \frac{(s_d/\Delta H)}{(s_K/\overline{K})}$$

in which s_d is the standard deviation of differences in head values, ΔH is the mean difference in head between adjacent nodes in the direction of mean flow, s_K and $\overline{K}$ are the sample standard deviation and mean values of conductivity, respectively. The empirical factor was found to decrease as s_K increased. It is interesting to note that this behavior is also predicted from (4.23), and the numerical factor obtained after rewriting (4.23) also decreases as the standard deviation of ln K increases. This agreement between results from the numerical simulations by McMillan (1966) with those obtained from the analyses developed herein lends support to the stochastic approach adopted for this work.

6.5 Summary

In this section we summarize results of comparisons made between the different solutions to the problem of steady groundwater flow in one dimension. Also summarized are the results of the comparison between

one- and three-dimensional stochastic analyses of groundwater flow.

6.5.1 One-Dimensional Results

Results of the one-dimensional analysis can be summarized as follows:

1. Solution of the problem of steady groundwater flow in one dimension in terms of the hydraulic resistivity, referred to as the exact solution, is to be preferred over the two approximate solutions when estimating flow. This is because the approximate solutions, obtained by linearizing the flow equation in terms of K and ln K, tend to underestimate both the variance of predicted hydraulic head and the mean hydraulic gradient considerably compared to the exact results.

2. The simple network design problems discussed in Chapter 3, showed the applicability and utility of the stochastic analysis of the flow problem in one dimension; their extension to multidimensional flow problems should be developed.

3. Linearizing the flow equation in terms of ln K is intuitively reasonable since the logarithm of a function is far less variable than the function itself. The analyses of section 3.3.3 showed that the results of the approximate solution in terms of ln K were indeed better than that of the case of linearizing in terms of K. This approach is also useful as a basis for comparison with the three-dimensional analysis in which linearization in terms of ln K was also used. Finally, utilizing ln K in the analysis provides a suitable mean hydraulic conductivity in multidimensional flow as shown by Warren and Price (1961).

4. The results of the one-dimensional spectral analysis gave insight to the form of covariance function characterizing fluctuations that was used in the more general three-dimensional analysis.

6.5.2 One-Dimensional Versus Three-Dimensional Results

Results of the comparisons carried out between the one- and three-dimensional forms of solution to the flow problem are summarized below.

1. The variance of predicted hydraulic head from the three-dimensional analysis was found to be an order of magnitude smaller than its corresponding value in one dimension. This is an important result because the errors in head observations will be significantly smaller than indicated by one-dimensional simulations (Freeze, 1975).

2. The agreement between the covariance function describing conductivity fluctuations in one dimension and that describing such fluctuations in three dimensions is reasonable for $\xi/\ell < 2$. For $\xi/\ell > 2$, the one-dimensional autocorrelation becomes negative and remains so while the three-dimensional autocorrelation asymptotically approaches zero as ξ/ℓ increases (see figure 6-5).

3. The spectral density function of hydraulic conductivity fluctuations obtained from integrating the spectrum of the three-dimensional problem shows a wider range of wave numbers for conductivity fluctuations as compared to the spectrum resulting from solution of the one-dimensional flow problem (see figure 6-9).

4. The autocovariance of hydraulic head fluctuations, $R_{\phi\phi}(\xi,\chi)$, is a two parameter function, namely, the separation distance ξ, and the angle χ, that ξ makes with the direction of mean flow. Evaluation of $R_{\phi\phi}(\xi,\chi)$ demonstrated that hydraulic head fluctuations have consistently higher values for all values of ξ/λ in the direction perpendicular to that of the mean flow direction (i. e. at $\chi = \pi/2$) while $R_{\phi\phi}(\xi,\chi)$ is smallest in the direction of flow where $\chi = 0$ (see figure 6-11).

5. The autocovariance of hydraulic head fluctuations in three dimensions is anisotropic since it depends on the angle χ that the separation vector makes with direction of mean flow. It is interesting to note that while the hydraulic conductivity field (or input) was assumed to be statistically isotropic, the resulting hydraulic head (or output) is statistically anisotropic.

CHAPTER 7

CONCLUSIONS

Several major results of significance in relation to the effects of spatial variation of hydraulic conductivity of aquifer materials on groundwater flow have been established. These fall into the following categories:

Flow of Groundwater in One Dimension

1. Among the three methods followed for the solution of the problem of groundwater flow in one dimension, the exact analysis in terms of the hydraulic resistivity W is valid for any value of the fluctuations W' since any function can be expressed in terms of its mean and a fluctuation about the mean with no limitation on the size or amplitude of the fluctuation part.

2. The approximate analyses by linearizing in terms of K and ln K are valid for small perturbations. Linearizing in terms of ln K is more accurate than in terms of K itself since variation in ln K are much smaller than that of K. The approximate solutions, however, tend to underestimate both the standard deviation of hydraulic head and the mean hydraulic gradient considerably compared to that of the exact results. Consequently, the linearized solutions are limited in comparison with the exact results especially for natural flow systems where σ is commonly indicated to be greater than 0.2.

3. Based on the previous conclusion it follows that in estimating flow quantities in one dimension using Darcy's equation, one would have to work with the hydraulic resistivity W and not the hydraulic conductivity.

4. The mean conditions for the input (or conductivity) are consistent with that found by Warren and Price (1961) since the logarithmic mean is equal to the log of the geometric mean which represented the mean permeability of the different blocks used in their simulations.

5. It has been shown that the one-dimensional flow is a two parameter problem, namely, the standard deviation of ln K and the correlation length, ℓ, of the medium, characterizing the average distance over which neighboring conductivity values are positively correlated.

6. The analysis of the permeameter example demonstrated the usefulness of the theoretical results in establishing the spacing between two hydraulic head measurements required to estimate the hydraulic conductivity or the hydraulic resistivity with a given degree of accuracy.

7. Results from the aquitard example may be useful in estimating the length of core material that would be required for a hydraulic conductivity measurement to be made with a certain degree of accuracy.

Flow of Groundwater in Three Dimensions

1. The main conclusion to be derived from results of solving the problem of groundwater flow in three dimensions is the observed reduction in variance of predicted hydraulic head. Compared to the variance of predicted head in one dimension, the variance obtained from the three-dimensional analysis of the flow is an order of magnitude smaller. Serious errors would result if analyses of groundwater flow in one dimension are used for predictions of flow conditions in natural systems which are inherently three-dimensional.

2. The autocorrelation of hydraulic head fluctuations in three dimensions is statistically anisotropic, although the hydraulic conductivity field (or input) was assumed to be stastistically isotropic.

3. The flow system has a filtering effect as evidenced by the displacement of the peaks of the spectra (see figure 6-12) of the input (conductivity) and the output (hydraulic head).

4. The relationship between the standard deviation of log K and that of hydraulic head obtained from this study is in agreement in the structure and behavior to a similar relationship obtained from three-dimensional simulations (McMillan, 1966). This lends support to the stochastic approach utilized in this study.

Stochastic Analyses of Permeability and Porosity Data

1. The form of the autocovariance function assumed to characterize fluctuations in hydraulic conductivity of aquifer materials appears to be appropriate as evidenced by the good agreement between it and the covariance of actual data.

2. Values of the integral scale determined from a large set of core data of samples from different parts of an aquifer in northeastern Illinois showed little variation. This observation lends support to the contention that the integral scale characterizing permeability fluctuations is a physical parameter.

3. The existence of a length scale describing correlation of neighboring values of a hydrologic parameter enhances the applicability of the simple network design problems discussed earlier since the analysis of these problems indicated the need for such a parameter.

REFERENCES

Agterberg, F. P., Developments in Geomathematics, 596 pp. Elservier Pub. Co., Ltd., Amsterdam, 1974.

Aitchison, J., and J. A. C. Brown, The Lognormal Distribution, 176 pp., Cambridge Univ. Press, London, 1957.

Asfari, A., and P. A. Witherspoon, Numerical simulation of naturally fractured reservoirs, Soc. Petrol. Eng. J., (in press) 1973.

Bagnold, R. A., Deposition in the process of hydraulic transport, Sedimentology, 10, 45-56, 1968.

Bear, J., Dynamics of Fluids in Porous Media, 764 pp., Elservier Pub. Co., Ltd., Amsterdam, 1972.

Bennion, D. W., and J. C. Griffiths, A stochastic model for predicting variations in reservoir rock properties, Trans. AIME, 237, part 2, 9-16, 1966.

Bennion, D. W., and A. C. A. Hope, Mathematical modelling of reservoir rock properties, J. Canadian Petrol. Technol., 1-10, April-June, 1974.

Bibby, R., and D. K. Sunada, Statistical error analysis of a numerical model of confined groundwater flow, Proceedings, First International Symposium on Stochastic Hydraulics, C. L. Chiu (Ed.), 591-612, 1971.

Bouwer, H., Planning and interpreting soil permeability measurements, J. Irrig. Drain. Div. Amer. Soc. Civil Eng., 95(IR3), 391-402, 1969.

Breiman, L., Probability and Stochastic Processes: with a View Toward Applications, 324 pp., Houghton Mifflin Co., Boston, 1969.

Brust, K. J., C. H. M. van Bavel, and G. B. Stirk, Hydraulic properties of a clay-loam soil and the field measurement of water uptake by roots, 3, Soil Sci. Soc. Amer. Proc., 32(3), 322-326, 1968.

Bulnes, A. C., An application of statistical methods to core analysis data of dolomitic limestone, Trans. AIME, 165, Petrol. Div., 223-240, 1946.

Butler, S. S., and D. L. Gundlach, Discharge and travel time for groundwater conduits, J. Irrig. Drain. Div. Amer. Soc. Civil Eng., 100(IR1), 17-29, 1974.

Buyevich, Y. A., A. I. Leonov, and V. M. Safrai, Variations in filtration velocity due to random large scale fluctuations in porosity, J. Fluid. Mech., 37, part 2, 371-381, 1969.

Cardwell, W. T., Jr., and R. L. Parsons, Average permeabilities of heterogeneous oil sands, Trans. AIME, 160, part 2, 34-42, 1945.

Coelho, M. A., Spatial variability of water related soil physical properties, Ph.D. Thesis, 97 pp., Univ. of Arizona, Tucson, 1974.

Cohen, P., Specific yield and particle size relations of quaternary alluvium, Humboldt River valley, Nevada, U. S. Geological Survey Water-Supply Paper 1669-M, 1963.

Csallany, S., and W. C. Walton, Yields of shallow dolomite wells in northern Illinois, Illinois State Water Survey Rept. Invest. 46, 1963.

Davis, S. N., Porosity and permeability of natural materials, Ch. 2 in Flow Through Porous Media, R. J. M. DeWeist (Ed.), Academic Press, New York, 53-89, 1969.

Dixon, W. J., (Ed.), BMD: Biomedical Computer programs, BMD02T, 517-540, Univ. of California Press, Berkeley, 1974.

Dwight, H. B., Tables of Integrals and Other Mathematical Data, 336 pp., The Macmillan Company, New York, 1961.

Emsellem, Y., and G. De Marsily, An automatic solution for the inverse problem, Water Resour. Res., 7(5), 1264-1283, 1971.

Erdelyi, A., (Ed.), Tables of Integral Transforms, vol. 1, Bateman Manuscript Project, 391 pp., McGraw-Hill, New York, 1954.

Eriksson, E., Groundwater time-series: An exercise in stochastic hydrology, Nord. Hydrol., 1(3), 181-205, 1970a.

Eriksson, E., Cross-spectrum analysis of groundwater levels in an esker, Nord. Hydrol., 1(4), 245-259, 1970b.

Freeze, R. A., Theoretical analysis of regional groundwater flow, Ph.D. Thesis, 304 pp., Univ. of California, Berkeley, 1966.

Freeze, R. A., Regionalization of hydrologic parameters for use in mathematical models of groundwater flow, 24th International Geological Congress, Sec. 11, 177-190, 1972.

Freeze, R. A., A stochastic-conceptual analysis of one-dimensional groundwater flow in nonuniform homogeneous media, Water Resour. Res., 11(5), 725-741, 1975.

Gambolati, G., P. Gatto, and R. A. Freeze, Mathematical simulation of the subsidence of Venice, 2. Results, Water Resour. Res., 10(3), 563-577, 1974.

Gelhar, L. W., Stochastic analysis of phreatic aquifers, Water Resour. Res., 9(3), 721-733, 1974.

Gelhar, L. W., P. Y. Ko, H. H. Kwai, and J. L. Wilson, Stochastic modelling of groundwater systems, Rept. No. 189, R. M. Parsons Lab. for Water Resources and Hydrodynamics, Massachusetts Institute of Technology, Cambridge, Mass., 1974.

Gelhar, L. W., Effects of hydraulic conductivity variations on groundwater flows, Paper to be presented at the Second International Symposium on Stochastic Hydraulics to be held in Lund, Sweden, August 2-4, 1976.

Gradshteyn, I. S., and I. M. Ryzhik, Tables of Integrals, Series, and Products, 1086 pp., Academic Press, New York, 1965.

Greenkorn, R. A., C. R. Johnson, and L. K. Shallenberger, Directional permeability of heterogeneous anisotropic porous media, Trans. AIME, 231, part 2, 124-132, 1964.

Griffiths, J. C., The Scientific Method in Analysis of Sediments, 508 pp., McGraw-Hill, New York, 1967.

Hannan, E. J., Time Series Analysis, 152 pp., Metheun & Co., Ltd., London, 1960.

Heller, J. P., Observations on diffusion and mixing in porous media, Proceedings, Second International Symposium on Fundamentals of Transport Phenomena in Porous Media, IAHR and ISSS, Univ. of Guelph, Ontario, Canada, 1, 1-26, 1972.

Illinois State Water Survey, Feasibility study on desalting brackish water from the Mt. Simon aquifer in northeastern Illinois, Contract No. 14-30-2924 with the Department of the Interior, Office of Saline Water, 120 pp., 1973.

Jackson, R. E., J. A. Gilliland, and K. Adamowski, Time series analysis of the hydrologic regimen of a groundwater discharge area, Water Resour. Res., 9(5), 1411-1419, 1973.

Jenkins, G. M., and D. G. Watts, Spectral Analysis and Its Applications, 525 pp., Holden-Day, Inc., San Francisco, 1968.

Julian, P. R., Variance spectrum analysis, Water Resour. Res., 3(3), 831-845, 1967.

Koch, G. S. Jr., and R. F. Link, Statistical Analysis of Geologic Data, 2 vols: v. 1, 375 pp.; v. 2, 438 pp., John Wiley and Sons, Inc., New York, 1972.

Krumbein, W. C., Application of the logarithmic moments to size frequency distributions of sediments, J. Sediment. Petrol, 6(1), 35-47, 1936.

Krumbein, W. C., and M. F. Dacey, Markov chains and embedded Markov chains in geology, J. Intern. Assoc. Math. Geology, 1(1), 79-96, 1969.

Krumbein, W. C., and F. A. Graybill, An Introduction to Statistical Models in Geology, 475 pp., McGraw-Hill, New York, 1965.

Krumbein, W. C., and G. D. Monk, Permeability as a function of the size parameters of sedimentary particles, Amer. Inst. Mining Metall. Eng. Tech. Pub. 1492, 153-163, 1942.

Law, J., A statistical approach to the interstitial heterogeneity of sand reservoirs, Trans. AIME, 155, Petrol. Div., 202-222, 1944.

Lippmann, M. J., Two-dimensional stochastic model of a heterogeneous geologic system, Ph.D. Thesis, 135 pp., Univ. of California, Berkeley, 1973.

Lumley, J. L., Stochastic Tools in Turbulence, 194 pp., Academic Press, New York, 1970.

Lumley, J. L., and H. A. Panofsky, The Structure of Atmospheric Turbulence, 239 pp., John Wiley and Sons, Inc., New York, 1964.

Masch, F. D., and K. J. Denny, Grain size distribution and its effects on the permeability of unconsolidated sands, Water Resour. Res., 2(4), 665-677, 1966.

Mason, D. D., J. F. Lutz, and R. G. Petersen, Hydraulic conductivity as related to certain soil properties in a number of great soil groups - Sampling errors involved, Soil Sci. Soc. Amer. Proc., 21(5), 554-560, 1957.

Mast, R. F., and P. E. Potter, Sedimentary structures, sand shape fabrics and permeability, 2, J. Geology, 71(5), 548-565, 1963.

Matern, B., Metoder att uppskatta noggrannheten vid linje-och provytetaxering (Methods of estimating the accuracy of line and sample plot surveys), Meddelanden fran Statens Skogsforskning-sinstitut, 36, 1-117, 1947.

McMillan, W. D., Theoretical analysis of groundwater basins operations, Tech. Rept. No. 6-25, 167 pp., Hydraulic Lab., Univ. of California, Berkeley, 1966.

Merriam, D. F., (Ed.), Geostatistics: a Colloquium, 177 pp., Plenum Press, New York, 1970.

Monin, A. S., and A. M. Yaglom, Statistical Fluid Mechanics, 769 pp., The M.I.T. Press, Cambridge, Mass., 1971.

Nelson, R. W., In-place determination of permeability distribution for heterogeneous porous media through analysis of energy dissipation, Soc. Petrol. Eng. J., 8(1), 33-42, 1968.

Nelson, R. W., and W. L. McCollum, Transient energy dissipation methods of measuring permeability distributions in unconfined heterogeneous porous materials, 51 pp., Open file report, Contract No. 14-08-0001-11994, Water Resour. Div., U. S. Geological Survey, 1969.

Nielsen, D. R., J. W. Biggar, and K. T. Erh, Spatial variability of field-measured soil-water properties, Hilgardia, 42(7), 215-259, 1973.

Pettijohn, F. J., P. E. Potter, and R. Siever, Sand and Sandstone, 618 pp., Springer-Verlag, New York, 1972.

Polasek, T. L., and C. A. Hutchinson, Jr., Characterization of non-uniformities within a sandstone reservoir from a fluid mechanics standpoint, In: 7th World Petroleum Cong. Proc., 2, 397-407, Elsevier Pub. Co., Ltd., Amsterdam, 1967.

Prats, M., The influence of oriented arrays of thin impermeable shale lenses or of highly conductive natural fractures on apparent permeability anisotropy, J. Petrol. Technol., 24, 1219-1221, October, 1972.

Pryor, W. A., Permeability-porosity patterns and variations in some Holocene sand bodies, Amer. Assoc. Petrol. Geologists Bull., 57(1), 162-189, 1973.

Rodrigues-Iturbe, I., and J. M. Mejia, The design of rainfall networks in time and space, Water Resour. Res., 10(4), 713-728, 1974.

Rogowski, A. S., Watershed physics: Soil variability criteria, Water Resour. Res., 8(4), 1015-1023, 1972.

Rose, H. G., and H. F. Smith, Particles and permeability: A method of determining permeability and specific capacity from effective grain size, Water Well J., 11(3), p. 10, 1957.

Sagar, B., and C. C. Kisiel, Limits of deterministic predictability of saturated flow equations, Proceedings, Second International Symposium on Fundamentals of Transport Phenomena in Porous Media, IAHR and ISSS, Univ. of Guelph, Ontario, Canada, 1, 194-205, 1972.

Seaber, P. R., and E. F. Hollyday, Statistical analysis of regional aquifers, (abs.), Geol. Soc. of Amer., Special Paper No. 101: Abstracts for 1966, 1968.

Stockton, J. G., and A. W. Warrick, Spatial variability of unsaturated hydraulic conductivity, Soil Sci. Soc. Amer. Proc., 35(5), 847-848, 1971.

Theis, C. V., Aquifers and models, Proceedings of the National Symposium on Ground-Water Hydrology, Amer. Water Resour. Assoc., San Francisco, 138-148, November 6-8, 1967.

Todd, D. K., Ground Water Hydrology, 336 pp., John Wiley and Sons, Inc., New York, 1959.

Toth, J., A theoretical analysis of groundwater flow in small drainage basins, J. Geophys. Res., 68(16), 4795-4812, 1963.

U. S. Geological Survey, Definitions of selected ground-water terms - Revisions and conceptual refinements, Water-Supply Paper 1988, 21, pp., 1972.

Visocky, A. P., Private Communications, 1975.

Vistelius, A. B., Studies in Mathematical Geology, 294 pp., Consulting Bureau, New York, 1967.

Warren, J. E., and H. S. Price, Flow in heterogeneous porous media, Soc. Petrol. Eng. J., 1, 153-169, September, 1961.

Warren, J. E., F. F. Skiba, and H. S. Price, An evaluation of the significance of permeability measurements, J. Petrol. Technol., 13, 739-744, August, 1961.

Whittle, P., On stationary processes in the plane, Biometrika, 41, 434-449, 1954.

Willardson, L. S., and R. L. Hurst, Sample size estimates in permeability studies, J. Irrig. Drain. Div. Amer. Soc. Civil Eng., 91(IR1), 1-9, 1965.

Wu, T. H., S. K. Vyas, and N. Y. Chang, Probabilistic analysis of seepage, J. Soil Mech. Found. Div. Amer. Soc. Civil Eng., 99(SM4), 323-340, 1973.

Yevjevich, V., Stochasticity in geophysical and hydrological time series, Nord. Hydrol., 2(4), 217-242, 1971.

APPENDIX - A

Representation Theorem For a Stationary Stochastic Process

A.1 Stationary or Homogeneous Random Processes. A random process X(t) is said to be strictly stationary if its statistics are not affected by a shift in the time origin. In particular, the probability density function of X(t) is independent of time. That is to say that the two processes X(t) and X(t + τ) have the same statistics for any τ. Since most of the methods used in time series analysis are based upon the first and second moments, i.e., means and variances, it is reasonable to define a less restrictive type of a stationary process.

A random process is said to be stationary in the wide sense if its expected value is a constant and its autocorrelation function depends only on the time difference τ. In terms of the probability density function, p(X), we can write the mean as

$$\overline{X} \equiv \mu_X = E[X(t)] = \int_{-\infty}^{\infty} Xp(X)dX \tag{A.1}$$

and the covariance as

$$R_{XX}(\tau) = E[X(t)\ X(t+\tau)]$$

$$= \iint_{-\infty}^{\infty} X_1 X_2 p(X_1, X_2)\ dX_1 dX_2 \tag{A.2}$$

where $X_1 = X(t)$, $X_2 = X(t + \tau)$ and $p(X_1, X_2)$ is the joint probability density function (Lumley and Panofsky, 1964, p. 13). The quantity $R_{XX}(0)$ is known as the variance.

If we are working with a space series, i.e. a process which is a function of space or distance instead of time (e.g. hydraulic conductivity measurements), then our independent variable is space or distance instead of time. Hence, we speak of a homogeneous process instead of a stationary process if space is our independent variable rather than time; the above discussion holds true for stationary as well as for homogeneous processes. But why are we interested in stationary or homogeneous processes? We are interested in stationarity (or homogeneity) since it brings a major simplification into our calculations, that is it permits the introduction of time (or space) averages which are meaningful in the sense that their values represent properties of the process that we can actually measure (Lumley and Panofsky, 1964, p. 14).

A.2 Representation Theorem For a Stochastic Process. The subsequent discussion follows essentially Lumley and Panofsky (1964). Fourier representation of periodic functions is a very useful tool in linear analysis. However, random functions are neither periodic nor integrable, so that neither Fourier series nor integrals may be used in the ordinary sense. However, stationary (or homogeneous) processes can be represented in the complex form as

$$X(\xi) = \int_{-\infty}^{\infty} e^{ik\xi}\, dZ(k) \qquad (A.3)$$

which is known as Cramer representation of a stationary process or stochastic Fourier-Stieltjes integral. The integral is written in this way because the process Z(k) may not have derivatives. The differences dZ(k) represent complex amplitudes of the Fourier modes of wave number k. This

process has orthogonal increments, i.e., nonoverlapping differences are uncorrelated or

$$\left.\begin{aligned} E[dZ(k_1)\ dZ^*(k_2)] &= 0 && k_1 \neq k_2 \\ &= dF(k) = \Phi(k)\ dk && k_1 = k_2 = k \end{aligned}\right\} \tag{A.4}$$

with

$$F(k) = \int_{-\infty}^{k} \Phi(k')\ dk' \tag{A.5}$$

where the asterisk denotes the complex conjugate. Equation (A.5) is used to write the autocovariances in the form

$$R_{XX}(\xi) = \int_{-\infty}^{\infty} e^{ik\xi}\ dF(k) = \int_{-\infty}^{\infty} e^{ik\xi}\ \Phi(k)\ dk \tag{A.6}$$

The set of theorems represented by (A.3) through (A.6) is called the Wiener-Khintchine theorem, and it enables random functions to be expanded in terms of Fourier-Stieltjes integrals which is a useful tool in solving differential equations involving random processes. Note that F(k) is known as a spectral distribution, since F(k) gives the contribution to the variance $R_{XX}(0)$ from wave numbers below k, whereas $\Phi(k)$, the spectral density or spectrum, represents the distribution of variance over wave number. The spectrum can be obtained from the inverse Fourier transform of the covariance function $R(\xi)$ of the process $X(\xi)$ as

$$\Phi(k) = \frac{1}{2\pi} \int_{-\infty}^{\infty} e^{-ik\xi}\ R(\xi)\ d\xi \tag{A.7}$$

As a result of (A.7), spectra have the following properties. Through a change of variables, using (A.7), we find that

$$\Phi(k) = \Phi(-k) \tag{A.8}$$

i.e., the spectrum is an even quantity. In addition, from (A.7), (A.4), and (A.5) we obtain

$$\Phi(k) \quad \text{real}, \quad \Phi(k) \geq 0 \tag{A.9}$$

Making use of the symmetry of the spectrum, the covariance function (A.6) can be expressed as a cosine transform

$$R(\xi) = \int_{-\infty}^{\infty} \cos\, k\xi\Phi(k)\, dk = 2 \int_{0}^{\infty} \cos\, k\xi\Phi(k)\, dk \tag{A.10}$$

APPENDIX - B

Derivation of the Variance, $\overline{e'^2}$, of Discharge

In this appendix we present the algebraic steps necessary to arrive at (3.62) representing the variance in discharge, $\overline{e'^2}$. We start out by recalling the expression for $\overline{e'^2}$

$$\overline{e'^2} = \overline{\left(\frac{W'_3}{\bar{W}}\right)^2} + 2\overline{\left(\frac{\phi'}{\Delta\bar{\phi}}\right)^2} - 2\frac{\overline{W'_3\phi'_1}}{\Delta\bar{\phi}\bar{W}} + 2\frac{\overline{W'_3\phi'_2}}{\Delta\bar{\phi}\bar{W}} - 2\frac{\overline{\phi'_1\phi'_2}}{\Delta\bar{\phi}} \tag{3.56}$$

where

$$\overline{\phi'_1\phi'_2} = \frac{q^2\overline{W'^2}}{a^2}(1 + aL)\,\bar{e}^{aL} \tag{3.13}$$

$$\overline{\phi'^2} = \frac{q^2\overline{W'^2}}{a^2} \tag{3.14}$$

$$\Delta\bar{\phi} = q\bar{W}L \tag{3.52}$$

$$\overline{W'_3\phi'_1} \equiv \overline{\phi'_1W'_3} = R_{W\phi}(\xi) = R_{W\phi}(d) \qquad , \qquad d > 0 \tag{3.59}$$

and

$$\overline{W'_3\phi'_2} \equiv \overline{\phi'_2W'_3} = R_{\phi W}(L-d) = R_{W\phi}(d-L) \qquad , \qquad d-L \leq 0 \tag{3.60}$$

in which $R_{W\phi}(\xi)$ is given by

$$R_{W\phi}(\xi) = \begin{cases} q\xi\ \overline{W'^2_3}\ e^{-a\xi} & ;\quad \xi > 0 \\ q\xi\ \overline{W'^2_3}\ e^{a\xi} & ;\quad \xi \leq 0 \end{cases}$$

Substituting the above expressions into (3.56) yields

$$\overline{e'^2} = \overline{\left(\frac{W'_3}{\overline{W}}\right)^2} + \frac{2}{a^2L^2}\overline{\left(\frac{W'_3}{\overline{W}}\right)^2} - \frac{2}{a^2L^2}\overline{\left(\frac{W'_3}{\overline{W}}\right)^2}(1 + aL)\ e^{-aL}$$

$$- \frac{2d}{L}\overline{\left(\frac{W'_3}{\overline{W}}\right)^2} e^{-ad} + \frac{2(d - L)}{L}\overline{\left(\frac{W'_3}{\overline{W}}\right)^2} e^{a(d-L)}$$

Hence,

$$\frac{\overline{e'^2}}{(W'_3/\overline{W})^2} = \left\{1 + \frac{2}{(aL)^2}\left[1 - (1 + aL)\ e^{-aL}\right] + 2\left(\frac{d}{L} - 1\right) e^{a(d-L)} - \frac{2d}{L} e^{-ad}\right\}$$

which is the required expression.

APPENDIX - C

Transformation From Cartesian to Spherical Coordinates

To simplify evaluation of integrals of autocovariance functions and spectra in three dimensions we transformed the rectangular elemental volume $d\vec{\xi}$ or $d\vec{k}$ to an elemental volume in spherical coordinates; this is done as follows. We first write the following expressions relating the coordinates in rectangular coordinates (k_1, k_2, k_3) to those in spherical coordinates (k, ζ, θ):

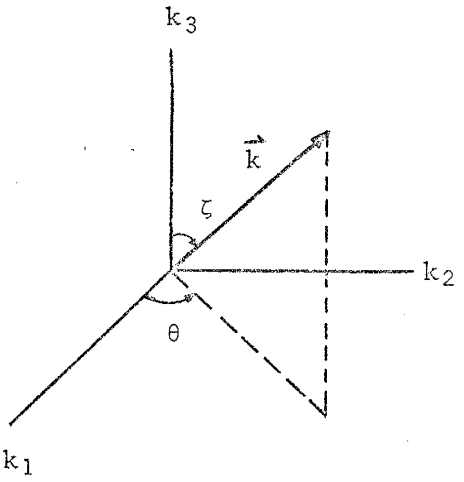

$$\left.\begin{aligned} k_1 &= k \sin\zeta \cos\theta \\ k_2 &= k \sin\zeta \sin\theta, \text{ and} \\ k_3 &= k \cos\zeta \end{aligned}\right\} \qquad (C.1)$$

Now using the Jacobian of the rectangular coordinates k_1, k_2, and k_3 with respect to the spherical coordinates k, ζ, and θ, we arrive, after simple algebraic manipulation (see any standard calculus text), to the elemental volume in spherical coordinates

$$dV = k^2 \sin\zeta \, dk d\zeta d\theta \qquad (C.2)$$

where the limits of the spherical coordinates are

$$\left.\begin{aligned} 0 < k < \infty \\ 0 < \zeta < \pi \\ 0 < \theta < 2\pi \end{aligned}\right\} \qquad (C.3)$$

Equation (C.2) is used for the transformation of integrals from rectangular to spherical coordinates while (C.3) is utilized for the evaluation of the resulting integrals.

Finally, we note that the above derivations were performed for the wave number vector $\vec{k}$ realizing, however, that the same procedure holds for the separation vector $\vec{\xi}$, or any other vector for that matter.

APPENDIX - D

Evaluation of Three-Dimensional Autocorrelation Function of Hydraulic Head Fluctuations

Recall that the autocovariance $R_{\phi\phi}(\xi,\chi)$ of hydraulic head fluctuations in three dimensions is given by (4.21) as

$$R_{\phi\phi}(\xi,\chi) = C \int_{k=0}^{\infty} \int_{\alpha=0}^{2\pi} \int_{y=-1}^{1} \frac{(y^2 \cos^2\chi + \sin^2\chi \cos^2\alpha - y^2 \sin^2\chi \cos^2\alpha) \cos k\xi y}{(\gamma^2 + k^2)^2} \, dy d\alpha dk \qquad (4.21)$$

in which

$$C = \frac{\gamma J_o^2 \overline{f'^2}}{\pi^2}$$

Let us first integrate the above expression with respect to k so that

$$I \equiv \int_{k=0}^{\infty} \frac{\cos ak}{(\gamma^2 + k^2)^2} \, dk = \frac{\pi}{4\gamma^3} (1 + a\gamma) \, e^{-a\gamma} \qquad \text{for } a > 0, \ \gamma > 0 \qquad (D.1)$$

where $a = \xi y$.

If $a < 0$, we set $a = -a'$, $a' > 0$ or $a' = |a|$, hence (D.1) becomes

$$I = \frac{\pi}{4\gamma^3} (1 + |a|\gamma) \, e^{-|a|\gamma}$$

Substituting in (4.21) leads to

$$R_{\phi\phi}(\xi,\chi) = \frac{\pi\, J_o^2\, \overline{f'^2}\, \gamma}{4\pi^2\gamma^3} \int_{\alpha=0}^{2\pi} \int_{y=-1}^{1} (1 + \gamma|\xi y|)\, \bar{e}^{\gamma|\xi y|}\, x$$

$$(y^2 \cos^2\chi + \sin^2\chi \cos^2\alpha - y^2 \sin^2\chi \cos^2\alpha)\, dy d\alpha$$

Setting $B = (1 + \gamma|\xi y|)\, \bar{e}^{\gamma|\xi y|}$, the above expression reduces to

$$R_{\phi\phi}(\xi,\chi) = \frac{J_o^2\, \overline{f'^2}}{4\pi\gamma^2} \left\{ \int_{\alpha=0}^{2\pi} \int_{-1}^{1} B[y^2 \cos^2\chi + \sin^2\chi \cos^2\alpha - y^2 \sin^2\chi \cos^2\alpha] \right.$$

$$\left. x\, dy d\alpha \right\}$$

Setting $A = \frac{J_o^2\, \overline{f'^2}}{4\pi\gamma^2}$ and integrating this expression term by term with respect to the angle α gives

$$R_{\phi\phi}(\xi,\chi) = A \left\{ \int_{-1}^{1} 2\pi\, B\, y^2 \cos^2\chi\, dy \right.$$

$$+ \frac{1}{2} \int_{-1}^{1} B \sin^2\chi\, (\alpha + \sin\alpha \cos\alpha) \Big|_{o}^{2\pi} dy$$

$$\left. - \frac{1}{2} \int_{-1}^{1} B\, y^2 \sin^2\chi\, (\alpha + \sin\alpha \cos\alpha) \Big|_{o}^{2\pi} dy \right\}$$

The above expression can be written in the form

$$R_{\phi\phi}(\xi,\chi) = \pi A \left\{ \int_{-1}^{1} (1 + \gamma|\xi y|)\, \bar{e}^{\gamma|\xi y|}\, [2y^2 \cos^2\chi + \sin^2\chi(1 - y^2)]\, dy \right\}$$

(D.2)

Taking $\xi > 0$ in (D.2) causes no loss of generality in our results, and since the integrand is an even function in y we can write the above integral as twice its value from 0 to 1

$$R_{\phi\phi}(\xi,\chi) = 2\pi A \left\{ \int_0^1 (1 + \gamma\xi\, y\,)\, e^{-\gamma\xi y}\, [2y^2 \cos^2\chi + \sin^2\chi(1-y^2]dy \right\} \tag{D.3}$$

We now proceed to evaluate (D.3) by making use of the following trigonometric identity:

$$\sin^2\chi = 1 - \cos^2\chi$$

to rewrite the following part of the integrand:

$$2y^2\cos^2\chi + \sin^2\chi(1-y^2) = 2y^2\cos^2\chi + (1-\cos^2\chi)(1-y^2)$$

$$= y^2\,(3\cos^2\chi - 1) - (\cos^2\chi - 1)$$

Substituting the above expression in (D.3) leads to

$$R_{\phi\phi}(\xi,\chi) = 2\pi A \int_0^1 (1 + \gamma\xi y)\, e^{-\gamma\xi y}\, [y^2\,(3\cos^2\chi - 1) - (\cos^2\chi - 1)]dy \tag{D.4}$$

We break up this expression to simplify its evaluation and label each integral as follows:

$$I_1 = \int_0^1 (3\cos^2\chi - 1)\, y^2\, e^{-\gamma\xi y}\, dy$$

$$I_2 = -\int_o^1 (\cos^2 \chi - 1)\ e^{-\gamma\xi y}\ dy$$

$$I_3 = \int_o^1 \gamma\xi y^3\ (3\cos^2 \chi - 1)\ e^{-\gamma\xi y}\ dy$$

and

$$I_4 = -\int_o^1 \gamma\xi y\ (\cos^2 \chi - 1)\ e^{-\gamma\xi y}\ dy$$

Performing the integrations we obtain using tables of integrals (Dwight, 1961)

$$I_1 = \int_o^1 (3\cos^2 \chi - 1)\ y^2\ e^{-\gamma\xi y}\ dy$$

$$= (3\cos^2 \chi - 1)\left[\frac{2(1 - e^{-\gamma\xi})}{(\gamma\xi)^3} - e^{-\gamma\xi}\left(\frac{1}{\gamma\xi} + \frac{2}{(\gamma\xi)^2}\right)\right] \quad ;$$

$$I_2 = -\frac{(\cos^2 \chi - 1)}{\gamma\xi}\ (e^{-\gamma\xi} - 1) \quad ;$$

$$I_3 = \int_o^1 \gamma\xi y^3\ \ (3\cos^2 \chi - 1)\ e^{-\gamma\xi y}\ dy$$

$$= \gamma\xi(3\cos^2 \chi - 1)\left[\frac{y^3\ e^{-\gamma\xi y}}{(-\gamma\xi)}\Bigg|_{y=0}^{1} - \frac{3}{(-\gamma\xi)}\int_o^1 y^2\ e^{-\gamma\xi y}\ dy\right]$$

$$I_3 = (3\cos^2\chi - 1)\left\{-e^{-\gamma\xi} + \left[-\frac{3e^{-\gamma\xi}}{\gamma\xi}\left(1 + \frac{2}{\gamma\xi} + \frac{2}{(\gamma\xi)^2}\right) + \frac{6}{(\gamma\xi)^2}\right]\right\} \quad ;$$

and finally

$$I_4 = \int_0^1 \gamma\xi\,(\cos^2\chi - 1)\, y\, e^{-\gamma\xi y}\, dy$$

$$= -(\cos^2\chi - 1)\left[e^{-\gamma\xi}\left(1 + \frac{1}{\gamma\xi}\right) - \frac{1}{\gamma\xi}\right]$$

Substituting the values of the above integrals into (D.4), the auto-covariance $R_{\phi\phi}(\xi,\chi)$ of hydraulic head fluctuations is given by

$$R_{\phi\phi}(\xi,\chi) = 2\pi A\left\{-(3\cos^2\chi - 1)\left[\frac{e^{-\gamma\xi}}{\gamma\xi}\left(1 + \frac{2}{\gamma\xi} + \frac{2}{(\gamma\xi)^2}\right) + \frac{2}{(\gamma\xi)^3}\right]\right.$$

$$+ (\cos^2\chi - 1)\,\frac{(e^{-\gamma\xi} - 1)}{\gamma\xi}$$

$$+ (3\cos^2\chi - 1)\left[-e^{-\gamma\xi} + \left[-\frac{3e^{-\gamma\xi}}{\gamma\xi}\left(1 + \frac{2}{\gamma\xi} + \frac{2}{(\gamma\xi)^2}\right) + \frac{6}{(\gamma\xi)^3}\right]\right]$$

$$\left. + (\cos^2\chi - 1)\left[e^{-\gamma\xi}\left(1 + \frac{1}{\gamma\xi}\right) - \frac{1}{\gamma\xi}\right]\right\}$$

which can be reduced to

$$R_{\phi\phi}(\xi,\chi) = \frac{J_o^2\,\overline{f'^2}}{2\gamma^2}\left\{(\cos^2\chi - 1)\left[e^{-\gamma\xi} + \frac{2(e^{-\gamma\xi} - 1)}{\gamma\xi}\right]\right.$$

$$+ (3\cos^2\chi - 1)\left[(1 - e^{-\gamma\xi})\frac{8}{(\gamma\xi)^3} - e^{-\gamma\xi}\left[1 + \frac{4}{\gamma\xi} + \frac{8}{(\gamma\xi)^2}\right]\right]\Bigg\} \qquad (4.21)$$

Equation (4.21) is the expression sought at the beginning of this appendix.

APPENDIX - E

Variance of Hydraulic Head Fluctuations in Three Dimensions

An expression for the variance $\overline{\phi'^2}$ of hydraulic head fluctuations is obtained by taking the limit of (4.21) as $\xi \to 0$ which leads to

$$R_{\phi\phi}(0,\chi) = \frac{J_o^2\,\overline{f'^2}}{2\gamma^2}\left\{(\cos^2\chi - 1)\,[-1]\right.$$

$$+ (3\cos^2\chi - 1)\left[\frac{8}{(\gamma\xi)^3}\left[1 - \left(1 - \gamma\xi + \frac{(\gamma\xi)^2}{2} - \frac{(\gamma\xi)^3}{6}\right)\right]\right.$$

$$\left.\left. - \left(1 - \gamma\xi + \frac{(\gamma\xi)^2}{2} - \frac{(\gamma\xi)^3}{6}\right)\left(1 + \frac{4}{\gamma\xi} + \frac{8}{(\gamma\xi)^2}\right)\right]\right\}$$

in which the exponential functions have been expanded in terms of power series. Performing the algebraic operations involved in the above expression, in the limit as $\xi \to 0$, results in

$$R_{\phi\phi}(0,\chi) = \frac{J_o^2\,\overline{f'^2}}{2\gamma^2}\left[\sin^2\chi + \frac{1}{3}(3\cos^2\chi - 1)\right]$$

$$= \frac{J_o^2\,\overline{f'^2}}{2\gamma^2}\left[\sin^2\chi + \cos^2\chi - \frac{1}{3}\right]$$

Hence, the variance ϕ'^2 of hydraulic head fluctuations in three dimensions is

$$R_{\phi\phi}(0,\chi) \equiv \overline{\phi'^2} = \frac{J_o^2\,\overline{f'^2}}{3\gamma^2} \qquad (4.23)$$

which is the desired expression.

APPENDIX - F

Lists of Permeability and Porosity Core Data From Mt. Simon Aquifer, Northeastern Illinois

Remarks

1) Porosity values are given in percent

2) Permeability values are given in millidarcys.

HORIZONTAL PERMEABILITY DATA FOR SET NO. IL036H

1	1.17	4.57	0.10	0.10	0.10	0.96	0.10	0.89
9	1.05	1.91	7.87	2.46	0.10	0.10	0.10	0.10
17	0.10	18.70	0.89	6.93	2.44	2.07	0.89	4.72
25	5.15	2.40	1.43	1.27	1.22	5.92	17.50	29.00
33	3.24	1.17	1.00	31.20	37.60	114.00	73.60	1.24
41	221.00	19.00	51.70	31.20	99.00	0.10	5.15	4.45
49	7.65	0.10	41.70	35.60	34.00	45.50	68.60	56.00
57	66.00	56.00	119.00	0.10	0.10	2.04	14.90	6.93
65	8.90	27.40	58.00	16.50	23.40	29.00	34.00	25.80
73	66.00	11.90	14.70	9.65	35.60	0.89	2.36	10.20
81	0.89	3.37	4.20	5.71	0.10	0.10	0.10	1.52
89	2.84	2.12	13.70	62.20	18.30	27.40	29.00	2.54
97	2.23	1.52	2.36	1.56	2.23	3.12	6.93	2.33
105	8.38	4.57	35.60	37.60	24.90	24.90	3.95	3.12
113	7.00	23.40	32.50	2.92	11.30	0.91	4.57	35.60
121	41.70	32.50	104.00	32.50	56.00	87.30	85.00	51.70
129	231.00	249.00	175.00	354.00	670.00	415.00	385.00	185.00
137	455.00	486.00	820.00	211.00	0.10	11.40	85.00	43.20
145	0.10	5.25	4.64	0.10	35.60	4.34	43.20	53.90
153	112.00	51.70	37.60	85.00	43.20	104.00	66.00	19.50
161	23.40	29.00	29.00	56.00	80.30	37.60	78.00	73.60
169	47.80	5.60	0.10	5.46	0.10	4.72	5.60	0.10
177	6.47	0.10	7.36	51.70	2.29	8.38	5.15	0.10
185	0.10	5.33	8.15	9.90	7.00	27.40	8.13	9.90
193	2.36							

VERTICAL PERMEABILITY DATA FOR SET NO. IL036V

1	10.40	0.89	0.10	0.10	0.10	0.10	0.10	0.10
9	2.99	4.25	8.65	0.10	0.10	0.10	0.10	1.37
17	0.10	34.00	0.89	32.50	0.10	1.88	6.86	4.57
25	1.61	2.07	1.52	6.11	2.54	2.99	7.00	27.40
33	1.56	0.91	19.50	31.20	4.34	107.00	82.20	0.89
41	4.20	25.80	60.00	22.10	10.90	0.10	185.00	29.00
49	14.70	0.10	66.00	5.15	7.11	62.20	34.00	73.60
57	51.70	34.00	1.72	0.10	0.10	1.37	11.10	1.22
65	31.20	32.50	2.40	9.28	35.60	24.90	24.90	41.70
73	19.50	10.20	38.80	6.22	34.00	0.10	0.89	2.44
81	2.07	11.90	2.44	2.99	0.10	0.10	0.10	7.60
89	5.33	23.40	0.89	4.20	35.60	0.10	2.99	7.65
97	4.45	60.00	8.90	10.90	43.20	4.09	23.40	12.70
105	8.90	1.61	13.20	5.25	56.00	37.60	4.09	6.22
113	2.40	1.42	3.30	10.30	5.92	1.56	4.72	3.67
121	0.89	1.88	2.44	5.25	12.40	1.56	3.77	3.77
129	5.15	3.43	12.10	2.07	2.12	385.00	37.60	20.60
137	35.60	9.65	250.00	15.50	0.10	23.40	0.10	5.15
145	0.10	0.89	2.54	0.10	5.25	0.89	5.71	5.60
153	27.40	22.10	25.80	112.00	29.00	49.00	53.90	29.00
161	10.20	16.50	22.10	15.50	24.90	14.70	32.50	10.20
169	37.60	8.25	0.10	0.10	0.10	2.84	1.47	1.00
177	3.59	0.10	6.11	3.43	1.13	6.72	1.08	0.89
185	0.10	37.60	24.90	14.70	15.50	19.50	19.50	3.18
193	0.89							

POROSITY DATA FOR SET NO. IL036

1	13.40	4.70	9.00	10.80	8.80	10.50	7.40	3.30
9	14.20	8.80	3.00	11.60	7.20	9.40	5.80	6.80
17	1.80	1.70	1.50	2.20	13.00	5.80	12.40	10.50
25	11.50	12.00	13.50	17.30	9.60	9.20	11.00	9.50
33	12.50	15.50	11.10	8.80	9.70	12.10	13.00	6.50
41	14.80	11.60	14.60	13.70	14.40	7.00	12.20	9.10
49	8.40	10.80	11.20	9.80	10.80	12.10	13.30	12.10
57	12.90	12.90	13.60	5.00	7.20	10.50	11.50	9.90
65	11.80	10.60	9.40	11.10	12.50	11.70	13.60	15.00
73	13.60	9.60	8.80	10.00	12.40	10.30	13.70	12.00
81	9.00	8.30	10.50	11.50	4.50	9.90	6.90	10.00
89	10.50	12.00	7.80	9.70	11.50	14.40	13.00	10.80
97	14.00	11.10	12.90	11.50	17.80	7.60	12.80	9.20
105	10.60	10.00	11.50	10.30	13.00	10.30	10.30	13.60
113	12.90	11.00	10.70	10.00	9.60	9.10	11.10	11.00
121	8.80	11.40	15.00	13.10	13.00	11.80	14.70	12.60
129	15.30	17.40	15.80	18.20	19.20	17.00	16.70	15.80
137	18.10	15.70	17.40	13.30	11.00	13.50	13.50	10.90
145	6.60	10.50	4.60	1.00	9.10	13.90	10.70	14.00
153	13.50	15.00	12.50	12.40	14.00	12.90	14.50	8.30
161	9.90	10.90	13.50	10.50	9.00	12.50	12.10	9.50
169	10.90	10.40	1.10	7.90	1.00	9.50	10.40	10.90
177	13.10	0.60	9.10	12.30	11.00	10.60	9.50	11.00
185	5.00	9.60	10.00	10.10	15.50	14.00	8.60	15.70
193	12.90							

HORIZONTAL PERMEABILITY DATA FOR SET NO. IL040H

1	2.40	2.69	2.87	53.90	4.20	1.88	0.10	2.74
9	1.66	0.10	0.10	31.20	2.74	10.80	5.08	3.12
17	4.02	6.11	25.80	6.11	37.60	2.03	18.30	4.64
25	198.00	10.20	13.70	24.90	43.20	11.90	13.70	6.74
33	2.87	35.60	43.20	53.90	51.70	94.40	47.60	31.20
41	6.74	2.07	4.09	2.16	18.30	10.90	99.00	41.70
49	34.00	37.60	45.50	45.50	37.60	12.70	35.60	37.60
57	27.40	35.60	38.80	29.00	35.60	45.50	206.00	35.60
65	119.00	160.00	104.00	0.10	0.10	8.25	35.60	37.60
73	51.70	80.30	94.40	51.70	23.40	32.50	10.20	41.70
81	16.50	34.00	18.30	29.00	18.30	51.70	20.60	45.50
89	17.30	51.70	38.80	35.60	618.00	60.00	29.00	10.20
97	15.50	13.70	0.10	15.50	34.00	16.50	22.10	3.12
105	1.17	10.20	0.10	102.00	47.80	53.90	92.00	68.60
113	11.90	37.60	34.00	25.80	6.35	32.50	18.30	41.70
121	64.00	82.20	2.69	2.20	8.90	7.11	3.30	2.36
129	0.10	0.10	0.10	22.10	43.20	51.70	13.30	32.50
137	14.70	53.90	64.00	47.80	31.20	14.70	104.00	68.60
145	104.00	60.00	34.00	35.60	35.60	35.60	25.80	16.50
153	43.20	53.90	41.70	49.50	32.50	34.00	51.70	31.20
161	38.80	37.60	16.50	18.30	43.20	43.20	31.20	29.00
169	38.80	94.40	0.10	0.10	35.60	19.50	31.20	47.80
177	49.50	47.80	35.60	41.70	25.80	37.60	104.00	51.70
185	19.50	37.60	32.50	51.70	3.85	18.30	56.00	20.60
193	19.50	11.90	6.03	49.50	31.20	78.00	9.91	25.80
201	35.60	5.25	9.65	17.50	43.20	43.20	0.10	0.10
209	8.25	4.09	0.10	24.90	34.00	25.80	31.20	71.00
217	53.90	10.20	22.10	43.20	18.30	5.60	41.70	4.95
225	29.00	1.61	41.70	17.50	29.00	22.10	12.70	24.90
233	25.80							

VERTICAL PERMEABILITY DATA FOR SET NO. IL040V

1	1.18	1.66	2.57	4.45	1.00	3.12	0.10	2.69
9	0.10	0.10	4.34	38.80	1.83	9.00	2.20	2.44
17	4.57	13.90	35.60	14.70	53.90	0.10	1.78	5.82
25	1.88	51.70	38.80	43.20	24.90	10.20	13.70	1.27
33	0.10	18.30	2.20	47.80	58.00	25.80	38.80	20.60
41	31.20	2.12	3.85	0.96	11.90	15.50	13.70	7.11
49	2.12	32.50	49.50	13.70	85.00	43.20	34.00	17.50
57	47.80	31.20	112.00	62.20	34.00	96.50	41.70	43.20
65	68.60	35.60	29.00	0.10	0.10	3.24	9.65	29.00
73	58.00	45.50	64.00	31.20	31.20	15.50	5.25	24.90
81	10.20	20.60	13.70	56.00	2.69	22.10	14.70	94.40
89	10.90	18.30	10.20	22.10	18.30	17.50	29.00	14.70
97	16.50	8.25	0.10	1.61	19.50	20.60	18.30	45.50
105	1.33	8.25	0.10	41.70	35.60	13.70	53.90	29.00
113	58.00	13.70	18.30	25.80	2.36	17.50	15.50	0.10
121	34.00	22.10	2.36	0.10	1.05	1.33	7.11	3.24
129	0.10	0.10	0.10	25.80	37.60	34.00	34.00	10.20
137	8.90	37.60	117.00	34.00	8.90	23.40	47.80	38.80
145	35.60	37.60	71.00	8.90	20.60	37.60	11.90	18.30
153	66.00	35.60	53.90	24.90	29.00	32.50	58.00	25.80
161	66.00	47.80	8.90	35.60	8.25	49.50	53.90	29.00
169	58.00	35.60	0.10	0.10	34.00	14.70	47.80	17.50
177	43.20	19.50	34.00	29.00	29.00	34.00	32.50	68.60
185	34.00	31.20	64.00	31.80	32.50	18.30	34.00	18.30
193	14.70	14.70	13.70	6.11	25.80	73.60	11.90	19.50
201	3.85	6.35	3.85	2.74	17.50	14.70	0.10	0.10
209	5.25	13.70	0.10	31.20	71.00	4.72	14.70	117.00
217	25.80	1.91	2.77	10.90	17.50	3.50	18.30	4.72
225	18.30	0.10	18.30	4.45	10.90	3.24	1.47	8.25
233	27.40							

POROSITY DATA FOR SET NO. IL040

1	13.20	15.40	10.50	10.50	16.60	8.00	12.30	8.00
9	10.80	11.70	8.50	11.00	7.50	9.70	5.00	14.50
17	11.70	9.70	7.30	8.00	12.40	8.80	11.00	8.80
25	9.80	12.40	9.90	9.00	9.60	6.90	9.50	9.60
33	7.70	11.00	8.90	14.50	13.50	12.70	11.50	8.10
41	10.60	9.00	10.80	6.70	10.50	6.50	7.50	9.00
49	8.50	9.80	7.80	11.00	11.00	9.80	10.00	14.80
57	16.70	14.50	13.70	17.40	14.00	18.00	17.60	11.50
65	13.10	13.20	14.00	5.00	5.50	16.40	10.50	15.50
73	13.10	15.70	17.30	13.50	15.50	13.10	12.40	10.60
81	10.70	12.00	10.70	10.20	12.20	11.20	11.50	12.50
89	12.80	11.90	12.50	10.10	14.50	9.50	8.80	9.80
97	7.00	7.00	8.80	7.00	9.90	12.80	10.50	12.00
105	14.00	8.30	13.50	14.30	13.90	11.50	12.00	13.10
113	12.60	10.00	12.80	12.20	15.30	10.00	10.50	16.00
121	11.30	12.10	18.20	15.10	12.30	9.50	12.20	10.50
129	0.80	1.00	0.80	12.50	9.60	10.00	9.50	10.00
137	13.70	12.20	13.30	11.80	12.60	13.30	12.80	14.20
145	11.00	10.50	11.70	12.80	9.80	10.20	10.60	12.00
153	13.60	12.80	13.00	12.10	12.40	10.60	11.60	11.70
161	11.80	15.00	10.60	10.40	13.10	11.80	12.00	11.50
169	12.50	13.40	11.70	11.50	10.90	12.80	14.70	11.90
177	13.50	11.50	14.00	14.70	13.80	13.80	14.30	12.00
185	13.30	17.70	13.40	11.70	11.70	10.70	12.90	14.30
193	14.00	11.50	14.50	13.40	12.60	15.40	13.80	7.90
201	9.80	7.30	10.70	9.80	10.90	10.30	9.50	2.00
209	8.70	7.50	9.10	13.40	9.80	13.80	15.00	15.90
217	10.30	8.00	10.30	9.20	10.30	10.20	9.10	11.60
225	10.50	6.00	10.30	9.20	10.00	9.20	9.80	11.50
233	11.00							

HORIZONTAL PERMEABILITY DATA FOR SET NO. IL042H

1	17.50	23.40	1.37	35.60	24.90	7.62	5.60	31.70
9	20.60	19.50	37.60	64.00	37.60	10.90	150.00	94.40
17	3.43	1.22	0.18	131.00	160.00	99.00	25.80	2.29
25	96.50	38.80	104.00	160.00	9.65	0.91	0.33	0.26
33	1.78	2.33	20.60	11.90	4.92	16.50	11.90	11.40
41	11.70	20.60	35.60	22.10	7.62	29.00	41.70	31.20
49	20.60	117.00	47.80	22.10	25.80	35.60	34.00	22.10
57	25.80	8.90	23.40	0.20	19.50	29.00	9.65	117.00
65	25.80	131.00	34.00	16.50	34.00	35.60	8.90	10.90
73	195.00	13.70	38.60	25.80	37.60	94.40	94.40	60.00
81	557.00	165.00	94.00	16.50	23.40	71.10	68.60	58.00
89	7.62	34.00	18.30	0.10	32.50	27.40	18.30	53.90
97	37.60	34.00	12.70	35.60	31.20	134.00	155.00	37.60
105	94.40	6.74	11.90	7.11	22.10	0.42	17.50	31.20
113	34.00	385.00	96.50	253.00	82.20	203.00	43.20	17.50
121	102.00	13.70	24.90	253.00	27.40	41.70	34.00	157.00
129	53.90	0.10	58.00	82.20	38.80	253.00	0.27	68.60
137	38.80	0.10	306.00	42.50	41.70	23.40	58.00	29.00
145	10.20	19.50	10.20	117.00	14.70	29.00	73.60	68.60
153	41.70	49.50	60.00	0.10	0.10	0.10	78.00	29.00
161	35.60	31.20	32.50	32.50	49.50	96.50	68.60	34.00
169	1.56	25.80	0.10	0.10	0.13	38.80	20.60	10.20
177	24.90	24.90	31.20	19.50	25.80	142.00	274.00	584.00
185	58.00	109.00	138.00	107.00	112.00	17.50	25.80	18.30
193	25.80	18.30	8.25	10.90	43.20	112.00	35.60	68.60
201	247.00	41.70	14.70	104.00	172.00	618.00	274.00	279.00
209	180.00	249.00	53.90	14.70	2.20			

VERTICAL PERMEABILITY DATA FOR SET NO. IL042V

1	34.00	3.95	1.33	2.03	29.00	9.65	3.30	12.20
9	19.50	22.10	16.50	32.50	185.00	41.70	17.50	15.70
17	1.61	0.96	0.12	32.50	20.60	29.00	35.60	1.05
25	4.25	35.60	2.03	9.65	7.11	2.57	0.10	1.42
33	0.17	2.38	23.40	14.70	2.33	1.05	1.52	0.88
41	31.20	37.60	1.88	15.50	8.25	24.90	22.10	29.00
49	37.60	35.60	47.80	37.60	37.60	32.50	34.00	4.02
57	34.00	25.80	10.20	0.10	6.35	6.35	8.90	4.45
65	35.60	18.30	29.00	10.90	35.60	31.20	1.78	4.64
73	13.70	13.70	35.60	19.50	56.00	37.60	31.20	104.00
81	80.30	43.20	25.80	34.00	47.80	138.00	31.20	31.20
89	0.91	17.50	25.80	0.10	11.90	38.80	22.10	20.60
97	22.10	11.90	18.30	41.70	15.50	127.00	66.00	25.80
105	38.80	13.70	8.25	19.50	4.64	0.10	104.00	80.30
113	53.90	104.00	104.00	73.60	138.00	47.80	37.60	23.40
121	62.20	37.60	45.50	43.20	24.70	82.20	35.60	51.70
129	29.00	0.10	13.70	62.20	23.40	41.70	0.10	18.30
137	47.80	0.10	68.60	102.00	10.20	56.00	152.00	24.90
145	18.30	20.60	8.25	4.57	15.50	60.00	68.60	104.00
153	37.60	38.80	35.60	0.10	0.10	0.10	49.50	19.50
161	51.70	49.50	43.20	64.00	142.00	51.70	32.50	41.70
169	5.25	60.00	0.10	0.10	0.10	25.80	82.20	41.70
177	37.60	31.20	45.50	35.60	71.00	37.60	218.00	114.00
185	231.00	60.00	104.00	73.60	104.00	47.80	15.50	58.00
193	7.11	15.50	0.10	11.90	250.00	58.00	45.50	58.00
201	53.90	38.80	25.80	53.90	117.00	203.00	66.00	188.00
209	208.00	150.00	99.00	35.60	1.37			

POROSITY DATA FOR SET NO. IL042

1	16.30	8.70	14.40	11.00	11.90	14.20	14.00	11.30
9	12.30	9.20	14.10	13.40	12.70	6.70	12.90	15.40
17	12.50	6.80	6.90	11.30	14.10	14.50	9.20	9.20
25	12.60	10.80	12.60	11.90	6.30	8.30	5.90	6.30
33	8.50	11.10	10.60	7.10	6.20	8.10	7.60	8.50
41	8.10	8.60	11.60	12.80	9.20	11.10	8.50	9.90
49	10.60	11.80	11.00	10.90	10.20	11.00	8.40	11.00
57	11.00	7.60	11.50	6.90	9.90	9.40	7.20	7.70
65	13.50	12.50	10.60	9.30	11.00	9.20	11.50	9.50
73	12.70	11.40	10.40	12.00	13.10	13.50	10.80	13.40
81	14.60	14.80	16.20	14.50	10.20	13.50	10.60	10.80
89	7.40	10.50	11.80	13.90	12.00	11.00	11.30	12.30
97	11.10	10.50	9.90	12.60	11.10	12.00	12.30	11.20
105	10.50	11.00	9.60	11.70	10.70	11.70	16.60	10.50
113	13.30	15.00	15.30	13.90	15.00	12.90	12.00	15.00
121	16.00	11.80	16.30	12.60	13.10	11.90	11.50	15.90
129	14.30	2.40	10.00	11.70	12.80	13.40	15.00	11.80
137	13.50	4.00	15.40	15.70	10.00	14.80	11.70	16.00
145	13.00	12.50	13.00	8.80	9.50	14.40	12.20	13.40
153	13.80	11.00	10.90	1.00	2.00	1.50	9.00	11.20
161	13.70	12.00	11.90	12.20	13.50	13.90	15.00	12.50
169	17.50	10.60	2.70	1.60	1.50	11.00	9.50	10.70
177	9.80	11.20	10.50	14.00	17.00	22.00	16.00	16.20
185	15.00	15.70	15.50	15.20	15.20	15.60	12.00	12.40
193	14.40	13.50	7.50	11.50	19.00	14.80	17.00	15.50
201	15.00	16.00	14.90	16.00	15.00	15.90	14.50	17.50
209	16.40	16.70	16.70	14.00	11.90			

HORIZONTAL PERMEABILITY DATA FOR SET NO. IL052H

1	0.70	0.70	0.48	0.25	7.10	0.39	0.22	0.25
9	0.48	2.10	1.10	4.30	4.40	4.10	5.50	2.20
17	1.20	0.11	2.80	0.48	4.10	2.70	3.30	3.20
25	3.10	5.00	1.50	0.26	1.50	8.40	5.70	0.12
33	7.80	35.00	27.00	1.70	54.00	180.00	11.00	34.00
41	10.00	57.00	25.00	11.00	7.40	7.50	168.00	81.00
49	29.00	13.00	16.00	65.00	29.00	31.00	19.00	23.00
57	74.00	60.00	54.00	3.80	24.00	21.00	17.00	34.00
65	10.00	36.00	26.00	16.00	17.00	191.00	19.00	4.30
73	29.00	6.20	45.00	14.00	0.31	25.00	3.20	23.00
81	30.00	30.00	1.30	16.00	72.00	189.00	66.00	32.00
89	83.00	69.00	204.00	34.00	37.00	7.90	1.80	39.00
97	22.00	30.00	13.00	7.90	21.00	15.00	242.00	226.00
105	13.00	14.00	9.40	0.05	27.00	38.00	864.00	226.00
113	433.00	168.00	14.00	13.00	25.00	3.90	44.00	27.00
121	77.00	32.00	127.00	45.00	36.00	68.00	74.00	189.00
129	40.00	59.00	9.50	61.00	17.00	96.00	36.00	666.00
137	162.00	95.00	257.00	42.00	30.00	8.30	8.60	48.00
145	12.00	23.00	67.00	54.00	116.00	1220.00	228.00	320.00
153	274.00	1085.00	4.30	12.00	5.10	2.00	78.00	31.00
161	62.00	51.00	70.00	1.50				

VERTICAL PERMEABILITY DATA FOR SET NO. IL052V

1	0.09	0.63	0.08	0.03	2.00	0.43	0.26	0.50
9	0.12	0.23	0.19	13.00	1.10	1.40	0.11	4.80
17	5.10	0.11	2.20	1.70	9.90	0.63	2.00	1.70
25	0.33	4.10	2.40	0.91	1.90	6.90	9.80	0.09
33	2.90	18.00	24.00	1.80	4.00	2.70	6.80	22.00
41	31.00	17.00	1.40	2.00	0.83	8.30	117.00	115.00
49	25.00	12.00	27.00	68.00	89.00	22.00	8.90	8.20
57	125.00	8.90	21.00	20.00	25.00	1.20	26.00	9.30
65	11.00	14.00	50.00	16.00	42.00	31.00	0.70	7.80
73	19.00	6.40	7.70	26.00	0.10	26.00	1.40	28.00
81	6.00	8.70	3.50	8.70	167.00	6.00	6.90	59.00
89	150.00	23.00	16.00	10.00	15.00	27.00	4.40	7.90
97	9.90	11.00	6.20	8.90	4.20	33.00	13.00	8.10
105	8.60	5.20	12.00	0.06	16.00	137.00	304.00	140.00
113	69.00	73.00	40.00	62.00	11.00	17.00	23.00	38.00
121	11.00	24.00	65.00	48.00	49.00	31.00	22.00	24.00
129	21.00	60.00	34.00	19.00	31.00	104.00	56.00	77.00
137	67.00	13.00	27.00	27.00	20.00	30.00	31.00	9.50
145	9.60	2.70	11.00	39.00	97.00	100.00	30.00	40.00
153	38.00	0.86	4.70	14.00	32.00	0.22	40.00	26.00
161	64.00	51.00	191.00	277.00				

POROSITY DATA FOR SET NO. IL052

1	9.00	21.00	17.60	8.30	12.20	8.40	9.30	24.40
9	17.60	16.50	22.00	14.10	6.30	11.00	7.40	7.70
17	10.90	23.90	18.20	14.20	9.30	5.80	21.20	23.50
25	19.30	6.70	6.50	19.10	5.50	14.60	10.20	6.30
33	14.20	11.50	10.70	8.40	9.80	16.60	13.80	14.90
41	14.60	13.70	12.10	12.10	19.50	7.00	12.30	11.20
49	7.20	9.60	7.20	14.30	15.60	11.00	7.90	8.00
57	11.30	14.10	10.30	8.30	14.60	12.30	10.00	12.50
65	15.30	11.10	14.00	10.40	9.90	9.00	11.70	9.10
73	12.00	9.70	9.80	13.70	8.80	12.10	18.10	16.50
81	11.10	12.50	6.70	15.40	16.60	15.50	13.90	13.80
89	13.90	13.90	14.00	11.70	13.60	9.10	13.70	14.10
97	11.00	14.20	8.80	10.80	13.10	8.40	11.80	12.20
105	8.40	8.50	13.10	2.80	14.10	14.40	15.10	13.30
113	13.80	18.60	18.60	14.00	11.90	13.20	13.20	14.20
121	12.90	14.80	15.70	16.70	15.70	16.90	10.50	15.50
129	17.00	12.10	14.00	14.10	12.60	15.80	13.80	22.30
137	16.20	15.10	13.60	14.20	10.20	9.10	11.90	10.40
145	11.30	8.00	13.40	11.90	16.20	17.20	13.20	14.60
153	12.10	17.50	17.00	8.10	11.30	13.20	14.40	13.30
161	14.40	15.30	12.30	10.30				

HORIZONTAL PERMEABILITY DATA FOR SET NO. IL056H

1	1.60	7.50	2.10	1.90	2.90	1.60	0.57	5.10
9	6.10	7.90	8.00	3.70	7.20	6.10	2.10	6.40
17	5.70	5.90	2.30	3.00	2.60	1.90	1.80	0.10
25	1.30	9.20	13.00	11.00	8.50	2.20	5.90	3.60
33	11.00	13.00	2.60	10.00	14.00	6.20	2.30	8.40
41	13.00	7.40	43.00	9.10	8.70	4.10	5.00	11.00
49	3.60	4.80	0.10	0.10	63.00	69.00	326.00	58.00
57	66.00	33.00	20.00	1.40	6.60	3.50	10.00	7.40
65	25.00	10.00	4.00	5.40	0.10	0.43	0.48	2.70
73	7.20	1.90	0.31	14.00	71.00	31.00	57.00	56.00
81	65.00	81.00	11.00	2.50	7.50	5.70	5.00	7.60
89	5.20	5.10	6.80	3.20	0.10	4.50	8.10	18.00
97	8.70	15.00	7.80	9.00	2.80	2.90	1.10	1.10
105	2.90	3.30	3.10	6.70	8.40	2.90	17.00	4.50
113	5.50	5.10	4.50	7.70	4.90	5.80	0.10	0.10
121	5.20	2.10	8.30	37.00	18.00	39.00	41.00	50.00
129	43.00	59.00	25.00	20.00	19.00	38.00	29.00	42.00
137	0.10	0.32	0.10	1.90	3.20	17.00	30.00	0.28
145	0.58	0.10	1.70	1.10	2.20	5.10	41.00	13.00
153	22.00	64.00	133.00	96.00	40.00	48.00	7.90	32.00
161	15.00	0.58	7.00	13.00	5.20	0.58	0.53	5.40
169	36.00	6.00	6.00	1.80	0.10	0.10	0.10	0.10
177	14.00	9.90	15.00	20.00	2.90	0.10	3.20	0.10
185	1.10	3.90	3.50	0.34	0.24	6.30	16.00	19.00
193	58.00	34.00	85.00	110.00	79.00	32.00	36.00	3.20
201	6.80	9.30	62.00	33.00	25.00	23.00	6.00	31.00
209	31.00	6.10	5.10	43.00	26.00	53.00	76.00	27.00
217	0.43	0.36	0.10	0.52	0.66	20.00	69.00	115.00
225	93.00	53.00	38.00	70.00	48.00	8.50	75.00	82.00
233	78.00	28.00	36.00	113.00	0.10	0.54	0.28	6.40
241	18.00	8.60	11.00	0.25	6.80	9.50	6.30	66.00
249	91.00	56.00	40.00	35.00	41.00	0.35	0.10	0.15
257	0.10	36.00	12.00	95.00	43.00	44.00	65.00	54.00
265	26.00	0.98	6.20	30.00	0.10	28.00	33.00	26.00
273	6.20	3.20	51.00	0.93	32.00	9.10	6.50	0.10
281	0.10	0.10	3.70	0.33	0.67	4.80	2.60	26.00
289	23.00	22.00	58.00	8.50	11.00	44.00	9.40	34.00
297	7.30	7.10	7.10	5.50	30.00	0.10	1.30	

VERTICAL PERMEABILITY DATA FOR SET NO. IL056V

1	1.90	1.80	1.20	1.30	1.20	0.55	1.40	1.30
9	5.90	1.30	8.70	3.80	6.40	6.70	1.90	4.70
17	2.00	10.00	2.30	4.20	3.00	6.90	2.50	0.33
25	2.20	4.20	2.00	7.20	3.40	5.70	19.00	5.30
33	4.50	6.00	6.40	4.50	9.20	6.50	1.90	7.60
41	5.80	175.00	20.00	18.00	10.00	5.80	4.50	20.00
49	5.10	7.60	0.10	0.10	18.00	102.00	15.00	6.80
57	13.00	49.00	24.00	0.39	4.10	2.50	20.00	43.00
65	7.60	23.00	15.00	14.00	0.10	0.23	0.10	6.00
73	4.50	0.89	0.10	7.20	21.00	9.90	25.00	20.00
81	36.00	1.00	1.40	3.70	13.00	28.00	6.30	4.70
89	12.00	9.70	12.00	2.70	0.10	3.60	4.90	25.00
97	3.90	7.10	7.00	6.20	4.50	5.20	0.10	0.10
105	0.10	3.90	5.40	9.50	1.20	2.00	3.30	6.00
113	24.00	6.10	4.00	36.00	28.00	15.00	0.10	0.10
121	4.70	4.50	7.90	16.00	15.00	29.00	60.00	45.00
129	45.00	37.00	21.00	17.00	7.70	6.80	26.00	18.00
137	0.10	0.10	0.10	3.00	4.20	7.00	2.00	0.10
145	0.22	0.10	0.90	0.60	2.10	2.80	11.00	34.00
153	66.00	23.00	28.00	20.00	28.00	39.00	6.80	2.80
161	1.60	1.40	6.30	2.30	2.10	0.10	0.10	3.40
169	5.20	6.60	4.70	2.60	0.10	0.10	0.10	0.10
177	13.00	13.00	6.20	6.90	4.50	0.10	1.90	0.10
185	0.35	3.00	2.60	0.20	0.92	5.00	4.20	14.00
193	41.00	22.00	50.00	48.00	13.00	20.00	4.40	4.40
201	2.20	9.80	13.00	9.50	26.00	13.00	2.40	17.00
209	18.00	1.90	2.30	4.80	12.00	2.50	12.00	45.00
217	0.43	0.10	0.10	0.33	0.66	5.00	5.70	21.00
225	18.00	57.00	14.00	21.00	42.00	5.70	13.00	19.00
233	18.00	6.90	93.00	15.00	0.10	0.15	0.17	6.50
241	10.00	13.00	5.90	0.75	2.80	6.50	7.50	28.00
249	34.00	22.00	8.80	24.00	8.50	0.55	0.10	0.10
257	0.24	10.00	9.00	5.80	20.00	45.00	18.00	23.00
265	8.50	0.81	3.70	4.90	0.10	21.00	24.00	32.00
273	5.90	11.00	20.00	30.00	19.00	20.00	6.30	0.10
281	0.10	0.10	0.10	0.10	0.10	1.30	2.10	34.00
289	13.00	18.00	19.00	37.00	48.00	15.00	7.50	8.90
297	4.10	2.60	8.40	2.60	45.00	0.10	1.10	

POROSITY DATA FOR SET NO. IL056

1	11.30	9.00	8.60	8.10	9.30	9.00	7.70	8.70
9	11.20	8.90	11.10	12.10	10.40	12.80	11.70	9.90
17	11.00	11.60	11.90	11.70	10.60	10.80	12.70	15.70
25	7.80	10.40	10.60	13.00	13.80	12.00	8.00	14.20
33	12.00	13.70	10.00	11.00	12.50	13.50	14.60	10.40
41	9.30	9.80	16.80	12.00	17.80	13.60	14.20	12.50
49	12.40	14.20	10.60	3.70	13.50	10.50	14.10	14.00
57	19.50	14.00	13.80	16.10	12.80	12.50	13.40	13.00
65	11.20	12.20	12.00	9.60	4.50	8.40	4.00	8.50
73	18.20	7.70	10.20	14.30	13.50	13.40	13.60	13.00
81	12.00	14.70	11.60	10.80	14.70	13.10	11.00	11.90
89	10.30	11.80	12.50	13.40	2.30	9.70	12.90	17.80
97	14.20	11.80	12.40	11.30	10.40	7.10	13.20	11.00
105	11.90	10.50	10.10	9.90	9.90	11.00	10.40	10.00
113	10.10	10.00	12.10	11.10	11.80	11.40	6.00	3.30
121	8.70	11.80	10.00	11.40	13.30	14.10	13.90	14.50
129	14.00	13.80	13.40	12.70	10.30	12.40	10.90	12.10
137	3.30	14.70	9.00	9.90	10.20	9.10	10.00	8.10
145	10.50	7.90	15.80	9.90	9.40	10.00	11.20	12.80
153	13.10	14.30	13.80	11.70	14.50	14.70	13.50	11.70
161	10.70	7.70	9.20	9.20	7.60	8.80	6.70	8.80
169	9.60	11.90	10.10	9.70	3.10	8.20	4.50	6.80
177	10.40	10.20	10.20	11.70	9.10	12.80	9.30	11.00
185	10.80	9.20	10.30	8.80	8.00	10.90	11.30	10.70
193	13.10	13.90	15.40	13.80	13.90	12.50	11.00	9.30
201	9.40	11.60	11.80	10.80	12.30	13.70	15.10	11.70
209	12.80	9.00	8.70	11.90	13.20	12.00	13.20	13.70
217	9.60	7.30	9.50	10.30	12.40	8.20	11.80	12.10
225	13.70	13.70	11.80	13.70	13.10	12.50	12.50	13.40
233	12.30	14.90	9.40	11.00	2.00	5.60	7.20	7.40
241	10.10	10.20	8.30	7.20	9.90	11.20	8.70	12.50
249	11.50	12.10	12.40	12.40	11.80	11.30	5.90	12.50
257	8.60	9.40	10.90	10.30	12.50	9.80	10.70	10.20
265	6.30	12.40	9.90	8.30	2.90	10.70	11.50	10.00
273	10.70	10.10	12.50	12.30	16.10	11.50	9.80	8.30
281	5.50	4.40	11.50	9.70	7.10	7.90	8.50	11.10
289	9.50	12.10	13.30	13.30	12.00	10.30	11.10	12.30
297	10.60	11.70	8.20	9.20	9.20	1.80	6.50	

HORIZONTAL PERMEABILITY DATA FOR SET NO. IL062H

1	3.80	0.32	0.53	0.10	0.11	3.00	0.10	1.00
9	0.10	0.92	0.10	0.58	1.90	0.14	0.29	0.10
17	0.10	54.00	17.00	1.80	7.90	8.30	0.10	1.90
25	0.63	1.40	0.14	27.00	10.00	28.00	15.00	5.50
33	38.00	1.40	67.00	5.50	7.60	8.30	10.00	1.60
41	0.10	20.00	0.29	0.80	6.60	9.20	0.10	0.10
49	0.83	2.50	4.90	5.50	9.50	2.00	0.10	36.00
57	7.50	77.00	4.30	7.50	54.00	1.20	3.20	1.10
65	0.12	0.10	0.34	0.10	2.40	4.90	4.00	45.00
73	25.00	62.00	5.10	2.10	2.80	1.30	16.00	6.20
81	1.30	0.10	3.70	4.20	5.90	2.20	0.29	22.00
89	0.10	0.13	2.30	0.27	1.70	0.10	1.50	2.00
97	65.00	0.16	0.10	3.60	6.20	0.89	90.00	280.00
105	775.00	11.00	7.80	1.10	0.50	0.10	0.40	0.33
113	2.70	8.80	8.10	6.80	46.00	0.65	3.80	6.80
121	23.00	1.60	1.40	0.10	3.30	10.00	3.30	1.50
129	0.49	0.21	32.00	0.10	58.00	48.00	40.00	122.00
137	30.00	93.00	20.00	34.00	27.00	8.20	31.00	0.14
145	3.70	12.00	26.00	38.00	61.00	41.00	20.00	14.00
153	74.00	96.00	43.00	74.00	71.00	65.00	37.00	95.00
161	20.00							

VERTICAL PERMEABILITY DATA FOR SET NO. IL062V

1	0.10	0.10	0.30	0.10	0.10	0.78	0.10	0.72
9	0.10	0.36	0.10	0.92	0.52	0.10	0.11	0.10
17	0.24	5.10	2.20	1.90	0.87	6.00	0.10	0.77
25	0.36	0.17	0.24	1.30	5.30	17.00	2.00	2.70
33	20.00	0.31	4.00	1.50	0.96	4.20	0.83	1.80
41	0.20	2.40	0.10	0.10	2.00	6.80	0.17	0.13
49	0.40	2.10	3.50	2.20	4.00	0.87	0.10	2.10
57	3.50	5.00	1.30	5.80	22.00	1.10	3.20	0.36
65	0.10	0.10	0.10	0.10	1.90	6.90	5.80	35.00
73	14.00	3.10	5.20	1.30	1.10	1.20	1.30	0.58
81	1.30	0.10	0.31	0.58	3.10	1.70	0.31	8.30
89	0.10	0.10	2.00	0.10	0.56	0.10	1.80	0.10
97	1.20	0.10	0.10	1.80	2.60	1.00	42.00	75.00
105	16.00	0.91	2.20	0.10	0.21	0.10	0.10	0.10
113	1.80	7.00	3.40	4.90	10.00	0.68	0.46	1.60
121	0.63	0.10	0.10	0.10	3.10	3.20	1.50	0.16
129	0.10	0.10	0.29	0.10	49.00	17.00	19.00	30.00
137	4.80	37.00	8.90	9.70	6.90	6.10	10.00	0.10
145	2.80	6.40	5.10	13.00	7.70	18.00	25.00	18.00
153	38.00	42.00	26.00	10.00	19.00	42.00	14.00	68.00
161	12.00							

POROSITY DATA FOR SET NO. IL062

1	6.40	11.40	10.50	5.00	5.30	12.90	5.50	9.10
9	6.80	15.60	9.20	13.10	7.10	15.40	9.50	6.10
17	6.30	9.30	10.10	10.40	13.20	12.00	9.50	8.20
25	9.40	8.70	8.90	9.10	10.80	13.30	14.00	9.30
33	10.50	6.40	9.80	8.70	9.60	9.00	9.80	11.00
41	10.40	9.40	8.30	16.20	7.80	12.20	8.40	6.80
49	6.20	8.70	14.00	9.70	8.70	10.80	6.70	12.10
57	11.30	12.30	8.30	11.50	12.30	8.00	11.00	10.30
65	8.90	8.00	12.00	12.10	9.90	10.00	9.50	11.00
73	11.90	11.20	6.70	7.80	10.30	8.60	13.70	11.00
81	11.40	8.00	9.60	8.20	9.90	8.20	8.50	9.10
89	9.10	8.70	8.40	7.30	7.10	9.20	7.40	9.50
97	11.10	7.10	5.60	7.80	9.60	8.30	17.70	14.20
105	15.20	10.50	8.70	10.60	6.90	8.60	7.50	7.40
113	8.70	10.70	10.70	11.80	12.00	8.70	8.60	10.50
121	11.00	7.50	5.90	7.40	8.70	7.80	9.50	7.60
129	8.20	6.80	8.90	8.00	14.10	14.80	15.20	16.10
137	14.30	15.00	13.40	12.30	10.10	11.30	10.00	11.20
145	7.50	7.80	10.00	10.20	13.00	10.70	10.60	11.10
153	10.60	10.50	12.20	12.20	11.60	11.70	12.00	12.70
161	10.90							

HORIZONTAL PERMEABILITY DATA FOR SET NO. IL064H

1	0.10	0.10	0.10	0.10	27.00	7.50	3.70	3.00
9	39.00	3.30	6.50	2.70	7.90	53.00	7.50	9.20
17	3.10	28.00	10.00	8.30	0.59	24.00	3.90	49.00
25	15.00	7.80	4.50	1.70	1.00	0.10	0.10	0.10
33	4.90	3.50	82.00	2.00	1.70	0.10	0.10	2.60
41	0.10	0.83	1.30	3.80	2.80	0.47	6.50	13.00
49	25.00	7.40	0.10	0.97	0.10	0.10	0.10	0.10
57	3.60	3.50	3.00	0.10	124.00	3.00	2.70	49.00
65	0.10	3.60	1.30	0.10	4.00	9.30	30.00	13.00
73	8.90	47.00	0.10	7.50	3.10	24.00	79.00	59.00
81	32.00	36.00	29.00	69.00	98.00	17.00	48.00	6.80
89	1.80	8.80	11.00	8.30	11.00	34.00	3.10	2.10
97	7.60	2.20	2.20	10.00	2.00	1.90	0.10	0.10
105	0.10	6.40	35.00	16.00	21.00	7.20	0.10	0.90
113	1.70	2.50	7.60	7.10	32.00	4.40	20.00	76.00
121	39.00	27.00	56.00	131.00	123.00	17.00	46.00	5.50
129	20.00	20.00	22.00	106.00	51.00	60.00	41.00	24.00
137	27.00	29.00	48.00	2.30	25.00	32.00	2.30	2.10
145	0.81	19.00	35.00	39.00	0.10			

VERTICAL PERMEABILITY DATA FOR SET NO. IL064V

1	0.10	0.10	0.10	0.10	1.50	5.70	6.70	2.00
9	1.30	1.70	5.10	3.80	5.60	10.00	13.00	9.60
17	4.90	14.00	11.00	4.10	0.79	2.00	4.90	2.00
25	3.30	0.62	0.10	0.10	0.78	0.10	0.55	0.10
33	2.70	1.00	2.90	0.85	1.90	0.65	0.10	0.62
41	0.10	0.62	0.81	0.10	1.20	0.10	1.80	9.40
49	24.00	2.80	0.10	0.43	0.10	0.10	0.10	0.10
57	3.10	3.00	0.77	0.10	40.00	1.70	1.50	29.00
65	0.10	0.10	0.10	0.10	0.10	7.40	7.80	6.10
73	8.20	11.00	0.10	6.10	2.40	5.10	41.00	5.90
81	34.00	4.90	18.00	25.00	113.00	18.00	9.40	4.30
89	2.90	7.20	2.90	11.00	24.00	2.10	0.27	0.70
97	2.20	3.40	0.10	1.50	2.00	1.20	0.10	0.10
105	0.10	0.87	2.20	9.90	2.90	4.10	0.10	0.10
113	0.38	2.00	1.60	9.00	26.00	1.50	5.30	39.00
121	39.00	42.00	32.00	40.00	19.00	17.00	7.70	5.10
129	9.80	5.00	5.60	40.00	33.00	43.00	9.70	25.00
137	32.00	6.90	8.00	3.80	3.20	44.00	1.70	1.70
145	1.30	2.30	6.40	45.00	0.10			

POROSITY DATA FOR SET NO. IL064

1	4.50	3.50	10.80	5.40	11.20	12.30	8.30	11.80
9	9.70	9.00	11.00	11.00	6.10	9.70	10.90	10.90
17	9.40	9.80	10.70	7.60	5.30	8.70	10.80	11.90
25	7.10	7.90	5.70	14.80	13.30	13.30	9.80	6.90
33	8.60	8.20	9.20	8.40	9.10	5.70	5.90	6.60
41	5.50	6.70	7.20	8.00	10.40	5.70	9.70	13.60
49	14.80	10.20	8.10	6.40	8.20	3.40	6.10	4.40
57	10.30	8.70	10.00	6.20	14.80	14.70	12.60	12.60
65	12.50	7.70	10.70	3.70	7.10	8.40	8.90	10.70
73	9.70	9.40	5.90	11.20	8.30	9.90	10.60	8.30
81	9.30	10.10	10.40	11.10	13.50	11.20	9.60	7.10
89	6.60	8.80	7.80	11.80	8.10	10.10	6.30	7.40
97	9.60	9.30	9.00	8.60	9.60	8.80	12.00	9.30
105	8.90	11.50	11.40	10.30	9.80	7.20	4.00	7.80
113	7.00	7.80	8.20	7.80	10.70	7.80	10.10	12.80
121	14.60	13.00	12.60	15.30	15.00	15.40	12.90	8.00
129	11.70	10.80	10.50	10.80	12.70	11.90	13.20	12.00
137	13.40	11.50	11.30	12.30	12.00	13.20	7.20	7.70
145	8.50	8.90	10.00	12.90	2.80			

HORIZONTAL PERMEABILITY DATA FOR SET NO. IL066H

1	0.56	0.10	0.18	0.10	0.72	1.40	0.28	0.12
9	0.10	0.10	0.10	0.10	0.45	0.96	5.70	1.70
17	1.50	0.10	0.10	8.10	1.70	1.80	9.00	2.70
25	3.50	1.20	4.00	7.50	9.80	29.00	3.50	12.00
33	6.80	2.00	1.50	0.14	0.10	0.10	1.80	4.20
41	1.40	4.70	19.00	62.00	20.00	0.90	0.43	0.10
49	0.34	19.00	30.00	4.60	0.59	0.56	2.50	1.40
57	0.53	0.21	0.10	2.20	0.38	0.76	2.00	11.00
65	2.80	44.00	87.00	2.80	1.30	5.20	0.10	1.20
73	24.00	3.50	24.00	1.80	23.00	0.75	1.60	6.40
81	9.00	25.00	6.80	29.00	3.70	6.60	6.10	4.70
89	1.30	14.00	14.00	8.30	7.30	18.00	12.00	3.70
97	52.00	8.00	7.70	12.00	7.90	45.00	10.00	13.00
105	4.00	11.00	1.60	42.00	6.90	7.60	3.50	0.93
113	3.10	1.90	1.70	15.00	12.00	9.50	29.00	24.00
121	15.00	22.00	33.00	35.00	50.00	44.00	35.00	48.00
129	106.00	29.00	25.00	8.50	16.00	24.00	115.00	121.00
137	40.00	9.40	26.00	7.60	27.00	28.00	28.00	25.00
145	11.00	27.00	82.00	35.00	53.00	120.00	45.00	55.00
153	44.00	58.00	53.00	0.35	6.70	12.00	27.00	9.30
161	13.00	47.00	41.00	26.00	0.10	0.10	0.10	18.00
169	43.00	107.00	16.00	23.00	10.00	8.30	6.00	3.20
177	0.10	2.40	6.10	30.00	10.00	32.00	24.00	8.60
185	5.60	0.26	0.82	0.75	0.69	7.60	7.40	8.00
193	5.70	2.20	0.10	0.10	0.10	0.45	6.70	24.00
201	11.00	7.20	4.50	1.40	11.00	19.00	31.00	9.90
209	20.00	0.10	0.11	0.10	0.10	0.10	0.10	52.00
217	8.50							

VERTICAL PERMEABILITY DATA FOR SET NO. IL066V

1	0.11	0.10	0.10	0.10	0.13	0.93	0.13	0.11
9	0.10	0.10	0.10	0.10	0.12	1.10	4.60	1.20
17	1.40	0.10	0.10	12.00	2.20	1.30	2.50	0.52
25	3.60	0.97	2.00	1.10	2.60	18.00	6.70	6.50
33	1.40	1.50	0.10	0.10	0.10	0.10	1.30	1.20
41	2.00	2.10	1.60	3.20	2.00	0.10	0.10	0.10
49	0.10	6.30	11.00	2.20	0.60	0.10	0.25	0.10
57	0.10	0.10	0.10	1.40	0.35	1.40	1.90	2.70
65	2.30	31.00	56.00	0.60	1.10	3.50	0.10	0.10
73	8.30	5.10	10.00	0.56	14.00	0.16	2.00	3.70
81	8.70	17.00	4.40	6.40	5.40	3.20	6.70	0.25
89	0.10	3.00	5.70	17.00	12.00	11.00	3.60	5.60
97	16.00	4.00	6.30	9.50	9.20	22.00	5.60	7.40
105	1.20	6.80	0.35	3.80	7.50	8.70	1.50	1.80
113	0.15	0.92	1.50	10.00	3.80	10.00	33.00	6.40
121	11.00	23.00	16.00	25.00	45.00	38.00	34.00	53.00
129	61.00	39.00	25.00	6.90	13.00	47.00	25.00	36.00
137	32.00	8.90	7.90	9.30	13.00	6.50	8.20	9.00
145	8.80	32.00	27.00	43.00	41.00	27.00	27.00	11.00
153	20.00	26.00	33.00	0.14	4.80	9.20	18.00	6.40
161	8.40	10.00	9.20	16.00	0.10	0.10	0.10	9.40
169	15.00	41.00	0.11	12.00	16.00	4.60	3.60	2.80
177	0.10	2.80	4.00	5.40	6.20	3.50	8.80	7.20
185	2.00	0.35	0.10	0.10	0.16	3.10	1.00	1.70
193	2.80	1.70	0.10	0.10	0.10	0.10	0.67	5.90
201	2.80	0.87	2.10	0.14	7.40	4.20	29.00	7.20
209	11.00	0.10	0.10	0.10	0.10	0.10	0.10	37.00
217	5.20							

POROSITY DATA FOR SET NO. IL066

1	6.30	10.60	11.20	9.40	8.50	9.50	8.40	7.70
9	14.10	4.20	6.50	8.30	10.80	6.10	8.00	8.80
17	9.50	7.90	6.20	10.20	8.40	7.00	8.40	7.80
25	8.50	7.30	9.70	8.50	8.60	12.80	8.50	12.30
33	11.00	8.70	6.70	8.70	12.80	3.40	9.70	9.80
41	10.90	13.10	11.20	11.90	10.40	6.80	7.70	3.70
49	6.90	12.60	14.10	13.90	6.60	9.20	9.40	7.30
57	6.20	6.50	5.90	10.50	8.30	6.40	12.30	11.40
65	12.60	11.50	14.60	8.20	9.80	11.80	5.90	7.60
73	10.20	7.90	9.00	11.40	13.70	8.60	10.10	11.90
81	10.50	12.00	9.60	10.80	8.10	9.30	10.40	7.70
89	11.50	9.50	10.80	9.50	9.00	11.00	7.90	9.00
97	9.80	9.80	8.70	11.50	9.20	10.20	9.60	9.40
105	10.50	11.40	7.60	11.00	11.60	11.10	8.60	9.10
113	8.30	7.70	8.10	13.30	10.10	11.00	12.90	13.10
121	12.20	12.10	11.40	14.50	15.40	16.20	14.90	14.90
129	16.40	16.90	15.10	10.80	13.10	11.70	11.60	14.80
137	16.10	11.00	11.30	11.90	10.90	13.00	10.90	13.20
145	11.30	13.30	13.60	14.40	14.70	16.00	14.80	13.70
153	14.10	13.50	13.90	11.40	10.10	13.80	11.50	11.20
161	12.60	11.40	12.40	11.80	5.80	7.60	5.30	14.80
169	14.20	13.60	13.40	13.90	13.40	11.30	10.40	17.30
177	9.10	11.00	11.10	11.70	11.60	11.40	12.20	12.20
185	10.60	8.40	7.20	8.10	10.70	10.00	9.60	12.60
193	13.60	8.30	5.00	2.10	6.90	8.50	6.30	9.90
201	10.50	8.30	8.80	9.60	14.00	12.10	11.30	11.40
209	13.30	11.20	5.80	11.70	7.80	3.90	5.70	13.20
217	11.80							

APPENDIX - G

Description of Mt. Simon Aquifer, Northeastern Illinois

The following description of Mt. Simon aquifer is summarized from a report by the Illinois State Water Survey (1973). The Mt. Simon Sandstone derives its name from an exposure on Mount Simon near Eau Claire, Wisconsin. It belongs to the Croixan series of the Cambrian system. In northeastern Illinois the Mt. Simon Sandstone consists of fine- to coarse-grained, unfossiliferous sandstone underlying fossiliferous sandstone, shale, and dolomite of the Eau Claire Formation.

The Mt. Simon Sandstone is present in all wells in northeastern Illinois that penetrate the base of the Eau Claire Formation. It is found at a depth of 1500 to 1900 feet over most of the area with a thickness ranging from 1200 up to 2800 feet. The top of the Mt. Simon Sandstone generally dips northwest to southeast at 10 feet per mile.

The Mt. Simon Sandstone is generally coarser, more poorly sorted, and more angular than sandstones of the other Cambrian or Ordovician formations in northeastern Illinois. Cores exhibit well developed cross-bedding, especially in the coarser grained beds. Red and green shales, a few inches to 15 feet in thickness, occur in the upper 300 feet and lower 600 feet. A few zones contain very fine quartz pebbles, and an arkosic zone is commonly found at the base of the Mt. Simon Sandstone.

Deposition of the Mt. Simon Sandstone most likely occurred in basins that had an influx of fresh water as suggested by the lack of marine fossils in it. The source of the sediments is believed to have been to the north, since the sandstones coarsen in that direction. Most

of the Cambrian and Ordovician rocks are less dolomitic to the north, forming, in southeastern Wisconsin, a more continuous sandstone sequence from the Mt. Simon Sandstone up through the St. Peter Sandstone (Ordovician). This series of sandstones plus the overlying Galena Dolomite are collectively referred to as the "sandstone aquifer".

In Northeastern Illinois the Mt. Simon Sandstone and the lower incoherent sandstone of the Eau Claire Formation are hydrologically connected and considered as one unit, the Mt. Simon aquifer. In southeastern Wisconsin, the recharge area of the Mt. Simon, this aquifer is the lowermost unit of the "sandstone aquifer", which behaves hydrologically as one unit. Recharge to the sandstone aquifer takes place as precipitation percolates down through glacial drift and, where present, overlying bedrock units.

Groundwater in the Mt. Simon aquifer occurs under artesian conditions because part of the Eau Claire Formation acts as a confining layer and head differences exist between the Mt. Simon aquifer and shallow aquifers. Groundwater movement is apparently downdip away from the recharge area and becomes increasingly vertical further southward as conditions become favorable for upward movement.

Average coefficients of transmissivity and storativity of the Mt. Simon were estimated to be 10,000 gpd/ft (gallons per day per foot) and 10^{-4} respectively. The ratio of vertical to horizontal permeability is generally 0.5.

APPENDIX - H

Derivation of the One-Dimensional Spectrum of Hydraulic Head From its Three-Dimensional Counterpart

In this appendix we evaluate the integral appearing in the expression of the one-dimensional spectrum of hydraulic head fluctuations given by (see section 6.3.3)

$$\phi_{\phi\phi}^{(1)}(k_1) = \frac{J_o^2 \overline{f'^2}}{\pi} \int_o^\infty \frac{\gamma k_1^2 \, d\tau^2}{(\tau^2 + k_1^2)^2 (\tau^2 + k_1^2 + \gamma^2)^2} \tag{6.31}$$

Setting

$$\left.\begin{aligned} A &= \frac{J_o^2 \overline{f'^2} \gamma}{\pi} \quad , \\ \tau^2 &= x \quad , \\ a &= k_1^2 \quad , \quad \text{and} \\ c &= k_1^2 + \gamma^2 \end{aligned}\right\} \tag{H.1}$$

reduces (6.31) to the form

$$\phi_{\phi\phi}^{(1)}(k_1) = Aa \int_o^\infty \frac{dx}{(a + x)^2 (c + x)^2} \tag{H.2}$$

Equation (H.2) is evaluated using tables of integrals (Dwight, 1961, p. 29) as

$$I \equiv a \int_o^\infty \frac{dx}{(a + x)^2 (c + x)^2} = a \left[\frac{-1}{(a - c)^2} \left[\frac{1}{(a + x)} + \frac{1}{c + x} \right] \right]_{x=0}^{\infty} +$$

$$+ \left[\frac{2a}{(a - c)^3} \ln \left| \frac{a + x}{c + x} \right| \right] \Bigg|_{x=0}^{\infty}$$

Using ℓ'Hospital rule on the second term leads to

$$I = \frac{1}{(a - c)^2} \left(1 + \frac{a}{c} \right) - \frac{2a}{(a - c)^3} \ln \left| \frac{a}{c} \right|$$

Substituting the quantities defined in (H.1) in the above expression yields

$$\Phi_{\phi\phi}^{(1)}(k_1) = \frac{J_o^2 \overline{f'^2}}{\pi \gamma^3} \left[\left(1 + \frac{1}{1 + (\gamma/k_1)^2} \right) + 2 \left(\frac{k_1}{\gamma} \right)^2 \ln \left(\frac{1}{1 + (\gamma/k_1)^2} \right) \right]$$

which is the desired expression for the one-dimensional spectrum of hydraulic head fluctuations.

APPENDIX - I

Derivation of the Variance of Hydraulic Head Fluctuations from the Spectrum, $\phi^{(1)}_{\phi\phi}(k_1)$

In Appendix - E we derived an expression for the variance of hydraulic head fluctuations from the autocorrelation function in three dimensions, $R_{\phi\phi}(\xi,\chi)$. We now use the spectrum of hydraulic head fluctuations given by (6.32) to see if we can obtain the same expression that was obtained in Appendix - E for the variance of hydraulic head which is defined as

$$\overline{\phi'^2} = \int_{-\infty}^{\infty} \phi^{(1)}_{\phi\phi}(k_1)\, dk_1 \qquad (I.1)$$

Substituting the value of $\phi^{(1)}_{\phi\phi}(k_1)$ from (6.32) in the above expression yields

$$\overline{\phi'^2} = \int_{-\infty}^{\infty} \frac{J_o^2 \overline{f'^2}}{\pi\gamma^3} \left[\left[1 + \frac{k_1^2}{k_1^2+\gamma^2} \right] + \frac{2\, k_1^2}{\gamma^2} \ln \left(\frac{k_1^2}{k_1^2+\gamma^2} \right) \right] dk_1$$

Setting $\dfrac{J_o^2 \overline{f'^2}}{\pi\gamma^3} = A$ and integrating gives the following expression for the variance of hydraulic head fluctuations:

$$\overline{\phi'^2} = A \left[\frac{2}{3} k_1 - \frac{2k^3}{3\gamma^2} \ln \left(1 + \frac{\gamma^2}{k_1^2} \right) + \frac{\gamma}{3} \tan^{-1} \frac{k_1}{\gamma} \right] \Bigg|_{-\infty}^{\infty}$$

Expanding the logarithmic term as a power series yields

$$\overline{\phi'^2} = A\left[\frac{2}{3}k_1 + \frac{\gamma}{3}\tan^{-1}\frac{k_1}{\gamma} - \frac{2k_1^3}{3\gamma^2}\left(\frac{\gamma^2}{k_1^2} - \frac{\gamma^4}{2k_1^4} + \frac{\gamma^6}{3k_1^6} - \cdots + \cdots\right)\right]_{-\infty}^{\infty}$$

$$= \frac{A\gamma\pi}{3}$$

Substituting the value of A and evaluating the above expression at the indicated limits results in

$$\overline{\phi'^2} = \frac{J_o^2\overline{f'^2}}{3\gamma^2}$$

which is indentical to the expression obtained earlier from the covariance of hydraulic head fluctuations in three dimensions.

APPENDIX - J

Confidence Limits for the Spectral Density Functions

The sampling distribution of a smoothed estimate of a spectral density function is approximately chi-square with ν degrees of freedom (Jenkins and Watts, 1968, p. 254). Hence, for a spectral density $\Phi_{ff}(k)$ based upon an estimate $\hat{\Phi}_{ff}(k)$ computed for a number of lags, M and a total record length N, a $1 - \alpha$ confidence interval is given by

$$\frac{\nu\ \hat{\Phi}_{ff}(k)}{\chi^2_\nu(\alpha/2)} \leq \Phi_{ff}(k) \leq \frac{\nu\ \hat{\Phi}_{ff}(k)}{\chi^2_\nu(1-\alpha/2)} \qquad \text{(J.1)}$$

where $\nu = 2.667\ \frac{N}{M}$ for the Tukey window used in the computations presented in earlier chapters.

The confidence intervals given by (J.1) would have to be computed for each spectral estimate if the spectrum is plotted on a linear scale. However, if the spectrum is plotted on logarithmic scale, the confidence interval for the spectrum is represented by a constant interval about the spectral estimate (Jenkins and Watts, 1968). Thus, using (J.1) the confidence interval for $\log \Phi_{ff}(k)$ is

$$\log \hat{\Phi}_{ff}(k) + \log \frac{\nu}{\chi^2_\nu(\alpha/2)} \leq \log \Phi_{ff}(k) \leq \log \Phi_{ff}(k) + \log \frac{\nu}{\chi^2_\nu(1-\alpha/2)} \qquad \text{(J.2)}$$

Consequently, when plotting the computed spectrum, the confidence interval for all wave numbers or frequencies can be indicated by a

single vertical line. Figure 3.10 in Jenkins and Watts (1968) was used to read off values of $\log \frac{\nu}{\chi^2_\nu(\alpha/2)}$ and $\log \frac{\nu}{\chi^2_\nu(1-\nu/2)}$ for the confidence intervals presented in Chapter 5.

This dissertation is accepted on behalf of the faculty of the Institute by the following committee:

Lynn W. Gillam
Adviser

Allan L. Gilligan

John R. MacGillivray

July 23, 1976
Date